WEARABLE RF SENSORS FOR NON-INVASIVE DETECTION OF BLOOD GLUCOSE LEVELS

by

Tuba Yilmaz

A thesis submitted in partial fulfilment of
the requirements for the degree of

Doctor of Philosophy
School of Electronics Engineering and Computer Science

at the

Queen Mary, University of London

September 14, 2013

To My Family

Abstract

Radio frequency (RF) techniques have the potential to provide blood glucose readings through sensing the glucose dependent change in dielectric properties of the biological tissue. Such technique can enable much desired non-invasive and continuous monitoring of blood glucose level. In this work, we present realistic glucose dependence of dielectric properties as well as basic understanding of resonator behaviour while radiating towards the lossy biological tissue.

To investigate the potential of RF techniques, two resonators, operating at microwave frequencies when placed radiating towards the biological tissue, are designed and fabricated. The spiral resonator is tested with liquid and semi-solid phantoms containing different amounts of sugar. An analytical formulation to retrieve the dielectric properties of the biological tissues is improved. In order to perform realistic tests, novel tissue mimicking materials for an extremely wide frequency range are proposed. Glucose dependance of the blood mimicking material dielectric properties are further investigated by adding realistic glucose amounts to the blood mimicking material and dielectric spectroscopy is performed. Next, a single pole Cole-Cole model is fitted to the median of the dielectric property measurements. In addition, a patch resonator is simulated with four-layered digital phantom and tested with the four-layered physical tissue mimicking phantom.

Finally, a double parameter measurement platform is constructed by combining the patch resonator and a commercial force sensor to perform controlled experiments with humans. Also, the force dependant response of the patch resonator is quantified. Soda tests is performed on five subjects with the platform, all subjects were asked to apply the same level of force. Spiral resonator is also

applied to examine the glucose changes of two human subjects during the soda test. The results suggests that, although the glucose-dependance of the dielectric properties is relatively small, the input impedance of a microwave resonator is still sensitive to such small alterations.

Acknowledgments

I would like to express my deepest gratitude to my advisor Prof. Yang Hao for providing guidance and encouragement throughout my PhD study. I would like to thank Prof. Clive Parini and Dr. Akram Alomany for serving in my committee during mid-exams. I would also like to thank Dr. Robert Foster for fruitful discussions and being an example to me with his attention to meticulous detail.

Special thanks to my colleagues for providing a peaceful and friendly environment to work. I also enjoyed very much during my PhD studies our intellectual and cultural exchange. I would especially like to thank Di, Khaleda, Alice, Paolo, Allessio, Qammer, Olex, Yifeng, Marie, Khalid, Rihannon, Jiefu, Anestis, Oscar, Max, and Wenxuan for their support and friendship.

I would like to give the most of the credit to my family, without their support, guidance, and sacrifices, beginning from my childhood, this dissertation would not be possible. I am grateful to my late grandfather for religiously believing in the power of education. I would also like thank my mother who always supported and pushed me to perform at my best. Special thanks to my father who has been a big influence to me with his compassion. I would like to thank Ahmad for his constant support during my PhD, without his encouragement and patience this thesis would never been possible.

Finally, I would like to thank Allah for not giving up on me and giving me all the opportunities throughout my life.

List of Publications

Book Chapters:

1. Robert Foster, **Tuba Yilmaz**, Max Munoz and Yang Hao, "Wearable Sensors", in "Autonomous Sensor Networks: Collective Sensing Strategies for Analytical Purpose", Chapter 5, Daniel Filippini (Ed.), Springer, 2013, ISBN-13 978-3642346477.

Journal Publications:

1. **Tuba Yilmaz**, Robert Foster, Yang Hao, "Broad-Band Tissue Mimicking Phantoms for Evaluating Non-Invasive Monitoring of Blood Glucose Levels.", IEEE Transactions on Antennas and Propogation.*(Under Review).*

2. **Tuba Yilmaz**, Robert Foster, Yang Hao, "Dielectric Property Retrieval of Biological Tissues for Blood Glucose Monitoring.", IEEE Transactions on Microwave Theory and Techniques.*(Under Review).*

3. **Tuba Yilmaz**, Robert Foster, Yang Hao, "Detecting Vital Signs with Wearable Wireless Sensors." Sensors 2010, no. 12, pp. 10837-10862 *(Review Article).*

Conference Proceedings:

1. **Tuba Yilmaz**, Max Munoz, Robert Foster, Yang Hao, "Wearable Wireless Sensors", International Workshop on Antenna Technology (IWAT), Karlsruhe, Germany, March 2013.

2. **Tuba Yilmaz**, Max Munoz, Robert Foster, Yang Hao, "Towards Non-invasive and Continuous Monitoring of Vital Signs",I ET workshop on Today's RF Tomorrow's Medicine, London, UK, February 2013.

3. **Tuba Yilmaz** ,Robert Foster,and Yang Hao, "Patch Resonator for Non-invasive Detection of Dielectric Property Changes in Biological Tissues." IEEE International Symposium on Antennas and Propagation and USNC-URSI National Radio Science Meeting 2012, Chicago, USA.

4. **Tuba Yilmaz*** and Yang Hao, "Enabling Microwave Devices for Chronic Disease Management." QMUL, Research Open Day 2012, London, UK. ***Best Antenna Poster Award***.

5. Yang Hao, Alessio Brizzi, Robert Foster, Max Munoz, Alice Pellegrini, **Tuba Yilmaz**, "Antennas and propagation for body-centric wireless communications: Current status, applications and future trend," Electromagnetics; Applications and Student Innovation (iWEM), 2012 IEEE International Workshop on , vol., no., pp.1-2, 6-9 Aug. 2012.

6. **Tuba Yilmaz*** and Yang Hao, "Enabling Microwave Devices for Chronic Disease Management." the 24th. London Hopper Colloquium 2011, London, UK. ***IBM Best Poster Award***.

7. **Tuba Yilmaz** and Yang Hao, "Sensing of Dielectric Property Alterations in Biological Tissues at Microwave Frequencies." LAPC 2011, Loughborough, UK.

8. **Tuba Yilmaz** and Yang Hao, "Compact Resonators for Permittivity Reconstruction of Biological Tissues." XXX URSI General Assembly 2011, Istanbul, Turkey.

9. **Tuba Yilmaz** and Yang Hao, "Electrical Property Characterization of Blood Glucose for On-body Sensors." EUCAP 2011, Rome, Italy.

10. F. Keshmiri, **T. Yilmaz**, Y. Hao, and C. Craeye, "MOM Analysis of Antenna Devoted to BAN." EUCAP 2011 Rome, Itally.

11. **Tuba Yilmaz** and Yang Hao, "Non-invasive Sensing of Blood Glucose Using Wearable Microwave Sensors." European Microwave Week 2011, Manchester, UK.

Table of Contents

List of Figures

List of Tables

Glossary

AES	Advanced encryption standard, 52
BAN	Body area network, 49
BG	Blood Glucose, 38
BGL	Blood Glucose Level, 35
BMM	Blood Mimicking Material, 157
BP	Blood pressure, 35
DGBE	Diethylene Glycol Butyl Ether, 72
E-health systems	Providing ubiquitous healthcare available to everyone, 1
ECG	Electrocardiograph, 35
EM	Electromagnetic, 1
EMFi	Electromechanical film, 46
EMI	Electromagnetic interference, 59
Ex-vivo	To perform experiments in an artificial environment outside the living organism, 13
FCC	Federal Communications Commission, 52
FDA	Food and drug administration, 39
FDTD	Finite difference time domain, 55
GFSK	Gaussian frequency-shift keying, 51
HbA1c	Haemoglobin A1c, 4
HFSS	High frequency structure simulator, 59
HSCA	Horn-shaped self-complementary antenna, 57
In-vivo	To perform experiment by using a living organism as opposed to a partial or dead organism, 13
IS	Impedance spectroscopy, 39
ISM	Industrial scientific medical, 51
LOS	Line of sight, 55

LOS	Non-line of sight, 55
Lumpectomy	A surgical operation in which a lump is removed from the breast, 14
Mastectomy	A surgical operation to remove a breast, 14
MEMS	Micro-electromechanical systems, 37
MICS	Medical implant communication service, 41
MLR	Multiple Linear Regression, 111
NHS	National Health Service, 2
NIR	Near Infrared, 7
OQPSK	Offset quadrature phase-shift keying, 52
PDA	Personal digital assistant, 50
PICA	Planar inverted cone antenna, 57
PNA	Performance Network Analyzer, 15
PPG	Photoplethysmogram, 37
PSO	Particle Swarm Optimization, 111
PTT	Pulse wave transit time, 37
PVDF	Polyvinylidenefluoride, 46
RF	Radio Frequency, 9
RFID	Radio-frequency identification, 59
RMSE	Root Mean Square Error, 90
SAR	Specific Absorbtion Rate, 93
SNR	Signal-to-noise ratio, 57
SPO_2	Blood oxygen saturation, 47
Telemedicine	The remote diagnosis and treatment of patients by means of telecommunications technology., 35
TPh	Tissue phantom, 69
UWB	Ultra-wide band, 11
VNA	Vector Network Analyzer, 39
WBSN	Wireless Body Area Network, 34
WBSN	Wireless body sensor network, 53
WHO	World Health Organization, 2
WLAN	Wireless local area network, 58

WPAN Wireless personal area network, 51

Chapter 1

Introduction

The emergence of wireless technologies and advancement in on-body sensor design can enable changes to the conventional healthcare system, replacing it with e-health systems, centred on the individual [1]. So-called E-health systems can provide healtcare for everyone at anywhere [2]. And it is anticipated to reduce healthcare costs via disease prevention and individualised provision of care in decentralised health systems, including virtual healthcare providers, with hospitals reserved for more targeted care scenarios [3, 4, 5].

A vital element of ubiquitous healthcare systems is wearable vital sign monitoring devices. Such devices are currently under development towards seamless integration with the daily routine of the user. Seamless integration requires non-invasive, real-time, and continuous monitoring of the vital signs [6]. Many chronic diseases and emergency scenarios can be successfully managed with wide deployment of such sensors. However, design and testing of such sensors is very challenging and requires comprehensive understanding of biological parameters to be sensed in the human body. From an electromagnetic (EM) perspective, disease related changes cause molecular alterations in the biological tissue; thus, lead to changes to dielectric properties of the tissue. Therefore, such changes can

be detected by using EM techniques.

1.1 Research Objectives

The goal of this thesis is to propose an electromagnetic technique which can be used to sense the changes in blood glucose level. The approach should be non-invasive, robust, and applicable to normal, pre-diabetic, and diabetic subjects. Towards the development of the non-invasive blood glucose monitoring device, the aim is to explore the relationship between the blood glucose level and dielectric properties of biological tissue. Then, establish a relation between the response of the proposed microwave device and the blood glucose through a champaign of numerical simulations and measurements. The research objectives of this dissertation are;

1. Assessment of the effect of blood glucose level on the dielectric properties of blood at microwave frequencies;

2. Numerical investigation of the response of microwave resonators to dielectric property change;

3. Design of controlled experiments to measure the effect of the blood glucose level to microwave resonator response;

4. Investigation of the other biological and external factors that can effect the microwave resonator response.

To the best of author's knowledge, results arising from this research have not been presented by others in the literature before.

1.2 Motivation

Chronic diseases presents a significant challenge to healthcare services worldwide. Currently, chronic diseases are incurable; thus, further complications of such diseases can only be prevented with effective management. The World Health Organization (WHO) has reported that such conditions will be the leading cause of

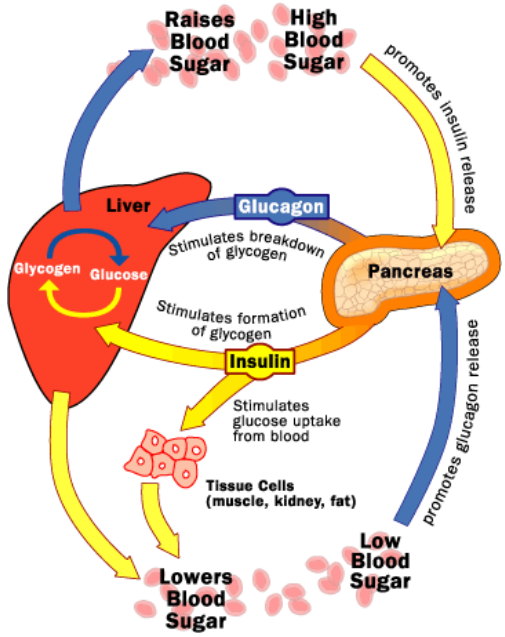

Figure 1.1: Glucose regulation mechanism of the body [10]

disability by 2020 and if not successfully managed, they will potentially become one of the most expensive problems in healthcare [7]. Additionally, according to a National Health Service (NHS) report, WHO data indicates that 75% of the total global population have at least one chronic condition and 50% have two or more [7].

Within the last decade, changes in lifestyle and nutrition made diabetes one of the most commonly-seen chronic conditions. There are 2.2 million people with diabetes in England, and over 250 million people worldwide suffering from the disease [8]. Diabetes is a prevalent metabolic disorder, occurs due to the malfunction of glucose regulation mechanism shown in Fig. 1.1, without a certain cause. There are two main types of diabetes, known as Type 1 and Type 2 [9].

Type 1 diabetes is an autoimmune disease, usually develops during at an early age. Type 1 diabetes affects $400,000$ patients in the UK and of these, more than $29,000$ are children [11]. The immune system attacks the insulin producing beta cells in the pancreas [12]. Thus the body's glucose regulation system lacks the insulin secretion. Disease is managed through insulin injections to prevent an abnormal increase in the blood glucose level and patients are strongly adviced to adopt a healthy lifestyle. There is no cure for Type 1 diabetes; however, several treatment possibilities, such as beta cell or pancreas transplantation, are under

investigation [13].

Type 2 diabetes is more prevalent among people over 40 years old [14]. However, nowadays with the high intake of processed foods among youth, the assessed age for the risk group is dropping rapidly [15]. One of the significant cause of type 2 diabetes is *insulin resistance* [16]. *Insulin resistance* is the condition in which the body is able to produce the required amount of insulin but the muscle, fat, and liver cells fail to respond to it [17]. As the threshold of required insulin for proper functioning of the cells increases, the pancreas increases the amount of the insulin produced to regulate the blood glucose level. Thus, insulin resistance causes high insulin level in the blood stream, as well as high glucose level. Fasting glucose level of a non-diabetic patient with insulin resistance is 5.5 mmol/l (100 mg/dl) or above [18].

Diabetes is a chronic condition and, if it is left untreated, it is a leading cause of kidney failure, blindness in adults, and limb amputation. Also, diabetes significantly increases the risk of stroke, coronary heart disease, and it is the 5th leading cause of death [7]. Blood glucose level of a healthy individual is between 3.5 to 5.5 mmol/l (80-100 mg/dl) before meals and are less than 8 mmol/l (150 mg/dl) two hours after meals [19]. Normal change of the blood glucose level with different food intake are shown in Fig. 1.2.

For a diabetic patient it is vital to keep the blood glucose level at normal range. One important step for long-term evaluation of the blood glucose was taken with the introduction of the test named HbA1c [21]. In the blood stream, hemoglobin coexist with glucose molecules, for both diabetes patients and healthy people. The glucose molecules stick to hemoglobin to form haemoglobin A1c, termed HbA1c [22]. HbA1c molecules lasts around 12 weeks, so the long-term management of blood glucose level can be evaluated by measuring the HbA1c level about every 3 months [23]. For non-diabetes people, the HbA1c level should be less than 5%, and for patients with well-managed diabetes, it should be less than 6% [24]. If a person is undiagnosed and in the $5 - 6\%$ HbA1c range, they are diagnosed as pre-diabetes. Also, the HbA1c test can be used as a diabetes diagnosis tool[25]. It is estimated that there are about $900,000$ people living with diabetes in the UK without diagnosis [26]. On occasion, the disease might not

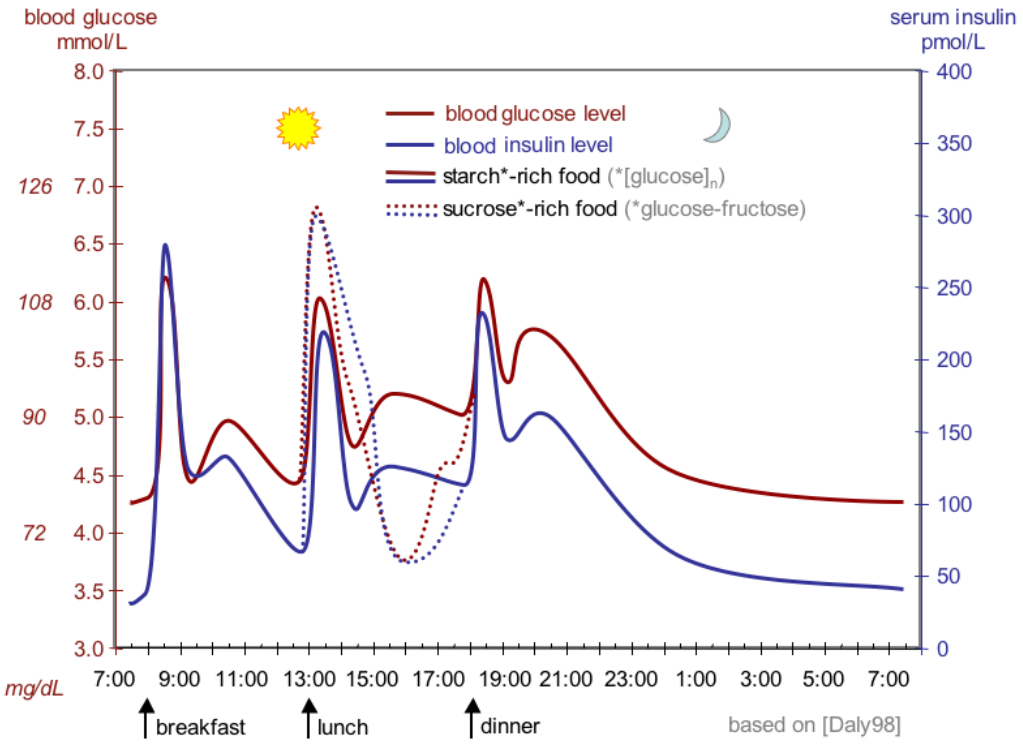

Figure 1.2: Change of blood glucose level and insulin level in the blood stream [20]
.

show any symptoms and, during clinical visits, the blood glucose measurements can be within the normal range. However, in between the doctor visits, the patient can experience abnormal blood glucose fluctuations. In such cases, many people suffering from diabetes can leave the clinic without diagnosis. Although HbA1c is an important measurement tool for both tracking the diabetes management and as a diagnosis tool for diabetes, it can only be effective in long-term performance evaluations of diabetes management. Thus, there is still a need to monitor blood glucose level in real-time and continuously, such monitoring approach will also help to prevent the blood glucose spikes in between the HbA1c tests. The benefits of the continuous monitoring over HbA1c are well-documented [27]:

- continuous monitoring can reduce the HbA1c level, by regulating the daily glucose level through real time information;
- with continuous monitoring, an episode of sugar coma can be prevented;
- continuous monitoring can show the immediate effect of the medication or diet on blood glucose level.

Figure 1.3: Mobile blood glucometer [31] .

Therefore, the continuous monitoring of the blood glucose level is vital for proper management of the diabetes diseases. Currently, off-the-shelf continuous monitoring devices are available from Medtronics [27, 28]. The continuous glucose monitoring (CGM) from Medtronics is composed of two main components: 1) glucose sensor; and 2) CGM display [29]. The glucose sensor has a needle-type electrode which is inserted under the skin that measures the glucose level from the subcutaneous liquid. The needle-type sensor is attached to an adhesive patch, which keeps the needle stable for 3 days. The needle sensor should be replaced every few days. The glucose sensor is also attached to a transmitter which performs wireless transfer of the collected data to the CGM display. CGM display shows the blood glucose level at any given time during the day; also warns the user when the glucose level drops to low or spikes to high values. In addition, the CGM display records the data; thus, the patient can always check historical data. Although this approach provides continuous monitoring, it is still invasive and the patients supposed to change the sensor every 3 days due to the contamination and drop in performance [30]. Thus, there is still a need to develop a device that can function long-term and can be seamlessly integrated with the patient's daily routine.

The other current option for blood glucose monitoring is the mobile blood glucometers, shown in Fig. 1.3, over 42 types of glucometers are available in the

UK [32]. The patients prick their finger with a lancet and draw the blood out. The blood drop is placed on a strip and the strip is inserted in to a monitor, where they can read the blood glucose level. The method is not only physically painful and invasive, but also does not provide the continuous reading for the patient. Also in order to regulate the blood glucose level with the finger pricking method, patients are recommended to measure their blood glucose level minimum 4 times a day [33].

One of the drawbacks of the finger pricking method is the failures in readings [34]. There are a number of reasons for such failures. The failures can be categorised as technical and methodological failures. The technical failures are due to damaged strips. The strips should be kept in a cool dry place avoiding to be exposed to light. Additionally, once the capped strip tube is opened, the strips should be consumed in 30 days. The humidity can alter the readings [35]. Also, the lancet should be changed very often to avoid irritation and infection. The erroneous readings can come from methodological errors as well, such as not dropping the blood on to the strip thoroughly [36]. The hygiene of the measurement site, usually the finger, is also important. The hydration of the patient is vital for a correct reading [37]. Before the reading, the hands can be washed with warm water to increase the circulation and to remove any contaminant in the withdrawal site [38]. In addition, the reading should be recorded and should be compared with the previous results to check the consistency of the reading. Therefore, using the ambulatory monitoring kit requires responsible handling of the measurements. Thus the diabetes patient must understand these issues, in order to properly manage the disease. Also, such kits cost between $12 to $24 per unit, the kits are requiring refills for both stripes and lancets, which also discourages patients from taking more frequent readings [39]. Therefore, it is essential to develop a simple, non-invasive, inexpensive, continuous, and user-friendly gulucometer.

One of the proposed technique for non-invasive measurement of the blood glucose level is near infrared (NIR) spectroscopy. The NIR is measuring the scattered signal from the analytes in the tissue. NIR can be applied in four different measurement configurations: transmission, diffuse reflectance, transflectance, and

photoacoustic [40]. For transmission the probing radiation applied from one side of a tissue medium and received from the other end of the media. However, this measurement technique restricts the measurement site. In diffuse reflectance technique the incident photons are radiated and received from the one side of the tissue. However, the photons are concentrated at the surface of the tissue. For example, for the skin tissue the incident photons are mostly reflected from the epidermis layer of the tissue. Thus, such technique can not penetrate into the deeper layers of the tissue where transcutaneous tissue fluid is kept. Scattering from deeper regions, such as dermis layer of the skin tissue, is achieved by utilizing transflectance measurement method. The technique is applied with placing an optical source fiber to the surface of the tissue and placing another optical fiber on the surface of the tissue with a distance as a receiver. Distance between the fibers controls the penetration depth which increases with the increase in distance. Finally, photoacoustic sensing is performed by locating the tissue under test to a chamber and launching a beam that is modulated at an acoustic frequency. The absorbed light creates heating which then results in acoustic waves. Such waves are detected by using a sensitive microphone. However, this technique is also concentrated on the surface of the tissue which greatly limits the applicability of no-invasive glucose sensing. Although NIR data displays correlation with the blood glucose data there is obstacles on collection of reliable information non-invasively from the human body. One issue is the time lag between the change in blood glucose level and change in interstitial fluid glucose level. Change of interstitial fluid glucose level depend on many factors including blood perfusion speed and metabolic rate; thus, the time lag can be between 2-45 minutes [41]. Another issue is scattering from the other analytes, such as protein, in blood and interstitial fluid [42]. Therefore, there is still a need to carry n further research and analysis techniques to improve the reliability of the NIR techniques for non-invasive blood glucose monitoring.

Ultrasound technique also utilized in the literature to aid non-invasive measurement of blood glucose level. In [43], ultrasound waved are used to enhance the permeability characteristics of the skin to extract glucose analyte as one the major problems in non-invasive transdermal diagnostics is obtaining sufficient

quantities of analyte for detection. Reported study suggest that by exposing the skin to 20 kHz ultrasound wave for a limited amount of time the permeability of the skin can be enhanced for up to 3 hours. However, the safety of the application, when used in a repetitive manner, not yet examined. Study also reported a time lag between the results and measurements performed with a reference glucose measurement method and suggested that the transdermal analytes may have been sourced from the capilary veins between the dermis and epidermis. A similar study is performed on pigs by applying 20 kHz ultrasound for 20 minutes and measuring the blood glucose levels with a biosensor [44]. Although promising results are obtained from the reported studies there is still a need to asses the long term effect of the ultrasound exposure to human skin.

An alternative and relatively unexplored area for such applications uses radio frequency (RF) techniques. This thesis explores the microwave and RF applications, focusing on the alterations in the dielectric properties of the blood and subcutaneous tissue and its reflection to the response of the RF device, for non-invasive and continuous monitoring of the blood glucose level.

1.3 Theory

Dielectric properties are parameters that quantify the behaviour of the materials when subject to an electric field. The dielectric properties can be explained through Maxwell's equations. When time varying fields are considered in a medium, the Maxwell's equations are represented at point form as follows;

$$\vec{\nabla} \cdot \vec{D} = \rho_v \tag{1.1}$$

$$\vec{\nabla} \times \vec{E} = -\frac{\partial \vec{B}}{\partial t} \tag{1.2}$$

$$\vec{\nabla} \cdot \vec{B} = 0 \tag{1.3}$$

$$\vec{\nabla} \times \vec{H} = \vec{j_c} + \frac{\partial \vec{D}}{\partial t} \tag{1.4}$$

Where $\vec{D}$ is the electric flux density, $\vec{B}$ is magnetic flux density ρ_v is volume charge density, $\vec{j_c}$ is the conduction current density, $\vec{E}$ and $\vec{H}$ are the electric and magnetic field respectively. From the field equations, constitutive parameters, namely permittivity and conductivity, of the medium can be derived. To do so,

the equation 1.4 is rewritten in phasor form. Also by substituting constitutive equation $\vec{D} = \varepsilon_0 \varepsilon_r \vec{E}$ and $\vec{j_c} = \sigma \vec{E}$ we can obtain equation 1.5.

$$\vec{\nabla} \times \vec{H} = \sigma \vec{E} + j\omega \varepsilon_0 \varepsilon_r \vec{E} \tag{1.5}$$

$\epsilon_0 = 8.85 \times 10^{-12} F/M$ is the permittivity of the air medium. Permittivity relates to the ability of the material to store the energy, namely the ability of the material to align it's molecules in the direction of the applied field. The conductivity of the material represents the loss. The loss of power is presented by conduction current. The other form of loss in the dielectrics is in molecular level. The dipole molecules inside the material polarize, that is the molecules aligns itself, in the direction of the applied electric field. Since the Electric field is time varying, as the direction of the applied electric field changes the dipole molecules starts to rotate itself to remain aligned with the direction of the applied electric field. The rotation of the dipole molecules causes loss of the energy due to the friction. Thus, the equation 1.5 should be rewritten by adding $\omega \kappa'' \vec{E}$ term to include the other source of loss, shown in equation 1.6.

$$\vec{\nabla} \times \vec{H} = \sigma \vec{E} + \omega \kappa'' \vec{E} + j\omega \varepsilon_0 \varepsilon_r \vec{E} \tag{1.6}$$

$$\vec{\nabla} \times \vec{H} = j\omega (\varepsilon_0 \varepsilon_r - j \frac{\sigma + \omega \kappa''}{\omega}) \vec{E} \tag{1.7}$$

$$\vec{\nabla} \times \vec{H} = j\omega (\varepsilon_0 \varepsilon_r - j \frac{\sigma_e}{\omega}) \vec{E} \tag{1.8}$$

The effective conductivity is defined as $\sigma_e = \sigma + \omega \kappa''$, the equation 1.8 can be written as follows;

$$\vec{\nabla} \times \vec{H} = j\omega (\varepsilon' - j\varepsilon'') \vec{E} \tag{1.9}$$

In equation 1.9, real part of the complex permittivity ε' is defined as $\varepsilon_0 \varepsilon_r$ and the imaginary part of the complex permittivity ε'' is defined as $\frac{\sigma_e}{\omega}$. In this thesis, the change in relative permittivity ε_r and change in effective conductivity σ_e will be investigated.

From the definition of the permittivity and conductivity we can state that the relative permittivity and effective permittivity are depends on the molecular structure of the material. Thus a change in the dielectric properties of biological

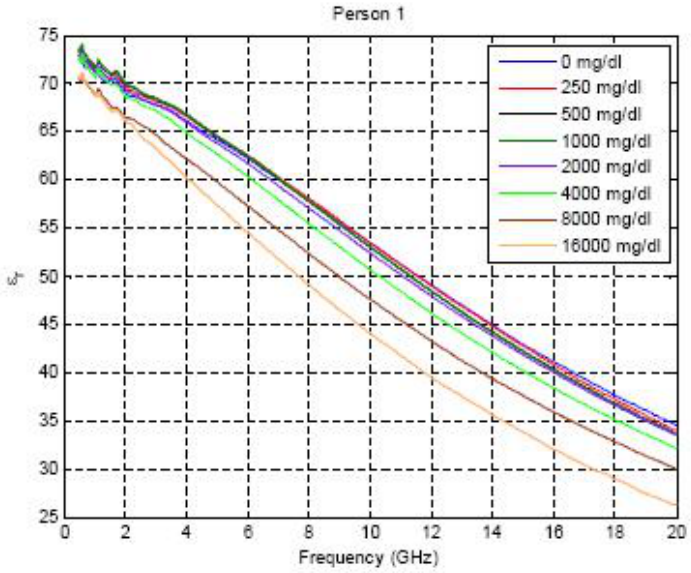

(a)

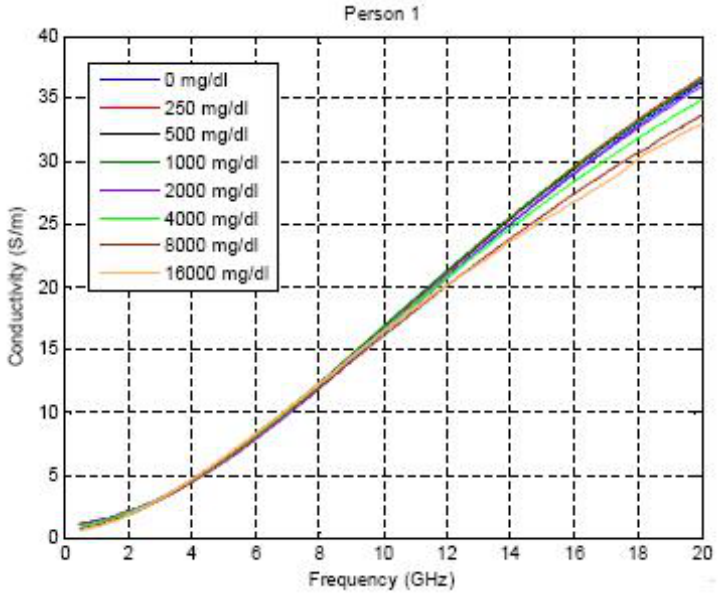

(b)

Figure 1.4: (a) Relative permittivity comparison of a blood plasma sample with different dextrose levels [45] (b) Effective conductivity comparison of a blood plasma sample with different dextrose levels [45] .

tissues is an indication of alterations in the molecular structure of the tissue such as malignancy in biological tissues, aging of the tissue, and the variation of the components in the biological tissue. Although the dielectric properties of the healthy and malignant tissues at ultra-wide band (UWB) frequencies are reported extensively in the literature, the effect of aging, gender, and chronic diseases to the dielectric properties of the biological tissues is still unknown [46, 47, 48].

It is well-known that the relative permittivity and effective conductivity of blood and subcutaneous fluids vary with the change in the blood glucose level [49]. However, there are a limited number of studies in the literature that quantify the changes in relative permittivity and effective conductivity with respect to blood glucose level. Topsakal et al. [45] performed dielectric property measurements by adding liquid D-glucose (dextrose) to blood plasma obtained from 12 healthy individuals. Dextrose level were increased with each measurement. Measurements were taken at room temperature by adding 250, 500, 1000, 2000, 4000, 8000, and 16000 miligram liquid dextrose to per deciliter blood plasma.

The experiments were performed with an Agilent's open-ended slim probe, that can take measurements up to 20 GHz. Although the experiment was performed on a small sample, the results provide an insight on the relationship between the glucose level and dielectric properties. Fig. 1.4 (a) and Fig. 1.4 (b) show the relative permittivity and effective conductivity, respectively, of a blood plasma sample with different dextrose levels [45]. Both the relative permittivity and effective conductivity of blood plasma were decreased while glucose level were increased. The results for relative permittivity are expected, as sugar is commonly used in the literature to decrease the relative permittivity of water when characterizing skin and other high water content tissue-mimicking materials [50].

Although this study [45] provides an insight to the change in dielectric properties, there is still a need to characterize the change in the dielectric properties of blood and subcutaneous fluid with adding realistic glucose amounts to blood plasma and quantifying the change. Note that the normal glucose levels are 80 mg/dl at fasting state and 140 mg/dl after meals. Realistic glucose dependance of dielectric properties is vital to design an RF device that is sensitive enough to quantify such changes.

Considering the relatively small change in the blood glucose level and resulting alterations in dielectric property change, narrowband resonance techniques are more suitable to detect such small changes. Narrowband technique is a more precise method when compared to broadband technique. The empirical relationship between the effective permittivity and resonance frequency of a resonator is given as follows [51]:

$$f_r = \frac{nc}{L_{eff}\sqrt{\varepsilon_{eff}}} \tag{1.10}$$

In equation 1.10, f_r is the the operation frequency, L_{eff} is the effective length of the resonator. ε_{eff} is the effective relative permittivity, that is a proportional, based on the electric field distribution, combination of relative permittivity of the surrounding dielectric and relative permittivity of the resonator substrate. n is the mode of the resonator, namely if the resonator has multiple operation frequencies the considered number of the operation frequency; for example, if the resonator is operating at a dual mode and user is considering the 2^{nd} mode n should be 2. Finally, c is the speed of light in free space. The equation presents a clear relationship between the permittivity of the dielectric medium and the characteristic response of the resonator.

In the light of the previously reported literature on the dielectric property change of the blood and subcutaneous tissue, this thesis is proposing to quantify the dielectric property dependance to the realistic blood glucose alterations with broadband techniques. This thesis is also proposing narrowband resonators to sense the glucose dependent relative permittivity change in the anthropomorphic media.

1.4 Methodology

Dielectric properties of biological tissues have been studied in the literature using different techniques. The most suitable method for dielectric property retrieval can be decided according to the desired frequency of operation. For example, an open-ended coax probe is desirable when a broadband measurement response is needed. Other important parameters are the required degree of sensitivity, level of invasiveness, sample size, sample temperature, and the measurement procedure.

Dielectric properties of biological tissues at microwave frequencies have been studied since 1951, first introduced by Cook et al. [52]. Although a considerable amount of knowledge has been accumulated on the dielectric behavior of biological tissues for over a half century, it is still a complex procedure to perform *in-vivo*

and *ex-vivo* experiments for dielectric property retrieval. Usually, high water content tissues, such as muscle, skin, and blood, have high conductivity; thus, it is hard to perform measurements using resonant methods unless the calibration is performed with a material having similar dielectric properties to high water content tissues. Therefore, an open-ended coaxial probe has been extensively used in the literature to obtain ultra-wide band measurement results. Although a comprehensive review in dielectric property measurement techniques is beyond the scope of this thesis, in the following sections, a review on techniques, including coaxial probes and resonant methods, is given.

1.4.1 Open-Ended Coaxial Probe

Open-ended coaxial probes have been used in the literature for non-destructive measurement of broadband dielectric properties of the biological tissues extensively [53, 54, 55, 56]. The two most important advantages of the coaxial probe technique are (1) the probe can be used for broadband measurements, where usually current commercial probes can provide up to 50 GHz measurement; and (2) in general, there is no need for sample preparation, that is, liquid and arbitrarily-shaped semi-solid materials can easily be used. For biological tissues, *in-vivo* and *ex-vivo* measurements can be performed. However, the measurement precision of the open-ended probe is low when compared to narrowband techniques, such as the cavity resonance technique.

One important area where the open-ended coaxial probe has been investigated and used widely is the dielectric property characterization of healthy, benign, and malignant breast tissues. It is particularly a challenging area, as the physical size and composition of the tissue samples tend to vary depending on the surgical procedure, which can be a breast reduction surgery, partial or total mastectomy , and lumpectomy . For example, the tissue specimen excised through a breast reduction surgery can be heterogeneous including fibroglandular and fatty tissues. Also, a surgery performed to excise the malignant or benign tumor, namely lumpectomy, can be heterogeneous including both the tumor and the healthy tissue. Thus, the coaxial probes, featuring small apertures and small sensing

volume, are suitable to perform broadband dielectric property characterization on such arbitrarily-shaped and composed biological tissues. Because, small sensing volume and small aperture can ensure that the measurement is taken from a homogeneous tissue sample even if the excised sample is heterogeneous in composition.

Open-ended coaxial probes are also widely used to assess the dielectric properties of liquids and agricultural products [57]. Commercial dielectric probes can easily measure the dielectric properties of homogeneous liquids with a good precision. However, when measuring liquid, it is important to check the probe tip for air bubbles. The air bubble can affect the dielectric property measurements significantly.

Usually, the dielectric material inside the probe is a stable and non-reactive material, such as glass or teflon. Some probes features air as an insulating material. However, to prevent the possible damage over time and to keep the response stable, usually glass and teflon material are preferred. Use of such materials also allows the probe to be used in a range of temperatures by preventing corrosion damage due to the heat. Conventionally, experiments are performed by mounting the coax probe to a network analyzer and placing the dielectric sample at the tip of the probe. The complex permittivity of the sample can be obtained from the measurement of several parameters depending on the field interaction with the sample at the tip of the probe. Traditionally, the reflection coefficient is measured at the tip of the probe with a vector network analyzer (VNA) and, by utilizing different numerical and analytical models, the reflection coefficient is converted to dielectric properties of the material under test [53, 58, 59, 60].

One of the most commonly used commercial coaxial probe is the Agilent 85070E dielectric probe kit [61]. The probe kit comes with a software where the ε_r' (The real part of complex permittivity), ε_r'' (the imaginary part of permittivity), tan (δ) (loss tangent $tan\ (\delta) = \frac{\sigma_e}{\omega\varepsilon'}$), and Cole-Cole fitting formats can be viewed. Depending on the probe type, the measurements can be performed from 200 MHz to 50 GHz. The software can be installed on a computer with Windows operating system and a VNA can be controlled through the computer. For a Performance Network Analyzer (PNA), the software can be directly installed to

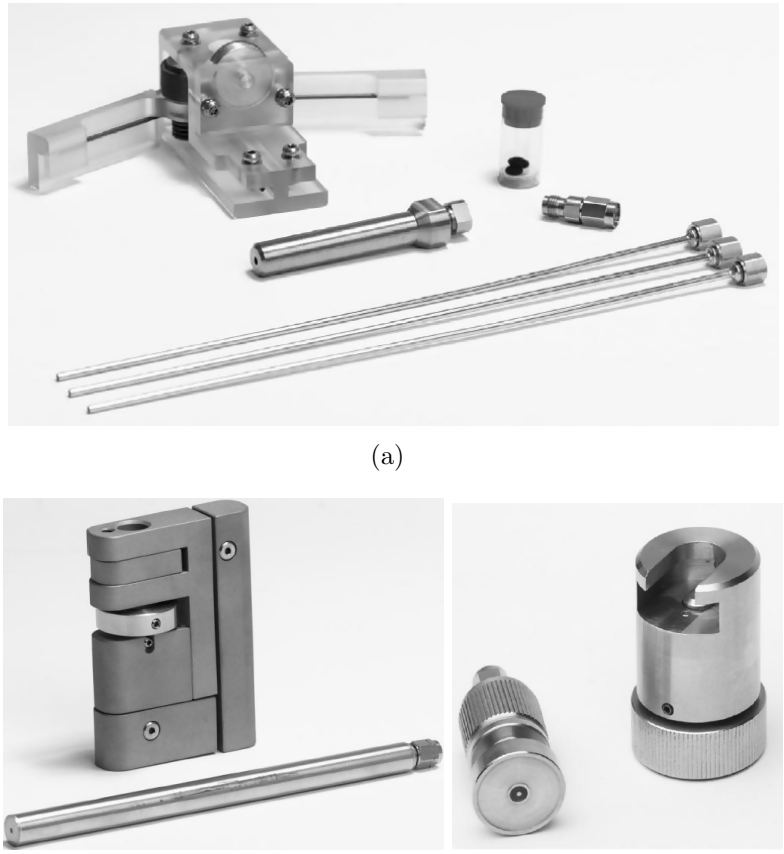

(a)

(b) (c)

Figure 1.5: Agilent 85070E dielectric probe kit: (a) slim probe, (b) precision probe, (c) high temperature probe [61].

the network analyzer. All three probes in the kit need to be calibrated before taking measurements; the calibration is performed in three steps with air, short (the short is provided with the kit), and a known liquid. The known liquid can be any liquid, but the Cole-Cole parameters of the liquid should be entered in the software in order to perform correct calibration. The default calibration liquid is de-ionozed water. Other procedures that must be followed include setting the measurement frequency range, number of data points, and temperature of the calibration liquid. The software has a friendly user interface, and during calibration, it guides the user through the three steps.

The Agilent's coaxial probe is modelled as a coaxial aperture opening on an infinite ground plane with semi-finite material load. The assumptions are justified due to the reflection from the boundaries of the material will not be sensed at the probe aperture if the material is lossy enough. The modelling of the probe

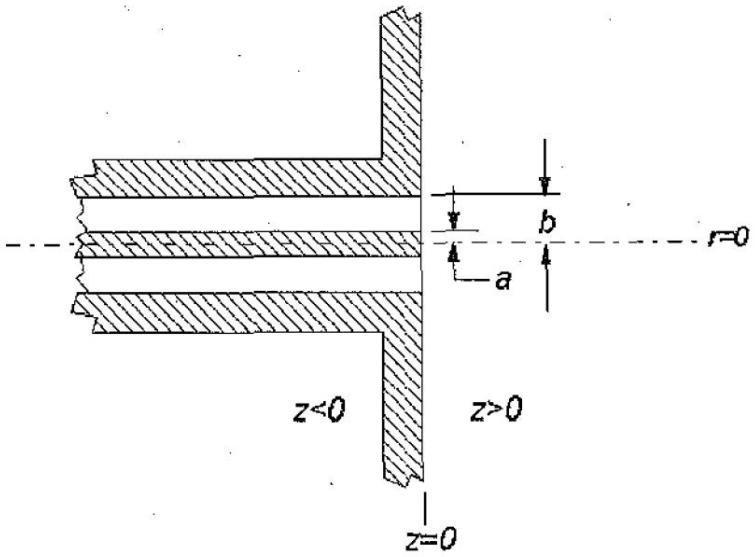

Figure 1.6: Modelled aperture opening of the coaxial probe on infinite ground plane [62].

is shown in Fig. 1.6, (a) and (b) represents the radius of the inner and outer conductor, respectively. This problem is solved by equating the tangential magnetic fields on the aperture $z = 0$. Solution to the forward problem gives the reflection coefficient for a given sample permittivity and solution to the inverse problem gives the sample permittivity for a given reflection coefficient. The normalized admittance for the described coaxial probe model is given as follows;

$$Y_L = \frac{jk_m^2}{\pi k_c \; ln(\frac{a}{b})} \int_a^b \int_a^b \int_0^\pi cos(\phi) \frac{e^{-jk_m R}}{R} d\phi dr dr' \tag{1.11}$$

where,

$$R = \sqrt{r^2 + r'^2 - 2rr'cos(\phi)}$$

$$k_c = w\sqrt{\varepsilon_c \varepsilon_0 \mu_0}$$

$$k_m = w\sqrt{\varepsilon_m \varepsilon_0 \mu_0}$$

ε_c is the permittivity of the dielectric between the inner and outer conductor of the coaxial line. ε_m is the permittivity of the sample at the aperture of the probe. Exponential expression given in equation 1.11 can be expanded with Taylor series, which yields integrals independent from the medium properties.

After the computation of the integrals, a polynomial expression can be obtained which has a low computational cost. However, the resulted polynomial does not include the higher order modes thus a correction technique usually employed to obtain the best match.

The other measurement error source is systematic errors. Such errors are corrected with vector error correction, termed 'calibration'. By measuring three standards, that is terminating the aperture with air, short, and distilled water the reflection coefficient of the probe aperture is measured to correct the systematic errors. The air, short, and distilled water are readily available calibration materials and distilled water with 200 ml beaker can simulate semi-infinite sample, due to the dipole losses, for Agilent's dielectric probes.

The Agilent 85070E dielectric probe kit features three probes, including a slim form, a precision, and a high temperature probe, shown Fig 1.5 (a), Fig 1.5 (b), and Fig 1.5 (c), respectively. The slim probe is more suitable for liquids and small sized soft semi-solids. The aperture of the slim probe is 2.2 mm and slim design allows the insertion of the probe into the chemical reaction chambers and fermentation tanks. The slim form probe can take measurements from 500 MHz to 50 GHz. The precision probe can take measurements from 500 MHz to 50 GHz as well and can be utilized for temperatures between -40° C to 200° C. The aperture of the probe is 9.5 mm. The dielectric insulating material in the coaxial probe is boroslicate glass. The probe can be used for measuring liquid, semi-solid, and flat surfaced solid materials. High temperature probe can take measurements from 200 MHz to 20 GHz between -40° C to 200° C. The aperture of the probe is 3.5 mm. The high temperature probe is further discussed in Chapter 3. Note that the sample size should be bigger than the aperture of the probe. Thickness of the sample depends on the sensing volume of the probe; however, one can measure the effect of the thickness by placing a short under the material. If the response of the probe remains the same, that means the material thickness is enough. In this thesis, Agilent's open-ended high temperature probe is used for broadband dielectric property measurement of the tissue simulating materials.

1.4.2 Waveguide, Cavity, and Resonance Techniques

The waveguide technique is one of the popular methods to measure dielectric properties of materials at microwave and milli-meter wave frequencies. For dielectric property measurements, conventionally, a rectangular waveguide with four shorted walls is filled with the sample and connected from two sides to a network analyzer with coaxial cables for sending and receiving the energy. Different testing configurations for rectangular waveguide such as waveguide probes shorted with dielectric material, have been proposed in the literature [63, 64, 65, 66]. It is possible to collect measurements at different modes and at the cut-off frequency. The cut-off frequency is related to the dielectric properties of the material filling the waveguide.

The main limitation for this technique is that the sample should fill the waveguide in width and height dimensions. Usually for biological tissues, the tissue need to be excised, so it is not possible to perform *in- vivo* measurements with the waveguide technique. This technique is suitable for materials that can be shaped to fit inside the waveguide.

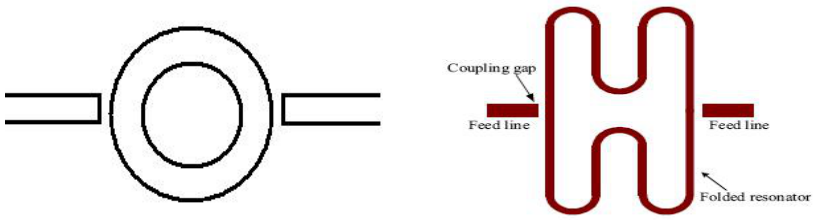

Figure 1.7: (a) A traditional ring resonator (b) Folded ring resonator proposed in [67].

Cavity technique is another kind of popular narrowband method for measurement of dielectric properties; the real part of the complex permittivity is calculated from the shift of the resonance frequency, and the imaginary part is retrieved from the change of the cavity quality factor, which can be found from the bandwidth at the operation frequency. To increase the sensitivity of the cavity technique, the sample is placed inside the cavity at a position where the electric field is a maximum. Depending on the field distribution inside the cavity electric, field probes can be used for detection purposes.

Other techniques proposed in the literature include resonant and resonant perturbation methods. Usually the resonant technique, such as the use of ring or folded ring resonators shown in Fig. 1.7 (a) and Fig. 1.7 (b) [67, 68, 69, 70], is suitable for measurement of low-loss dielectric materials. The limitation for resonant techniques is that dielectric properties can be retrieved only at the resonant frequency. Usually, the retrieval of parameters is performed either with numerical iterations or analytical models. However, resonators such as ring resonators are easy to fabricate, with high accuracy, low cost, and can be made conformal. These resonators can be used for samples with irregular shapes. Additionally, the resonant sensors can be printed on flexible substrates, such as textiles, and can easily be mounted on the human body. However, at low microwave frequencies, the miniaturization of such structures can present a challenge.

Other measurement techniques include free-space method [71, 72, 73]. The free-space method is suitable for planar or materials with sheet like samples. The measurements are taken by placing the sample between a receiver and a transmitter antenna. The free space method is a non-contact and non-destructive permittivity reconstruction technique. The method is mostly suitable for medium loss materials.

1.4.3 Tissue Mimicking Materials

Anthropomorphic tissue mimicking materials closely repeating the dielectric properties and the shape of the tissues have been invaluable for pre-clinical testing of ultrasound imaging, microwave imaging, and implantable devices [74, 75, 76]. To construct such phantoms it is important to measure the dielectric properties of the biological tissue. A number of studies have been reported int he literature on the dielectric properties of the biological tissue. One significant comprehensive study have been reported by Gabriel et al. [46, 47, 77]. According to the measurement results the biological tissues are classified as low-water, intermediate-water, and high-water content tissues. The water content signifies the magnitude of the relative permittivity of the tissue. That is, high-water content tissues tend

to have high relative permittivities and low-water content tissues have low relative permittivities. Dielectric properties of some tissues at 2.45 GHz is given in Table 1.1.

Table 1.1: Dielectric properties of the tissues at 2.45 GHz [78]

Tissue name	*Relative permittivity*	*Conductivity* $[S/m]$	*Wavelength* $[m]$
Body Fluid	68.208	2.4781	0.014689
Blood	58.264	2.5448	0.015834
Muscle	52.729	1.7388	0.016731
Aorta	42.531	1.4353	0.018623
$Skin_{wet}$	42.853	1.5919	0.018524
$Skin_{dry}$	38.007	1.464	0.019657
Bone Cancellous	18.548	0.80517	0.028067
Fat	5.2801	0.10452	0.053113

Bone and fat are classified as low-water content tissues. Aorta, skin_{dry}, and skin_{wet} are categorised as intermediate-water content tissues. High-water content tissues given in Table 1.1 are body fluid, blood, and muscle.

Another use of the tissue mimicking materials is the controlled manipulation of the parameters. In this thesis, by changing the dextrose level at a blood mimicking material the dielectric properties are measured. Such approach allow us to manipulate one parameter at a time and observe the EM response. The advantage of this technique is the EM response is only effected from a single parameter; however, such manipulation is much difficult to perform at human body as multiple sensors are needed to track other parameters.

1.5 Possibility and Challenges

An important challenge is to distinguish the response of the RF or microwave device to other vital signs. Change of the temperature, hearth rate, respiration rate, blood pressure, and many other environmental variables can affect the response of the RF or microwave device. Therefore, the experiments should be performed by changing one parameter at a time to understand the limitations of the method. For example, while changing the blood glucose level temperature,

blood pressure, heart rate, etc., should be kept constant. This requires an intelligent design of experiments, in this study we are proposing to work with tissue mimicking materials to change a single parameter at a time to understand the behaviour of the resonant structure.

Performing non-invasive human tests for blood glucose detection is challenging. The change in external parameters should be controlled such as applied force. And the effect of other vital signs should be measured as well. Response of the resulting non-invasive glucometer can be calibrated according to the known vital and external parameters.

There are many other challenges regarding the monitoring of the blood glucose level non-invasively and continuously with RF or microwave techniques that are not only hardware-related, but also software issues. One of the software related issues is protecting the privacy of the patients.

1.6 Thesis Organization

The rest of the dissertation is organized as follows.

Chapter 2 provides an extensive literature and industry review for the state of the art of vital signs monitoring, including blood pressure, blood glucose, and cardiac activity monitoring techniques. Current constraints to achieve truly non-invasive and multi-parameter monitoring are discussed in depth.

In *Chapter 3*, recipes and dielectric property measurements for liquid, semi-solid, and gel-like tissue mimicking phantoms are presented. The liquid and semi-solid phantoms are used to test the spiral resonator, to retrieve the relative permittivity of the phantom. Two broadband (0.3 GHz to 3 GHz) tissue mimicking materials for dry skin and blood tissues are given. The validity of the phantoms are verified via comparison with the literature data [78]. Also, ultra-wide band tissue mimicking materials are presented for wet skin, fat, blood, and muscle tissues. The capabilities of these tissue mimicking materials are not limited to the experiments proposed in this thesis; depending on the frequency range, the tissue mimicking phantoms can be used to validate the performance of any RF or microwave device designed for biological app lications. A comparison

of the dielectric of the phantoms is made with experimental values properties for the biological tissues from the literature, as well as with for previously proposed tissue mimicking materials, to validate the performance of the phantoms.

Chapter 4 presents a spiral resonator for retrieval of dielectric properties of lossy materials. The spiral resonator is tested with liquid and semi-solid phantoms and the S-parameter response of the resonator is recorded. From the collected response of the resonator the dielectric properties are retrieved using an empirical formulation and a form of calibration. In order to modify and improve the accuracy the empirical formulation, simulations with different superstrates having variety of dielectric properties are performed. Then, by employing particle swarm optimisation and multiple linear regression, the modified empirical formulation is characterized. Finally, a sensitivity analysis of the resonator response to the change in effective permittivity is demonstrated by simulating and measuring the response of the resonator with phantoms having different thicknesses.

Chapter 5 describes the design and testing of a patch resonator, as well as the dielectric property measurement and analysis of a blood mimicking material with realistic glucose indexes. The blood mimicking material proposed in Chapter 3 is characterised and realistic glucose amounts are added. The dielectric properties of the each phantom with different glucose level is measured by employing Agilent's open-ended high temperature dielectric probe. The resonator is mounted at the bottom of a container. The skin, fat, and muscle mimicking phantoms, presented in Chapter 3, are characterized and a four-layered tissue mimicking material placed above the patch resonator. The blood layer is alternated with a higher glucose index blood layer and the S-parameter response of the resonator is measured. Then the input impedance of the resonator is calculated. Measured input impedance results are also compared with the simulations.

In *Chapter* 6, experiments with human subjects under controlled laboratory environment are reported. A doulbe-sensing platform is constructed by combining the patch resonator and a commercial force sensor. Force dependent response of the patch resonator is quantified. To investigate the glucose dependent response of the patch resonator soda tests are performed with 5 subjects by manipulating the blood glucose levels through rapid ingestion of sugar rich drink under constant

applied force. Soda test is also performed with spiral resonator on 2 subjects. The response of the sensors are compared with reference data.

Finally, in *Chapter* 7, the summary of the dissertation and the potential future work is presented. Potential future work includes measuring the dielectric properties of other tissues with realistic blood glucose amounts to assess the change of the overall subcutaneous dielectric property change, investigation of the temperature dependence of blood dielectric properties with different glucose indexes, and building a durable testing fixture for further human experiments.

References

[1] [Online]. Available: http://www.who.int/eht/en/eHealth_HCD.pdf

[2] S. Ouma and M. E. Herselman, "E-health in rural areas: Case of developing countries," *International Journal of Biological and Life Sciences*, March 2008.

[3] D. Lam and G. DeSouza, "Virtual dermatologist: An application of 3d modeling to tele-healthcare," in *e-Health Networking Applications and Services (Healthcom), 2011 13th IEEE International Conference on*, june 2011, pp. 28 –33.

[4] J. Sim, J. James, M. McDonald, P. Maude, T. Ryan, S. Scutter, and D. Wood, "Virtual learning in healthcare disciplines: Learning via avatars," in *INTED2012 Proceedings*, ser. 6th International Technology, Education and Development Conference. IATED, 5-7 March, 2012 2012, pp. 5999–6000.

[5] M. Najafi, S. Aghtar, K. Sartipi, and N. Archer, "Virtual remote nursing system," in *Consumer Communications and Networking Conference (CCNC), 2011 IEEE*, jan. 2011, pp. 13 –17.

[6] T. Yilmaz, R. Foster, and Y. Hao, "Detecting vital signs with wearable wireless sensors," *Sensors*, vol. 10, no. 12, pp. 10 837–10 862, 2010. [Online]. Available: http://www.mdpi.com/1424-8220/10/12/10837/

[7] [Online]. Available: http://www.dh.gov.uk

[8] [Online]. Available: http://www.diabetes.org.uk/Documents/Reports/Diabetes_in_the_UK_2010.pdf

[9] "Main types of diabetes." [Online]. Available: http://www.diabetes.org.uk/Guide-to-diabetes/What-type-of-diabetes-do-I-have/

[10] [Online]. Available: http://www.diabeteshealthysolutions.com

[11] "NHS Type 1 diabetes." [Online]. Available: http://www.nhs.uk/Conditions/Diabetes-type1/Pages/Introduction.aspx

[12] "JDRF Type 1 diabetes." [Online]. Available: http://www.jdrf.org.uk/life-with-type-1-diabetes/what-is-type-1-diabetes?gclid=CNeLvomdkbkCFYWz3godn0EAWQ

[13] "Wikipedia Type 1 diabetes." [Online]. Available: http://en.wikipedia.org/wiki/Diabetes_mellitus_type_1

[14] [Online]. Available: http://www.diabetes.org.uk/Guide-to-diabetes/Type-2-diabetes

[15] [Online]. Available: http://www.jdrf.org/

[16] "Insulin levels." [Online]. Available: http://www.columbia.edu/itc/hs/medical/clerkships/primcare/case/diabetes/diabetes01_07.html

[17] [Online]. Available: http://en.wikipedia.org/wiki/Insulin_resistance

[18] [Online]. Available: http://www.ncbi.nlm.nih.gov/pubmedhealth/PMH0004546/

[19] [Online]. Available: http://www.medicinenet.com/script/main/art.asp?articlekey=17384

[20] [Online]. Available: http://en.wikipedia.org/wiki/Blood_sugar

[21] [Online]. Available: http://medweb.bham.ac.uk/easdec/prevention/what_is_the_hba1c.htm

[22] [Online]. Available: http://www.mydiabetesmyway.scot.nhs.uk/resources/leaflets/hba1c.pdf

[23] [Online]. Available: http://www.diabetes.org.uk/Guide-to-diabetes/Monitoring/Blood_glucose/Glycated_haemoglobin_HbA1c_and_fructosamine/

[24] [Online]. Available: http://www.diabetesdaily.com/voices/2011/11/what-is-an-hba1c/

[25] S. A. Mostafa, K. Khunti, E. S. Kilpatrick, D. Webb, B. T. Srinivasan, L. J. Gray, and M. J. Davies, "Diagnostic performance of using one- or two-hba1c cut-point strategies to detect undiagnosed type 2 diabetes and impaired glucose regulation within a multi-ethnic population," *Diabetes and Vascular Disease Research*, pp. 84–92, 2012.

[26] [Online]. Available: http://www.diabetes.org.uk/Documents/Reports/State-of-the-Nation-2012.pdf

[27] [Online]. Available: http://www.medtronic-diabetes.co.uk/product-information/paradigm-veo/continuous-glucose-monitoring.html

[28] J. Mastrototaro, "The minimed continuous glucose monitoring system," *Diabetes Technol Therapeut*, vol. 2, pp. 13–18, 2000.

[29] [Online]. Available: http://www.medtronicdiabetes.com/products/guardiancgm

[30] T. M. Gross, B. W. Bode, D. Einhorn, D. M. Kayne, J. H. Reed, and N. H. White, "Performance evaluation of the minimed continuous glucose monitoring system during patient home use," *Diabetes Technol Therapeut*, pp. 49–56, 2000.

[31] [Online]. Available: http://optipunkt.com/pl/sklep/produkt/accu-chek-active-diabetes-blood-glucose-meter-kit.html

[32] [Online]. Available: http://www.diabetes.co.uk/diabetes_care/blood_glucose_monitor_guide.html

[33] [Online]. Available: http://www.patient.co.uk/doctor/Self-Monitoring-Blood-Glucose-(SMBG)-in-Diabetes-Mellitus.htm

[34] B. H. Ginsberg, "Factors affecting blood glucose monitoring: Sources of errors in measurement," *Journal of Diabetes Science and Technology*, vol. 3, pp. 903 –913, july 2009.

[35] [Online]. Available: http://www.pharmacytimes.com/publications/issue/2006/2006-07/2006-07-5704

[36] [Online]. Available: http://www.diabetes.co.uk/blood-glucose-meters/blood-glucose-meter-accuracy.html

[37] [Online]. Available: http://www.livestrong.com/article/239458-how-does-dehydration-affect-blood-glucose-levels/

[38] J. Hortensius, R. J. Slingerland, N. Kleefstra, S. J. J. Logtenberg, K. H. Groenier, S. T. Houweling, and H. J. G. Bilo, "Self-monitoring of blood glucose: The use of the first or the second drop of blood," *Diabetes Care*, pp. 903–913, March 2011.

[39] U. L. Malanda, L. M. C. Welschen, I. I. Riphagen, J. M. Dekker, G. Nijpels, and S. D. M. Bot, *Self-monitoring of blood glucose in patients with type 2 diabetes mellitus who are not using insulin.* John Wiley and Sons, Ltd, 2012.

[40] M. A. Arnold, J. Olesberg, and G. W. Small, "Near infrared spectroscopy for non-invasive glucose sensing," in *In Vivo Glucose Sensing*, D. D. Cunningham and J. A. Stenken, Eds. USA: John Wiley and Sons, 2010.

[41] N. S. Oliver, C. Toumazou, A. E. G. Cass, and D. G. Johnston, "Glucose sensors: a review of current and emerging technology," *Diabetic Medicine*, vol. 26, no. 3, p. 197210, 2009.

[42] L. A. Marquardt, M. A. Arnold, and G. W. Small, "Near-infrared spectroscopic measurement of glucose in a protein matrix," *Analytical Chemistry*, vol. 65, no. 22, pp. 3271–3278, 1993, pMID: 8291678. [Online]. Available: http://pubs.acs.org/doi/abs/10.1021/ac00070a018

[43] J. Kost, S. Mitragotri, R. A. Gabbay, M. Pishko, and R. Langer, "Transdermal monitoring of glucose and other analytes using ultrasound," *Nature Medicine*, vol. 6, no. 3, pp. 1078–8956, 2000. [Online]. Available: http://dx.doi.org/10.1038/73213

[44] E. OPark, J. Werner, J. Beebe, S. Chan, and N. B. Smith, "Noninvasive ultrasonic glucose sensing with large pigs (200 pounds) using a lightweight cymbal transducer array and biosensors," *Journal of Diabetes Science Technology*, vol. 3, no. 3, p. 517523, 2009.

[45] E. Topsakal, E. C. Moreland, T. Karacolak, and M. Acar, "The impact of glucose concentration in blood plasma on relative dielectric constant and conductivity," in *National Science Meeting URSI*, 2008.

[46] C. Gabriel, S. Gabriel, and E. Corthout, "The dielectric properties of biological tissues: I. literature survey," *Physics in Medicine and Biology*, vol. 41, no. 11, p. 2231, 1996. [Online]. Available: http://stacks.iop.org/0031-9155/41/i=11/a=001

[47] S. Gabriel, R. W. Lau, and C. Gabriel, "The dielectric properties of biological tissues: Ii. measurements in the frequency range 10 hz to 20 ghz," *Physics in Medicine and Biology*, vol. 41, no. 11, p. 2251, 1996. [Online]. Available: http://stacks.iop.org/0031-9155/41/i=11/a=002

[48] M. Lazebnik, D. Popovic, L. McCartney, C. B. Watkins, M. J. Lindstrom, J. Harter, S. Sewall, T. Ogilvie, A. Magliocco, T. M. Breslin, W. Temple, D. Mew, J. H. Booske, M. Okoniewski, and S. C. Hagness, "A large-scale study of the ultrawideband microwave dielectric properties of normal, benign, and malignant breast tissues obtained from cancer surgeries," *Physics in Medicine and Biology*, vol. 52, pp. 6093–6115, 2007.

[49] Y. Hayashi, L. Livshits, A. Caduff, and Y. Feldman, "Dielectric spectroscopy study of specific glucose influence on human erythrocyte membranes," *Journal of Physics D: Applied Physics*, vol. 36, no. 4, pp. 369–374, 2003. [Online]. Available: http://stacks.iop.org/0022-3727/36/i=4/a=307

[50] T. Karacolak, A. Hood, and E. Topsakal, "Design of a dual-band implantable antenna and development of skin mimicking gels for continuous glucose monitoring," *Microwave Theory and Techniques, IEEE Transactions on*, vol. 56, no. 4, pp. 1001 –1008, april 2008.

[51] S. Seewattanapon, T. Wattakeekamthorn, T. Somwong, and P. Akkaraekthalin, "A microstrip folded resonator sensor for measurement of dielectric constant," in *Electrical Engineering/Electronics, Computer, Telecommunications and Information Technology, 2008. ECTI-CON 2008. 5th International Conference on*, vol. 1, may 2008, pp. 245 –248.

[52] H. F. Cook, "The dielectric behaviour of some types of human tissues at microwave frequencies," *British Journal of Applied Physics*, vol. 2, no. 10, p. 295, 1951. [Online]. Available: http://stacks.iop.org/0508-3443/2/i=10/a=304

[53] M. A. Stuchly and S. S. Stuchly, "Coaxial line reflection methods for measuring dielectric properties of biological substances at radio and microwave frequencies-a review," *Instrumentation and Measurement, IEEE Transactions on*, vol. 29, no. 3, pp. 176 –183, Sept. 1980.

[54] D. Popovic, L. McCartney, C. Beasley, M. Lazebnik, M. Okoniewski, S. Hagness, and J. Booske, "Precision open-ended coaxial probes for in vivo and ex vivo dielectric spectroscopy of biological tissues at microwave frequencies," *Microwave Theory and Techniques, IEEE Transactions on*, vol. 53, no. 5, pp. 1713 – 1722, May. 2005.

[55] T. Athey, M. Stuchly, and S. Stuchly, "Measurement of radio frequency permittivity of biological tissues with an open-ended coaxial line: Part i," *Microwave Theory and Techniques, IEEE Transactions on*, vol. 30, no. 1, pp. 82 –86, jan. 1982.

[56] M. Stuchly, T. Athey, G. Samaras, and G. Taylor, "Measurement of radio frequency permittivity of biological tissues with an open-ended coaxial line: Part ii - experimental results," *Microwave Theory and Techniques, IEEE Transactions on*, vol. 30, no. 1, pp. 87 –92, jan. 1982.

[57] N. Sheen and I. Woodhead, "An open-ended coaxial probe for broad-band permittivity measurement of agricultural products," *Journal of Agricultural Engineering Research*, vol. 74, no. 2, pp. 193 – 202, 1999. [Online]. Available: http://www.sciencedirect.com/science/article/pii/S0021863499904444

[58] D. Misra, "A quasi-static analysis of open-ended coaxial lines (short paper)," *Microwave Theory and Techniques, IEEE Transactions on*, vol. 35, no. 10, pp. 925 – 928, oct 1987.

[59] C. Gabriel, T. Y. A. Chan, and E. H. Grant, "Admittance models for open ended coaxial probes and their place in dielectric spectroscopy," *Physics in Medicine and Biology*, vol. 39, no. 12, p. 2183, 1994. [Online]. Available: http://stacks.iop.org/0031-9155/39/i=12/a=004

[60] J. Anderson, C. Sibbald, and S. Stuchly, "Dielectric measurements using a rational function model," *Microwave Theory and Techniques, IEEE Transactions on*, vol. 42, no. 2, pp. 199 –204, feb 1994.

[61] "Agilent 85070e dielectric probe kit 200 mhz to 50 ghz technical overview." [Online]. Available: http://cp.literature.agilent.com/litweb/pdf/5989-0222EN.pdf

[62] D. Blackham and R. D. Pollard, "An improved technique for permittivity measurements using a coaxial probe," *Instrumentation and Measurement, IEEE Transactions on*, vol. 46, no. 5, pp. 1093–1099, 1997.

[63] R. Zajicek, T. Smejkal, L. Oppl, and J. Vrba, "Waveguide probes for complex permittivity measurement," in *Microwave Techniques, 2008. COMITE 2008. 14th Conference on*, Apr. 2008, pp. 1 –4.

[64] J. Sheen, "Microwave dielectric properties measurements using the waveguide reflection dielectric resonator," in *Instrumentation and Measurement Technology Conference Proceedings, 2007. IMTC 2007. IEEE*, May. 2007, pp. 1 –4.

[65] K. Rajab, K.-F. Fuh, R. Mittra, and M. Lanagan, "Dielectric property measurement using a resonant nonradiative dielectric waveguide structure," *Microwave and Wireless Components Letters, IEEE*, vol. 15, no. 2, pp. 104 – 106, Feb. 2005.

[66] M. Ghasr, D. Simms, and R. Zoughi, "Multimodal solution for a waveguide radiating into multilayered structures ;dielectric property and thickness evaluation," *Instrumentation and Measurement, IEEE Transactions on*, vol. 58, no. 5, pp. 1505 –1513, May. 2009.

[67] S. Seewattanapon, T. Wattakeekamthorn, T. Somwong, and P. Akkaraekthalin, "A microstrip folded resonator sensor for measurement of dielectric constant," in *Electrical Engineering/Electronics, Computer, Telecommunications and Information Technology, 2008. ECTI-CON 2008. 5th International Conference on*, vol. 1, May. 2008, pp. 245 –248.

[68] M. Afsar, H. Ding, and K. Tourshan, "A new open-resonator technique at 60 ghz for permittivity and loss-tangent measurement of low-loss materials," in *Microwave Symposium Digest, 1999 IEEE MTT-S International*, vol. 4, 1999, pp. 1755 –1758 vol.4.

[69] S. Seewattanapon and P. Akkaraekthalin, "A dual microstrip resonator for liquid dielectric constant measurement," in *Microwave Conference, 2008. APMC 2008. Asia-Pacific*, Dec. 2008, pp. 1 –4.

[70] P. Bernard and J. Gautray, "Measurement of dielectric constant using a microstrip ring resonator," *Microwave Theory and Techniques, IEEE Transactions on*, vol. 39, no. 3, pp. 592 –595, Mar. 1991.

[71] F. Zaki, Z. Awang, N. Baba, A. Zoolfakar, R. Bakar, M. Zolkapli, and N. Fadzlina, "A free-space method for measurement of complex permittivity of double-layer dielectric materials at microwave frequencies," in *Research and Development (SCOReD), 2010 IEEE Student Conference on*, 2010, pp. 12–15.

[72] S. B. Kumar, U. Raveendranath, K. T. Mohanan, P.and Mathew, M. Hajian, and L. P. Ligthart, "A simple free-space method for measuring the complex permittivity of single and compound dielectric materials," *Microw. Opt. Technol. Lett.*, vol. 26, p. 117119, 2000.

[73] D. Ghodgaonkar, V. Varadan, and V. K. Varadan, "A free-space method for measurement of dielectric constants and loss tangents at microwave frequencies," *Instrumentation and Measurement, IEEE Transactions on*, vol. 38, no. 3, pp. 789–793, 1989.

[74] A. Sani, A. Alomainy, and Y. Hao, "Numerical characterization and link budget evaluation of wireless implants considering different digital human phantoms," *Microwave Theory and Techniques, IEEE Transactions on*, vol. 57, no. 10, pp. 2605 –2613, Oct. 2009.

[75] T. Yilmaz, T. Karacolak, and E. Topsakal, "Characterization and testing of a skin mimicking material for implantable antennas operating at ism band (2.4 ghz-2.48 ghz)," *Antennas and Wireless Propagation Letters, IEEE*, vol. 7, pp. 418 –420, 2008.

[76] M. Lazebnik, E. L. Madsen, G. R. Frank, and S. C. Hagness, "Tissue-mimicking phantom materials for narrowband and ultrawideband microwave applications," *Physics in Medicine and Biology*, vol. 50, no. 18, p. 4245, 2005. [Online]. Available: http://stacks.iop.org/0031-9155/50/i=18/a=001

[77] C. Gabriel, R. W. Lau, and S. Gabriel, "The dielectric properties of biological tissues: Iii. parametric models for the dielectric spectrum of tissues," *Physics in Medicine and Biology*, vol. 41, no. 11, p. 2271, 1996. [Online]. Available: http://stacks.iop.org/0031-9155/41/i=11/a=003

[78] Itallian National Research Council, URL: http://niremf.ifac.cnr.it/tissprop/.

Chapter 2

Vital Signs Monitoring: Current State of the Art

The design of wearable physiological measurement systems has been a growing research interest in the last decade, due to the potential applications in medicine, sports, and security [1, 2, 3]. With the increase in the size of the elderly population, as well as the emergence of chronic diseases because of the changes in lifestyle, there has been a need to monitor the health status of individuals in their daily routine to prevent fatal disorders. The adoption of mobile healthcare technology is promising to enhance the quality of life for chronic disease patients and the elderly, as well as healthy individuals. Furthermore, it offers the potential to alter the current heathcare system by enabling out-patient care and preventing unnecessary hospitalisations. Designing a telemetry system for health monitoring is a very cumbersome task. There are many key issues to be addressed, including:

- designing reliable sensors;
- ensuring the reliable transmission of vital sign data;
- providing privacy and security for individuals.

Mobility is both a key benefit of such systems and a constraint on their design. To achieve the benefit, wireless physiological sensors must be small, low-weight, power efficient. The radio channel on and around the body has a distinctive nature. For instance, antennas designed to operate at a given frequency in free space, will operate at a lower frequency when placed on the body so-called 'detuning' [4]. This is due to the complex permittivity difference between the body and the air medium. Note that the human body is lossy at microwave frequencies, which is making the body a hostile environment for electromagnetic wave prorogation. Path losses of radio component are increased on-body compared with those in free space. There are also shadowing issues; for example, if a transmitter antenna operating at 2.45 GHz is placed on the abdomen of a human subject it is expected that a shadow region will appear at the back of the subject. Also, the on-body radio channel is dynamic, due to the continuous variation in posture and movement. In this chapter, a detailed review of recent publications is given on research on chronic disease management and on-body propagation issues. The remainder of this chapter is divided into two main sections; the first examines recent research on the measurement of the major physiological parameters, termed 'vital signs'. The second examines wearable wireless sensors from an electromagnetic perspective, discussing such issues as communications protocols, antenna design and radio channel propagation on and around the body.

2.0.1 Future of Healthcare

The emergence of wireless technologies and advancements in on-body sensor design can enable change in the conventional healthcare system, replacing it with wearable healthcare systems, centered on the individual. Wearable monitoring systems, shown in Fig 2.1, can provide real-time reading of physiological data, as well as better information regarding the general health of individuals. Disease prevention is an important step in healthcare revolution; thus, the market for monitoring devices is not only for patients but also for individuals who would like lead a healthier life. The ultimate aim of the new healthcare system is to prevent the advancement of the disease [5]. In the current healthcare system,

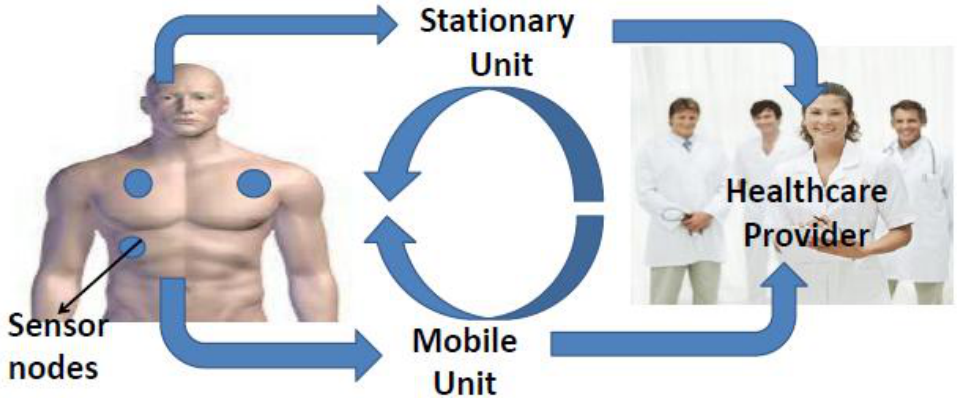

Figure 2.1: Future of healthcare

acquiring the medical data is expensive and it requires multiple visits to hospital. Thus, it is necessary to develop an easy access method to medical data with inexpensive monitoring devices. Through such technology the patients can transfer their physiological readings from anywhere and even acquire a diagnosis without paying a visit to a clinic.

Another important role of real-time monitoring is to provide immediate help for patients or elderly in an emergency situation. Currently, there are systems launched for critically ill patients as emergency home-care solutions. This is done by placing a button on to a patient. In an emergency situation, if the patient pushes the button, the home system calls the healthcare service immediately. However, if the patient fails to push the provided button, the systems fails to call the help in an emergency. Therefore, if the physiological signs are monitored continuously and non-invasively, there is no need for the patient to make the judgement whether or not to call the emergency. Based on the severity of the abnormal vital signs, the system can warn either the patient or the emergency service. Thus, it is very important to develop vital signs monitoring devices that can provide continuous and real-time information to the patients.

Many attempts have been made to monitor the vital signs non-invasively and continuously, both for wearable devices and home or hospital care. One recently reported study proposed a piezoelectric system, which was integrated to the four legs of the home or hospital bed, to monitor bio-signals such as hearth beat, respiratory rate, and the movements while the person is lying on the bed [6]. Monitoring respiration during sleep is very important for people suffering from

sleep apnea in order to target the effective treatment. Another study proposes a diagnosis method for pre-diabetes that measures the functioning of the sudomotor dysfunction, which is a condition present in pre-diabetes patients. Measuring the galvanic skin response tests the proper functioning of the sudomotor [7]. Galvanic skin response is measured by placing two electrodes on the skin to asses the skin conductivity which is related to the sweat levels, ions, and sweat ducks. Early diagnosis of glucose intolerance is important since, such diagnosis can prolong the duration of the pre-diabetes stage by delaying the progress of the disease, thus improving the life quality for patients. In [8], a millimetre wave system is proposed for monitoring the breathing rate and heart rate by measuring the shift on the phase of the back scattered electromagnetic wave.

With the expanding research on monitoring the vital signs, it is expected that the market for vital signs monitoring devices will grow by 8 billion dollars by 2018. However, current monitoring devices are still obtrusive and unreliable. Chronic diseases, including diabetes, heart failure, chronic obstructive pulmonary disease, and dementia, currently have no cure. Such diseases should be managed effectively. Thus, vital-sign monitoring systems will reduce healthcare costs by prevention of further disease complications and enhance the quality of life with disease management.

2.1 Vital Sign Monitoring

There are a number of health issues whose treatment benefits from continuous vital sign monitoring. Traditionally, when this approach is deemed necessary, it results in the hospitalisation of the patient, with expensive equipment and medical personnel on hand; in some cases, the patient may remain at home, but the use of bulky and expensive equipment remains. Much effort has gone into the development of small, wearable devices over recent years, with benefits including lower cost, greater mobility for the patient and, potentially, improved physiological data for the physicians to analyse when attempting to diagnose the condition. Wirelessly-enabling these devices provides greater mobility and improves the efficiency with which available bandwidth is used [9]. A review of

wireless body sensor networks (WBSNs) for healthcare applications was given in [9], including a design strategy for such wireless sensor networks.

There are a number of demographic changes to the world populations, particularly in the West, that are driving the move towards the use of WBSNs and vital sign monitoring. The two most significant changes are the ageing of the population and the rise in obesity levels. Both of these factors increase the risk of developing various conditions that require significant medical intervention and, thus, significant cost. Governments around the world have acknowledged this fact and are seeking ways of delivering healthcare more efficiently, including the use of 'personal health systems' and telemedicine techniques.

The two conditions of most interest currently are diabetes and cardiovascular disease and its related conditions. In developed countries, typically 24% of the population suffers from diabetes and the further complications of the disease, such as cardiovascular disease, can only be prevented with frequent monitoring of blood glucose level (BGL) [10].

Hypertension is another common health problem which has no obvious symptoms [11]. Healthy dietary choices, lifestyle changes and use of medicine can improve the condition of the patient. In order to control the risks associated with the disease, it is crucial to monitor the blood pressure (BP) of the patient frequently. For middle-aged and older subjects, high blood pressure is an important indicator for cardiovascular diseases, which are amongst the leading cause of sudden deaths globally [11].

Vital sign monitoring systems will, therefore, involve monitoring one or more of the following:

- blood glucose level;
- blood pressure;
- pulse rate;
- electrocardiograph (ECG) patterns;
- respiration rate;

- respiration effectiveness (e.g., blood oxygen saturation).

These are discussed in more detail in the following sections.

2.1.1 Monitoring Blood Pressure

Traditionally, monitoring of blood pressure is performed in a clinic with trained personnel by mounting inflatable pressure cuffs with stethoscopes to the patient's arm – the so-called auscultatory method [12]. This type of measurement does not achieve continuous monitoring and the patient is required to be in a certain posture in the clinical environment, which causes the *white-coat effect*. The white-coat effect is known to be the falsification of BP measurements, usually with transient peaks in BP, due to the stress caused by being present in a clinical environment [13]. Current alternatives are ambulatory monitoring and home-monitoring devices, where patients can monitor their own BP.

One of the common techniques used in ambulatory/home monitoring devices is the oscillometric method [12]. Home monitoring devices generally include a fully automatic inflatable cuff which can be mounted on the patient's wrist and measures the blood pressure of the radial artery by relating external pressure with the magnitude of arterial volume pulsations.

Although oscillometric monitoring systems are convenient to avoid the transient rise of BP due to the white-coat effect, the periodic interruptions of the blood flow and continuous usage of such devices may cause unwanted side effects, such as sleep disruptions at night-time, skin irritations and an increase in stress level [14]. Vasotrac (Medwave Inc., Arden Hills, MN, USA) is an example of a watch-type ambulatory non-invasive BP monitoring device [15, 16]. It includes a circular sensor (this must sit on top of the radial artery in the wrist), a digital monitor and a disposable adhesive plaster to estimate the location of artery. After collection of data, the sensor response is taken and processed by a controller unit and displayed on the digital screen. Although Vasotrac is a cuff-less device, an external pressure is required for reliable measurements. Vasotrac is a good alternative for infrequent ambulatory monitoring; it is, however, unsuitable for continuous monitoring.

Many different methods have been used to measure BP non-invasively. For example, the ultrasonic method, introduced in 1961, relates the Doppler shift of the ultrasound response and the velocity of blood [17]. The frequency shift of the scattered ultrasound with the change in the velocity of the particles in blood is observed by placing two piezoelectric crystals in a plastic tube. The Doppler shift technique is proven to be an effective method for measuring the systolic BP of infants [18].

Measuring the BP through pulse wave transit time (PTT) is another cuff-less technique and a candidate method for continuous monitoring of BP [19]. When measuring the PTT, the heart activity is usually monitored with an ECG sensor and a photoplethysmogram (PPG) sensor is placed on a finger, wrist or earlobe to track the pulse travelling from the heart to the peripheral point. Note that Photoplethysmogram sensor takes volumetric measurement of an organ optically by measuring changes in light absorbtion. Simply, if the arterial pressure is higher, the pulse travels faster. Recently, a wrist module was developed to measure BP by integrating a PPG sensor and ECG sensor into a watch-type monitoring device [20, 21]. However, the reliability of measurements and calibration of the device are still issues under investigation.

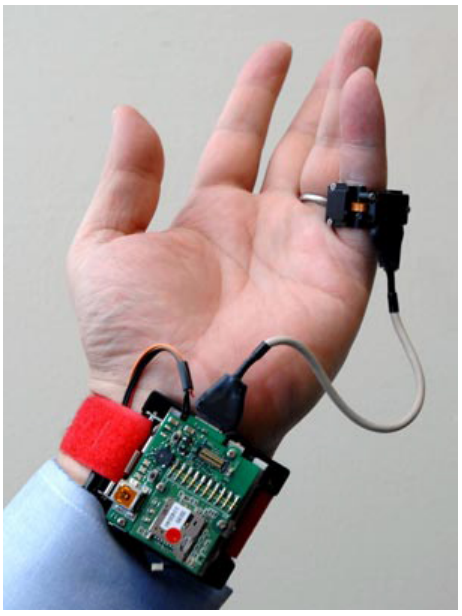

Figure 2.2: Blood pressure sensor by MIT, ppg sensor measuring the pulse on the wrist and on the finger [22]

More recently, another cuff-less design was developed by using combined PTT

and oscillometric methods [22, 23, 24]. The system estimates the BP by placing two sensors along the artery; typically, these are at the wrist and index finger, as shown in Fig. 2.2. However, measuring the blood pressure in this fashion is challenging, due to instabilities in hydrostatic pressure caused by the change of hand position with respect to the heart. Conventional ambulatory BP meters require patients to sit and raise their hand to the heart level. In order to overcome this challenge, a MEMS accelerometer is used to adjust the height of the hand with respect to the heart, to set the hydrostatic pressure offset for the PTT sensor. This approach allows the patients move their hands freely by calibrating the PTT sensor response according to the change in hydrostatic pressure. One benefit is that the local pressure applied to the tissue is trivial compared to the traditional oscillometric devices and does not interrupt the blood flow. Thus, this design is a promising approach to achieve continuous, non-invasive and unobtrusive monitoring of blood pressure and is one of the cutting-edge technologies under investigation at this time.

2.1.2 Monitoring the Blood Glucose Levels

Most commercial blood glucose (BG) monitoring devices employ invasive techniques; usually, a blood sample must be obtained by pricking the finger with a lancet. The blood sample obtained is then exposed to a strip and the BGL calculated by inserting the strip into a digital monitor. Diabetic patients should perform the task at least 4 times a day for tight metabolic control. However, the finger pricking task is reported to be a painful procedure, leading some to take fewer samples, hence risking problems induced by poor BGL management.

Some commercial systems (e.g., Medtronic's MiniMed and Guardian products [25]) are termed 'minimally-invasive' continuous monitoring systems. Typically, a (disposable) bio-sensor needle is inserted under the skin on the abdomen and the BGL is derived from the glucose level in the interstitial tissue fluid. In Medtronic's product [25], the needle unit is self-contained and includes all electronics required to capture the signal, process it and communicate it wirelessly to a second body-worn unit that acts as the user-interface. Recently, a feasibility study conducted

to examine a similar system concept, with the aim of extending the lifetime of the bio-sensor needle [26]. This involved both design and optimisation of the bio-sensor and the use of signal processing techniques to extract the maximum useful information possible. Work is on-going in this area.

A non-invasive continuous self-monitoring system is key to improve the management of diabetes. In recent years, there has been a considerable progress in research on minimally-invasive or non-invasive monitoring techniques. One example is the GlucoWatch Biographer, a minimally-invasive device measuring BGL through extraction of transdermal fluid. This device was developed by Cygnus, Inc., and was commercially available for some time [27]. However, the Food and Drug Administration (FDA) in the United States later banned the commercial use of the device, due to complaints from users claiming that the device caused a mild-to-moderate amount of skin irritation. The device essentially drew the interstitial fluid through the skin with a low electrical current; therefore, there was a 10-15 minute time lag compared to traditional glucometers, note that the time lag between the change in interstitial fluid and blood glucose level could be 2-45 minutes [28].

Impedance spectroscopy (IS) is another highly investigated method; it measures the change in the electrical properties of blood non-invasively. Variation in BGL affects the electrical properties of erythrocyte (red blood cell) membranes; this causes alterations in the electrolyte balance of skin and subcutaneous tissue [29, 30]. These variations can be detected with the IS technique by measuring the magnitude of impedance $|Z|$ with an RLC resonant circuit [31] or a vector network analyser (VNA). Although IS is sensitive to BG variation, the alterations in other bodily parameters (such as sweat levels, changes in the posture and temperature levels) can affect the measurement results. In order to reduce the effect of the other parameters, a multi-sensor approach has recently been developed [32, 33]. The new arm module, shown in Fig. 2.3, includes eight sensors; three of them are capacitive electrodes in long, medium and short lengths and operating at different frequencies, developed by Solianis Monitoring AG. The medium-length and long electrode signals can penetrate into the deeper layers of tissue, providing information related to changes in glucose levels; the short electrode signal penetrates to

the surface layer of skin, providing data related to other parameters. Additionally, there is a sweat sensor, an accelerometer and an optical reflection sensor, which are combined in an arm module on elasticized cloth. Note that accelerometer can identify the forces such as gravity around the device understanding the tilt and orientation of the device and optical reflection sensor is used for skin blood flow measurement. The arm module was tested under controlled conditions with ten male diabetic patients; however, further investigation is crucial to understand the true performance of the developed module in non-laboratory environments.

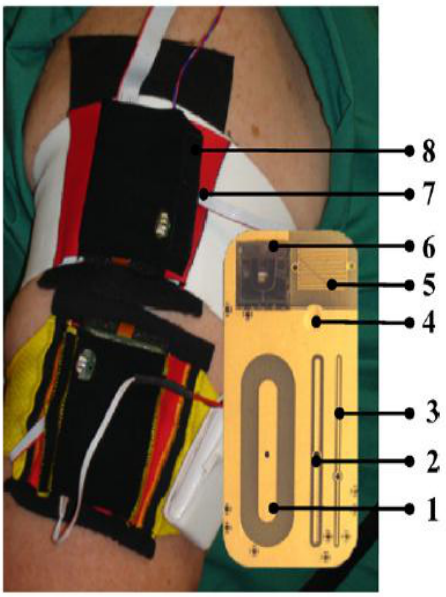

Figure 2.3: Arm module proposed in [32] (1) deep, (2) mid and (3) shallow electrodes. (4) Temperature sensor. (5) Sweat sensor. (6) Siliconwafer based optical reflection sensor. (7) Humidity sensor. (8) 3-axes acceleration sensor.

It is well-known that alterations in BGL affects the electrical properties of blood, as well as the electrical properties of subcutaneous tissue, at microwave frequencies. In order to measure the change in the electrical properties of interstitial fluid with respect to glucose levels, an *in-vitro* study performed by collecting the blood plasmas of twelve healthy volunteers [34]. The electrical properties of blood plasma were measured between 100 MHz and 20 GHz using Agilent's open-ended slim coaxial probe kit; this was performed by adding dextrose to the plasma sample in concentration from 0 mg/dl to 16000 mg/dl. According to the measured results, the conductivity values between 15 GHz and 20 GHz were more sensitive to changes in the glucose concentrations in the blood plasma. Please

refer to *Chapter* 1 for Fig. 1.4 (a) and (b).

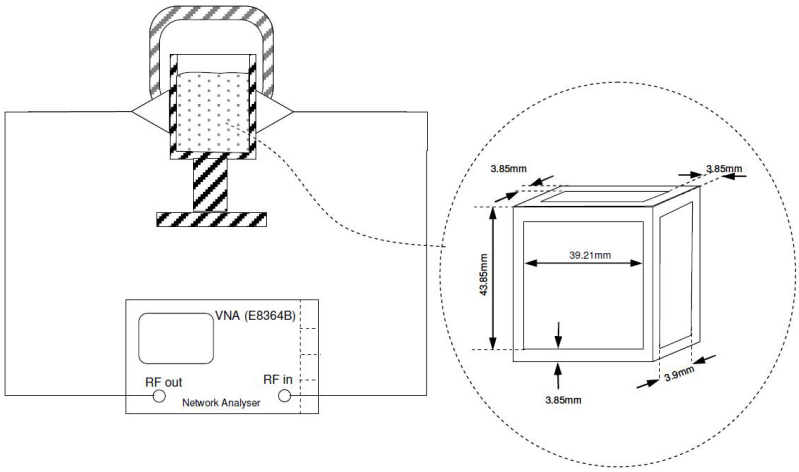

Figure 2.4: Experimental set-up for measurements: a cubic cell sandwiched between two antennas [35] .

Another experiment was performed to relate the change in microwave resonance characteristics with the alterations in BGL [35, 36]. A blood sample containing 6 mmol/dl of glucose was poured in a cubic test cell and exposed to low power microwave energy between 10 GHz to 20 GHz. This was achieved by placing two SMA coaxial-to-waveguide 18 (WR62) E-field adaptors on each side of the test cell, shown in Fig. 2.4. The blood sample was swapped with another blood sample containing 14 mmol/dl glucose; for both cases, the S_{21} magnitude response of the system (i.e., the transmission coefficient or transfer function) was measured with an Agilent 8720ET VNA. The observed minimum in the S_{21} response for the first sample occurred at 13.130 GHz; for the second test sample, the frequency of the minimum shifted upwards by 332 MHz, occurring at 13.452 GHz. The frequency shift occurs due to the permittivity change in the blood glucose levels. Also, it was observed that the Q factor (a measure of the bandwidth and loss in a system) for the first sample was higher than for the second sample. Both experiments showed that microwave detection is a promising approach to detect blood glucose level non-invasively. However, *in-vivo* measurements of electrical properties, as well as the effect of other parameters in blood on the electrical properties, should be further investigated.

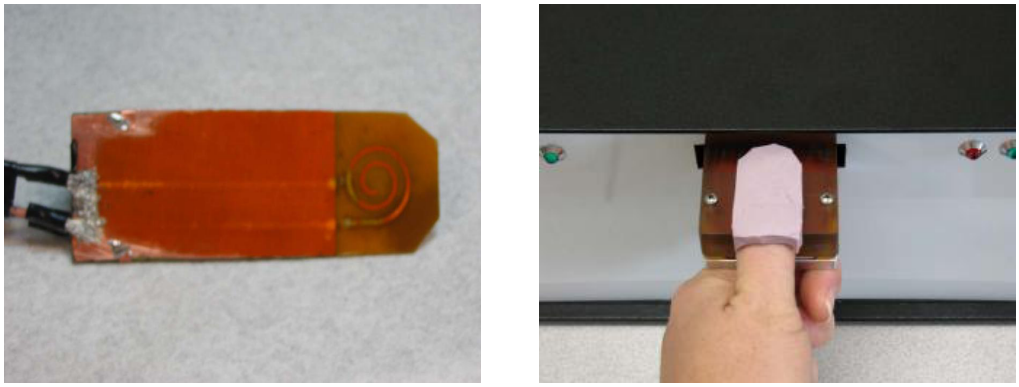

(a) (b)

Figure 2.5: (a) Initial design of microwave sensor (b) Modified microwave sensor with silicon positioning aid [37].

Recently, a spiral-shaped microwave sensor, shown in Fig. 2.5, has been developed and tested for non-invasive monitoring of BGL [37]. The sensor design was evolved from the microstrip ring-resonator. Testing of the sensor was performed with a 'soda test', in which the author fasted for at least eight hours before consuming a soda drink with high sugar content to increase the BGL rapidly. During the soda test, the author measured the sensor response for two hours at ten minute intervals, by placing the spiral part against the wrist. Meanwhile, the blood glucose level was tracked with a commercial glucometer. The first maximum of the S_{21} response was tracked. The structure is designed to operate at Medical Implant Communication Service (MICS) band (401-406 MHz); however, when placed to the human wrist it is operating at 465 MHz. During the soda test the first maximum of the S_{21} was increased by 8.5 MHz, shown in Fig. 2.6. However, the author did not show a comparison between the glucose level and the peak shift. Also, the applied pressure was not measured during the experiment. It is known that the applied pressure changes the resonance response significantly.

In order to control the effect of the pressure, the sensor is mounted on a fixed structure with a pressure sensor. This time sensor is modified to take measurements from the thumb, shown in Fig. 2.5 (b). 5 subjects are asked to measure the capillary blood glucose level with off-the-shelf monitoring devices. Then the subjects were asked to place their thumb on top of the resonator with controlled pressure. Then the response of the resonator is recorded. The data

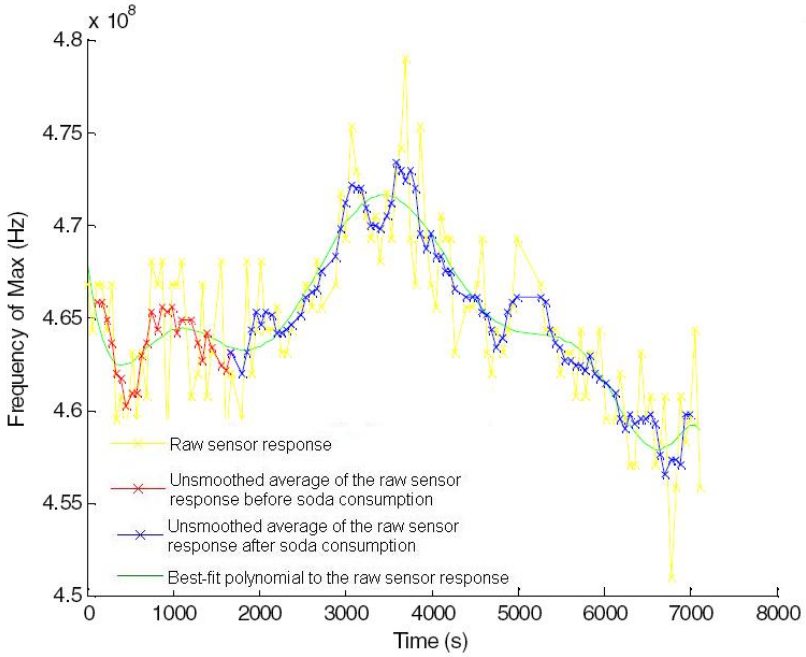

Figure 2.6: Change of the first maximum of S_{21} during the soda test performed by placing the resonator towards the wrist every ten minutes with a male subject [37].

collected from the subjects are used to calibrate the sensor, given in [37]; however, the author did not give the details of the algorithm and no quantification of the error is given. The calibration results are shown however the technique have not been tested with subjects. Although this approach showed promising results, the designed sensor is still bulky for home monitoring. Also, there is a need to validate the performance of the sensor with subjects. Additionally, as mentioned in the [37], calibration is limited with healthy individuals the blood glucose level are fluctuating between 80 mg/dl to 130 mg/dl.

Another preliminary study was published recently on non-invasive measurement of BGL using millimeter-waves [38, 39]. In the study, the return loss of the system measured by placing different glucose solutions as a load. Although the change in the frequency of resonance, as well as the Q factor, is in an acceptable range, human tissue is, in reality, very lossy; therefore, the penetration depth at higher frequencies will be very low.

Usually, in near-infrared spectroscopy, the peripheral tissue is exposed to the near infrared radiation and the transmission or reflection from the tissue is measured. The blood glucose data is extracted through analysis of the measured tissue response. In [40], the validity of the extracted glucose values from measured

spectral absorption was discussed. The absorption of the radiation by glucose is very small, compared with absorption from background tissues. Experiments were performed using a protein solution with beef fat; under controlled conditions, the near infrared measurements were taken whilst altering the glucose levels. It was observed that, although no glucose was present, the measurement results was predicting its presence. Recently, algorithms for better estimation of the blood analytes were developed using Raman spectroscopy [41]. ([40, 41] contain a good overview of the challenges that must be overcome by spectroscopic methods of determining BGL for the interested reader.) Deleterious effects of scattering and absorption from the surrounding environment, termed as turbidity is one of the major causes of intensity and shape distortions in Raman spectra. The proposed method corrects intensity and shape distortions of the Raman spectra; it was tested with a set of tissue phantoms with same concentration of Raman scatterers but with different background turbidities. This method presents a promising approach on correcting intrinsic line shapes and intensity information. More recently, an algorithm was developed to estimate the BGL change from the change in the glucose level in transcutaneous tissue [42]. However, alterations in the glucose level of interstitial fluid lags behind the change in BGL. This time lag should be addressed and estimation should be performed accordingly.

2.1.3 Monitoring The Cardiac Activity

Conventional monitoring of cardiac activity is performed in a clinical setting in real-time during a visit to the facility, by recording electrocardiograph (ECG) signals. Monitoring the heart activity through ECG signals is a very common technique, performed by placing at least three electrodes to the skin to measure the electrical activity of the heart. Traditionally, Holter monitors are used for ambulatory monitoring during the recovery period after cardiac surgeries [43]. Although Holter monitors are capable of providing continuous monitoring, the central unit of these monitors is bulky and each electrode is connected to the central unit with wires. Therefore, use of the Holter monitor interrupts the daily routine of the patient and is not feasible for unobtrusive continuous monitoring.

Over the past few years, with the advancement in wireless technologies, Holter monitors have been miniaturized and evolved into complete wire-free monitoring devices such as capacitive electrodes. Although ambulatory wire-free devices look promising for continuous monitoring, there is still a need for further development of such devices.

Development of an ideal electrode for ambulatory devices is vital to achieve continuous unobtrusive monitoring. Commonly-used electrodes for clinical applications are gel-type Ag/AgCl wet electrodes. Even though these electrodes have been reliable, compact and low-cost, continuous usage of wet electrodes causes skin irritations, since these electrodes employs conductive adhesives in order to maintain the resistive electrical contact with the skin. Also, the signal quality from these electrodes decreases significantly when the gel dries, due to the loss of proper contact with the skin. As an alternative to wet electrodes, dry electrodes were developed; however, most dry electrodes are not bio-compatible, since they are usually constructed with hard substrates. Also, when placed on skin, dry electrodes have a higher impedance than gel-type ones [44, 45]. More flexible dry electrodes have been developed by using conductive rubber or elastic materials instead of hard substrates [46]. Conductive-rubber-based electrodes use human sweat to maintain the contact with the skin, instead of conductive gel. These electrodes can be integrated into clothing. As well as being flexible, the conductive rubber is approved for short-term implants; thus, it is expected to cause the least skin irritation. However, these electrodes still require contact with the skin and long-term usage of rubber-based dry electrodes still causes skin irritation. Motion is another factor that affects the measurement results: it causes a change in external pressure and eventually affects the contact between the electrode and skin. Alternatively, insulated electrodes are capable of sensing ECG signals through clothing via capacitive sensing, without a resistive electrical contact with skin, as shown in Fig. 2.7 [47, 48]. Earlier versions of capacitive electrodes used uncomfortable materials in order to provide high capacitance. However, over the last few years, bio-compatible materials have been used and these electrodes have been integrated with small wireless sensing devices, termed 'motes'. Additionally, capacitive electrodes provide good signal quality regardless of motion. Thus,

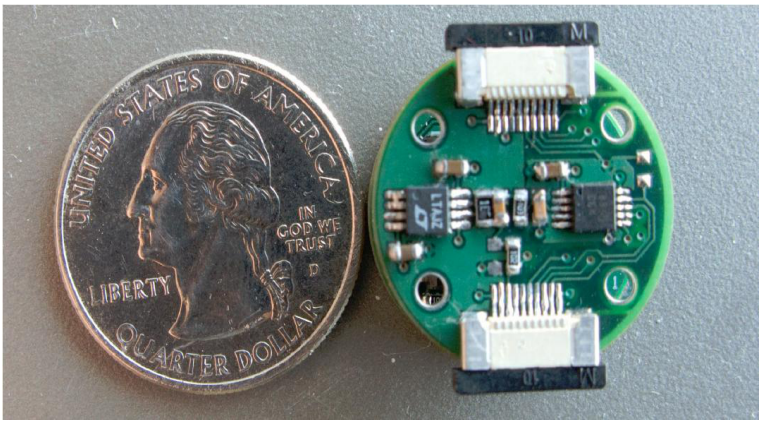

Figure 2.7: Capacitive electrodes proposed in [47].

insulated bio-electrodes are a promising approach for wireless cardiac monitoring and are an example of the current state-of-the-art technology in this field.

Mechanical cardiac activity can be tracked with microwave sensing. Microwave sensing does not require direct contact with the skin and employs a transmitter and a receiver in which the exact position of chest is detected by demodulating the phase of a scattered Doppler radar wave. Recently, a single-chip implementation of a Doppler radar technique has been presented [49]. However, a detailed morphology of the ECG is not available with the Doppler radar technique.

2.1.4 Monitoring Respiration

In clinical research, conventional non-invasive monitoring of respiration rate is performed by impedance pneumography and inductive plethysmography. Impedance pneumography measures the impedance change between two electrodes placed on the chest. Thus, this technique measures the movement of the chest caused by the respiration cycle. Impedance pneumography is prone to errors from posture changes and motion. Inductive plethysmography, on the other hand, employs two copper wires: one is placed around the abdomen, the other placed on the chest. During the respiration cycle, volumetric differences occur and this causes self-induction of the two wires. Inductive plethysmography is a more reliable technique compared to impedance pneumography.

Recently, a measurement system for drivers was introduced, where the respiration rate is derived by measuring the pressure applied to a gauge embedded in a seat belt [50]. Alternatively, a yarn-based piezo-resistive textile sensor has been developed to estimate the respiration rate through the strain output of the sensor when it is subjected to tensile strength [51]. Another study compares the measurements of heart rate and respiration cycle outputs of two different materials: one piezoelectric plastic polyvinylidenefluoride (PVDF) and the other electromechanical film (EMFi) embedded into clothing [52]. The PVDF sensor produces electrical signals with the mechanical changes in material. The EMFi sensor has two electrodes embedded in fabric and connected to each other with conductive wires. Although this study found similar results between the two sensors, the study was performed when the subjects were in a resting state. Other non-invasive measurement techniques include estimating the respiration rates through cardiac activity.

2.1.5 Multi-parameter monitoring

Ideally, monitoring systems for mobile health should be unobtrusive, incorporate multiple sensors, give real-time feedback and provide wireless communication with on-line data evaluation. To this end, several papers have been published and commercial multi-parameter sensors have also been produced. Of these commercial products, devices for performance monitoring (such as the Nike iPod kit and 'adidas miCoach') have been successful. However, these devices are limited to measuring one or two parameters and are not suitable for monitoring chronic disease patients. Combining sensors for vital sign monitoring has been studied by research groups in academia, as well as in industry. LifeShirt (Vivometrics Inc., USA) is an example of a multi-parameter monitoring system [53]. LifeShirt includes a garment, analysis software and a data recorder. Respiration, ECG, activity, and posture are monitored with the sensors attached to the garment. The device has been tested in many clinical settings and has been used successfully in animal studies as well. Even though LifeShirt is a promising invention, it is lacking wireless nodes to provide real-time data transfer. 'WEALTHY' is

another textile-based garment developed to monitor ECG, respiration, activity, and temperature measurements [54]. ECG monitoring is performed with knitted yarn-based sensors integrated into the wearable garment. When the patient is in a resting state, good quality signals are obtained; however, during physical activity, the movement of the arm causes significant noise. Therefore, hydrogel is required to maintain the ohmic connection with the skin. The system employs piezoresistive sensors for respiration and activity sensing. The main goal of textile-based systems is to develop a wearable and washable garment for monitoring vital signs data; they are usually aimed at cardiac, asthma and sleep apnea patients. Another study on multiple health monitoring devices is 'AMON', shown

Figure 2.8: AMON wrist module [55].

in Fig. 2.8, which employs a miniaturized wrist-type device and a stationary device [55, 56]. AMON is capable of monitoring blood oxygen saturation (SPO_2), temperature and activity continuously. Note that SPO_2 is the amount of oxygen carried by the red blood cell indicating how well the respiratory system is functioning and the ratio fluctuates between 90% to 95% for healthy humans. It employs a reflectance sensor for SPO_2 measurement. The reflectance sensor detects the SPO_2 level by measuring the absorbance levels of two different signals with two wavelengths. The activity of the individual is measured by acceleration sensors. Besides the aforementioned sensors, the wrist-type device also employs an oscillometric blood pressure sensor and single lead ECG monitoring. The ECG and blood pressure measurements are taken three times a day or upon

the request of the patient. ECG monitoring is performed with gold electrodes (which has higher impedance) and is converted into a twelve lead ECG signal at the stationary unit; therefore, the reliability of the ECG results is questionable. Additionally, for blood pressure monitoring, AMON incorporates the traditional inflatable cuffs; thus, the mobility of the patient is restricted during the measurement. The advantage of the AMON system is that the system includes a mobile communication (GSM) transceiver, which enables data exchange with the healthcare provider. Moreover, the device can perform data analysis on-line, enabling real-time feedback and emergency detection. Many other devices combining several sensors to monitor multiple parameters are available, such as SenseWear [57], Escort Guardian [58], Micropack [59], Smartshirt [60] and VTAMN [61]. These products and studies have been reviewed in the literature numerous times; thus, a detailed review of them is not included.

2.2 Wireless Technologies

Current physiological monitoring systems offer different means of communication between on-body sensors and the main data-capture unit. The simplest way of providing secure data transfer between the sensors and the main unit is wires. The implementation of wires in such systems is easy and low-cost; an obvious example of this technique is the aforementioned Holter monitor. However, these monitoring devices are obtrusive, presenting a challenge to patients in continuing their daily routine; in addition, the risk of wire tangling may mean that system failure is more likely. Over the past few decades, a number of alternative communication techniques have emerged. One is the use of so-called 'smart clothes' for on-body communications, where electronic devices (and, usually, interconnections in the form of wires) are embedded and woven into the fabrics. However, smart clothes are expensive and may force the end user to ignore personal preferences. Another innovative approach is communicating through biological channels (biochannels); here, the human body is used as a communication channel by allowing data transmission between near electronic devices through near field electrostatic coupling [62]. One limitation is that only small amounts of data (on average

2.4 kbps) can be transmitted through bio-channels; therefore, their use is not desirable for body area networks (BANs).

There are three general scenarios for wireless body-centric communications [4]:

- *off-body*, where a device located on a body communicates with one or more devices located off-body;
- *on-body*, where a number of devices located on the body communicate with each other;
- *in-body*, where some (or all) of the devices on-body are implanted, rather than worn (e.g., pace-makers).

The latter two cases can be grouped together under the term '*intra-body communications*'. Where the off-body case deals with communications between wireless BANs (WBANs), it is termed '*inter-body communications*'. It should be noted that the off-body case can cover propagation distances ranging from less than a metre up to tens of metres, whereas the intra-body cases will be less than two metres (the most extreme case could be a device near the foot communicating with a device near the head). Inter-operability of WBANs that may be located in close proximity is a critical issue. The off-body case is exemplified by mobile telephones; a great deal of research has examined how the performance of these devices is affected by proximity to the human body. This scenario will not be discussed further in this paper; the interested reader is directed to the literature (see, for example, [63, 64, 65, 66, 67, 68, 69]).

With the recent advancements in wireless technologies, wearable monitoring systems can operate without wires by integrating wireless modules with on-body sensors. Using wireless communication is beneficial in many ways. First and foremost, real-time monitoring of collected data can be achieved more easily, which is useful for launching alert mechanisms. In addition, wireless on-body sensors are more unobtrusive for patients, allowing them to continue with their daily routine more easily. Moreover, these systems enable out-patient care, potentially even after more significant operations, thus decreasing healthcare costs. Finally, by

allowing the individuals to track their own data with real-time feedback through smart-phones or PDAs, chronic disease sufferers can manage their disease more efficiently.

Providing reliable wireless transmission of data between on-body sensors (and also off-body to mobile, or stationary, devices) is a demanding task. There are a number of fundamental challenges that exist in understanding the propagation characteristics around the body, as well as the means of coupling radiated energy into these propagation channels through optimum antenna design [4]. From a communications perspective, different applications may have different bandwidth requirements, whilst all physiological data must be treated in a careful and secure manner; these lead to certain constraints on the optimum communications protocol for WBAN applications. Furthermore, the wireless module should be light-weight, low-power, low-cost and compatible with the remaining circuitry [9]; these constraints will also inform protocol and antenna design. Recent progress in addressing these challenges is reviewed in the following sections.

Whilst simple one-sensor systems are valid examples of the WBAN concept, it should be noted that the greatest realisation of the potential of a WBAN system is when applied to multiple sensor nodes on-body, such as the multi-parameter monitoring systems discussed in Section 2.1.5.

2.2.1 Wireless Communications Protocols

Several approaches have been developed for on-body wireless communication; for example, IEEE 802.15.1 (Bluetooth) is one of the widely-used standards for wireless *Personal Area Networks* (WPANs) – these differ from WBANs in the extent of the propagation range: WBANs cover the immediate area of the body (intra-body communications), whilst WPANs extend away from the body (off-body communications). However, some of the uses overlap and are difficult to distinguish; a typical example of Bluetooth usage for WBANs is transmission of voice data between a head-set and a cell phone [70]. Bluetooth-enabled devices can operate at the unlicensed industrial, scientific, and medical (ISM) band around 2.45GHz (2.40-2.48 GHz), divided into 79 channels, with a 1 Mbps data rate.

The modulation technique is Gaussian frequency-shift keying (GFSK) and it is capable of transmitting data to a range of between two to ten meters. Note that GFSK is a continuous phase frequency shift keying modulation technique which uses a Gaussian filter to smooth the binary frequency deviations. The maximum transmitted power is 0 dBm (1 mW). Multiple Bluetooth devices can form a piconet, a star-topology network consisting of a master device communicating with seven slave devices. This is the basic configuration, although multiple piconets can be linked into 'scatter-nets'. Recently, the lower layers of the Wi-Fi protocol (IEEE 802.11 PHY/MAC layers) were adopted for higher data throughput. For very low power requirement applications, such as body-worn wireless sensors, Bluetooth also offers a low-power option [71]. However, high power consumption is still a limitation for Bluetooth, compared to other enabling technologies; in addition, since it offers ad-hoc networking, it is vulnerable to security concerns.

Another wireless enabling technology is ZigBee, built on the IEEE 802.15.4 standard, used for low power and low data rate communication. It also operates at the 2.45 GHz ISM band, with 16 channels globally; the data-rate is 250 kbps and it is capable of transmitting data between 1 to 100 metres. A data rate of 250 kbps is considered adequate for most current health applications. The digital modulation scheme is offset quadrature phase-shift keying (OQPSK). It also operates at 915 MHz in America, with ten channels at a 40 kbps data-rate; and at 868 MHz on one channel in Europe, with a 20 kbps data-rate. Star, tree and mesh topologies are all supported network architectures. Data transmission security is protected by the use of the Advanced Encryption Standard (AES) in ZigBee [72]. The battery life for ZigBee is expected to be months, whereas battery life is limited to days for Bluetooth. The target market for ZigBee is low data-rate, low energy applications. With its simple architecture and the low power requirements, ZigBee is more suited to medical applications, compared to Bluetooth.

Ultra-wide band (UWB) technology has received attention lately as a promising method, since it offers high data rates for short ranges, as well as its very low power requirements. The US Federal Communications Commission (FCC) approved the 3.1–10.6 GHz band for UWB. UWB can provide high data rates

(1 Gbps) up to a distance of ten metres. Data transmission is limited to this short range due to the low power output of UWB systems.

Other wireless standards include the medical implant communication service (MICS) band (401-406 MHz), used for bi-directional communication between the implants and body-worn/external units. This band is authorized for implantable antennas [73, 74] that can be integrated into pacemakers and implantable sensors; however, there are regulatory constraints on its operation outside hospital environments that limit its usefulness in the wider WBAN market. Finally, the opening-up of spectrum in the millimeter-wave band (particularly around 60 GHz) has attracted attention for a number of short-range applications, particularly for indoor use. Although more analysis is required, due to the relatively immature nature of the field, it may offer the same advantages and disadvantages as UWB.

There is, at present, no single 'ideal' standard available for physiological measurement systems based on wireless body sensor networks (WBSNs) [72]. The IEEE 802.15.6 Task Group is seeking to address these issues and indications are that the new standard will have the following characteristics [72]:

- scalable data-rates, from 1 kbps to hundreds of Mbps, for use with sensors with differing bandwidth requirements;
- short-range, from two to five metres;
- network sizes of up to 100 devices will be allowed;
- it will guarantee very low latency in data paths;
- ultra-low power consumption, of the order of 0.1–1 mW, will be targeted;
- operation in the 2.36–2.40 GHz band is proposed, to take advantage of existing commercially-available technologies and mitigate potential interference.

It is unclear, at present, whether non-medical applications of wireless physiological measurement systems are envisaged for this standard, or whether it will be solely optimised for healthcare applications. It is the nature of standards development that much time is required; there are many parties, both part of and

exterior to the development process, who are awaiting the new standard with interest.

2.2.2 Antenna Design

Characterization of antennas is the key to establish reliable on-body data transmission between sensors and the main data-collecting node (this may be worn on-body or an external stationary or mobile unit). Antennas for WBAN communication are required to be compact, low-weight, conformal, high efficiency and compatible with the remaining circuitry for seamless integration. Designing antennas for WBAN applications is not a straight-forward task, since antenna performance is affected by various parameters, such as impedance matching and electromagnetic absorption when placed on-body. Therefore, when designing antennas for WBANs, careful consideration should be given to the presence of lossy human tissue. To this end, many antenna designs have been proposed for wearable applications, including textile antennas (i.e., antennas fabricated using textile-based materials).

The effect of the presence of the human body on antenna performance has been widely investigated in the literature. In a recent study, the free-space performance of different planar antennas operating in the 2.4 GHz ISM band was analysed and compared with the on-body performance [75]. The efficiency and gain of an on-body antenna can be affected by three main parameters:

1. antenna distance from the body;
2. antenna location on the body; and
3. the antenna type.

In order to test the effect of the antenna's distance from the body, six antennas (derived from the traditional dipole, monopole and loop antennas) were placed at separations of 1 mm, 4 mm and 8 mm away from the body. It was observed that the resonant frequency was detuned as the antennas were placed closer to human body. The human body has dispersive electrical properties and is very lossy at higher frequencies; therefore, the presence of the human body changes

the effective length of the antenna structure at the operating frequency of the antenna. The type of antenna is another important parameter that defines the magnitude of detuning: in the above study, it was concluded that the antennas with a ground-plane were less prone to the change in proximity to the human body, making them more suitable for WBAN applications.

The aforementioned antennas were also placed in different locations on the body, including the right and left ears, chest and ankles. According to the results, creeping waves were observed for a printed monopole antenna when placed on left chest; however, the waves decayed rapidly due to the lossy environment.

A button-shaped antenna, based on a Yagi microstrip array design and operating at 2.45 GHz, has been proposed for tele-medicine applications [76]. The directivity of the antenna was enhanced with director patches, in order to prevent back-radiation and minimise losses. 8 MHz bandwidth achieved at desired frequency, however, as we mentioned earlier the narrow bandwidth antennas is more likely to fail on reliable data transfer.

An innovative approach is liquid antennas for communication with implants. The electrical properties of on-body antenna substrates are very low, compared to those of the human body. The human body is mostly composed of water, which is among the materials with highest electrical properties (that is, relative permittivity and effective conductivity). Therefore, the near field of metal-based antennas when positioned on the skin is disturbed with the reflections from body. Due to the electrical property differences, the electromagnetic waves cannot penetrate the skin and are confined in the substrate. To prevent this phenomenon and provide better electrical property matching, a liquid antenna using a saline solution was designed [77]. The liquid is encapsulated with a bio-compatible material and simulated. The liquid antenna seems a promising approach for communication with implants.

The electrical properties of the organs and skin and muscle are different; therefore, the differences in the amount of muscle or fat, or even the skin, will cause differences in the observed antenna performance. These differences may be observed with respect to gender and age differences from one subject to another; they may also be expected to vary for the same subject over time. This shows

the importance of subject-specific characterisation of on-body antennas.

2.2.3 On-body Propagation

The channel variation between a transmitter and a receiver in an indoor or outdoor environment is caused by the interference between multiple scattered waves from the surrounding environment. Communication between antennas mounted on the body is achieved with both space waves (i.e., propagating through the air around the body) and surface (creeping) waves (i.e., propagating along the surface of the body, at the interface between air and body) [78]. The on-body propagation environment is, in some ways, similar to that in both indoor and outdoor environments, in that it is affected by scattering from the local environment. However, it differs from these propagation environments in that channel variation is affected mainly by the change in body posture. In fact, changes in the posture – hence, the geometry of the body channel – affects on-body propagation dramatically, including during even the simplest daily activities. The movement of the body parts changes the distance between antennas and causes channel variability; for example, antennas placed on a hand show dramatic channel variability [4]. Thus, on-body channel characterisation is a crucial task and needs to be studied for efficient antenna design. Two cases on-body and intra-

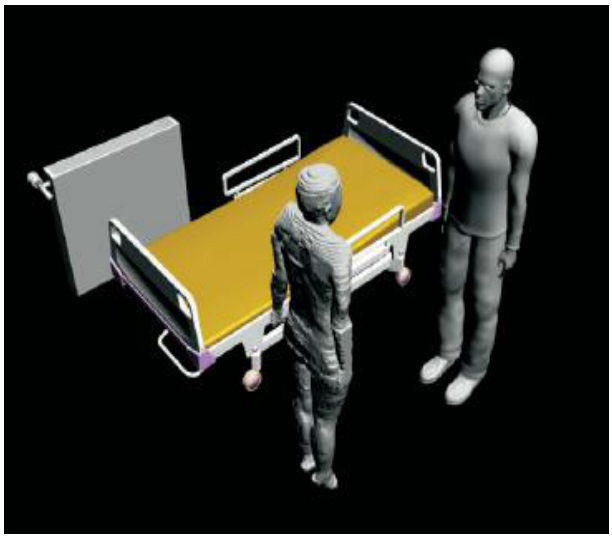

Figure 2.9: Inter-body propagation case in [79]

body propagation, shown in Fig. 2.9, have been considered in a subject-specific

study [79]. For on-body propagation, a patch antenna, operating at 2.45 GHz, was placed on the left chest; the receiver was placed alternately on the front and back of the subject to investigate both the line of sight (LOS) and non-line of sight (NLOS) cases. The simulation was performed using the parallel finite difference time domain (FDTD) method and the results verified with measurements. The study concluded that the propagation along the chest was highly dependent on the chest size, where the path-loss exponent increased when the receiver and transmitter were placed on larger chests. The variability of channel for intra-body communication case is vaguely effected from change of the subjects. It has been found that the WBAN channel characterisation is subject-specific if the received signal contains creeping waves around the body.

As mentioned previously, UWB has a great potential for WBAN applications. In a recent study, the UWB radio channel was investigated experimentally with two UWB antennas [80]. Horn-shaped self-complementary (HSCA) and planar inverted cone (PICA) antennas were used for the measurement campaign. The HSCA were placed parallel to the body and the PICA were placed perpendicular to the body, in order to model the dependence of on-body channels to space-wave and surface-wave propagation. The measurements were performed with 22 different postures in an anechoic chamber. Measurement results showed that, when the antennas were placed on the chest, the HSCA demonstrated stronger surface waves than those from the PICA. Additionally, it has been shown that bi-phase modulation outperforms pulse-position modulation (PPM) with very low transmitting power and low signal-to-noise ratio (SNR). A similar recent study on UWB analysed the effect of body movement on channel parameters by using tapered slot antennas operating in the 3-9 GHz band [81]. The measurements were performed in an anechoic chamber as well as in an indoor environment; one antenna was attached to the wrist and the other antenna successively to the head, ankle, chest and back. The path-loss exponent decreased for the indoor environment, compared to that found in the anechoic chamber, due to the multipath effect. It has been observed that the received power also depends on the dynamic behaviour of the body.

2.2.4 Security in Wireless Implantable/On-body Devices

The rapid expansion of the availability of mobile devices and wireless technologies enables the user/patient controlled usage of implantable and on-body devices. Cardiac pacemakers, insulin pumps and on-body cardiac monitoring devices are now integrated with wireless components in order to communicate with a stationary or a mobile unit, via a WBAN. Although integration of wireless technologies to such devices has many benefits, it also presents many challenges, including enabling the secure transmission of the collected private data, prevention of electromagnetic interference between different wireless devices and compatibility with the remaining circuitry, as well as compatibility with, and safety of, the biological tissues.

Secure transmission of private medical data needs to be ensured, during both WBAN transmissions and during the submission of the data to the cloud or healthcare provider through the Internet or cellular network. Although the requirements for security and privacy of medical data are high, other constraints (such as low power requirements) on wireless health monitoring systems place limits on what can be achieved on-body. Different system architectures have been proposed in the literature. In a recent study, the security of a remote cardiac monitoring system was analysed [82]. In this paper, data transfer was modelled from the sensors to the BAN gateway, then to a wireless router and through the Internet to the monitoring server. Data collection and processing was performed in the gateway, thus memory and power requirements were high. The gateway also included two types of wireless communication: a receiver for data collection from on-body/implantable sensors and a wirless local area network (WLAN) adapter to submit the processed medical data to the wireless router. The decision unit was the monitoring server, where the collected data was profiled: if the data indicated a critical case, the unit would activate an alarm.

In [82], off-the-shelf products were used for the sensor nodes, the electrode patches, the gateway 802.11 module and the commercial server with proper storage and feedback system. The proposed wireless architecture is prone to two major security threats; the system is vulnerable during the routine usage by the

patient and it is vulnerable to attacks during the transmission of the data to authorized personnel (such as the health care provider) through the web portal. During the transmission of collected data from on-body sensors, intruders could potentially attack from an unauthorized source and manipulate the vital signs data; alternatively, a denial-of-service attack could be used to prevent the collection of the sensor data by the WBAN gateway. This could cause a misinterpretation of the vital signs data and might generate a false alarm or the failure to detect a critical situation, such as a heart attack. The second vulnerability is at the link between the WBAN to the (Internet-based) monitoring server. This again could take many forms, including denial-of-service attacks and the unauthorized access to the medical data of the patient, violating privacy and confidentiality; one method might be through social engineering by targeting the healthcare providers.

Another study illustrates the privacy violation issues with different scenarios [83]. The scenarios includes the protection of the patient's rights to protect his own healthcare record, the privacy of the healthcare provider and the restrictions on the patient to access his own information due to the purpose of the treatment. The study also illustrates the role context may have in privacy protection of both healthcare provider and patient, such as location information. The development of a secure health information acquisition and distribution architecture is vital for the reliable usage of pervasive mobile healthcare systems.

2.2.5 Bio-compatibility and Electromagnetic Safety

The interaction between devices emitting electromagnetic waves is highly investigated in the literature. It is well-known that such devices can cause electromagnetic interference (EMI). Recently, a study on the effect of EMI to wireless healthcare devices was performed and the possible EMI scenarios investigated [84]. An example of EMI is the interaction between high priority medical devices, such as insulin pumps, and RFID tags which are used in hospitals in order to identify the blood or urine samples. If the insulin pump is exposed to an RFID signal at 915 MHz, it injects the insulin without the need of it. This effect

presents a high risk for diabetes patients. While there are several regulations that address the allowed levels of EMI between such devices, there are still areas where more can be done. Patients relying on implantable devices, such as insulin pumps and cardiac pacemakers, are still vulnerable to such effects.

Implantable sensors can be used either for diagnosis or sensing purposes (such as implantable antennas [85, 86]), or as life support agents (such as cardiac pacemakers, drug pumps, needle-type invasive blood glucose monitoring devices and neuron stimulators). Besides the power and small size requirements, implantable devices also need to be compatible with biological tissues in order to prevent possible infection and rejection of the device by the biological tissue. Usually, implantable devices should be covered with bio-compatible materials, such as medical-grade silicon; alternatively, bio-compatible materials should be used instrinsically during the production of the implantable device. In a recent study, stens, a bio-compatible material approved by FDA, was used as a radiating structure for wireless telemetry purposes [87]. A dipole antenna was built by using stens to acquire cardiac-related data, such as blood pressure, by integrating the dipole to an implantable haemo-dynamic monitor by Medtronic. The dipole operated at 5 GHz and had a total length of 30 mm. The antenna was first simulated with HFSS, encased in a muscle 'box'; *ex-vivo* measurements were also taken by immersing the dipole into a saline solution, simulating the electrolyte balance of the blood. Finally, *in-vivo* measurements were taken by implanting the dipole into a pig. The signals were received from the implanted stens-based dipole using a horn antenna; this proved the possibility of the usage of stens-based antennas for body telemetry.

Compared to implantable devices, on-body devices are less prone to the biocompatibility constraint. However, long-term skin contact with such devices can cause different forms of skin irritations. A popular example of this is the previously described $Ag - Cl$ electrode for cardiac monitoring. The adhesive gel used to ensure a good electrical contact usually causes skin irritation when used for a long time. Thus, on-body devices should either also be developed with biocompatible materials, or on-body devices should be truly non-invasive, where no skin contact is required for the acquisition of the desired data (this implies the

embedding of the on-body device into some wearable structure and material that can act as a protective layer to the skin).

2.3 Conclusions

In this chapter, the evolution of wearable systems for chronic disease management has been discussed, with examples drawn from the literature. An evaluation of current sensing technologies has been provided for the major physiological parameters (the vital signs), as well as a review of on-body communication from an electromagnetic perspective. Current sensors technology for vital sign monitoring is promising to alter the traditional chronic monitoring routine. However, designing non-invasive body-worn sensors is very challenging, often requiring a broad understanding of the nature of the disease and its effect on physiological parameters. Although there are sensors available off-the-shelf for cardiac and blood-pressure monitoring, there is still a need for improvement to achieve continuous and truly non-invasive monitoring of these parameters. The main constraints for sensor design are:

- low power requirements;
- reliability;
- security; and
- conformal design.

In order to achieve unobtrusive monitoring, implementation of wireless modules is vital. Integration of wireless modules to on-body sensors not only provides mobility for the patient, but also has the potential to change the conventional healthcare system with real-time feedback support. The limitations for wireless modules are low power requirements, reliable data transmission, compatibility with the sensor, and conformal antenna design. Although wireless protocols are available for on-body communication, there is still a need for development, in order to ease the existing constraints. It is hoped that the efforts of the IEEE 802.15.6 Task Group will bear fruit in this area.

Although the design and implementation of on-body monitoring systems presents a challenging task with several constraints, the benefits of employing multi-parameter monitoring systems for the prevention, prediction, and management of diseases are myriad. On-body monitoring systems with multiple sensors are not only capable of providing an extensive database of the patient's medical history: the simultaneous usage of multi-parameter monitoring sensors can also verify or correct the collected data, adding redundancy into a potentially safety-critical system; or the additional information can place a particular event detected into context. For example, the previously mentioned blood pressure monitoring system in [23] can be used in combination with ECG monitoring device for acquired data verification purposes: if there is a failure in the electronic circuitry or software of the cardiac-activity monitoring system, blood pressure monitoring device can be used instead, in particular for critically ill out-patients. Another example where a multi-parameter monitoring system could bring benefits is the combination of a blood-pressure monitor and blood-glucose level monitor: the BP monitor could provide context (in the form of blood flow rate differences) for the calculation of BGL by the BGL sensor, leading to improvements in the accuracy of the measurement. On the other hand, there may be alternative interpretations of certain symptoms (that is, there may be more than one cause) that could be more easily resolved given more information; for instance, a (sudden) drop in blood-sugar levels would be of more concern if the patient had been relatively inactive, compared to if the system had detected an increase in physical activity. Thus, multi-parameter monitoring systems will be more reliable and useful, compared to single-parameter monitoring devices.

References

[1] R. Wijesiriwardana, K. Mitcham, and T. Dias, "Fibre-meshed transducers based real time wearable physiological information monitoring system," in *Wearable Computers, 2004. ISWC 2004. Eighth International Symposium on*, vol. 1, oct.-3 nov. 2004, pp. 40 – 47.

[2] C. Mundt, K. Montgomery, U. Udoh, V. Barker, G. Thonier, A. Tellier, R. Ricks, R. Darling, Y. Cagle, N. Cabrol, S. Ruoss, J. Swain, J. Hines, and G. Kovacs, "A multiparameter wearable physiologic monitoring system for space and terrestrial applications," *Information Technology in Biomedicine, IEEE Transactions on*, vol. 9, no. 3, pp. 382 –391, sept. 2005.

[3] K. Malhi, S. Mukhopadhyay, J. Schnepper, M. Haefke, and H. Ewald, "A zigbee-based wearable physiological parameters monitoring system," *Sensors Journal, IEEE*, vol. 12, no. 3, pp. 423 –430, march 2012.

[4] P. S. Hall and Y. Hao, *Antennas and Propagation for Body-Centric Wireless Networks*. Artech House, 2006, iSBN 1-58053-493-7.

[5] A. Pedro and C. Binotto, D.and Pereira, "Improving preventive healthcare with high-tech telemedicine models," *Computing Now*, 2012. [Online]. Available: http://goo.gl/zVTjw4

[6] S. Nukaya, T. Shino, Y. Kurihara, K. Watanabe, and H. Tanaka, "Noninvasive bed sensing of human biosignals via piezoceramic devices sandwiched between the floor and bed," *Sensors Journal, IEEE*, vol. 12, no. 3, pp. 431 –438, march 2012.

[7] K. Khalfallah, H. Ayoub, J. Calvet, X. Neveu, P. Brunswick, S. Griveau, V. Lair, M. Cassir, and F. Bedioui, "Noninvasive galvanic skin sensor for early diagnosis of sudomotor dysfunction: Application to diabetes," *Sensors Journal, IEEE*, vol. 12, no. 3, pp. 456 –463, march 2012.

[8] H.-R. Chuang, H.-C. Kuo, F.-L. Lin, T.-H. Huang, C.-S. Kuo, and Y.-W. Ou, "60-ghz millimeter-wave life detection system (mlds) for noncontact human vital-signal monitoring," *Sensors Journal, IEEE*, vol. 12, no. 3, pp. 602 –609, march 2012.

[9] Y. Hao and R. Foster, "Wireless body sensor networks for health-monitoring applications," *Physiological Measurement*, vol. 29, no. 11, p. R27, 2008. [Online]. Available: http://stacks.iop.org/0967-3334/29/i=11/a=R01

[10] J. D. Newman and A. P. F. Turner, "Home blood glucose biosensors: a commercial perspective," *Biosensors and Bioelectronics*, vol. 20, pp. 2435–2453, 2005. [Online]. Available: http://dx.doi.org/10.1016/j.bios.2004.11.012

[11] K. L. Ong, "Prevalence, awareness, treatment, and control of hypertension among united states adults 19992004," *Hypertension*, vol. 49, p. 6975, 2006. [Online]. Available: http://hyper.ahajournals.org/content/49/1/69

[12] C. Y. Myung K. Park, Shirley W. Menard, "Comparison of auscultatory and oscillometric blood pressures," *Hypertension*, vol. 155, p. 5053, 2001.

[13] T. G. Pickering, D. Shimbo, and D. Hass, "Ambulatory blood-pressure monitoring," *The New England Journal of Medicine*, vol. 354, no. 22, pp. 2368–2374, 2006.

[14] J. C. T. B. Moraes, M. Cerulli, and P. Ng, "A strategy for determination of systolic, mean and diastolic blood pressures from oscillometric pulse profiles," in *Computers in Cardiology 2000*, 2000, pp. 211–214.

[15] K. G. Belani, J. J. Buckley, and M. O. Poliac, "Accuracy of radial artery blood pressure determination with the Vasotrac," *Canadian Journal of Anesthesia*, vol. 46, no. 5, pp. 488–496, 1999, 10.1007/BF03012951. [Online]. Available: http://dx.doi.org/10.1007/BF03012951

[16] M. E. McCann, D. Hill, K. C. Thomas, D. Zurakowski, and P. C. Laussen, "A comparison of radial artery blood pressure determination between the Vasotrac device and invasive arterial blood pressure monitoring in adolescents undergoing scoliosis surgery," *Anesthesia and Analgesia*, pp. 978–985, 2005.

[17] D. L. Franklin, W. Schlegel, and R. F. Rushme, "Blood flow measured by doppler frequency shift of back-scattered ultrasound," *Science*, vol. 134, no. 3478, pp. 564–565, 1961.

[18] A. M. Elseed, E. A. Shinebourne, and M. C. Joseph, "Assessment of techniques for measurement of blood pressure in infants and children," *Disease in Childhood*, vol. 48, pp. 932–936, 1973.

[19] B. Gribbin, A. Steptoe, and P. Sleight, "Pulse wave velocity as a measure of blood pressure change," *Psychophysiology*, vol. 3, no. 1, pp. 86–90, 1976.

[20] C. C. Y. Poon and Y. T. Zhang, "Cuff-less and noninvasive measurements of arterial blood pressure by pulse transit time," in *27th IEEE Int. Conf of Eng. in Med. and Biol. Soc., Shanghai, PRC*, 2005.

[21] C. C. Y. Poon, Y. M. Wong, and Y. T. Zhang, "M-health: The development of cuff-less and wearable blood pressure meters for use in body sensor networks," in *IEEE/NLM Life Science Systems and Applications Workshop*, 2006, pp. 1–2.

[22] A. Shaltis, P Reisner and H. Asada, "Wearable, cuff-less PPG-based blood pressure monitor with novel height sensor," in *28th Annual International Conference of the IEEE Engineering in Medicine and Biology Society.*, Aug. 2006, pp. 908–911.

[23] P. Shaltis, T. Reisner, and H. Asada, "Calibration of the photoplethysmogram to arterial blood pressure: Capabilities and limitations for continuous pressure monitoring," in *27th Annual International Conference of the IEEE-EMBS*, Jan. 2005, pp. 3970–3973.

[24] P. A. Shaltis, A. T. Reisner, and H. H. Asada, "Cuffless blood pressure monitoring using hydrostatic pressure changes," *IEEE Transactions on Biomedical Engineering*, vol. 55, no. 6, pp. 1775–1777, Jun. 2008.

[25] "Medtronic inc." [Online]. Available: http://www.medtronic.com/our-therapies/diabetes-management/index.htm

[26] P. Vadgama, Y. Hao, and R. Foster, "Wireless Implantable Sensors with Advanced On-Body Data Processing: NEAT Project FSE031 Final Report," Queen Mary, University of London, Mile End Road, Mile End, London, E1 4NS, UK, Tech. Rep., 2009, funded under the NEAT programme by the NHS National Institute for Health Research, UK; grant number FSE031. URL: http://www.nihr-ccf.org.uk.

[27] A. Sieg, R. H. Guy, and M. B. Delgado-Charro, "Noninvasive and minimally invasive methods for transdermal glucose monitoring," *Diabetes Technology and Therapeutics*, vol. 7, no. 1, pp. 174–197, 2005. [Online]. Available: http://www.liebertonline.com/doi/abs/10.1089/dia.2005.7.174

[28] N. S. Oliver, C. Toumazou, A. E. G. Cass, and D. G. Johnston, "Glucose sensors: a review of current and emerging technology," *Diabetic Medicine*, vol. 26, no. 3, p. 197210, 2009.

[29] Y. Hayashi, L. Livshits, A. Caduff, and Y. Feldman, "Dielectric spectroscopy study of specific glucose influence on human erythrocyte membranes," *Journal of Physics D: Applied Physics*, vol. 36, no. 4, pp. 369–374, 2003. [Online]. Available: http://stacks.iop.org/0022-3727/36/i=4/a=307

[30] T. A. Hillier, R. D. Abbott, and E. J. Barrett, "Hyponatremia: Evaluating the correction factor for hyperglycemia," *Am. J. Med.*, vol. 106, no. 4, pp. 399–403, 1999.

[31] A. Caduff and Y. Feldman, "Method and a device for measuring glucose," u.S. Patent 11/070,853, 27 Feb 2007.

[32] A. Caduff, M. Donath, M. Talary, S. Haug, D. Huber, W. A. Stahel, F. Dewarrat, L. S. Jonasson, H.-J. Krebs, and J. Klisic, "Multisensor concept for non-invasive physiological monitoring," in *Instrumentation and Measurement Technology Conference Proceedings, 2007. IMTC 2007. IEEE*, May. 2007, pp. 1–4.

[33] A. Caduff, M. S. Talary, M. Mueller, F. Dewarrat, J. Klisic, M. Donath, L. Heinemann, and W. A. Stahel, "Non-invasive glucose monitoring in patients with Type 1 diabetes: A Multisensor system combining sensors for dielectric and optical characterisation of skin," *Biosensors and Bioelectronics*, vol. 24, no. 9, pp. 2778–2784, Sept. 2009.

[34] E. Topsakal, E. C. Moreland, T. Karacolak, and M. Acar, "The impact of glucose concentration in blood plasma on relative dielectric constant and conductivity," in *National Science Meeting URSI*, 2008.

[35] C. Hancock and S. Chaudhry, "A non-invasive monitoring system," in *European Microwave Conference, 2007*, Oct. 2007, pp. 313–316.

[36] C. P. Hancock, "A non-invasive monitoring system," G.B. Patent 2428093, Jan. 17, 2007.

[37] B. Jean, E. Green, and M. McClung, "A microwave frequency sensor for non-invasive blood-glucose measurement," in *Sensors Applications Symposium, 2008. SAS 2008. IEEE*, Feb. 2008, pp. 4–7.

[38] Y. Nikawa and T. Michiyama, "Non-invasive measurement of blood-sugar level by reflection of millimeter-waves," in *Microwave Conference, 2006. APMC 2006. Asia-Pacific*, Dec. 2006, pp. 47–50.

[39] N. Y. and M. T., "Blood-sugar monitoring by reflection of millimeter wave," in *Microwave Conference, 2007. APMC 2007. Asia-Pacific*, Dec. 2007, pp. 1–4.

[40] M. A. Arnold, J. J. Burmeister, and G. W. Small, "Phantom glucose calibration models from simulated noninvasive human near-infrared spectra," *Analytical Chemistry*, vol. 70, no. 9, pp. 1773–1781, 1998. [Online]. Available: http://pubs.acs.org/doi/abs/10.1021/ac9710801

[41] I. Barman, G. P. Singh, R. R. Dasari, and M. S. Feld, "Turbidity-corrected raman spectroscopy for blood analyte detection," *Analytical Chemistry*, vol. 81, no. 11, pp. 4233–4240, 2009, pMID: 19413337. [Online]. Available: http://pubs.acs.org/doi/abs/10.1021/ac8025509

[42] I. Barman, C.-R. Kong, G. P. Singh, R. R. Dasari, and M. S. Feld, "Accurate spectroscopic calibration for noninvasive glucose monitoring by modeling the physiological glucose dynamics," *Analytical Chemistry*, vol. 82, no. 14, pp. 6104–6114, 2010. [Online]. Available: http://pubs.acs.org/doi/abs/10.1021/ac100810e

[43] P. J. Zimetbaum and M. E. Josephson, "The Evolving Role of Ambulatory Arrhythmia Monitoring in General Clinical Practice," *Annals of Internal Medicine*, vol. 130, no. 10, pp. 848–856, 1999. [Online]. Available: http://www.annals.org/content/130/10/848.abstract

[44] G. E. Bergey, R. D. Squires, and W. C. Sipple, "Electrocardiogram recording with pasteless electrodes," *Biomedical Engineering, IEEE Transactions on*, vol. BME-18, no. 3, pp. 206–211, May. 1971.

[45] A. Searle and L. Kirkup, "A direct comparison of wet, dry and insulating bioelectric recording electrodes," *Physiological Measurement*, vol. 21, no. 2, pp. 271–283, 2000. [Online]. Available: http://stacks.iop.org/0967-3334/21/i=2/a=307

[46] J. Muhlsteff and O. Such, "Dry electrodes for monitoring of vital signs in functional textiles," in *Engineering in Medicine and Biology Society, 2004. IEMBS '04. 26th Annual International Conference of the IEEE*, vol. 1, Sept. 2004, pp. 2212–2215.

[47] Y. M. Chi and G. Cauwenberghs, "Wireless non-contact EEG/ECG electrodes for body sensor networks," in *Body Sensor Networks (BSN), 2010 International Conference on*, Jun. 2010, pp. 297–301.

[48] R. Matthews, N. J. McDonald, I. Fridman, P. Hervieux, and T. Nielsen, "The invisible electrode zero prep time, ultra low capacitive sensing," in *Proceedings of the 11th International Conference on Human-Computer Interaction*, 2005.

[49] A. D. Droitcour, O. Boric-Lubecke, V. M. Lubecke, J. Lin, and G. T. A. Kovacs, "Range correlation and I/Q performance benefits in single-chip silicon Doppler radars for noncontact cardiopulmonary monitoring," *Microwave Theory and Techniques, IEEE Transactions on*, vol. 52, no. 3, pp. 838–848, Mar. 2004.

[50] A. Matsubara and S. Tanaka, "Unconstrained and noninvasive measurement of heartbeat and respiration for drivers using a strain gauge," in *SICE 2002. Proceedings of the 41st SICE Annual Conference*, vol. 2, Aug. 2002, pp. 1067–1068.

[51] J. W. Jeong, Y. W. Jang, I. Lee, S. Shin, and S. Kim, "Wearable respiratory rate monitoring using piezo-resistive fabric sensor," in *World Congress on Medical Physics and Biomedical Engineering, September 7 - 12, 2009, Munich, Germany*, ser. IFMBE Proceedings, R. Magjarevic, J. H. Nagel, O. Dössel, and W. C. Schlegel, Eds. Springer Berlin Heidelberg, Sept. 2009, vol. 25/5, pp. 282–284, 10.1007/978-3-642-03904-1_78. [Online]. Available: http://dx.doi.org/10.1007/978-3-642-03904-1_78

[52] S. Karki and J. Lekkala, "Film-type transducer materials PVDF and EMFi in the measurement of heart and respiration rates," in *Engineering in Medicine and Biology Society, 2008. EMBS 2008. 30th Annual International Conference of the IEEE*, Aug. 2008, pp. 530–533.

[53] P. Grossman, *Wearable eHealth Systems for Personalised Health Management: State of the Art and Future Challenges*, ser. Studies in Health Technology and Informatics. IOS Press, 2004, vol. 108, ch. The LifeShirt: A Multi-Function Ambulatory System Monitoring Health, Disease, and Medical Intervention in the Real World, pp. 133–141. [Online]. Available: http://iospress.metapress.com/content/JW4EPH0HPU5CAH7R

[54] R. Paradiso, G. Loriga, and N. Taccini, "A wearable health care system based on knitted integrated sensors," *Information Technology in Biomedicine, IEEE Transactions on*, vol. 9, no. 3, pp. 337–344, Sept. 2005.

[55] U. Anliker, J. Ward, P. Lukowicz, G. Troster, F. Dolveck, M. Baer, F. Keita, E. Schenker, F. Catarsi, L. Coluccini, A. Belardinelli, D. Shklarski, M. Alon, E. Hirt, R. Schmid, and M. Vuskovic, "AMON: a wearable multiparameter medical monitoring and alert system," *Information Technology in Biomedicine, IEEE Transactions on*, vol. 8, no. 4, pp. 415–427, Dec. 2004.

[56] P. Lukowicz, U. Anliker, J. Ward, G. Troster, E. Hirt, and C. Neufelt, "AMON: a wearable medical computer for high risk patients," in *Wearable Computers, 2002. (ISWC 2002). Proceedings. Sixth International Symposium on*, 2002, pp. 133–134.

[57] Bodymedia, Inc. URL: http://www.bodymedia.com/.

[58] Escort Guardian, Invivo Research, Inc. URL: http://www.invivoresearch.com/.

[59] Micropaq, Wellch Allyn, Inc. URL: http://www.monitoring.welchallyn.com/.

[60] Sensatex 2007, URL:http://www.sensatex.com.

[61] J. Weber, D. Blanc, A. Dittmar, B. Comet, C. Corroy, N. Noury, R. Baghai, S. Vaysse, and A. Blinowska, "Vtam - a new "biocloth" for ambulatory telemonitoring," in *Information Technology Applications in Biomedicine, 2003. 4th International IEEE EMBS Special Topic Conference on*, Apr. 2003, pp. 299 – 301.

[62] T. G. Zimmerman, "Personal area networks: Near-field intrabody communication," *IBM Systems Journal*, vol. 35, no. 3.4, pp. 609 –617, 1996.

[63] M. Okoniewski and M. Stuchly, "A study of the handset antenna and human body interaction," *Microwave Theory and Techniques, IEEE Transactions on*, vol. 44, no. 10, pp. 1855 –1864, Oct. 1996.

[64] M. Okoniewski and M. A. Stuchly, "Fdtd analysis of the handset antenna and human body interaction," in *Antennas and Propagation Society International Symposium, 1996. AP-S. Digest*, vol. 3, Jul. 1996, pp. 1668 –1673 vol.3.

[65] S. Amos, M. Smith, and D. Kitchener, "Modelling of handset antenna interactions with the user and sar reduction techniques," in *Antennas and Propagation, 1999. IEE National Conference on.*, Aug. 1999, pp. 12 –15.

[66] P. Vainikainen, J. Ollikainen, O. Kivekas, and K. Kelander, "Resonator-based analysis of the combination of mobile handset antenna and chassis," *Antennas and Propagation, IEEE Transactions on*, vol. 50, no. 10, pp. 1433 – 1444, Oct. 2002.

[67] O. Saraereh, M. Jayawardene, P. McEvoy, and J. Vardaxoglou, "Quad-band handset antenna operation for gsm900/dcs1800/pcs1900/umts," in *Wideband and Multi-band Antennas and Arrays, 2005. IEE (Ref. No. 2005/11059)*, Sep. 2005, pp. 129 – 133.

[68] W. Krzysztofik, "Meandered double-pifa antenna - handset / human interaction," in *Microwaves, Radar Wireless Communications, 2006. MIKON 2006. International Conference on*, May. 2006, pp. 119 –122.

[69] T. Cho, S. Nam, and H. Lee, "Penta-band internal antenna for mobile handset," in *Microwave Conference, 2009. APMC 2009. Asia Pacific*, Dec. 2009, pp. 2699 –2702.

[70] M. Ur Rehman, Y. Gao, Z. Wang, J. Zhang, Y. Alfadhl, X. Chen, C. Parini, Z. Ying, and T. Bolin, "Investigation of on-body bluetooth transmission," *Microwaves, Antennas Propagation, IET*, vol. 4, no. 7, pp. 871 –880, Jul. 2010.

[71] X.-F. Teng, Y.-T. Zhang, C. Poon, and P. Bonato, "Wearable medical systems for p-health," *Biomedical Engineering, IEEE Reviews in*, vol. 1, pp. 62 –74, 2008.

[72] A. Pantelopoulos and N. Bourbakis, "A survey on wearable sensor-based systems for health monitoring and prognosis," *Systems, Man, and Cybernetics, Part C: Applications and Reviews, IEEE Transactions on*, vol. 40, no. 1, pp. 1 –12, Jan. 2010.

[73] P. Soontornpipit, C. Furse, and Y. C. Chung, "Design of implantable microstrip antenna for communication with medical implants," *Microwave Theory and Techniques, IEEE Transactions on*, vol. 52, no. 8, pp. 1944 – 1951, Aug. 2004.

[74] T. Karacolak, A. Hood, and E. Topsakal, "Design of a dual-band implantable antenna and development of skin mimicking gels for continuous glucose monitoring," *Microwave Theory and Techniques, IEEE Transactions on*, vol. 56, no. 4, pp. 1001 –1008, Apr. 2008.

[75] A. Alomainy, Y. Hao, and D. Davenport, "Parametric study of wearable antennas with varying distances from the body and different on-body positions," in *Antennas and Propagation for Body-Centric Wireless Communications, 2007 IET Seminar on*, Apr. 2007, pp. 84 –89.

[76] H. Khaleel, H. Al-Rizzo, D. Rucker, and T. Elwi, "Wearable yagi microstrip antenna for telemedicine applications," in *Radio and Wireless Symposium (RWS), 2010 IEEE*, Jan. 2010, pp. 280 –283.

[77] A. Traille, L. Yang, A. Rida, and M. Tentzeris, "A novel liquid antenna for wearable bio-monitoring applications," in *Microwave Symposium Digest, 2008 IEEE MTT-S International*, Jun. 2008, pp. 923 –926.

[78] Y. Nechayev, P. Hall, I. Khan, and C. Constantinou, "Wireless channels and antennas for body-area networks," in *Wireless On-demand Network Systems and Services (WONS), 2010 Seventh International Conference on*, Feb. 2010, pp. 137 –144.

[79] Y. Zhao, A. Sani, Y. Hao, S. Lee, and G. Yang, "A subject-specific radio propagation study in wireless body area networks," in *Antennas Propagation Conference, 2009. LAPC 2009. Loughborough*, Nov. 2009, pp. 80 –83.

[80] A. Alomainy, Y. Hao, X. Hu, C. Parini, and P. Hall, "Uwb on-body radio propagation and system modelling for wireless body-centric networks," *Communications, IEE Proceedings-*, vol. 153, no. 1, pp. 107 – 114, Feb. 2006.

[81] Q. Abbasi, A. Sani, A. Alomainy, and Y. Hao, "Arm movements effect on ultra wideband on-body propagation channels and radio systems," in *Antennas Propagation Conference, 2009. LAPC 2009. Loughborough*, Nov. 2009, pp. 261 –264.

[82] S. Lim, T. H. Oh, Y. Choi, and T. Lakshman, "Security issues on wireless body area network for remote healthcare monitoring," Jun. 2010, pp. 327 –332.

[83] S. Ahamed, N. Talukder, and A. Kameas, "Towards privacy protection in pervasive healthcare," Sep. 2007, pp. 296 –303.

[84] D. Witters, S. Seidman, and H. Bassen, "EMC and wireless healthcare," Apr. 2010, pp. 5 –8.

[85] T. Chien, C. Cheng, H. Yang, and C. Luo, "Develop implantable ceramic antennas with no superstrate," Jul. 2010, pp. 1 –4.

[86] C.-M. Lee, T.-C. Yo, F.-J. Huang, and C.-H. Luo, "Dual-resonant x003c0;-shape with double l-strips pifa for implantable biotelemetry," *Electronics Letters*, vol. 44, no. 14, pp. 837 –838, Jul. 2008.

[87] E. Chow, B. Beier, Y. Ouyang, W. Chappell, and P. Irazoqui, "High frequency transcutaneous transmission using stents configured as a dipole radiator for cardiovascular implantable devices," Jun. 2009, pp. 1317 –1320.

Chapter 3

Tissue Mimicking Phantoms

Microwave resonators, antennas, and radio frequency (RF) devices, operating in the in-body and on-body environment, should be designed and tested considering lossy tissue surroundings. The dielectric properties of the biological medium, namely the key parameters to represent the medium during the design and testing of RF/microwave devices, are now widely available [1, 2, 3, 4]. Such data enabled researchers to replicate the lossy media during the numerical simulations of RF/microwave devices in electromagnetic simulation softwares and during testing of the proposed devices.

Within the past several decades, with the emergence of microwave and RF medical applications, the need for early stage testing of such devices has emerged. Until recently, such studies have been limited to numerical simulations. However, digital phantoms used in such simulation softwares are typically either homogeneous, or of low resolution [5, 6]. With the wide deployment of commercial ultra-wideband dielectric spectroscopy techniques, many different tissue phantom (TPh) physical materials have been proposed in the literature as an initial step to verify the proper functioning of RF or microwave devices [7, 8, 9]. Reported TPh materials can be classified based on different parameters such as frequency

of interest, tissue type, and matter state of the phantom. Throughout this thesis, the physical phantom materials are categorized based on the sate of the matter.

In this chapter, liquid and semi-solid phantom materials are presented. The liquid, and some of the proposed semi-solid phantoms presented are not intended to mimic the dielectric properties of biological tissues. Such phantoms are utilized to represent the lossy environment in order to assess the dielectric property dependance of the spiral resonator response, presented in Chapter 4. The intention is to investigate the behaviour of the proposed resonator in lossy environment. This chapter also presents novel recipes for semi-solid oil-in-gelatin dispersion TPh materials that are mimicking dielectric properties of biological tissues for an ultra-wide frequency band (0.3 to 20 GHz). Note that, throughout this thesis, wideband refers to 0.3 to 3 GHz, narrowband refers to MICS or ISM bands, and ultra-wide band refers to 0.3 to 20 GHz.The proposed TPh materials are produced by using off-the-shelf ingredients and the production lasted 2 hours. Then the characterized phantoms left to solidify overnight in room temperature. The proposed tissue mimicking phantoms are characterised by using few off-the-shelf ingredients; thus, the proposed phantoms can easily be replicated comparing to the previously proposed phantoms in the literature. The production time of the phantom is also shorter comparing to the previously proposed phantom materials.

The limitation of the proposed phantoms is as the water content of the tissue is increased the root mean square error between the proposed phantom dielectric properties and the tissue dielectric properties given in literature is increasing. This is due to the dispersion mechanism of the water. Mimicking the high variation of dielectric properties over a wide frequency range is challenging. Although the proposed phantoms is able to mimic the dielectric properties of high water content tissues within an acceptable error range, there is still a need to investigate the other materials/methods for phantom production to decrease the error.

This chapter is organized as follows: Section 3.1 presents the background of liquid and semi-solid phantom types used for testing the RF/microwave devices, while the probes used for dielectric spectroscopy are described in Section 3.2. Section 3.3 provides the recipes and dielectric property measurement results of

the liquid phantoms. The dielectric spectroscopy results and recipes for non-tissue-mimicking semi-solid phantoms are given in Section 3.4. Recipes for tissue mimicking materials, along with the dielectric property comparison with the literature data, is given in Section 3.5. Finally, conclusions are drawn in Section 3.6.

3.1 Background

Testing of on-body and implantable devices with animal or human subjects is a costly task, requiring approval from ethical committees and specific facilities to perform such experiments [10, 11]. However, preliminary tests can be performed with phantoms to verify the proper functioning of antennas and microwave devices [12, 13, 14]. Different types of phantoms are used in the literature, including digital phantoms to investigate on-body communications, physical phantoms to test the implantable antennas, hyperthermia, and for medical imaging (for example, microwave breast cancer and ultrasound imaging) purposes [15, 16, 17, 18, 19, 20].

Characterizing physical phantoms is a cumbersome task, requiring consideration of many parameters, such as the operation frequency, type of tissue, geometry, thickness, homogeneity, and degradation [21, 22]. Among different types of physical phantoms, we are focusing on characterisation of liquid and semi-solid (gel-like) phantoms, since the liquid and semi-solid phantoms are the simplest and inexpensive, as well as effective forms of physical phantoms.

The liquid phantoms in the literature have been extensively used for specific absorbtion rate *(SAR)* measurements [23, 24, 25]. The liquid phantom is designed to mimic the dielectric properties of the tissue of interest and encapsulated with a thin shell which has low dielectric properties. Dielectric property limits for the encapsulating shell have been given in the literature [26, 27]: the relative permittivity should be less than 5 and the dissipation factor should be less than 0.05. For SAR measurements the electric field distribution is measured with probes and often by drilling the shell at the point of interest to insert the probe. Although liquid phantoms are effective when mapping a field distribution inside the body, collecting measurements from surface points is challenging due to the physical

limitations. In addition, by using liquid phantoms, the body is assumed to be homogeneous; thus, liquid phantoms are arguably most suitable for feasibility and other early stage studies.

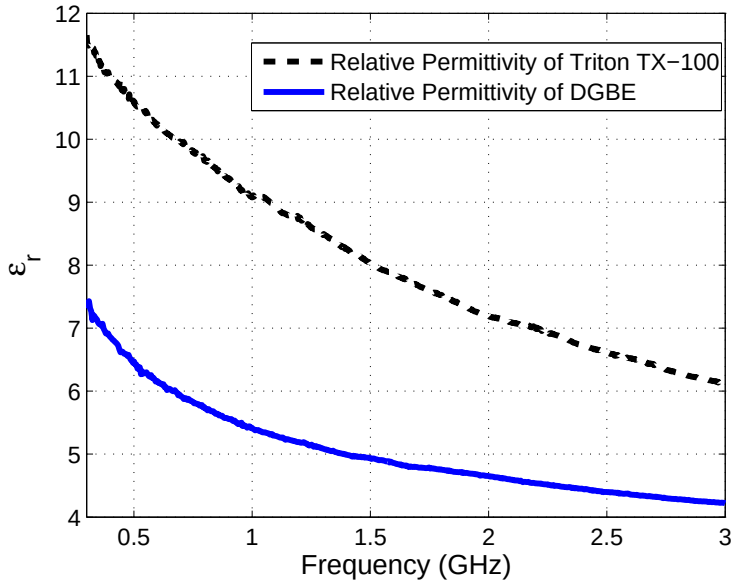

(a)

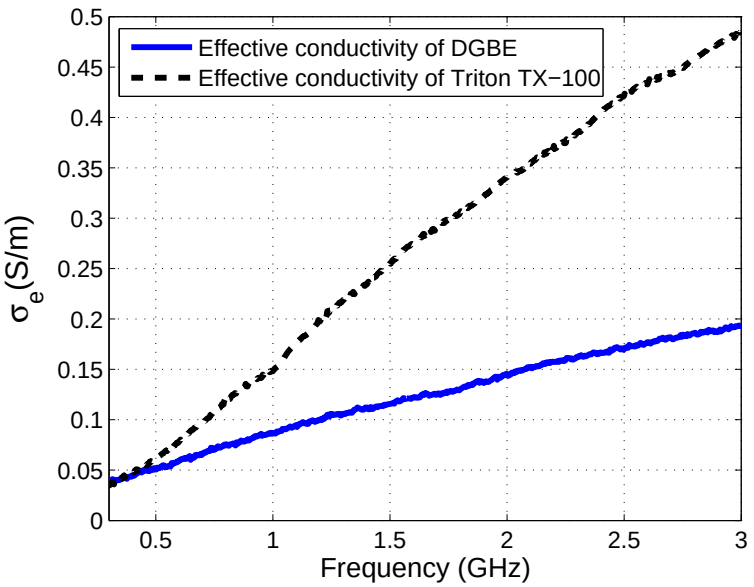

(b)

Figure 3.1: Dielectric property measurements of liquids: (a) Relative permittivity of the Triton TX-100 and DGBE; (b) effective conductivity of the Triton TX-100 and DGBE [8].

In addition to SAR measurements, the liquid phantoms can be used for testing of implantable antennas. In [17], a liquid phantom was developed to test a dual

band implantable antenna. The antenna was designed to operate under the skin; thus, it was tested with a skin mimicking material that emulated the dielectric properties of the skin_{wet} tissue in the 2.45 GHz ISM band (2.45-2.48 GHz). The skin mimicking material is characterized by using diethylene glycol butyl ether (DGBE) which is a type of glycol ether and used primarily as a solvent in coatings, inks, cleaners, and specialty fluids [28], Triton TX-100 which is a nonionic surfactant primarily used in detergents [29], sodium chloride (NaCl), and distilled water. Similarly, in [30], a MICS (402-405 MHz) band implantable antenna was tested with a head tissue simulating liquid phantom composed of distilled water, sugar, NaCl, and cellulose with the dielectric properties of $\varepsilon = 49.6$ and $\sigma = 0.51$ S/m at 402 MHz (very close to skin tissue properties). Note that the liquid phantoms in the literature are generally proposed to mimic the intermediate content tissues, such as skin tissue or high-water content tissues, suh as muscle. However, it could be possible to mimic the low-water content tissues, such as fat and bone, as some chemicals (DGBE and Triton TX100) can demonstrate low dielectric properties. Fig 3.1 shows the dielectric properties of DGBE and Triton from 0.3 to 3 GHz [8]. Liquid phantoms were also utilized in the literature for hyperthermia and microwave ablation [31, 32].

Semi-solid phantoms presents a more realistic representation of the complex nature of the human body; thus, the phantoms can be used at a later research stage, but before clinical experiments. Semi-solid phantoms are used to mimic both high-water and low-water content tissues in the literature [33, 34, 35, 36]. The high-water content tissues have high relative permittivity, such as blood, skin, and muscle. Conversely, the low-water content tissues have low relative permittivity. Fat tissue, having dielectric properties lower than 10, is a good example of low-water content tissues. Bone is another example of low-water content tissue. The application of semi-solid tissue mimicking materials presented in the literature include testing of microwave imaging techniques [37]. Semi-solid phantoms were also utilized to test ultrasound imaging devices [38]. Another application among reported studies is utilization of the semi-solid materials to map the electric field and associated temperature distribution in the body for

radio-frequency hyperthermia applications [39]. Semi-solid phantoms is also suitable for building anthropomorphic heterogenous phantoms [37]. Such phantoms enables the realistic verification of the proper functioning of RF or microwave devices. Conventionally, with the addition of preservatives (such as Proxel CRL, thimerosal), to prevent bacterial invasion, semi-solid phantoms can last from six weeks up to two years [34, 36, 40]. Some of the anthropomorphic heterogenous phantoms composed of semi-solid tissue mimicking materials can be taken apart and reassembled when the measurements are needed to be repeated or can be used for another measurement. The combination of the reasonable self-life, elasticity, low cost, and ease of fabrication make these phantoms a good candidate for pre-clinical studies.

Many different ingredients have been used to mimic the dielectric properties of biological tissues with semi-solid phantoms. The gelling agents proposed in the literature include TX-150 (commonly referred as *super stuff*), flour, agarose, carrageenan [41], polyacrylamide [42], and gelatine. TX-150 is chemically classified as an organic hydrate. It is most suitable when the phantom needs to be cut or reshaped, because TX-150 provides a re-healing cross-link with the dough like consistency [43]. Stable gelling can be obtained by using a minimum amount of 12% TX-150 [34]. Another commonly used solidifier is flour which is an off-the-shelf gelling agent. However, it is cumbersome to compose TPh materials with flour since a large amount od flour is needed to jellify any liquid [44]. The addition of the flour to water decreases the dielectric properties. Also flour TPh phantoms reacts with air very quickly thus the phantoms should be kept in air tight containers. An alternate coagulator is agarose which is usually available in white powder form. It is obtained from plants [45]. Agarose is dissolvable in water at 85°C; when cooled below 36°C, the mixture solidifies [46]. Agarose is an effective gelling agent; thus, a small amount of agarose is enough to form a gel-like material. Therefore, agarose does not affect the dielectric properties significantly [34, 47]. However, agarose gels are prone to water loss. Similarly, carrageenan is a plant based jellifying agent. Another commonly used congealing material is gelatine. Gelatine based tissue mimicking materials have been well-studied in the literature [48, 49, 50]. Gelatine is an animal based jellifying agent,

commonly obtained from calf skin or bones, that is commercially widely available in granular form [51]. Gelatine dissolves above 40°C, and water gelatine solutions usually solidify below 30°C. In this work, we are using gelatine as the congealing agent for the TPh phantoms. Additionally, flour is used to solidify the sugar phantoms in Section 3.4, for testing of spiral resonator proposed in Chapter 4.

In this chapter, we are proposing liquid, semi-solid, and semi-solid TPh materials. The recipes and the steps for characterization of such phantoms are shown along with the dielectric property measurements. Note that measurements for liquid phantoms were performed with the MCL probe and measurements for semi-solid TPh materials were performed with Agilent's high temperature dielectric probe.

3.2 Dielectric Probes

In this section, utilized dielectric spectroscopy instrumentations are described. Two types of probes have been used. The first probe is a slim open-ended coaxial probe, referred as MCL probe, used for measuring the dielectric properties of the liquid phantoms [52]. The second probe is Agilent's open-ended high temperature dielectric probe, utilized for measuring the dielectric properties of all semi-solid phantoms.

The MCL probe is a custom-made probe. It can only collect relative permittivity and effective conductivity data from 200 MHz to 5 GHz. Before collecting the dielectric properties of the liquid phantoms, the frequency range, the temperature, and the number of points is set. Next, the probe is calibrated with a three-step procedure. The procedure is as follows:

1. The probe tip was left open for air measurement;
2. The probe tip was then terminated with a foil-wrapped elastic block for short measurement;
3. The probe tip was then loaded by immersing it in de-ionized water for known load measurement.

After calibration, the measurements are taken with the liquid phantoms by immersing the probe into the solutions. One important experimental issue during the calibration and measurements is avoiding the air bubble that is likely to form at the tip of the probe when immersed into the liquid. In such cases, the air bubble was burst with a clean flexible wire during the measurements.

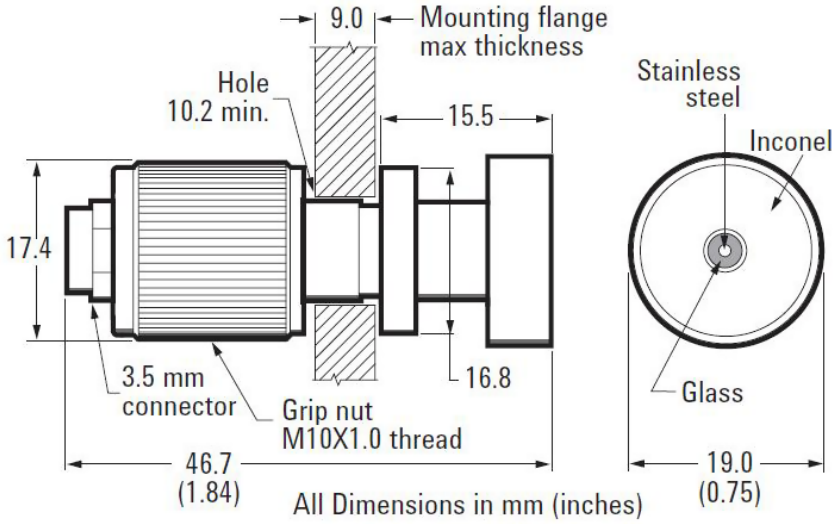

Figure 3.2: Dimensions of high temperature dielectric probe [53].

Agilent's open ended high temperature dielectric probe and the shorting block, shown in Chapter 1 Fig. 1.5 (c), was described in Section 1.4.1 [53]. The dielectric probe has a flange with a 19.0 mm diameter and the aperture size is 3.5 mm in diameter. The Immersible length of the probe is 35 mm; other dimensions of the probe are shown in Fig 3.2. Before calibration, the probe is fixed to a hook, provided by Agilent which is included in the dielectric probe kit, by using the grip nut. The calibration procedure described for the MCL probe is followed for calibration of the high temperature open ended dielectric probe. However, for the second step instead of using foil provided Agilent shorting is used. To verify the calibration, a measurement with de-ionized water is collected after each calibration. Note that other calibration liquids can be used; in particular, ethanol is recommended as a calibration liquid.

Fig. 3.3 shows the measurement set-up of for dielectric spectroscopy with Agilent's high temperature probe. To ensure a good contact between the probe and the sample, the probe was partially immersed into the sample. The gel-like

nature of the samples allowed the immersion. Measurements were taken at room temperature (23°C). Note that the temperature of the environment was measured with thermometer. All dielectric property measurements were carried out with samples having a minimum thickness of 20 mm. Note that for Agilent's high temperature dielectric probe the minimum thickness sample should be greater than $\frac{20}{\sqrt{|\varepsilon_c|}}$ mm [53]. This criteria was verified for all measurements performed in this thesis.

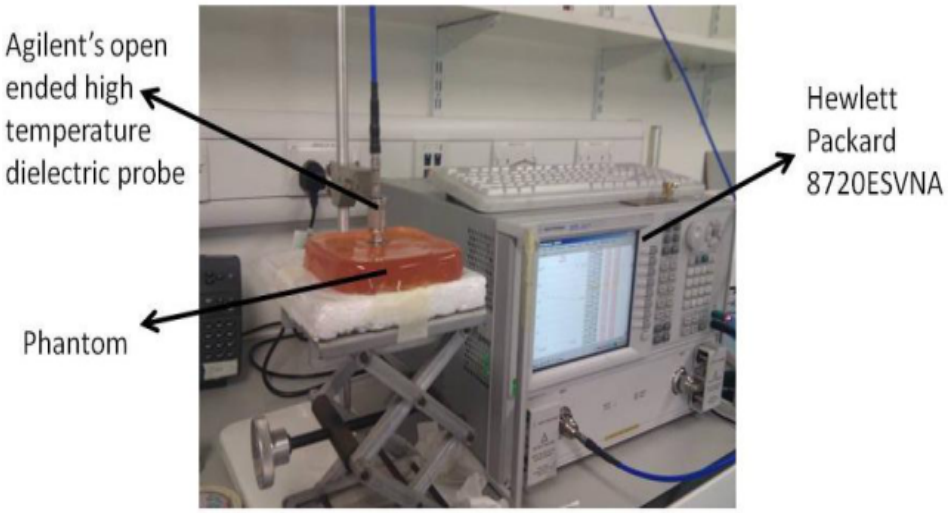

Figure 3.3: Measurement set-up for dielectric spectroscopy with Agilent's open ended high temperature probe.

During dielectric spectroscopy of the semi-solid phantoms different reference points both on the top and bottom surfaces of the phantoms were taken. First, the measurements from the top were collected from at least 5 different reference points. Two measurements were taken at each point: after collecting the first measurement at a given point, the probe was left in contact with the phantom for 3 to 5 minutes to ensure the proper contact between the probe aperture and the sample. Then another measurement was taken from the same point. The same measurement routine was repeated for the bottom surface of the phantoms.

3.3 Liquid Phantoms

Liquid phantoms are characterized to test the sensitivity of the spiral resonators presented in Chapter 4. Liquid phantoms are preferred, due to the ease of fabrication, low cost, and high precision measurements during dielectric spectroscopy. Note that the dielectric spectroscopy performed with open ended coaxial probes is more accurate when the sample is a transparent and homogeneous liquid. Because, the physical contact of the probe with the transparent homogeneous liquid sample can easily be ensured by eye inspection. However, using liquid phantoms has disadvantages. Preservative-free liquid phantoms degrade in 72 hours due to fungi formation in room temperature. In addition, the liquid phantoms can not be combined with another phantom to represent the anthropomorphic tissue environment.

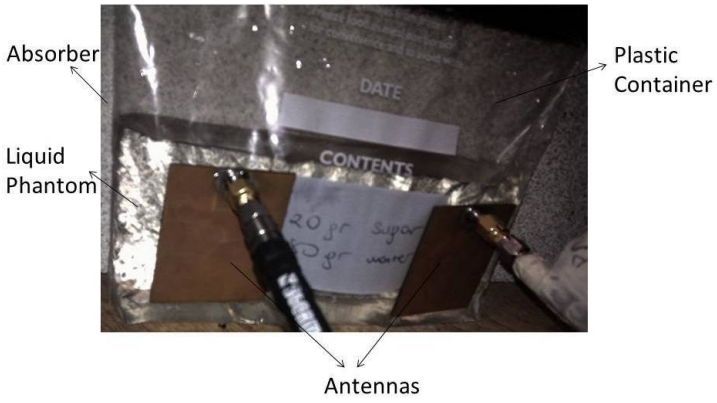

Figure 3.4: S_{21} measurement with a homogeneous sugar-water liquid phantom.

In this section, we proposed sugar-water phantoms. By changing the sugar amount in the phantom, the dielectric properties were altered. Phantoms are prepared by adding table sugar (sucrose) into distilled water. Five phantoms containing 10%, 20%, 30%, 40%, and 50% sugar by weight are composed. No other ingredients, such as solidifying agents or preservatives, were added to the phantoms. The dielectric properties of five phantoms were measured with the MCL probe [52]. The relative permittivity and effective conductivity of the phantoms are given in Fig. 3.5 (a) and Fig. 3.5 (b), respectively.

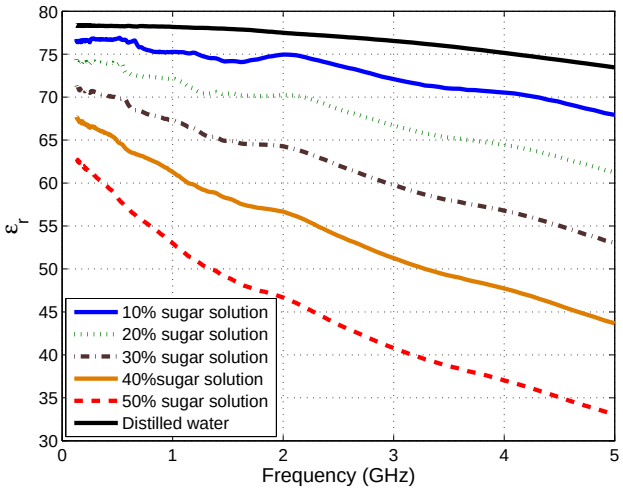

(a)

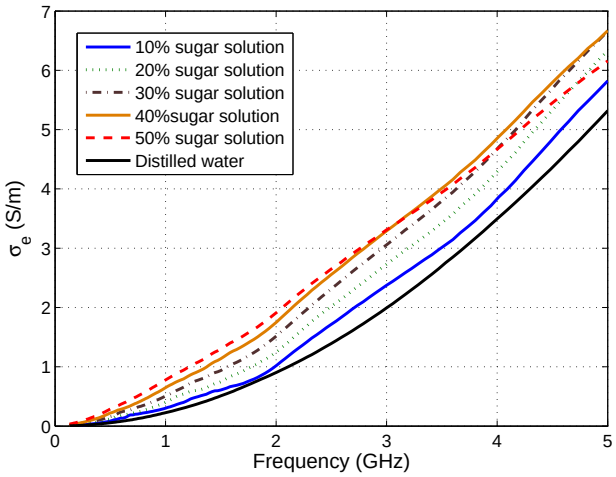

(b)

Figure 3.5: Dielectric property measurements of sugar-water liquid phantoms with MCL probe: (a) relative permittivity of the phantoms; (b) effective conductivity of the phantoms.

From the measurement results, it can be seen that dielectric properties of the phantoms vary significantly with respect to the amount of sugar added to the distilled water. As the amount of sugar added increased, the relative permittivity of the solution decreased. The results are expected, since they are similar to the previous examples in the literature [17, 47]. The effective conductivity of the solutions is increased as the sugar levels are increased, shown in Fig. 3.5 b. This is due to the change in electrolyte balance in solutions.

3.4 Semi-Solid Phantoms

Although liquid phantoms are suitable for preliminary tests of RF and microwave devices designed to operate in the vicinity of humans, the liquid phantoms introduce physical constraints, such as inconsistent geometry. In order to overcome such problems, we also characterized semi-solid phantoms, where geometry and thickness of the phantom can be kept constant.

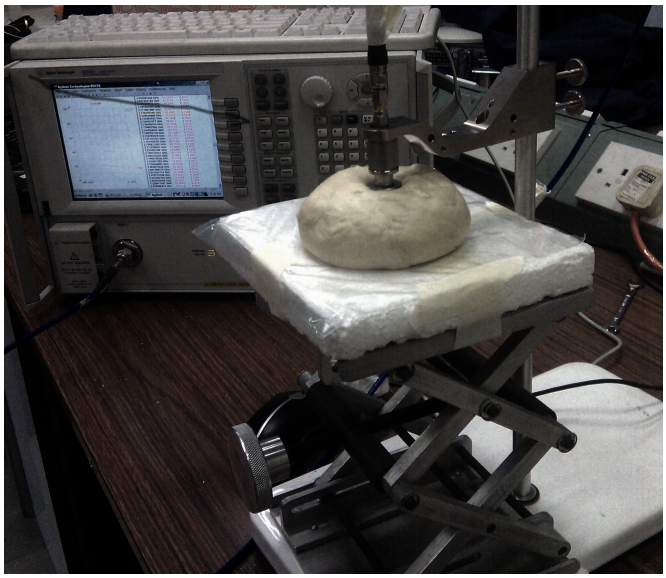

Figure 3.6: Dielectric property measurement of the semi-solid phantom with Agilent's high temperature open-ended dielectric probe.

Gel-like phantoms were produced by preparing 100 grams liquid sugar-water solutions with $5, 10, 15, 20, 25$, and 30 percent sugar by weight, then mixing each solution 179 grams of flour. Note that the amount of flour is chosen via trial to find the required amount of flour needed to solidify sugar-water solutions. The dielectric properties of the phantoms were measured with Agilent's high temperature open-ended dielectric probe kit. The relative permittivity and the effective conductivity measurements are given in Fig. 3.7 (a) and Fig. 3.7 (b), respectively. Although the sugar amount int he phantoms are increasing proportionally, the effective conductivity of the phantoms are not linearly changing with the change in sugar amount. Such trend could resulting from the measurement errors. The measurement errors are highly likely to occur for such phantoms due to the rapid change on the surface of the phantom when exposed to air. Note that the sensing volume of coaxial probes could be as small as 2 mm. Thus the changes in the

surface condition can have a direct effect on the measurement results.

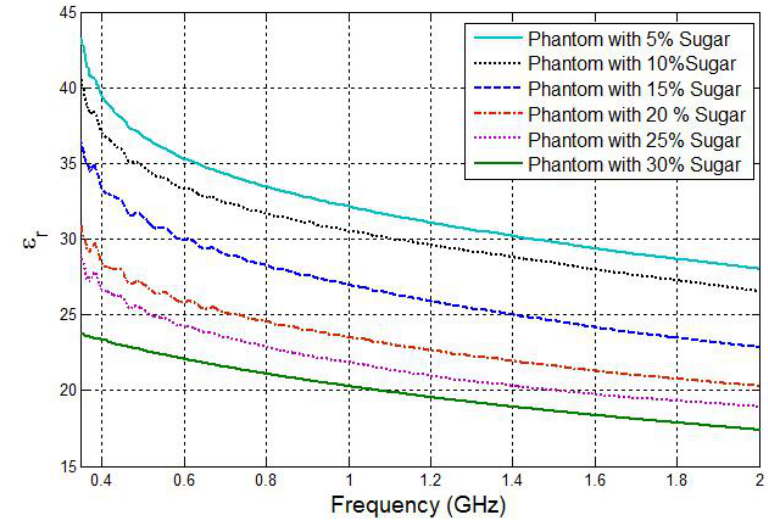

(a)

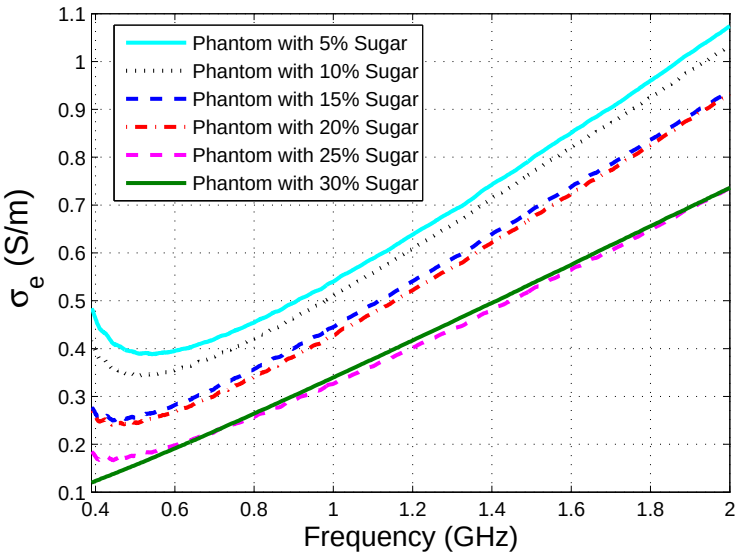

(b)

Figure 3.7: Dielectric property measurement of semi-solid phantoms with Agilent's high temperature open-ended coaxial probe: (a) relative permittivity of the phantoms; (b) effective conductivity of the phantoms.

Measurement results show that the relative permittiviy of the phantoms decreased as the sugar level increased. Also, the amount of flour in the phantom further decreases the dielectric properties of the mixture significantly. It is also worth noting that the flour can be used to make low-water content tissues, such as fat tissue. However, the prepared phantoms degrade very quickly: after exposing the phantoms to air for 60 minutes, the surface of the phantoms dries

up and forms a skin. The skin changes the dielectric properties of the dough, especially when measured with the dielectric probe, since the probe has a very small sensing volume. Note that during the measurements, the phantoms were kept inside plastic bags to prevent degradation.

The semi-solid phantoms were made to test the spiral resonator presented in Chapter 5. The need for semi-solid phantoms emerged because the experiments with liquid phantoms lacked repeatability, due to the inconsistent geometry. Note that the liquid can not be poured on top of the resonator due to the shorting problem. To do so, the spiral sensor must be covered with a superstrate or with a bio-compatible material. Traditionally in the literature, the implantable antennas are modified by covering it with a bio-compatible material to prevent the resonator to be in direct contact with biological tissue or, in this particular case, the liquid phantom [54]. The bio-compatible material is usually a silicone, whereas the superstrate is, in general, the same material as the substrate used during the design of the implantable antenna. Direct contact with a ionized liquid can cause shorting of the structure. To prevent the shorting of the structure, we developed semi-solid materials to control the shape and thickness of the phantom without changing the resonator design.

3.5 Tissue Mimicking Phantoms

TPh materials have been previously introduced in many different forms in the literature. The primary purpose of constructing phantoms is to perform pre-clinical tests for devices intended to be used in the vicinity of human body. TPh materials developed for RF telemetry or imaging purposes are mainly concerned with the dielectric properties of the biological tissues. An extensive study had been carried out by Gabriel et al. [1, 2, 3], on the measurement and parametric models for dielectric properties of biological tissues, which has been the primary reference source for tissue mimicking phantoms since 1996.

In order to define an ultimate test domain, that is closely emulating both the dielectric properties and shape of human tissue, it is important to characterize anthropomorphic phantoms. However, obtaining layered TPh materials is

a challenging task, since it requires prevention of diffusion between juxtaposed TPh materials. Recently, Lazebnik et al. [19] proposed oil-in-gelatine dispersion materials for microwave frequencies based on previously reported TPh materials for ultrasound imaging [38]. Such materials are suitable for composing anthropomorphic materials [37].

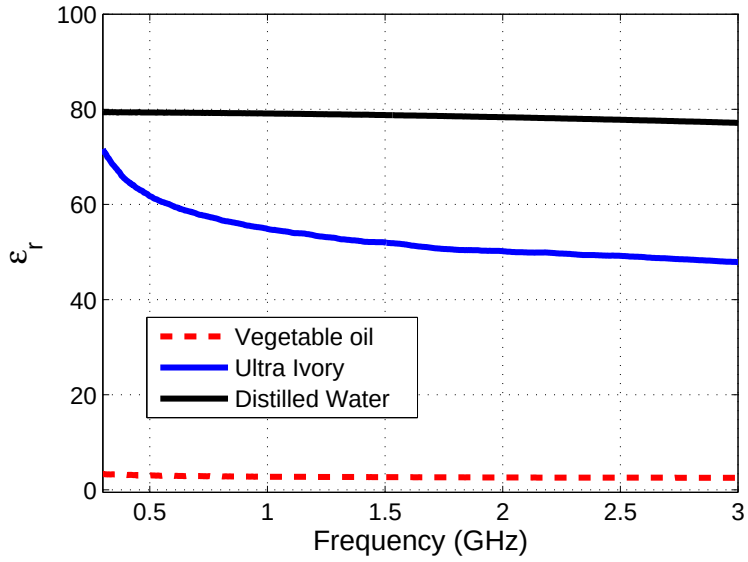

(a)

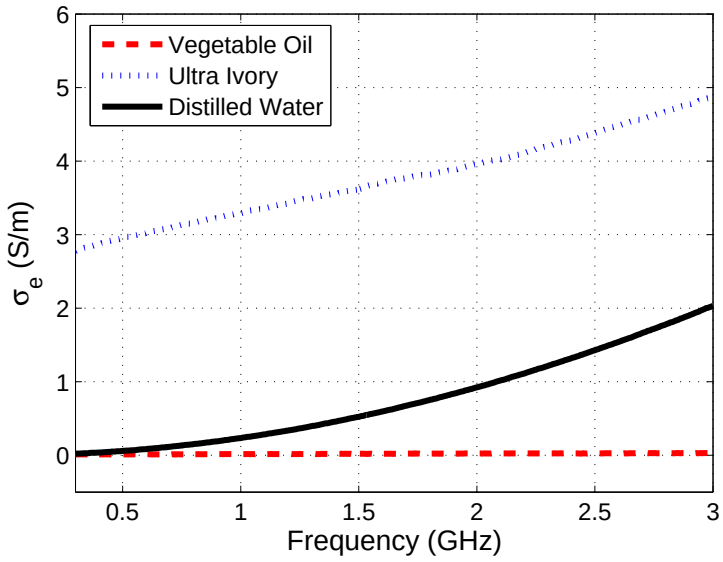

(b)

Figure 3.8: Dielectric property measurement of pure materials: (a) relative permittivity of the pure distilled water, vegetable oil, and Ultra Ivory; (b) effective conductivity of the pure distilled water, oil, and Ultra Ivory.

Additionally, oil-in-gelatine dispersion TPh materials are known to mimic the

dielectric properties of biological tissues for ultra-wide frequency band. The advantage of wide-band TPh materials is they can be used for both narrow and wide band applications. In this section, oil-in-gelatine materials have been developed with off-the-shelf ingredients to mimic high and low water content tissues for a wide frequency band.

Although [19] presents methods for constructing anthropomorphic heterogeneous phantoms, the presented procedure is complicated and the recipes includes chemicals and preservatives to lengthen the shelf-life of the phantoms. Also, the chemicals are only available from specific providers. Such phantoms can be developed with a simple procedure whilst avoiding these chemicals. Thus, we are proposing broad band tissue mimicking materials composed of off-the-self ingredients which can be characterised easily. In this section, the procedure used to develop semi-solid oil-in-gelatine dispersion phantoms using off-the-shelf ingredients is given.

Oil-in-gelatine dispersion materials are characterized using distilled water, NaCl (table salt), vegetable oil, dishwashing detergent (Ultra Ivory), and gelatine. Note that different oil types may have different dielectric properties, such potential difference is not investigated in this thesis. However, it is highly recommended to measure the dielectric properties if another type of oil is desired to be used for oil-in-gelatine dispersion phantom. The dielectric properties of pure distilled water, oil, and Ultra Ivory are given in Fig. 3.8. Throughout this thesis oil refers to vegetable oil. Distilled water and the dishwashing detergent have high relative permittivity and oil has very low relative permittivity. Depending on the water content of the tissue, the ingredients of the mimicking material are changed. It is well known that NaCl increases the effective conductivity of the TPh material dramatically due to the increase in electrolyte balance. During characterization of high and intermediate water content oil-in-gelatine dispersion materials, the amounts of distilled water, gelatine, and ultraivory are kept constant. the relative permittivity and the effective conductivity are adjusted by varying the amounts of oil and sodium chloride (NaCl).

Note that two different dishwashing detergents are used in this work, to enable the homogeneous distribution of the oil in the phantom material. Detergent$_1$ is

available in North America: a dishwashing liquid sold under the name of "Ultra Ivory". Detergent$_2$ is available in the United Kingdom: a dishwashing liquid named "Fairy Platinum Lemon". In Fig. 3.9, it is shown that the relative permittivity of the detergent$_1$ is approximately 10 higher than that of detergent$_2$ over the frequency range of 0.3 GHz to 20 GHz, and the effective conductivity of detergent$_1$ is also higher than detergent$_2$. The dielectric properties of the fat mimicking material are very low; thus, detergent$_2$ is preferred for the fat mimicking material. Any dishwashing liquid can be used in place of detergent$_1$ and detergent$_2$ as the detergent merely acts as a surfactant. However, measuring the dielectric properties is recommended before doing so, to obtain precise dielectric properties in the phantom.

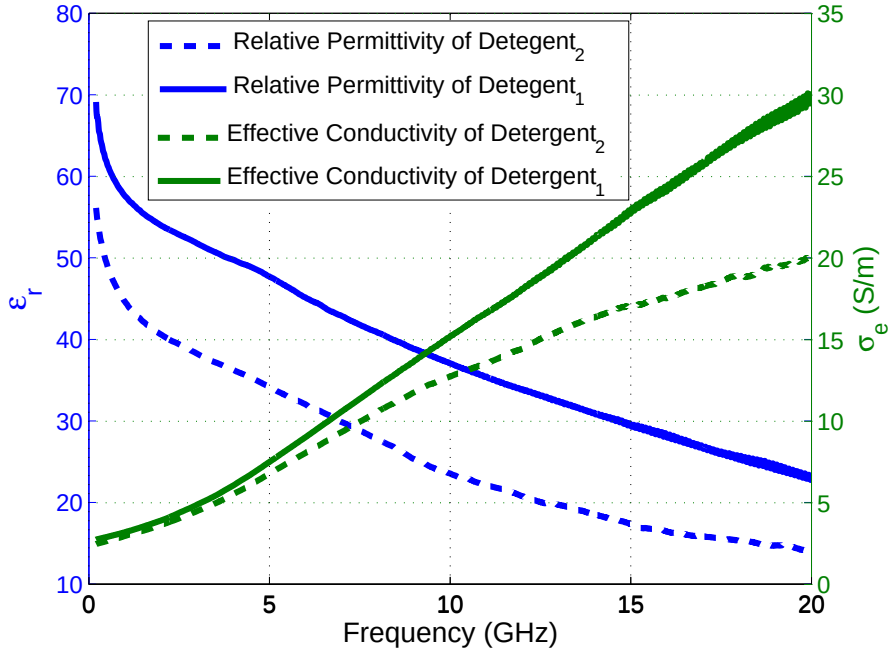

Figure 3.9: Measured dielectric properties of detergent$_1$ and detergent$_2$.

Skin, fat, blood, and muscle mimicking materials are composed by using oil-in-gelatine dispersion materials. Using a thermometer during the fabrication process is essential, since it is critical to measure the temperature precisely. In particular, when the phantom left to solidify at a high temperature, it will result in heterogenous distribution of the oil in the phantom. This elevates the electrical properties at the bottom and decreases the electrical properties at the surface of

the phantom. It is also important to measure the temperature of the ingredients when composing the TPh material. Note the process given below is repeated to characterize the skin, fat, blood, and muscle. The amount of ingredients in the phantom are varied, depending on the type of the tissue that is aimed to be mimicked. The process is completed in 2 hours on average. To obtain a semi-solid form, the phantom left overnight to congeal. Dielectric property measurements of TPh materials are collected approximately 24 hours of after fabrication. The physical phantoms are composed with the procedure below;

1. mix the gelatine and 100 g de-ionized water in a beaker;
2. cover the beaker with cling film and heat the mixture up to 80 °C in a hot water jacket or in a double boiler;
3. leave the mixture to cool until 35 °C;
4. add remaining room temperature de-ionized water and NaCl whilist stirring the mixture slowly;
5. add the room temperature dish washing detergent to the mixture and keep stirring slowly;
6. when the mixture reaches 28°C, add room temperature oil and keep stirring slowly until the mixture become homogeneous. At this point, the color of the mixture changes to white. Adding food colouring at this step allows the phantoms to be distinguished;
7. pour the homogeneous mixture into containers and leave it to solidify over night.

Using cling film is important to minimise water vaporization during the heating processes. Another recipe is also given for the blood mimicking material that does not include oil and mimics the narrow-band dielectric properties. This blood mimicking material is made using water, gelatine, sugar, and sodium chloride (NaCl) solution. Sugar is used to adjust the relative permittivity of the TPh material. The relative permittivity can be decreased by increasing the amount

of sugar, as seen in Fig. 3.5 (a). Initially, this recipe was created to obtain an easier procedure to mimic the dielectric properties of blood. However, it was still necessary to emulate the wide-band characteristics; thus, oil-in-gelatine blood mimicking phantoms were used instead in the experiments. However, the proposed sugar phantom can still be utilized for other experiments, such as testing of implatable or on-body antennas between 0.3 to 3 GHz.

Avoiding air bubbles while making the tissue mimicking phantoms is very important. Thus, the mixture should be handled with care; to minimize micro bubbles, the mixture can be filtered at the last step. If air bubbles form in the mixture, they will fly to the top of the phantom and form a non-smooth surface. Although it is impossible to avoid air bubbles completely, they can be minimized by stirring the mixture slowly.

After the phantom mixtures had solidified, dielectric property measurements were carried out with Agilent's open-ended high temperature dielectric probe, described in Section 3.2. To ensure a good contact, the probe was partially immersed into the phantom; however, while doing so, extreme care was taken to not to deform the skin of the phantom and not to put too much pressure on the phantom. The procedure is defined in Section 3.2. Twenty measurements in total were taken from each phantom. The dielectric property measurements shown in the following sections are the averaged measured dielectric properties.

3.5.1 Skin$_{dry}$ Mimicking Phantom Material

Skin in general can be characterized as an intermediate water content tissue. In terms of dielectric properties, skin can also be divided into two categories based on the water content [55]. The upper layer, which has a slightly lower water content and an average thickness of 0.015 mm around the wrist, is termed skin$_{dry}$. The inner layer, termed skin$_{wet}$, has a slightly higher water content and an average thickness around the wrist of 1 mm. Note that both the thickness and the dielectric properties can be different, depending on the age, gender, body mass index (BMI), and ethnicity. However, such effects have not been studied well in the literature. Thus, when referring to dielectric properties of biological tissues,

the effects of the parameters given above have not commonly been taken into account. This study is performed following the common assumption, the effect of other factors are ignored. Fig. 3.10 shows the dielectric property comparison of skin_{dry} and skin_{wet} tissues between 0.1 to 20 GHz. From the plots, it can be seen that the amount of water in skin_{dry} affects the dielectric properties of the tissue; that is, the lower percentage of water in tissue decreases the dielectric properties. The effect of the tissue water content for skin_{dry} and skin_{wet} is less significant at lower frequencies.

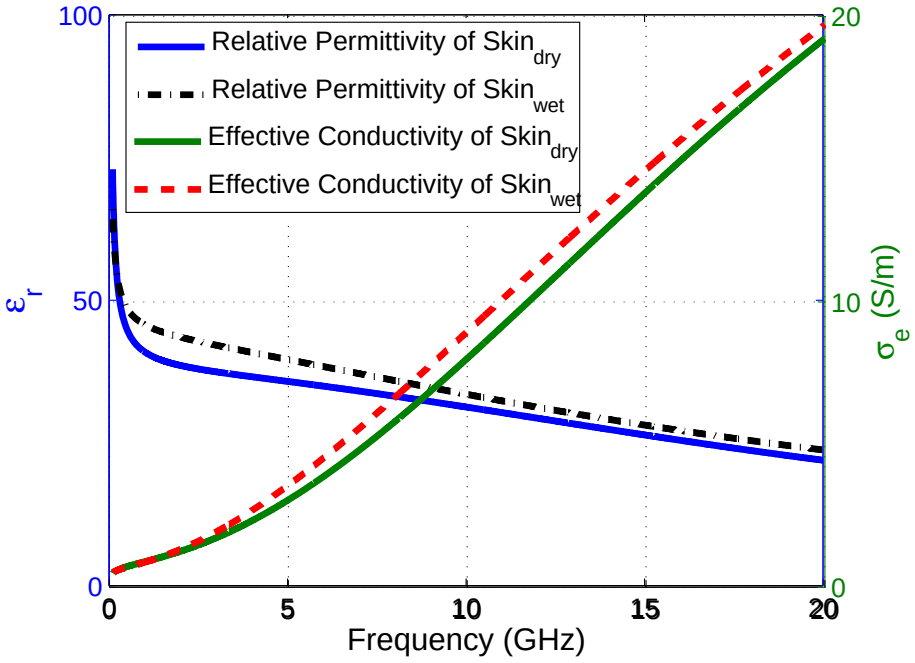

Figure 3.10: Comparison of dielectric properties of skin_{dry} and skin_{wet} tissues [1, 2].

In this section, a recipe is given for the skin_{dry} TPh material. It is composed using the oil-in-gelatine dispersion technique, described in Section 3.5. The ingredients and the amounts used to characterize skin_{dry} are given in Table 3.1. Although the frequencies above 3 GHz are ignored during the dielectric property measurements, we expect this recipe to mimic the dielectric properties of the skin_{dry} tissue up to 20 GHz.

$$\text{Error}_{\varepsilon_r} = \frac{|\varepsilon_{r_{human}} - \varepsilon_{r_{material}}|}{\varepsilon_{r_{human}}} \cdot 100\% \tag{3.1}$$

$$\text{Error}_{\sigma} = \frac{|\sigma_{human} - \sigma_{material}|}{\sigma_{human}} \cdot 100\% \tag{3.2}$$

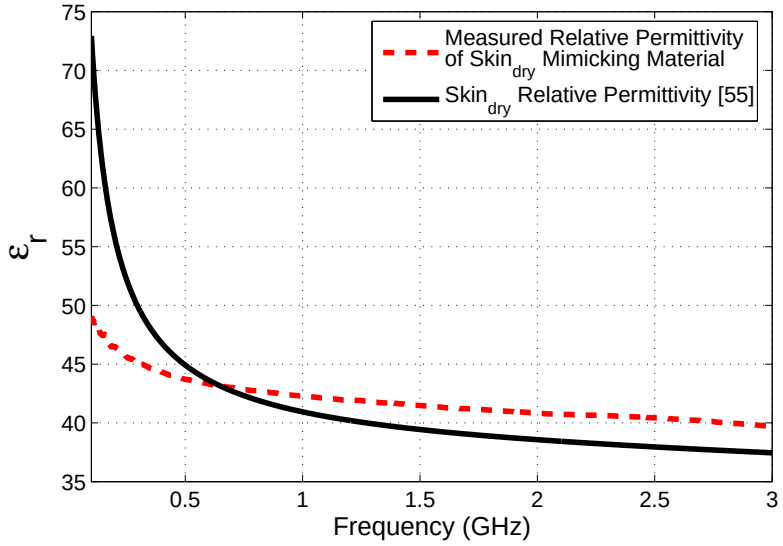

(a)

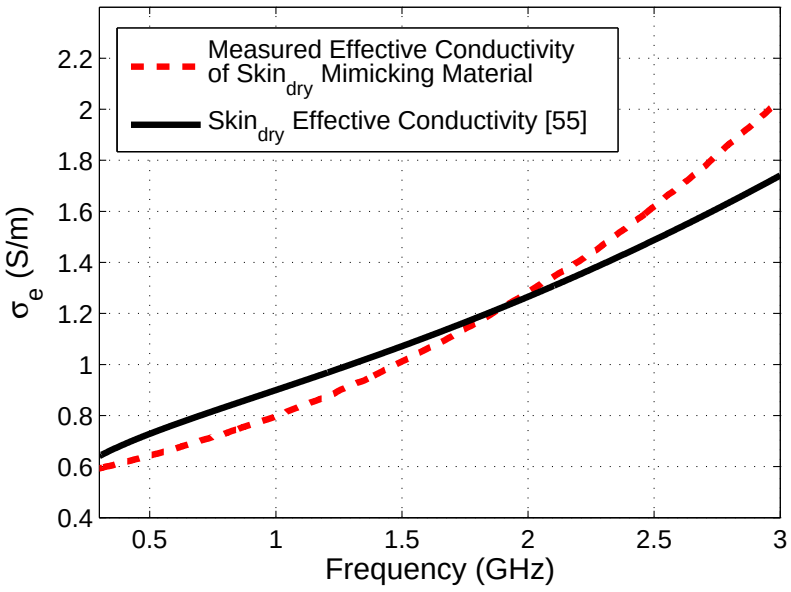

(b)

Figure 3.11: Dielectric property measurements and comparison with gabriel et al [55]: (a) relative permittivity of the skin$_{dry}$ phantom and skin$_{dry}$ tissue; (b) effective conductivity of the skin$_{dry}$ phantom and skin$_{dry}$ tissue.

The dielectric properties of the composed materials were measured with Agilent's high temperature open-ended coaxial probe [53]. The relative permittivity and effective conductivity for skin$_{dry}$ are given in Fig. 3.11 (a) and Fig. 3.11 (b),

respectively. The dielectric properties are compared with the literature data. From equation (3.1) the maximum difference between the measured relative permittivity of the skin_{dry} phantom and the literature data over the 0.3 to 3 GHz frequency range is less than *9.4%*. Similarly, for effective conductivity, from equation (3.2), the maximum difference is less than *0.2%*.

Table 3.1: Ingredients of Skin_{dry} Tissue Mimicking Phantom

Ingredient	*Amount*(g)	*Amount*$(\%)$
$Distilled\ Water$	230	58.9
$Gelatine$	34.1	8.7
$NaCl$	1.3	0.3
Oil	85	21.8
$Detergent_1$	40	10.3

A good agreement obtained between the literature data [55] and the dielectric properties of the characterised phantom. Although the dielectric properties of the phantom is given up to 3 GHz, the dispersive trend of the phantom dielectric properties is expected to agree with the human data up to 20 GHz. Due to the observed characteristics of the oil-in-gelatine dispersion phantom materials. The effective conductivity of the skin_{dry} phantom material shows excellent agrement in the frequency range of 0.3 to 3 GHz with the human data. The relative permittivity differs by 5 at 300 Mhz and it is expected that the difference will be more significant after 3 GHz. This level of error is expected for high water content tissues as it is difficult to match the dispersion trend at microwave frequency for high water content tissues.

3.5.2 Skin_{wet} Mimicking Phantom Material

The ingredients and proportions for the skin_{wet} oil-in-gelatine dispersion TPh material was given in Table 3.2. The food colouring ingredient is optional as it is merely to illustrate the phantom of different tissues and it does not affect their dielectric properties. This recipe was prepared with the procedure described in Section 3.5. Fig. 3.12 (a) and Fig. 3.12 (b) show the comparison of the measurements of relative permittivity and effective conductivity, respectively, with literature data. The measured dielectric property error, relative to the literature

data [55], is calculated using the root mean square error (RMSE) method, given in equation 3.3.

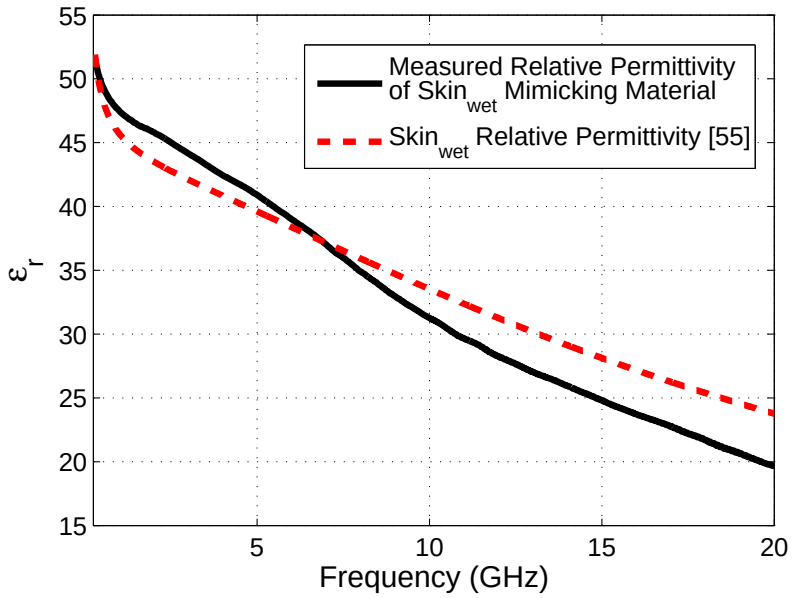

(a)

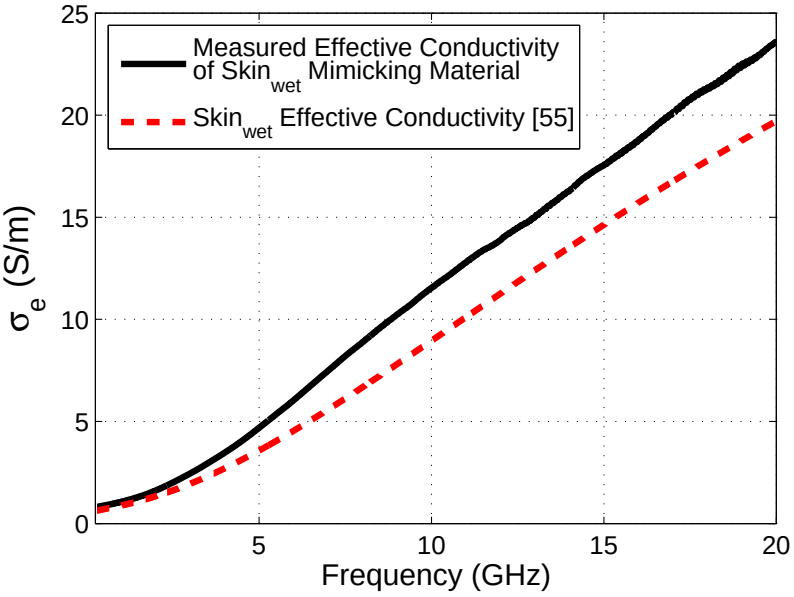

(b)

Figure 3.12: Dielectric property measurement and comparison with gabriel et al [55]: (a) relative permittivity of the skin$_{wet}$ phantom and skin$_{wet}$ tissue; (b) effective conductivity of the skin$_{wet}$ phantom and skin$_{wet}$ tissue.

$$\text{RMSE} = \sqrt{\frac{1}{N}\sum_{i=1}^{N}(x_i - \hat{x}_i)^2} \tag{3.3}$$

where x_i is the literature data, $\hat{x}_i$ is the measured data, and N is the number of frequency points. In this work, the number of frequency points, both for the literature data and the measurements, is 2500 for all TPh materials except skin_{dry} and narrowband blood TPh. Note that both measured relative permittivity and effective conductivity errors are represented in terms of RMSE. The RMSE values for skin_{wet} are 2.62 and 2.44 (S/m) for relative permittivity and effective conductivity, respectively. Further comparison with the existing phantom materials is given in Section 3.6.

Table 3.2: Ingredients of Skin_{wet} Tissue Mimicking Phantom

Ingredient	*Amount*(g)	*Amount*$(\%)$
Distilled Water	230	60.45
Gelatine	34.1	8.96
NaCl	1.4	0.37
Oil	75	19.71
$Detergent_1$	40	10.51
Food colouring	1.3	

The proposed skin_{wet} mimicking material is emulating the dielectric properties of the human skin_{wet} tissue very closely as the maximum difference between the tissue phantom material and the human data is 4.10 and 3.86 S/m for relative permittivity and effective conductivity, respectively. The phantom is following the dispersive trend of the tissue in the 0.3 to 20 GHz range. The phantom is also well suited for narrowband applications located in the 0.3 to 20 GHz range. The effective conductivity of the phantom is higher than the human data at high frequencies. If a better effective conductivity approximation is desired at higher frequencies, the amount of NaCl can be decreased.

3.5.3 Muscle Mimicking Phantom Material

Muscle tissue has slightly higher dielectric properties when compared to skin tissue. The recipe of the muscle TPh material is given in Table 3.3. The food

colouring is optional, as it has been added to the phantom to distinguish it while characterising anthropomorphic phantoms.

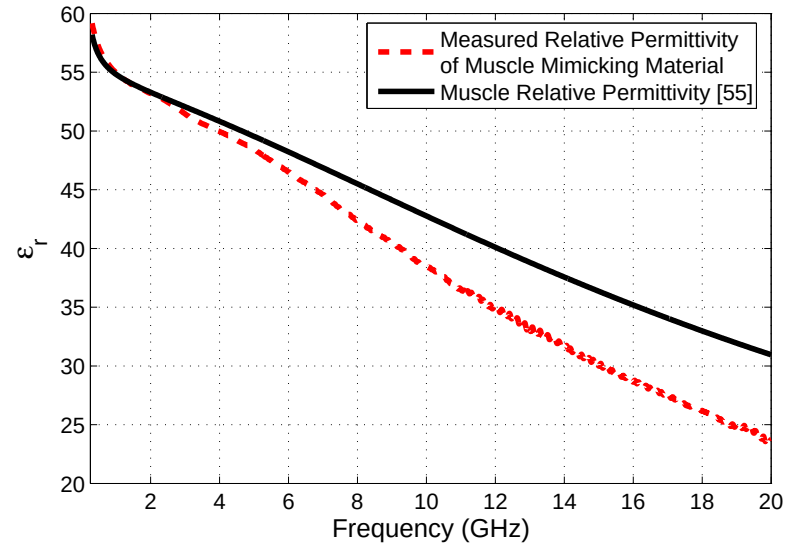

(a)

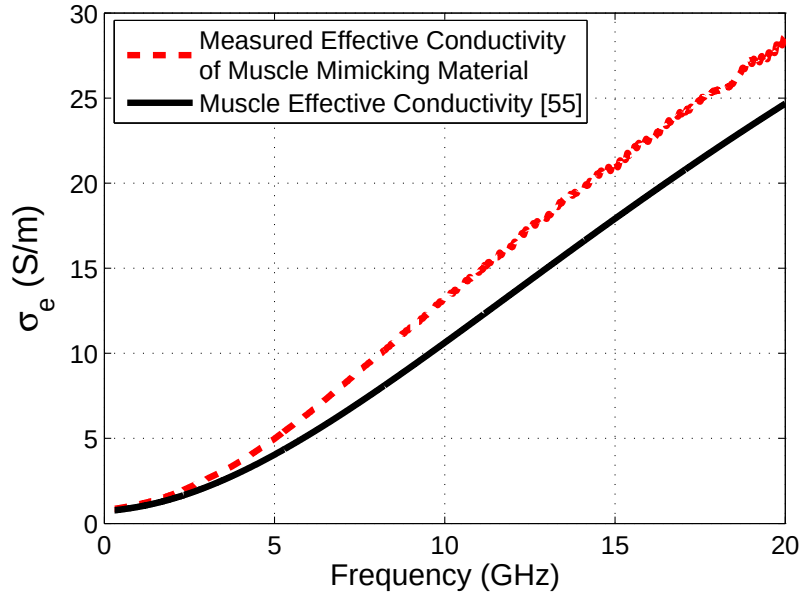

(b)

Figure 3.13: Dielectric property measurements and comparison with gabriel et al [55]: (a) relative permittivity of the muscle phantom and muscle tissue; (b) effective conductivity of the muscle phantom and muscle tissue.

Note that, for EM problems, such as investigation of on-body propagation or SAR measurements, the body is usually approximated with muscle tissue. Thus, in the literature, muscle tissue has been mimicked with different forms of TPh

materials, including liquid phantoms. The measured dielectric properties, along with a reference data comparison between 0.3 and 20 GHz, is given in Fig. 3.13 (a) and Fig. 3.13 (b) for relative permittivity and effective conductivity, respectively. The RMSE of the muscle mimicking material, with respect to the literature data, is 4.60 for relative permittivity and 2.49 (S/m) for effective conductivity, for the whole frequency range.

The muscle phantom material is mimicking the dielectric properties of the human data very well up to 10 GHz. Although the dispersive trend of the phantom is matching with the human tissue, the relative permittivity of the muscle phantom material is lower than the reported data with a maximum deviation of 7 from the human data. The phantom is still suitable for both ultra-wide band and narrowband applications. However, above 10 GHz if better match in relative permittivity is desired the amount of oil can be decreased. This will increase percentage of the water in the phantom material.

Table 3.3: Ingredients of Muscle Tissue Mimicking Phantom

Ingredient	*Amount*(g)	*Amount*$(\%)$
Distilled Water	230	67.59
Gelatine	34.1	10.02
$NaCl$	1.2	0.35
Oil	35	10.29
$Detergent_1$	40	11.75
Food colouring	1.3	

According to the electromagnetic mixing theory, the dielectric properties of a material can be formulated from the dielectric properties of it's constituents [56]. For example, effective permittivity of a biological tissue can be formulated through the dielectric properties of the cells, membranes, proteins, and tissue water. Although the mixing formulas may or may not suggest a linear relationship between the effective permittivity and the dielectric properties of the constituents, it is evident that the relative permittivity of the muscle mimicking material will increase with the increase in water content.

3.5.4 Fat Mimicking Phantom Material

Fat is categorized as a low water content tissue. The dielectric properties of fat tissue are very low. The composition of fat mimicking material is tricky, since it requires at least 80% oil to be present in the oil-in-gelatine dispersion TPh material. Therefore, in order to obtain a homogeneous phantom, the oil should be added just before the phantom starts to solidify (that is, very close to room temperature).

Figure 3.14: A sample of the solidified fat mimicking phantom material in a container.

Also, to keep the consistency of the material, the oil should be added to the rest of the ingredients slowly and whilst stirring continuously. The ingredients for the fat mimicking phantom are given in Table 3.4.

Table 3.4: Ingredients of Fat Tissue Mimicking Phantom

Ingredient	*Amount*(g)	*Amount*$(\%)$
Distilled Water	57.4	14
Gelatine	15	3.6
Oil	329.6	80
$Detergent_2$	10	2.4

A fat mimicking phantom is shown in Fig 3.14. The measured dielectric properties are given in Fig. 3.15 (a) and Fig. 3.15 (b) for relative permittivity and effective conductivity, along with a reference data comparison. The RMSE is calculated for the fat mimicking material as well; the RMSE values for relative permittivity and effective conductivity are 0.46 and 0.54 (S/m), respectively, for the whole frequency range.

Molecular relaxation theory suggests that if a polarizable material is subjected to a time varying electric field, the dipoles in the material will be oriented in the direction of the electric field [57]. The dipoles will then relax back to random orientation with

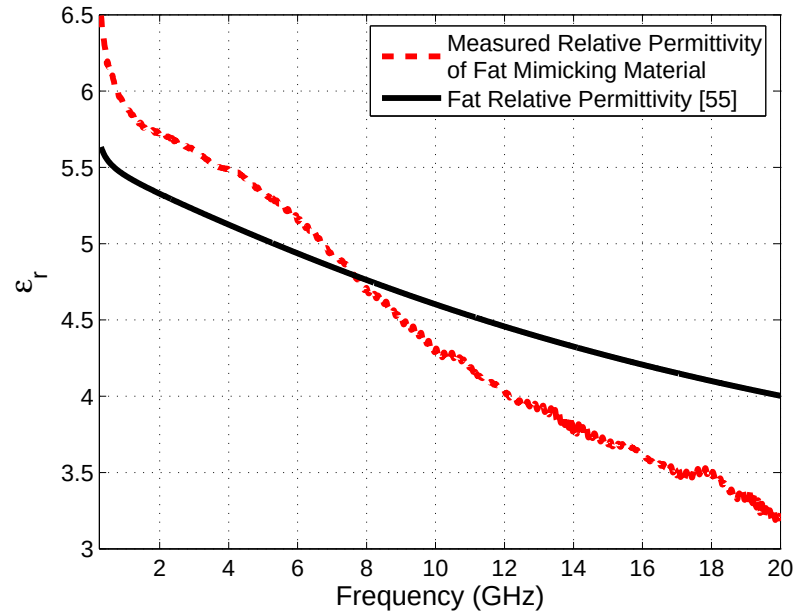

(a)

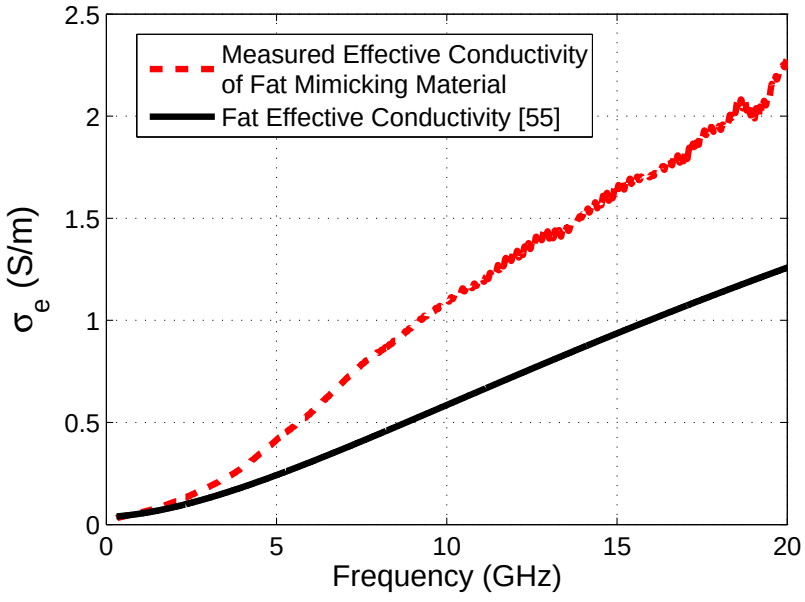

(b)

Figure 3.15: Dielectric property measurements and comparison with gabriel et al [55]: (a) relative permittivity of the fat phantom and fat tissue; (b) effective conductivity of the fat phantom and fat tissue.

time constant τ, which is related to relaxation frequency with $f_c = (2\pi\tau)^{-1}$. One major phenomena that governs the dielectric properties at GHz range is the γ dispersion. The γ dispersion is attributed to the dipolar orientation of free water molecules. Thus, the dielectric properties of the high water content tissues tend to be more frequency dispersive than low water content tissues. It can also be seen from Fig 3.15 (a) that the relative permittivity of the fat tissue is ranging from 6.5 to 3.5 between 0.3 to 20 GHz. The muscle tissue relative permittivity, shown in Fig. 3.13 (a), is ranging from 60 to 35 between 0.3 to 20 GHz. For Fat the dispersion is weaker thus the dispersion can be easily mimicked by the fat TPh material. Thus, the maximum difference between the TPh material and fat tissue is 0.8 and 1 S/m for relative permittivity and effective conductivity, respectively, suggesting an excellent match with the human data.

Note that the fat mimicking material degrades more rapidly than the other oil-in-gelatine dispersion phantoms, as the oil in the phantom material can separate easily if it is not kept in a cool place with air tight containers. Additionally, the fat mimicking material tends to be more fragile, compared to TPh materials containing less oil percentage. Thus, it should be handled with care, particularly, when composed as a thin layer form.

3.5.5 Narrowband Blood Mimicking Phantom Material

Blood has the highest relative permittivity when compared with muscle, skin, and fat tissues. Initially, the blood mimicking material was composed without oil, targeting narrowband applications. This thesis aims to characterize blood mimicking materials with different glucose indices, requiring fabrication of blood mimicking material multiple times. By including oil in the mixture, we obtain wideband phantoms; however, oil complicates the production procedure. Therefore, for convenience, the blood mimicking material fabrication was first carried out by using water-gelatine materials. The steps followed during fabrication of blood mimicking material are:

- Gelatine was mixed with 50 g water and heated to 70°C in a cling film covered beaker in a hot water jacket or in a double boiler;

- Sugar and NaCl were mixed with the rest of the water heated to 50°C in a cling film covered beaker, in a hot water jacket or in a double boiler;
- The two solutions were mixed at 28°C degrees.

Figure 3.16: A sample ofthe narrowband (0.3 - 1.5 GHz) blood mimicking phantom.

Table 3.5: Ingredients of Blood Tissue Mimicking Phantom

Ingredient	*Amount(g)*	*Amount(%)*
Distilled Water	230	69
Gelatine	34.1	10.2
NaCl	4.3	1.3
Sugar	65	19.5
Food colouring	1.3	

However, as the experiments progressed further, explained in Chapter 5, the investigation focused on oil-in-gelatin dispersion wideband blood Tph materials and the narrowband phantoms were not used in the experiments. The recipe

and dielectric property measurements are given in Section 3.5.6. A sample of the narrowband blood mimicking phantom material is shown in Fig 3.16. The phantom is transparent due to the lack of the oil ingredient in the recipe. The oil both gives dispersion and opaque white color to the phantom.

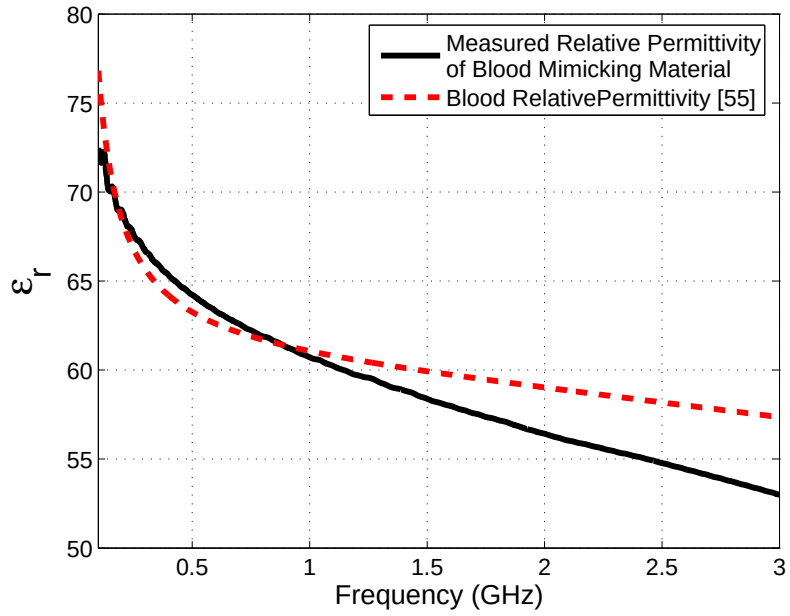

(a)

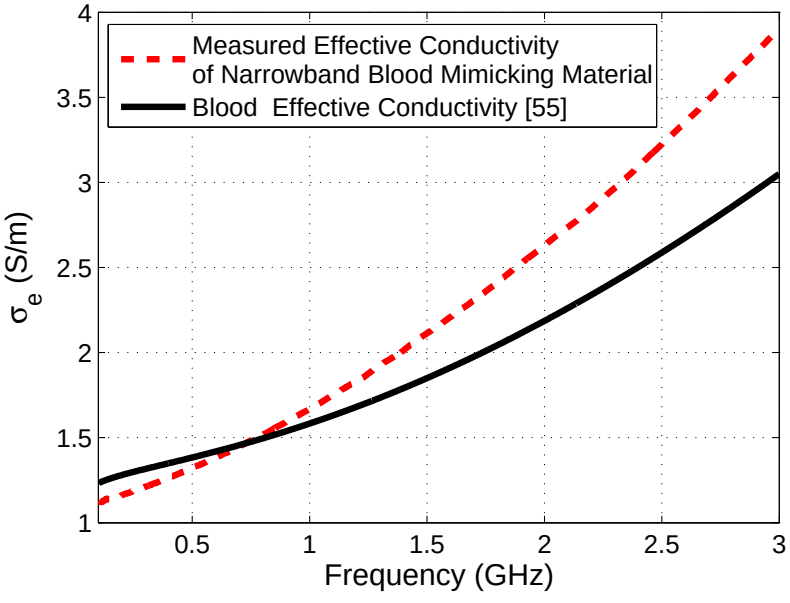

(b)

Figure 3.17: Dielectric property measurements and comparison with gabriel et al [55]: (a) relative permittivity of the narrowband blood phantom and blood ; (b) effective conductivity of the narrowband blood phantom and blood.

The ingredients for the narrowband blood mimicking phantom are given in Table 3.6. Measured dielectric properties are shown in Fig. 3.17 (a) and Fig. 3.17 (b) for the relative permittivity and effective conductivity, along with a reference data comparison. The mimicking error of the blood phantom material is less than *7.7%* for relative permittivity and less than *28%* for effective conductivity, from 300 MHz to 3 GHz. Note that the error percentages are calculated with equations given in 3.1 and 3.2 for relative permittivity and effective conductivity, respectively. Although, oil was not used to compose the blood mimicking material, the dielectric properties are mimicked with a reasonable error on the 0.3 to 3 GHz frequency band. The presented recipe can be used to test RF or microwave devices operating between 0.3 and 1.5 GHz, with very high accuracy.

3.5.6 Ultra-Wide Band Blood Mimicking Phantom Material

An ultra-wide band blood mimicking phantom material was designed using the oil-in-gelatine dispersion technique. This material contains the least amount of oil when compared to other TPh materials. The ingredients for the ultra-wide band blood TPh material are given in Table 3.6.

Table 3.6: Ingredients of Blood Tissue Mimicking Phantom

$Ingredient$	$Amount(g)$	$Amount(\%)$
$Distilled\ Water$	230	71.81
$Gelatine$	34.1	10.65
$NaCl$	1.2	0.38
Oil	15	4.68
$Detergent_1$	40	12.48

Comparison plots between the measured and literature data for relative permittivity and effective conductivity are shown in Fig. 3.18 (a) and Fig. 3.18 (b), respectively. The RMSE values are 5.04 and 1.06 (S/m) are for relative permittivity and effective conductivity, respectively, for the whole frequency range. The effective conductivity of the blood mimicking material agrees well with the literature data. Although there is a discrepancy at the high frequency of the relative permittivity, the blood Tph adequately mimics the dielectric properties

of the blood. The discrepancy of relative permittivity is due to the fact that the blood is a highly dispersive tissue. Although the dispersion is mimicked well, if a better match with the real tissue values is required, the oil content of the material should be decreased for higher frequencies. Validity of the phantom material will be further discussed in Section 3.6.

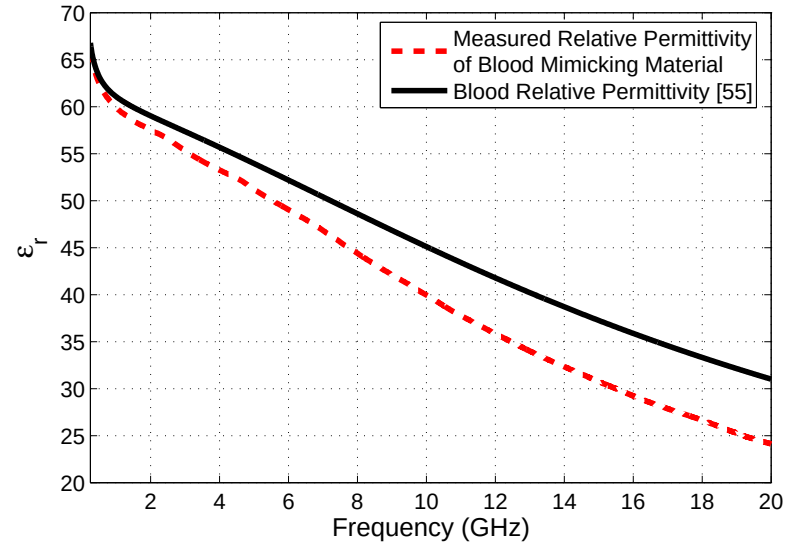

(a)

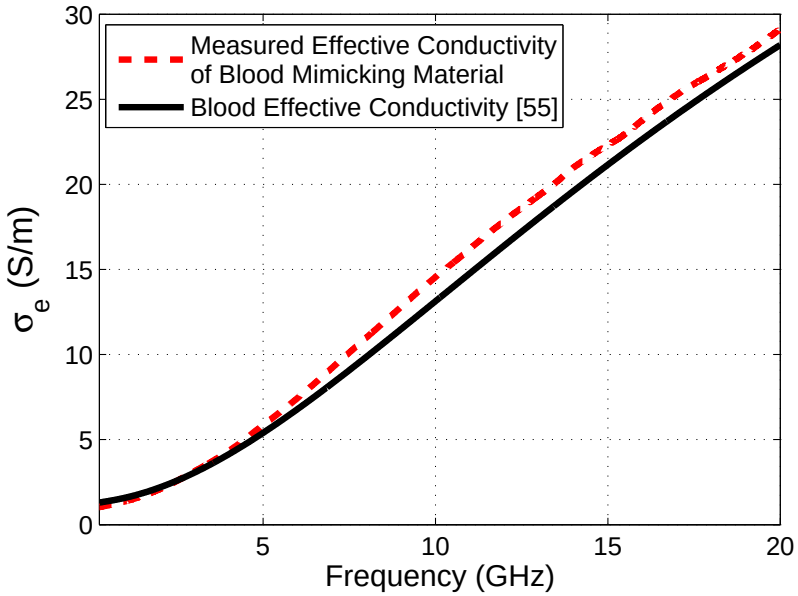

(b)

Figure 3.18: Dielectric property measurements and comparison with gabriel et al [55]: (a) relative permittivity of the blood phantom and blood; (b) effective conductivity of the blood phantom and blood.

3.6 Conclusions

In this chapter, recipes for liquid and semi-solid phantoms are given, together with validation measurements performed with open ended coaxial probes. Such phantoms were developed to carry out feasibility studies with the wireless glucose sensor proposed in Chapter 4. Additionally, tissue phantom materials, emulating the dielectric properties of the biological tissues for an ultra-wide frequency band, were proposed. The tissue phantom materials can be prepared by using off-the-shelf materials. Recipes and dielectric property measurements of the tissue phantom materials are given. Collected dielectric property measurements for tissue phantom materials were also compared with the tissue dielectric properties from the literature for validation purposes [55].

We also compared the maximum error of the proposed tissue phantom materials with the previously reported ultra-wide band tissue mimicking materials. In [19], dielectric properties of reported fat, muscle, and skin$_{wet}$ materials are plotted against the tissue properties from [2]. According to reported results we carried out a comparison between the fat, muscle, and wet skin mimicking materials proposed in this thesis to those proposed in [19] and in [37]. [19] classifies the tissues depending on the oil percentage. According to [19], the fat tissue corresponds to their 80% oil tissue phantom over the 0.5-20 GHz band. From the reported graphs in [19], the difference with respect to reported literature data [2] for relative permittivity and effective conductivity is around 2 and 1 S/m, respectively. In this study, the difference between our fat mimicking material, which also includes 80% oil, and reported data on fat tissue is less than 0.9 and 1 S/m for relative permittivity and effective conductivity, respectively, for the whole 0.3 to 20 GHz frequency range.

The wet skin mimicking material in this work is composed with 19% oil; the maximum relative permittivity and effective conductivity differences between the literature and measured data are 1.1 and 3.86 S/m, respectively. In [19], the maximum difference between the 20% oil content tissue phantom material and literature data on wet skin is 4−5 and 3 S/m, for relative permittivity and effective conductivity, respectively. In [37], a comparison between 30% oil tissue phantom

material and skin_{wet} tissue is proposed from 200 MHz to 6 GHz; the maximum difference is 4 and 0.7 S/m, for relative permittivity and effective conductivity, respectively.

For the muscle in [19], the maximum difference between the 10% oil tissue phantom material and literature data for relative permittivity and effective conductivity is 8 and 5 S/m, respectively. For the muscle tissue phantom material in this work, the maximum differences are 7.7 and 3.9 S/m, for relative permittivity and effective conductivity respectively.

From this comparison with the previously published data on oil-in-gelatine dispersion tissue phantom materials, we can state that the phantoms presented in this work mimic the dielectric properties of the $muscle$, $skin_{wet}$, and fat tissues with an acceptable, and sometimes improved, error range. Furthermore, the proposed recipes have an advantage over the previously published recipes as fewer ingredients are required. The trade-off is the probable reduction in the lifetime of the phantoms, though the extent of this has not being investigated at this point.

In addition, this work also presents a comparison between the measured dielectric properties of blood and ultra-wide band blood phantom material; the difference between these is less than 7 and 1.6 S/m for the whole frequency range. The validity of the other tissue phantom materials, based on the above comparisons with measured tissue properties and the previously published recipes, suggests that the blood tissue phantom material can be used for the whole frequency range. If one desires a better match at higher frequencies for the blood mimicking phantom, the water percentage of the phantom can be increased. Similarly, if a better match is desired for conductivities of the phantoms, the NaCl in the phantom mixture should be adjusted. Note that the blood tissue phantom has 4.6% oil content. It is also worth noting that these recipes can be optimised for high accuracy in narrow frequency bands.

This chapters reports novel, ultra-wide band tissue phantom materials that can mimic the dielectric properties of the skin_{wet}, skin_{dry}, muscle, blood, and fat tissue. The phantom materials are composed by using off-the-shelf ingredients and the production time is around 2 hours. Thus, the phantoms can be replicated

easily.

Although this thesis proposes narrow-band techniques for dielectric property sensing, the wideband phantoms are characterized based on two important reasons: (1) it is not clear what is the best frequency to use for monitoring of blood glucose levels, so wide-band phantoms are required to investigate this question; (2) it may ultimately prove the required accuracy for sensing blood glucose related changes, is only possible by using multiple frequencies, such as multiple resonances of a resonator, again requiring wide-band phantoms for investigation. In addition, the wide-band blood mimicking phantoms are also characterized to investigate the glucose-dependent dielectric properties of blood, the results are given in Chapter 5. This chapter presented recipes for wide-band materials; however, the recipes can be optimized for narrow-band applications.

References

[1] C. Gabriel, S. Gabriel, and E. Corthout, "The dielectric properties of biological tissues: I. literature survey," *Physics in Medicine and Biology*, vol. 41, no. 11, p. 2231, 1996. [Online]. Available: http://stacks.iop.org/0031-9155/41/i=11/a=001

[2] S. Gabriel, R. W. Lau, and C. Gabriel, "The dielectric properties of biological tissues: Ii. measurements in the frequency range 10 hz to 20 ghz," *Physics in Medicine and Biology*, vol. 41, no. 11, p. 2251, 1996. [Online]. Available: http://stacks.iop.org/0031-9155/41/i=11/a=002

[3] C. Gabriel, R. W. Lau, and S. Gabriel, "The dielectric properties of biological tissues: Iii. parametric models for the dielectric spectrum of tissues," *Physics in Medicine and Biology*, vol. 41, no. 11, p. 2271, 1996. [Online]. Available: http://stacks.iop.org/0031-9155/41/i=11/a=003

[4] F. A. Duck, *Physical Properties of Tissue: A Comprehensive Reference Book*. Harcourt, 1990.

[5] O. P. Gandhi, G. Lazzi, and C. Furse, "Electromagnetic absorption in the human head and neck for mobile telephones at 835 and 1900 mhz," *Microwave Theory and Techniques, IEEE Transactions on*, vol. 44, no. 10, pp. 1884–1897, Oct.

[6] T. Nagaoka, S. Watanabe, K. Sakurai, E. Kunieda, S. Watanabe, M. Taki, and Y. Yamanaka, "Development of realistic high-resolution whole-body voxel models of japanese adult males and females of average height and weight, and application of models to radio-frequency electromagnetic-field dosimetry," *Physics in Medicine and Biology*, vol. 49, no. 1, p. 1, 2004. [Online]. Available: http://stacks.iop.org/0031-9155/49/i=1/a=001

[7] M. Yvanoff and J. Venkataraman, "A feasibility study of tissue characterization using lc sensors," *Antennas and Propagation, IEEE Transactions on*, vol. 57, no. 4, pp. 885–893, April.

[8] T. Yilmaz, "Characterization of tissue mimicking materials for testing of implantable and on body antennas," Master's thesis, Mississippi State University, May 2009.

[9] A. Bakar, A. Abbosh, P. Sharpe, and M. Bialkowski, "Artificial breast phantom for microwave imaging modality," in *Biomedical Engineering and Sciences (IECBES), 2010 IEEE EMBS Conference on*, 30 2010-Dec. 2, pp. 385–388.

[10] [Online]. Available: http://www.mhra.gov.uk/Howweregulate/Devices/Registrationofmedicaldevices/index.htm

[11] [Online]. Available: http://www.initial.co.uk/medical-services/regulations/index.html

[12] Y. F.-M. Liu, W.-C. and M. Ghavami, "Miniaturized implantable broadband antenna for biotelemetry communication," *Microw. Opt. Technol. Lett.*, vol. 52, p. 24072409, 2008.

[13] M. Asili, R. Green, S. Seran, and E. Topsakal, "A small implantable antenna for medradio and ism bands," *Antennas and Wireless Propagation Letters, IEEE*, vol. 11, pp. 1683–1685.

[14] R. Warty, M. R. Tofighi, U. Kawoos, and A. Rosen, "Characterization of implantable antennas for intracranial pressure monitoring: Reflection by and transmission through a scalp phantom," *Microwave Theory and Techniques, IEEE Transactions on*, vol. 56, no. 10, pp. 2366–2376, Oct.

[15] M.-C. Gosselin, S. Kuhn, A. Christ, M. Zefferer, E. Cherubini, J. F. Bakker, G. C. van Rhoon, and N. Kuster, "Experimental evaluation of the sar induced in head phantoms of three- and eight-year-old children," *IEICE TRANSACTIONS on Communications*, vol. E95-B, no. 10, pp. 3215–3224, 2012.

[16] A. Sani, A. Alomainy, and Y. Hao, "Numerical characterization and link budget evaluation of wireless implants considering different digital human phantoms," *Microwave Theory and Techniques, IEEE Transactions on*, vol. 57, no. 10, pp. 2605 –2613, Oct. 2009.

[17] T. Yilmaz, T. Karacolak, and E. Topsakal, "Characterization and testing of a skin mimicking material for implantable antennas operating at ism band (2.4 ghz-2.48 ghz)," *Antennas and Wireless Propagation Letters, IEEE*, vol. 7, pp. 418 –420, 2008.

[18] M. P. Robinson, M. J. Richardson, J. L. Green, and A. W. Preece, "New materials for dielectric simulation of tissues," *Physics in Medicine and Biology*, vol. 36, no. 12, p. 1565, 1991. [Online]. Available: http://stacks.iop.org/0031-9155/36/i=12/a=002

[19] M. Lazebnik, E. L. Madsen, G. R. Frank, and S. C. Hagness, "Tissue-mimicking phantom materials for narrowband and ultrawideband microwave applications," *Physics in Medicine and Biology*, vol. 50, no. 18, p. 4245, 2005. [Online]. Available: http://stacks.iop.org/0031-9155/50/i=18/a=001

[20] A. Hunt, A. Ristolainen, P. Ross, R. pik, A. Krumme, and M. Kruusmaa, "Low cost anatomically realistic renal biopsy phantoms for interventional radiology trainees," *European Journal of Radiology*, vol. 82, no. 4, pp. 594 – 600, 2013. [Online]. Available: http://www.sciencedirect.com/science/article/pii/S0720048X13000053

[21] E. L. Madsen, M. A. Hobson, H. Shi, T. Varghese, and G. R. Frank, "Tissue-mimicking agar/gelatin materials for use in heterogeneous elastography phantoms," *Physics in Medicine and Biology*, vol. 50, no. 23, p. 5597, 2005. [Online]. Available: http://stacks.iop.org/0031-9155/50/i=23/a=013

[22] Y. Yuan, C. Wyatt, P. Maccarini, P. Stauffer, O. Craciunescu, J. MacFall, M. Dewhirst, and S. K. Das, "A heterogeneous human tissue mimicking phantom for rf heating and mri thermal monitoring verification," *Physics in Medicine and Biology*, vol. 57, no. 7, p. 2021, 2012. [Online]. Available: http://stacks.iop.org/0031-9155/57/i=7/a=2021

[23] M. L. Lumori, "Gaussian beam modeling of sar enhancement in paraxial and non-paraxial regions of biological tissues," in *Progress In Electromagnetics Research M*, 2010, pp. 1–12.

[24] C. Furse, D. A. Christensen, and C. H. Durney, *Basic Introduction to Bioelectromagnetics*, 2nd ed. CRC Press, 2009.

[25] M. H. Durney, C. H. and M. F. Iskander, *Radio Frequency radiation dosimetry handbook*, 4th ed. Report USAFSAM-TR-85-73, USAF School of Aerospace Medicine, Aerospace MedicalDivision (AFSC), 1986.

[26] P. S. Hall and Y. Hao, *Antennas and Propagation for Body-Centric Wireless Networks*. Artech House, 2006, iSBN 1-58053-493-7.

[27] M. Y. Kanda, M. Ballen, S. Salins, C.-K. K. Chou, and Q. Balzano, "Formulation and characterization of tissue equivalent liquids used for rf densitometry and dosimetry measurements," *Microwave Theory and Techniques, IEEE Transactions on*, vol. 52, pp. 2046 – 2056, 2004.

[28] [Online]. Available: http://www.dow.com/productsafety/finder/dgbe.htm

[29] [Online]. Available: http://en.wikipedia.org/wiki/Triton

[30] J. Kim and Y. Rahmat-Samii, "Implanted antennas inside a human body: simulations, designs, and characterizations," *Microwave Theory and Techniques, IEEE Transactions on*, vol. 52, no. 8, pp. 1934 – 1943, aug. 2004.

[31] C. J. Schneider, N. Engelberts, and J. D. P. van Dijk, "Characteristics of a passive rf field probe with fibre-optic link for measurements in liquid hyperthermia phantoms," *Physics in Medicine and Biology*, vol. 36, no. 4, p. 461, 1991. [Online]. Available: http://stacks.iop.org/0031-9155/36/i=4/a=005

[32] J. Lin and Y.-J. Wang, "The cap-choke catheter antenna for microwave ablation treatment," *Biomedical Engineering, IEEE Transactions on*, vol. 43, no. 6, pp. 657–660, June.

[33] N. Chahat, M. Zhadobov, S. Alekseev, and R. Sauleau, "Human skin-equivalent phantom for on-body antenna measurements in 60 ghz band," *Electronics Letters*, vol. 48, no. 2, pp. 67–68, 19.

[34] M. Hagmann, R. Levin, L. Calloway, A. Osborn, and K. Foster, "Muscle-equivalent phantom materials for 10-100 mhz," *Microwave Theory and Techniques, IEEE Transactions on*, vol. 40, no. 4, pp. 760–762, Apr.

[35] K. Ito, K. Furuya, Y. Okano, and L. Hamada, "Adevelopment and characteristics of a biological tissue-equivalent phantom for microwaves," *Electron. Comm. Jpn. Pt. I*, p. 6777., 2001.

[36] M. Lazebnik, E. L. Madsen, G. R. Frank, and S. C. Hagness, "Tissue-mimicking phantom materials for narrowband and ultrawideband microwave applications," *Physics in Medicine and Biology*, vol. 50, no. 18, p. 4245, 2005. [Online]. Available: http://stacks.iop.org/0031-9155/50/i=18/a=001

[37] A. Mashal, F. Gao, and S. C. Hagness, "Heterogeneous anthropomorphic phantoms with realistic dielectric properties for microwave breast imaging experiments," *Microwave and Optical Technology Letters*, vol. 53, no. 8, pp. 1896–1902, 2011. [Online]. Available: http://dx.doi.org/10.1002/mop.26128

[38] E. L. Madsen, J. A. Zagzebski, and G. R. Frank, "Oil-in-gelatin dispersions for use as ultrasonically tissue-mimicking materials," *Ultrasound in Medicine and Biology*, vol. 8, no. 3, pp. 277 – 287, 1982. [Online]. Available: http://www.sciencedirect.com/science/article/pii/0301562982900345

[39] A. Guy, "Analyses of electromagnetic fields induced in biological tissues by thermographic studies on equivalent phantom models," *Microwave Theory and Techniques, IEEE Transactions on*, vol. 16, no. 2, pp. 205–214, February.

[40] E. L. Madsen, G. R. Frank, and F. Dong, "Liquid or solid ultrasonically tissue-mimicking materials with very low scatter," *Ultrasound in Medicine and Biology*, vol. 24, no. 4, pp. 535 – 542, 1998. [Online]. Available: http://www.sciencedirect.com/science/article/pii/S0301562998000131

[41] [Online]. Available: http://en.wikipedia.org/wiki/Carrageenan

[42] [Online]. Available: http://en.wikipedia.org/wiki/Polyacrylamide

[43] G. Mazzara, R. W. Briggs, Z. Wu, and B. G. Steinbach, "Use of a modified polysaccharide gel in developing a realistic breast phantom for mri," *Magnetic Resonance Imaging*, vol. 14, no. 6, pp. 639 – 648, 1996. [Online]. Available: http://www.sciencedirect.com/science/article/pii/0730725X96000549

[44] T. Yilmaz and Y. Hao, "Sensing of dielectric property alterations in biological tissues at microwave frequencies," in *Antennas and Propagation Conference (LAPC), 2011 Loughborough*, nov. 2011, pp. 1 –4.

[45] [Online]. Available: http://en.wikipedia.org/wiki/Agar

[46] [Online]. Available: http://www.sigmaaldrich.com/etc/medialib/docs/Sigma/Product_Information_Sheet/a9414pis.Par.0001.File.tmp/a9414pis.pdf

[47] T. Karacolak, A. Hood, and E. Topsakal, "Design of a dual-band implantable antenna and development of skin mimicking gels for continuous glucose monitoring," *Microwave Theory and Techniques, IEEE Transactions on*, vol. 56, no. 4, pp. 1001 –1008, Apr. 2008.

[48] M. Nadi, G. Prieur, and C. Marchal, "Development of a gelatin water phantom used for simulation of biological tissues in the 20-110 mhz band," in *Engineering in Medicine and Biology Society, 1990., Proceedings of the Twelfth Annual International Conference of the IEEE*, 1990, pp. 2099–2100.

[49] M. Nadi, C. Marchal, A. Rouane, A. Hedjiedj, D. Kourtiche, and G. Prieur, "Effect of temperature variations on the dielectric properties of a radiofrequency, gelatin water phantom," in *Engineering in Medicine and Biology Society, 1992 14th Annual International Conference of the IEEE*, vol. 1, 1992, pp. 268–269.

[50] E. L. Madsen, G. R. Frank, T. A. Krouskop, T. Varghese, F. Kallel, and J. Ophir, "Tissue-mimicking oil-in-gelatin dispersions for use in heterogeneous elastography phantoms," *Ultrasoundn Imaging*, no. 1, pp. 17–38, 2003. [Online]. Available: http://www.ncbi.nlm.nih.gov/pubmed/12747425

[51] [Online]. Available: https://webshop.fishersci.com/insight2_uk/getProduct.do?productCode=10774751&resultSetPosition=0

[52] "Letters to the editor," *Physics in Medicine and Biology*, vol. 42, no. 8, p. 1671, 1997. [Online]. Available: http://stacks.iop.org/0031-9155/42/i=8/a=015

[53] "Agilent 85070e dielectric probe kit 200 mhz to 50 ghz technical overview." [Online]. Available: http://cp.literature.agilent.com/litweb/pdf/5989-0222EN.pdf

[54] J. Ung and T. Karacolak, "A wideband implantable antenna for continuous health monitoring in the medradio and ism bands," *Antennas and Wireless Propagation Letters, IEEE*, vol. 11, pp. 1642–1645, 2012.

[55] Itallian National Research Council, URL: http://niremf.ifac.cnr.it/tissprop/.

[56] A. Sihvola, *Electromagnetic Mixing Formulas and Applications*. IET, 1999.

[57] P. Debye, *Polar Molecules*. The Chemical Catalog Company, inc., 1929. [Online]. Available: http://books.google.co.uk/books?id=eEAwAAAAIAAJ

Chapter 4

Spiral Resonators for Dielectric Property Retrieval of Biological Tissues

The use of radio-frequency techniques for blood glucose level (BGL) monitoring has been investigated in the past (see, for example, [1, 2, 3]). These studies typically concern about the changes in the S-parameter response of a resonator, which occurs due to the changes in dielectric properties of the propagation medium, the biological tissue. A change in BGL leads to a variation in the effective permittivity of the body, which can thus be detected, in principle, from resonator measurement. Thus far, the proposed RF/microwave techniques for BGL monitoring in the literature are mostly concerned about establishing a relation between the response of the RF/microwave device and the change in glucose levels.

In [4], a spiral resonator was tested with human subjects for non-invasive monitoring of BGL. However, human body is a complex environment and, in addition to BGL, other physiological parameters, such as blood pressure and body

temperature, also affect the effective permittivity of the body. Such physiological changes can affect the S-parameter response of the resonator; as a result, the repeatability of the measurements can be degraded. The resonator may detect shifts in effective permittivity that are caused by changes in biological tissue other than the desired change in BGL; therefore, there is a need to perform controlled measurements to address the actual response of the resonator due to the BGL change.

In this Chapter, a spiral resonator is presented for dielectric property retrieval. Following the designs as presented in [4], controlled experiments were performed with both liquid and semi-solid phantoms; the dielectric property measurements and recipes of the liquid and semi-solid phantoms are given in Chapter 3 Section 3.3 and Section 3.4, respectively. The first prototype was tested with liquid phantoms, and an analytical formulation used to retrieve their dielectric properties. However, due to the unforeseen physical restrictions of liquid phantoms, the S-parameter response of the resonator showed ripples; therefore, too many modes appeared in the S-parameter response. Thus, the experiments were performed with a second prototype using semi-solid phantoms. The semi-solid phantoms were placed directly on top of the resonator, whereas the liquid phantom was poured first into a plastic bag, and then placed above the resonator for measurement. Note that the plastic bag introduced a mismatch. All phantoms had different dielectric properties; a decreasing trend for relative permittivity for both liquid and semi-solid phantoms was obtained by varying the amount of sugar dissolved in the phantoms.

An analytical method was proposed to retrieve the dielectric properties from the S-parameter response of the spiral resonator. However, this retrieval method required measurement of two phantoms with known dielectric properties, as a means of calibration. The calibration method was rather inefficient and the retrieval error depended on the frequency shift during the calibration.

The analytical equation is then modified by utilizing simulation data and the dielectric property retrieval is performed with the modified equation. This method is applied to eliminate the need for calibration. The analytical formulation is a system of two equations with four unknowns, including the effective

length of the resonator (l_{eff}), filling factor (A), relative permittivity of the phantom ($\varepsilon_{\text{phantom}}$), and the frequency of operation (f_c). The filling factor and the effective length are both functions of the frequency of operation and phantom relative permittivity; thus, the analytical equation can be re-written with two variables, f_c and $\varepsilon_{\text{phantom}}$, in non-linear form. To do so, an initial set of data was obtained by simulating the resonator with digital phantoms having different dielectric properties. Then, by utilizing particle swarm optimization (PSO) and multiple linear regression (MLR), a single non-linear analytical equation was obtained. The obtained equation is solved with an iterative method. The new technique is more efficient, since the simulation data provides *a priori* information based on the ideal case, whereas the pure measurement data used for calibration, particularly when collected without much care (as may be the case with end-users), can lead to wrong retrieval values.

This chapter is organised as follows: the retrieval method with calibration is defined in Section 4.1. Section 4.2 describes the first prototype of the spiral resonator and experiments with liquid phantoms, as well as dielectric property retrieval. The design and testing of the second prototype, along with the measurements performed with liquid and semi-solid phantoms, are given in Section 5.1.2. An improvement of the retrieval method formulation is given in Section 4.3.3. Finally, the conclusions are drawn in Section 4.4.

4.1 Dielectric Property Retrieval

Dielectric properties of biological tissues have been studied extensively in the literature, especially to differentiate between malignant and healthy tissues [5, 6]. Traditionally, dielectric property measurements of biological tissues are performed with open-ended coaxial probes for ultra-wide-band applications. Narrow-band techniques are usually used for dielectric property retrieval of low relative permittivity and low loss materials. The coaxial probe technique, depending on the fabrication of the probe, can be used to retrieve broadband dielectric properties for wide range of materials; this probe is usually used to estimate the dielectric properties of unknown materials or liquids with a certain probable error.

However, the narrow-band techniques are known to be more accurate for the retrieval of the dielectric properties. From the reported studies, we know that, at microwave frequencies, a change in glucose levels does not affect the conductivity at 0.3-20 GHz range; however, the relative permittivity is expected to vary slightly [1, 7]. Therefore, there is a need to detect the dielectric property change with sensors of high sensitivity. Based on our experience we can state that by using a narrow-band high Q resonators (i.e., a resonance method) the dielectric properties of unknown materials can be detected with a good precision.

The equipment needed to perform the dielectric property measurements with an open-ended coaxial probe is bulky and costly. Thus, a more convenient technique is to use a planar device. In addition to the ease of integration with the remaining electronics, planar devices are less costly. Also precision coaxial probes have a low sensing volume; depending on the aperture, the sensing volume can be as low as 2 mm [8]. Therefore, by utilizing a narrow band resonator or antenna, the sensing volume can be increased.

Reported studies on dielectric properties of biological tissues are traditionally performed *in vitro* [1, 9, 10]. Thus, a greater understanding of the actual dielectric property change can be obtained by utilizing non-invasive sensing. Also, there is still a need for further investigation of the disease-related alterations in dielectric properties of biological tissues.

Our goal is to measure the effective change in relative permittivity non-invasively to sense the change in blood glucose level. As the blood glucose levels of a diabetes patient alters during their daily routine, the effective relative permittivity of the tissues therefore varies. By utilizing resonance methods, the effective relative permittivity can be retrieved to sense the glucose levels. To do so, an analytical formulation that can retrieve the dielectric property at the resonance frequency of the RF or microwave device is utilized. Note that the return loss is a measure of the effectiveness of power delivery from a transmission line to a load such as an antenna [11]. Resonance for a microstrip antenna is the impedance is real at a certain frequency, namely voltage and current are in phase. This section describes the empirical formulation used to retrieve the dielectric properties.

The proposed spiral resonator is essentially a microstrip transmission line;

it has resonances that are determined by the length of the line and the phase velocity ($\upsilon_p = c/\sqrt{\varepsilon_{eff}\mu_{eff}}$) in the effective medium formed by the substrate and the phantom under test. Both the substrate and the phantom are non-magnetic ($\mu_{eff} = 1$), thus the phase velocity is only dependant the effective permittivity (ε_{eff}) of the medium. The resonances can be expressed by [12]:

$$f_n = \frac{nc_0}{l_{\text{eff}}\sqrt{\varepsilon_{\text{eff}}}} \tag{4.1}$$

$$\implies \varepsilon_{\text{eff}} = \left(\frac{nc_0}{l_{\text{eff}}f_n}\right)^2 \tag{4.2}$$

where f_n is the resonance frequency, n indicates the mode (number of the resonance, assumed equal to one), c_0 is the speed of light, l_{eff} is the effective length of the microstrip line and ε_{eff} is the effective permittivity.

The effective permittivity can be related,at least, to a first order approximation, to the relative permittivities of the substrate (ε_r) and phantom (ε_{p}) by [13]:

$$\varepsilon_{\text{eff}} = A\varepsilon_r + (1 - A)\varepsilon_{\text{p}} \tag{4.3}$$

where A is an unknown representing the proportion of the electric field that is in the phantom, relative to that in the substrate (essentially a 'filling factor'). The effective length of the spiral resonator is difficult to determine, as it is a function of the substrate and superstrate relative permittivities the geometry of the line (i.e., width and substrate height) and the geometry of the coupled lines (i.e., their separation). To the best of the author's knowledge, there is no closed-form expression available to compute this. Hence, as the effective length is also unknown, measurements from two samples can be used to 'calibrate' the parameter retrieval by allowing l_{eff} and A to be found using simultaneous equations.

In order to calibrate the spiral resonator, it was assumed initially that these values were not strong functions of the change in relative permittivity, enabling them to be used for all concentrations of sugar. The calibration can be done by using two phantoms with known dielectric properties. In this work, we used two phantoms having dielectric properties close to the expected ('designed for') values, as determined by an alternative measurement technique (i.e., not the spiral

resonator). The operation frequency f_n together with the 'known' mode n, and phantom relative permittivity, are recorded for the two calibration phantoms. Note that the phantom relative permittivity is measured with MCL or Agilent's open-ended coaxial probe and, depending on the resonator's recorded operation frequency f_n, a single value of relative permittivity for the phantom is collected at the specified frequency point. The two equations, 4.2 and 4.3, obtained with two phantom measurements are then solved simultaneously and the effective length l_{eff}, the filling factor A are obtained. This process is can be seen as the measurement calibration. Then, by collecting the spiral resonator measurements with the desired phantoms, the dielectric property retrieval can be performed. Retrieval error for the calculated relative permittivities of the proposed liquid and semi-solid phantoms are calculated with equation 4.4. (ε_{p_s}) is the phantom relative permittivity, (ε_{p_c}) is the measured relative permittivity. It is emphasized that the reference dielectric properties of all liquid and semi-solid phantoms are measured with the MCL and Agilent's high temperature probes, respectively, as given in Chapter 3.

$$\text{Error}_{\%} = \frac{\left|\varepsilon_{\text{p}_c} - \varepsilon_{\text{p}_s}\right|}{\varepsilon_{\text{p}_c}} \cdot 100\% \tag{4.4}$$

4.2 Design of the spiral resonator: First Prototype

Based on an open-ended transmission line model given by Jean *et al.* [14], a two-port microstrip transmission line was designed and fabricated. The top view of the first prototype is given in Fig. 4.1, with dimensions in Table 4.1. This first prototype was designed and simulated with the CST Microwave Studio software and printed on a FR4 substrate with the relative permittivity and tangent loss of $\varepsilon_r = 4.9$ and $\tan(\delta) = 0.025$, respectively.

A comparison of the S_{11} response between measurement and simulation in free space is given, to verify proper functioning of the transmission line. A good agreement is obtained in between measured and simulated responses, as shown

in

Table 4.1: Dimensions of the Transmission Line: First Prototype

Parameter	*Length (mm)*	*Parameter*	*Length (mm)*	*Parameter*	*Length (mm)*
$L1$	95	W_1	33	a_2	6.5
L_f	77	W_s	1	a_3	5
L_p	69	a_1	3.5	a_4	8
L_c	10				

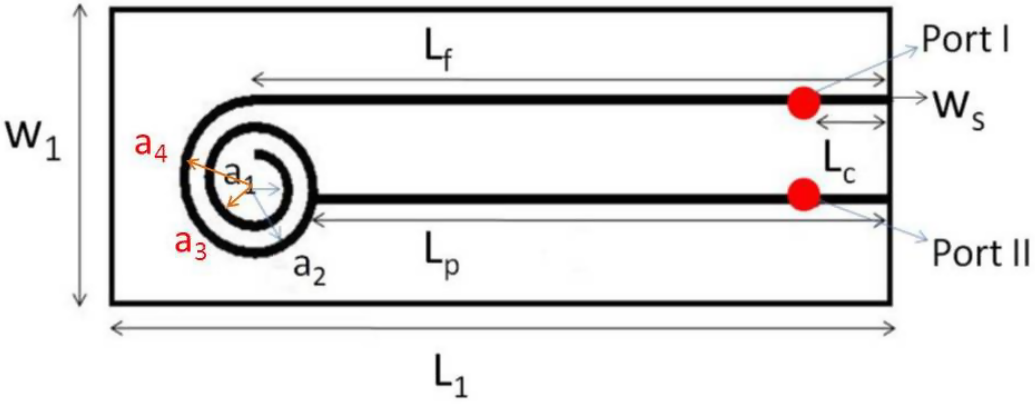

Figure 4.1: Spiral open-ended transmission line with full ground plane.

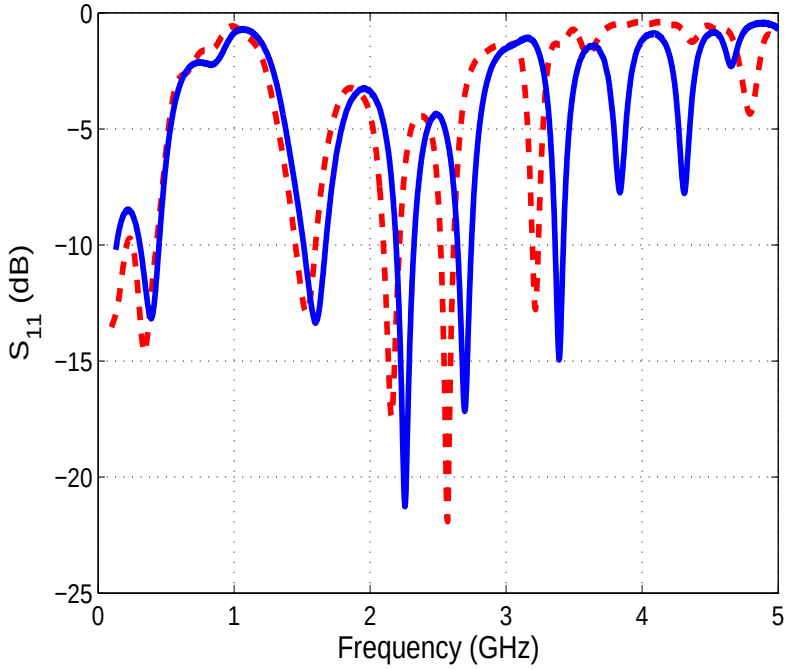

Figure 4.2: Comparison between measured and simulated S_{11} response of the first prototype .

Fig. 4.2. Note that all experiments are performed with vector network analyzer (Hewlett Packard 8720ESVNA). The thickness of the FR4 substrate is 1.6 mm and the thickness of the microstrip transmission line is 1 mm.

4.2.1 Experiments with Liquid Phantoms

Liquid phantoms proposed in Chapter 3 was poured into labeled plastic zip-lock bags and measurements are performed by placing phantoms with the plastic bags above the fabricated resonator. The thickness of all the phantoms were 5 cm. The response of the transmission line was tracked as the plastic bags containing different percentage of sugar solution were replaced with one another. Note that the liquid phantoms were not simulated as the dielectric properties of the phantoms were not known before the experiment and also the liquid experiments were preliminary. The S_{11} responses are given in Fig. 4.3.

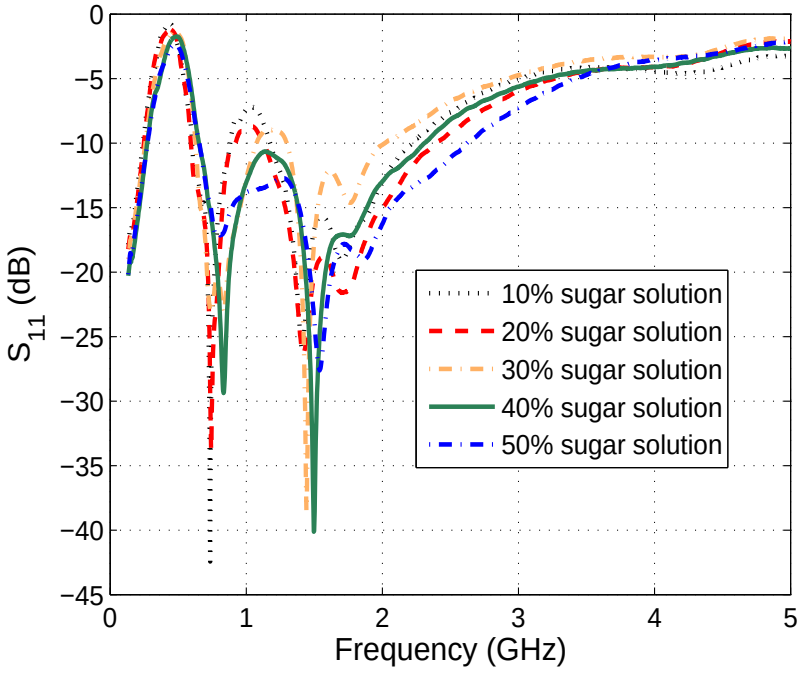

Figure 4.3: Measured S_{11} responses of the first prototype with different liquid phantoms.

It has been observed that the sensor response shows a significant amount of change when different solutions are placed above the sensor. As can be seen from Fig. 4.3, the resonance frequency shift to the right with increasing concentration.

Also, the relationship between the dielectric property change and sensor response is not linear. Thus, a non-linear mathematical expression is needed to describe the relation between the relative permittivity and the measured sensor response. The effective conductivity of the liquid phantoms also varies with the change in sugar percentage. However, in [1] it is reported that the conductivity of blood plasma does not change significantly with the variations in dextrose levels. Therefore, our priority is to investigate the relationship between the relative permittivity of the propagation medium and the sensor response.

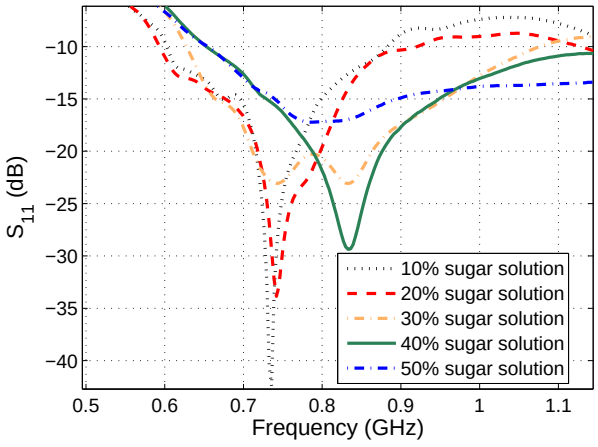

(a)

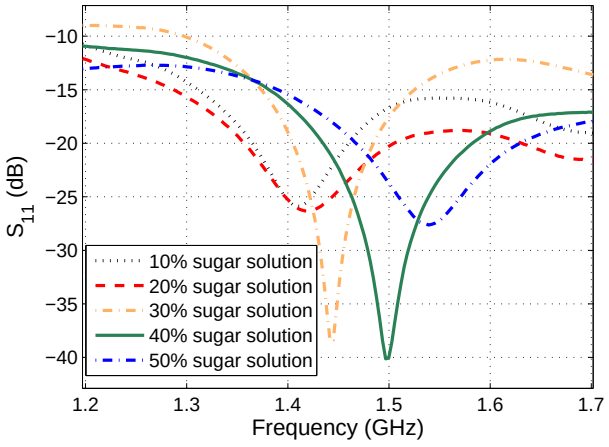

(b)

Figure 4.4: Zoomed version of the measured change in reflection response with different liquid phantoms shown in Fig 4.3: (a) S_{11} measurement at first mode, (b) S_{11} measurement at second mode .

A comparison between the calculated relative permittivity and the measured relative permittivity is given in Table 4.2. The dielectric property retrieval

method shown in Section 4.1 was used to calculate the the relative permittivity from the measured spiral resonator response. The measured relative permittivity is extracted from the MCL slim probe measurements, given in Chapter 3. Relative permittivities of the solutions are calculated at the first and second modes. The effective length l_{eff} and the filling factor A are calculated from the measurements performed with 10% and 20% sugar solution phantoms. Note that, for each mode, the calibration should be repeated for accurate retrieval of the relative permittivity. Also, for each mode, the 10% and 20% sugar solutions are used for calibration.

Table 4.2: Comparison Between Reconstructed and Measured Relative Permittivities of Solutions with First Prototype

Second Mode				
Phantom (%)	*Frequency (GHz)*	*Retrieved* ε_{phan}	*Measured* ε_{phan}	*Error %*
10%	0.735	75.71	75.64	0.0925
20%	0.741	72.401	72.38	0.0290
30%	0.751	66.73	68.15	2.0836
40%	0.836	25.18	62.49	59.7
50%	0.848	20.31	54.4	62.66
Third Mode				
Phantom (%)	*Frequency (GHz)*	*Retrieved* ε_{phan}	*Measured* ε_{phan}	*Error %*
10%	1.408	74.5	74.4	0.1344
20%	1.421	70.75	70.49	0.3688
30%	1.442	65.01	64.99	0.0308
40%	1.497	51.09	58.22	12.24
50%	1.539	41.4	48.69	14.97

In the second mode, reconstructed parameters for 40% and 50% solutions do not agree with the measured relative permittivities. This is due to the change in the resonance characteristics occurring when a solution with 30% sugar content placed on top of the structure. In S_{11} measurements, two notches are observed for 30% solution case. That is because the structure starts to resonate around the second notch's frequency as the solutions with higher sugar content placed above, shown in Fig. 4.4(a). Note that, for the 30% phantom in the second mode, the retrieval was performed for the first notch. In order to fix this error, a new calibration should be performed for the second notch and the effective length l_{eff} and filling factor A should be chosen accordingly. For the third mode,

the error is decreasing; the resonator shows more stable behavior, as shown in Fig. 4.4 (b). The error percentage is increases as the resonance shifts to the higher frequencies. For more precise measurements, the calibration should be repeated with known dielectrics around the desired frequency range. Additionally, the error percentage for the MCL probe should be considered; however, we do not have enough documentation to quantify the error for the MCL probe.

The dielectric property change of the sugar solutions is much higher than the glucose-dependent dielectric property change in biological tissues. Thus, one calibration for each mode will be sufficient for reconstruction of the relative permittivity of biological tissues with different blood glucose indices. The feasibility studies with sugar-water phantoms are needed to establish the basis of the study. However, the calibration method is still controversial, as it assumes the effective length and filling factor to be constant with the frequency. The improvement of this method is shown in the following sections.

4.3 Design of the spiral resonator: Second Prototype

The resonator presented in Section 4.2 is re-implemented by using CST Microwave Studio software on a Taconic TLC(30) substrate. The configuration of the resonator is given in Fig. 4.5(a). Fabricated resonator is shown in Fig. 4.5 (b). Substrate of the resonator had a thickness of 1.47 mm; the relative permittivity and the dissipation factor of the substrate are equal to 3 and 0.003, respectively. Dimensions of the resonator are given in Table 4.3.

Table 4.3: Dimensions of the Spiral Resonator

$Parameter$	$Value\ (mm)$	$Parameter$	$Value\ (mm)$	$Parameter$	$Value\ (mm)$
a_1	8	L_{subs}	95	L_c	47
a_2	6.5	L_{s1}	7.51	w_{subs}	33
a_3	5	L_{s2}	15	w_{s1}	3.98
a_4	3.5	L_p	9	w_{s2}	2.207
a_5	2	L_f	11	w_{s3}	1
a_6	0.5				

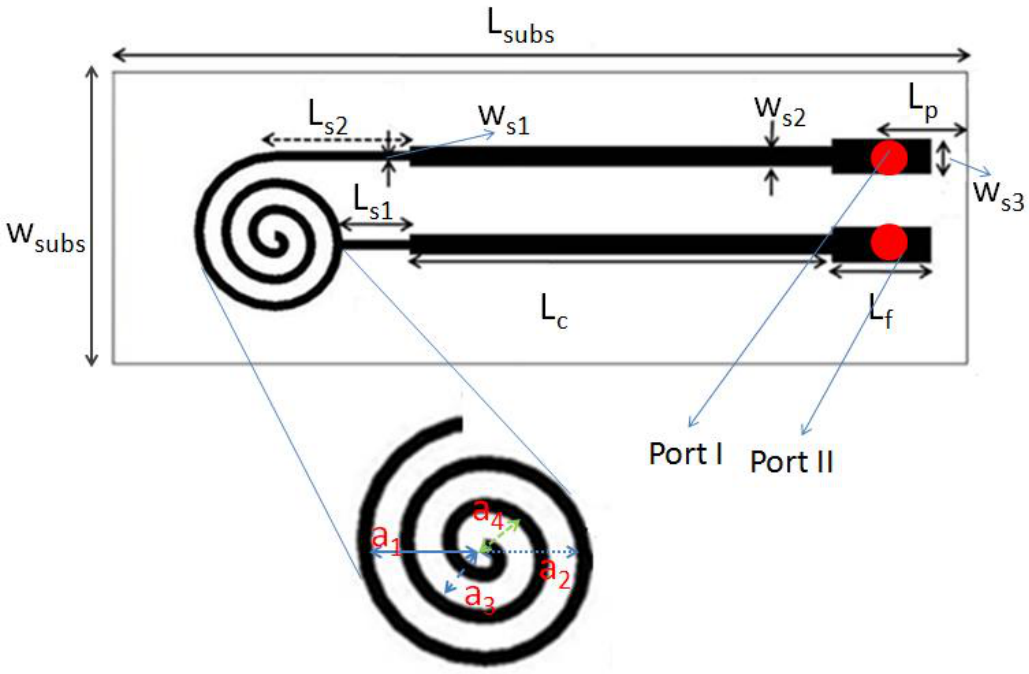

(a)

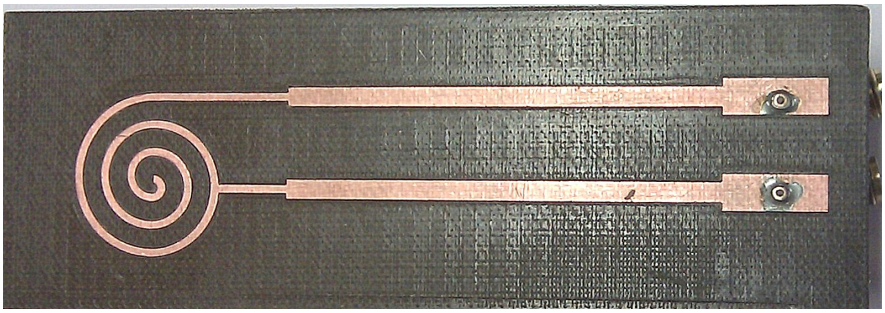

(b)

Figure 4.5: Second prototype of the spiral Resonator: (a) structure; and (b) manufactured prototype.

The simulated and measured S_{11} responses of the spiral resonator in air medium are shown in Fig. 4.6. Due to fabrication errors, the second notch at 1.8 GHz is shifted to right (to a higher frequency) by 140 MHz. Similarly, the third notch is shifted to right by 103 MHz. Although there is a shift in the operation frequencies, the fabricated resonator shows similar behaviour to the simulated resonator, which confirms the proper functioning of the fabricated resonator. The resonator was used to retrieve the dielectric properties of the liquid and semi-solid phantoms. The relative permittivity was retrieved for semi-solid

phantoms, using both empirical and modified analytical equations. The dielectric properties of the liquid phantoms are retrieved with the empirical formulation only.

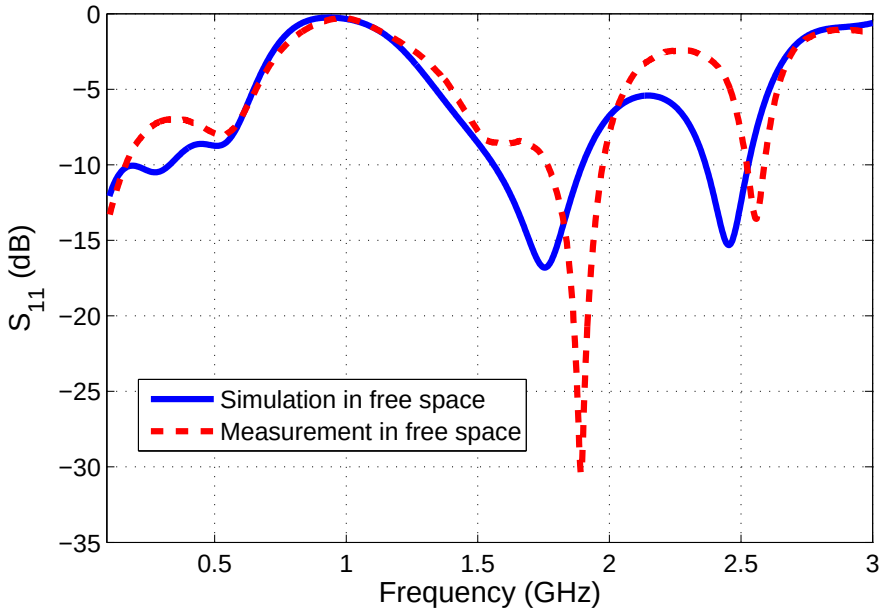

Figure 4.6: Unloaded Performance of the Spiral Resonator S_{11} in magnitude.

4.3.1 Testing of the Second Prototype with Liquid Phantoms

Experiments with liquid phantoms were performed in an anechoic chamber, to minimise the environmental effects. The liquid phantoms, given in Chapter 3 were again used to test the resonator. Liquid phantoms were poured into ziplock plastic bags. Second prototype of the resonator was fixed on a styrofoam. Response of the resonator was collected by placing phantoms with different sugar concentrations above the resonator. The thickness of all the phantoms was 5 cm. S_{11} measurement results are shown in Fig. 4.7. From the S_{11} responses, the first mode occurs around 90 MHz; second, third, and forth modes occur around 700 MHz, 1.3 GHz, and 1.45 GHz respectively.

In this section, we are focusing on the second and third mode of the resonator, since the first mode occurs at a very low frequency. The fourth mode is not considered as the matching is weak. For the empirical retrieval method, the

measured dielectric properties of the 10% and 20% sugar solutions are used to calculate the effective length l_{eff} and the coefficient A, so-called calibration.

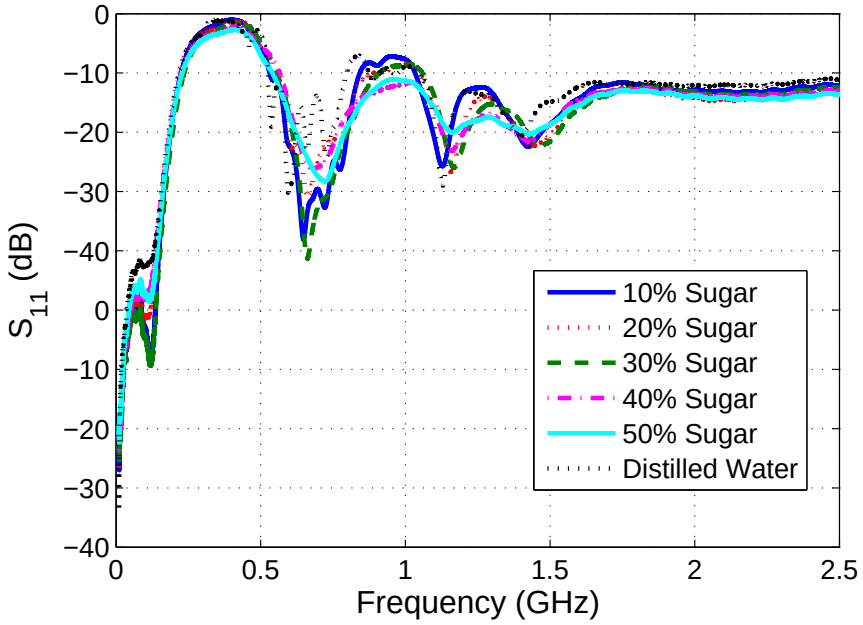

Figure 4.7: S_{11} measurement results with liquid phantoms containing different amount of sugar.

Table 4.4: Comparison Between Reconstructed and Measured Relative Permittivities of Solutions with 2^{nd} Prototype

Second Mode				
Phantom (%)	*Frequency (GHz)*	*Retrieved* ε_{phan}	*Measured* ε_{phan}	*Error (%)*
10	0.6472	76.46	76.47	0.0131
20	0.6620	72.53	72.55	0.027
30	0.6658	71.58	68.48	4.52
40	0.6866	66.72	63.32	5.37
50	0.7227	58.91	55.73	5.71
Third Mode				
Phantom (%)	*Frequency (GHz)*	*Retrieved* ε_{phan}	*Measured* ε_{phan}	*Error (%)*
10	1.129	75.14	75.15	0.01
20	1.157	71.14	71.15	0.01
30	1.169	69.52	66.47	4.61
40	1.171	69.25	59.90	15.61
50	1.181	67.94	51.35	32.31

The relative permittivities of the phantoms are calculated by using equation (4.2) and (4.3) and calculated values are compared to those measured by the MCL probe. Table 4.4 shows the measured and calculated relative permittivity

at the second and third modes of the resonator. Error of the retrieved relative permittivity is calculated with equation 4.4. Error percentage for all phantoms at the second mode is less than 6%.

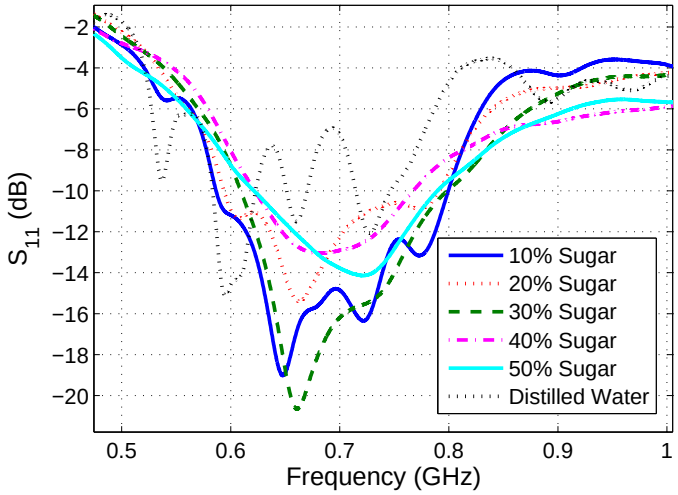

(a)

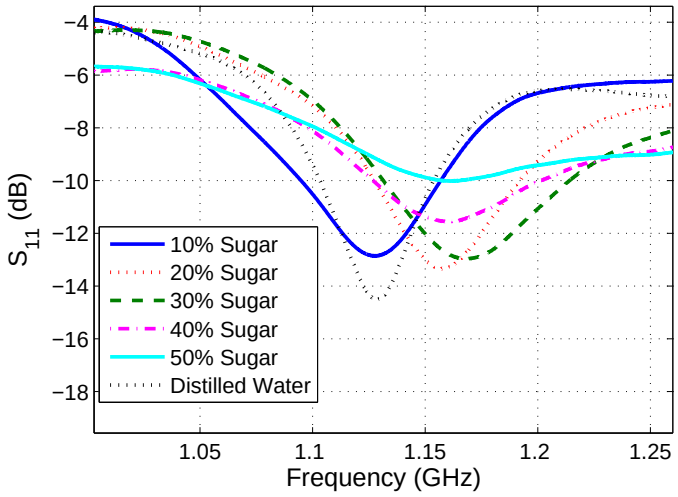

(b)

Figure 4.8: Zoomed version of the measured change in reflection response with different liquid phantoms shown in Fig 4.7:(a) S11 measurement at second resonance, (b) S11 measurement at third resonance .

The error starts to increase for the 30% phantom. In the second mode, calibration is performed based on the relative permittivity and resonance frequencies of the 10% and 20% sugar solutions. The difference in relative permittivity between the two calibration solutions is 3.92 units, and the resonance shift is 148 MHz. The difference between 20% and 30% sugar solutions is 4.07 units and the shift is 38

MHz. So the shift in frequency should be bigger for the calibrated equation to come up with closer values to the measured relative permittivities. Note that, by calibrating the resonator with 10% and 20% sugar solutions and taking the l_{eff} and A as constants, we are assuming that the behaviour of the resonator is linear.

The error for the third mode increases for higher sugar concentrations. This is due to the matching at the third mode, which degraded when the 40% and 50% solutions were placed above the resonator. Such behaviour is expected, due to the significant change in both relative permittivity and effective conductivity for 40% and 50% solutions. When the resonator response is checked, the depth of the notch is 11.56 dB and 10.01 dB, for 40% and 50% sugar liquid phantoms, respectively. This indicates that the resonance disappears if a higher percentage of sugar concentration is placed above the resonator. Also, it is expected the higher order modes have lower Q factors.

The repeatability of the liquid phantom measurements was also investigated. Measurements are repeated 10 times in the anechoic chamber. However, due to the mismatch introduced by the plastic bag and the unstable geometry of the liquid phantom, shifts in the resonance frequency were produced. Also, during the measurements, it was understood that the thickness of the phantom has a crucial role on the effective permittivity; thus, on the resonance of the sensor. With the plastic zip-lock bags, keeping a constant phantom thickness is cumbersome. Thus, the repeatability of the measurements with liquid phantoms is quite a challenge. One way to overcome such physical restrictions is to place a superstrate on top of the resonator, or covering the resonator with a bio-compatible material, such as medical-grade silicone, which is traditionally used for implantable antennas [15, 16]. Then the sensor can be mounted on the bottom of a container and the liquid phantom can be poured into the container. By keeping the thickness of the liquid phantom constant, the experiments can be repeated. However, such alterations would change the effective permittivity of the superstrate; therefore, electromagnetic behavior of the sensor. Another way to overcome this challenge is using semi-solid of phantoms. Thus, gel-like phantoms were also examined and the repeatability of the measurements are quantified in Section 4.3.2.

4.3.2 Testing of the Second Prototype with Semi-solid Phantoms

Conceptually, the experimental methodology is simple. First, the semi-solid physical phantoms, proposed in Chapter 3, are prepared; second, the dielectric properties of each phantom are measured across a wide frequency band using a vector network analyzer (Hewlett Packard 8720ES VNA) with an open-ended coaxial probe, as a reference for the resonator; finally, the resonator is used with each phantom, and S_{11} (magnitude and phase) measurements performed with the VNA. The experiment set-up is shown in Fig. 4.9.

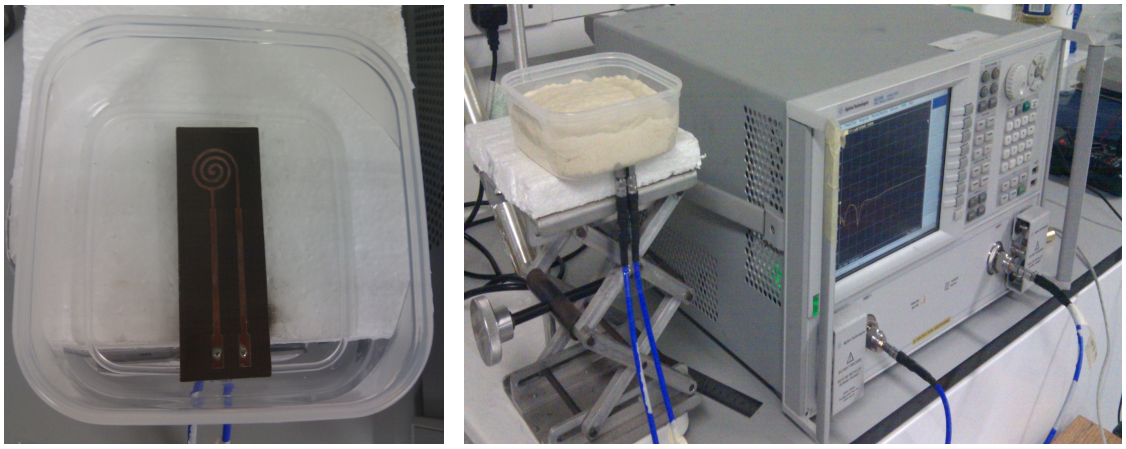

(a) (b)

Figure 4.9: Phantom measurements: (a) resonator mounted at the bottom of a container, (b) phantom material placed above the resonator.

The phantoms used are termed gel-like; they are semi-solid and require protection from the atmosphere when not in use. This was achieved by covering them with plastic bags. As previously reported in earlier sections, it had been observed that the resonant frequency of the sensor is affected by the thickness of the sample, the pressure applied to the resonator, and the surface condition of the phantom [17]. Thus, the thicknesses and weights of the phantoms were kept constant. Ten measurements in total were performed with the resonator mounted at the bottom of a container and each phantom placed just above the resonator. All measurements were performed at 21° C. Measured S_{11} responses with different phantoms are shown in Fig. 4.10. From the measured results, it

can be seen that the resonance does not change much; this is due to the close dielectric properties of the semi-solid phantoms.

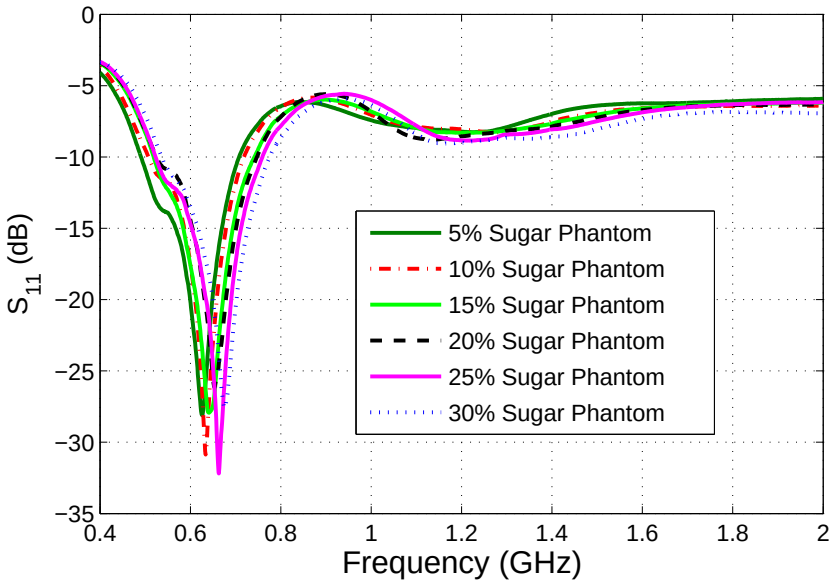

Figure 4.10: Performance of the spiral resonator with the semi-solid phantoms placed above, the averaged S_{11} measurements with $5-30\%$ sugar phantoms. .

Although the relative permittivity change in the semi-solid phantoms is still far from the realistic changes in the blood glucose levels [18], the semi-solid phantoms present a better representation when compared to liquid phantoms. Also, since the effective permittivity does not change significantly, the resonance is not at risk of disappearing within the range of sugar concentrations. Which means that the change of glucose amount in the blood is much lower than the proposed sugar amount change in the phantoms. As the error is increasing with the high change in the sugar amount, when this technique is applied to blood glucose change detection such error will not be apparent due to the low glucose fluctuation in blood.

Applied pressure is another factor that might affect the S_{11} measurements; therefore, after characterizing the homogeneous phantom, the weight of the samples are remeasured and the weight kept at 265 grams. The sensor is operating around 600 MHz when the phantoms are placed on top; the resonance frequency shifts to the higher frequencies as the relative permittivity of the phantoms decreases. Note that 600 MHz appears at the second mode; the first mode occurs

at a very low frequency and was therefore ignored.

Fig. 4.11 shows the measured resonant frequency with change in sugar concentration, for averaged S_{11} and insertion loss. It is evident that the S_{11} data shows a more controlled, almost linear, relationship with sugar concentration compared with the S_{21} data; however, the change in resonant frequency is confined to a relatively narrow (40 MHz) band of frequencies for the S_{11}, whereas the band of variation is almost three times that for the insertion loss (120 MHz).

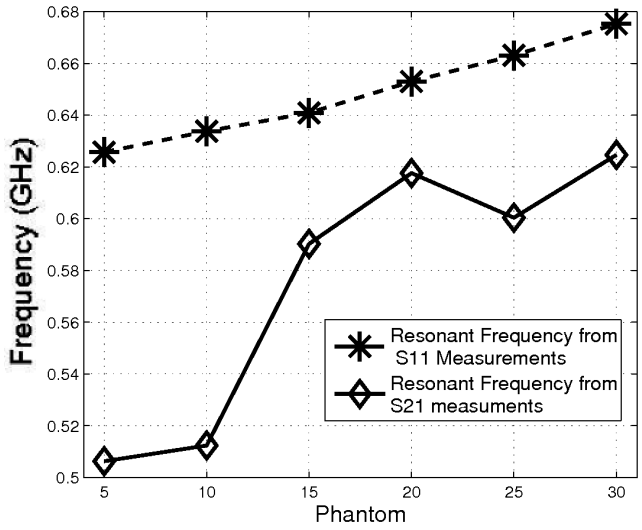

Figure 4.11: Variation of resonance frequency with the change of sample with different sugar concentration.

Dielectric properties measured with the coaxial probe at resonance frequencies are given in Table 4.5 and wide band measurements can be found in Chapter 3. The dielectric properties are retrieved with the empirical formulation described in Section 4.1.

To investigate the shift in S_{11} resonant frequency with respect to phantom further, the change in resonant frequency relative to that of the previous sample was plotted, shown in Fig. 4.12 (a). Here, the relationship between the increase in glucose concentration and increase in resonant frequency is shown to be non-linear.

Table 4.5: Retrieved and Measured Relative Permittivity Comparison of the Semi-solid Phantoms [19]

Parameter	Value			
Sugar %	30	25	20	15
Retrieved $\varepsilon_{\text{phantom}}$	24.269	26.377	28.182	30.063
Measured $\varepsilon_{\text{phantom}}$	21.654	23.809	25.637	29.310
Error %	12.07	10.78	9.92	2.56
f_c(MHz)	680.273	669.148	660.046	650.943

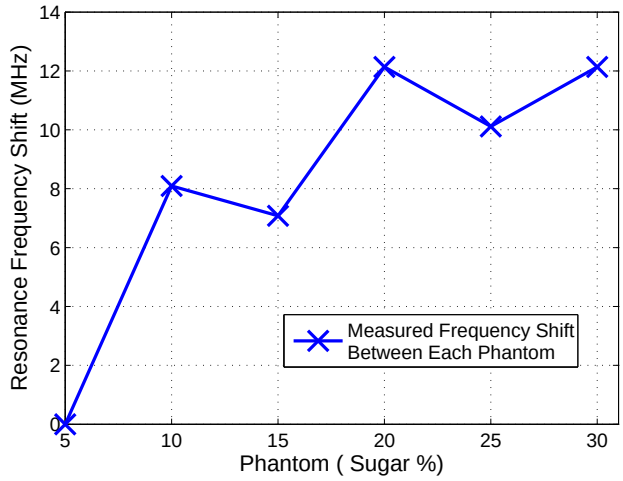

(a)

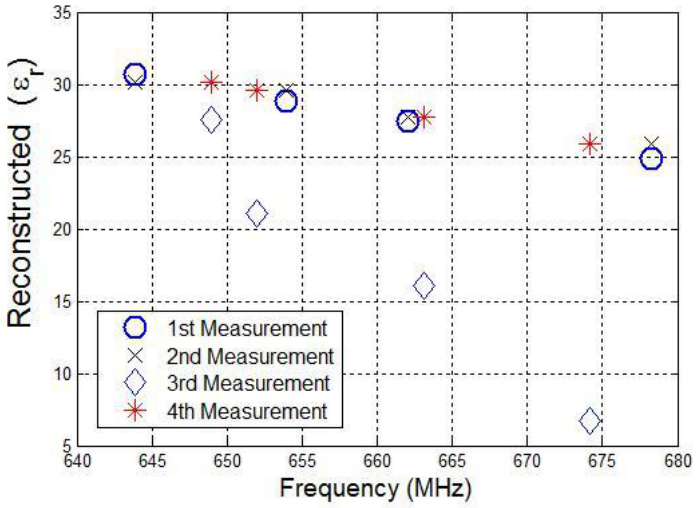

(b)

Figure 4.12: Analysis of S_{11}-based detection performance: (a) mean frequency shift between each successive phantom; (b) repeatability of retrieved relative permittivity .

Finally, Fig. 4.12(b) shows the retrieval error for the phantom's relative permittivity, with respect to the measured reference data. The measured reference relative permittivities found using the open-ended coaxial probe varied from 34 to 21 as the sugar concentration increased. The resonant frequencies are identified from the S_{11} data.

Although the maximum error in retrieved dielectric properties with the traditional analytical formulation is less than 13%, the gap between the measured and retrieved relative permittivity, termed the retrieval error, increased with decreasing phantom relative permittivity (increasing sugar concentration), as shown in Table 4.5. This indicates that the assumption that A and l_{eff} are not strongly affected by changes in the phantom relative permittivity is invalid. The dielectric properties (Table 4.5) were calculated considering only the frequencies consecutively increasing while the phantom relative permittivity was decreasing. In the calculations with traditional empirical method, the best four consecutive measurements were chosen and averaged, then the dielectric properties retrieved at the corresponding resonance frequencies. Note that the 5% and 10% sugar concentrations were used for calibrating the resonator, so the results are shown for 15% sugar concentration and above in Table 4.5.

4.3.3 Parameter Retrieval with Modified Analytical Method

Particle swarm optimization

Particle swarm optimization is an evolutionary algorithm first introduced by Kennedy and Eberhart in 1998; since then, the algorithm has been applied to solve many different problems, including electromagnetic problems, such as optimization of free space and implantable antenna geometries for maximum bandwidth, gain, or to tune the antenna for desired frequency of operation [20, 21, 22]. The algorithm finds an optimal solution to a problem from a pre-determined solution space by iteratively adjusting the trajectories of particles according to the personal best position of each particle and overall, global, best position of the swarm. The algorithm is powerful and simple and has a wide range of applications. More information is given, including the PSO terminology, in Appendix

A. In this work, the algorithm was used to solve a two-dimensional problem.

The previously introduced method required a calibration procedure [19]. Here, the calibration procedure is eliminated by utilizing simulation results to predict the values of the unknown parameters. In order to further decrease the retrieval error, the unknowns A and l_{eff} should both be expressed as functions of frequency (f_c) and phantom relative permittivity ($\varepsilon_{\text{phantom}}$). To do so, twelve digital homogeneous phantoms with different non-dispersive relative permittivities were placed above the resonator in CST Microwave Studio and the S-parameter responses of the resonator recorded. The digital homogeneous phantoms were 30 mm thick, with the relative permittivities ranging from 15 to 40.5. The simulated S_{11} response of the resonator is shown in Fig. 4.13 for the different phantoms.

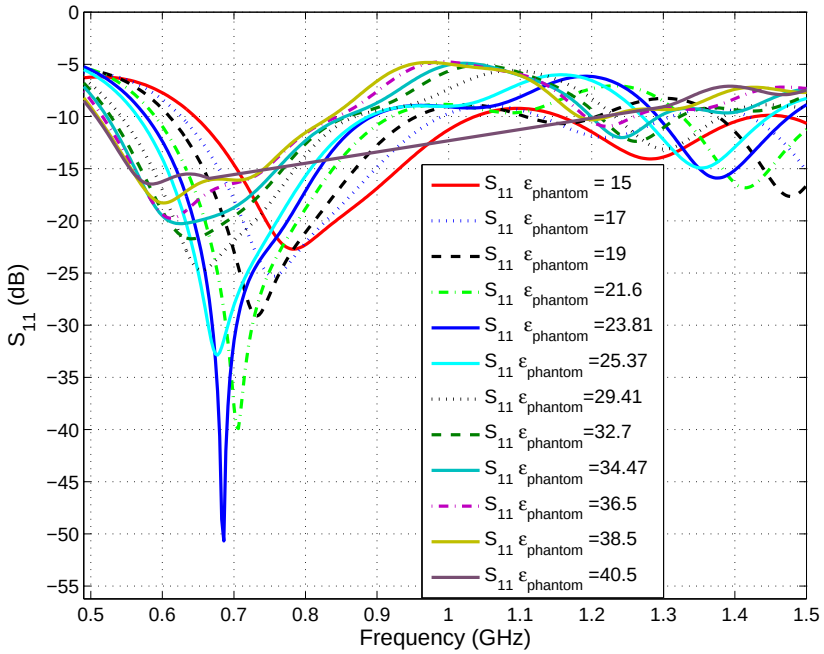

Figure 4.13: Simulations with phantoms.

From the recorded S_{11} simulation results, the operating frequencies of the resonator with different phantoms are determined. The PSO algorithm is applied to the analytical formulation in order to find the corresponding A and l_{eff} for each simulation. The algorithm is given the resonant frequency and the known phantom relative permittivity for each of the twelve CST simulations. The feasible solution space for A should be between zero to one, due to the construction of

equation (4.3), and the solution space for l_{eff} is chosen to be from 215.80 mm to 243.15 mm; this range is chosen considering the physical length (224.0520 mm) of the resonator. The fitness function for the algorithm is the phantom dielectric property retrieved from equation (4.3). The threshold is chosen as 0.009%. To calculate the threshold the absolute difference between the $\varepsilon_{\text{phantom}}$ and given $\varepsilon_{\text{phantom}}$ is calculated and the absolute difference is divided by given $\varepsilon_{\text{phantom}}$, then the percentage is calculated by multiplying with 100, given in equation 4.4. Note that the given $\varepsilon_{\text{phantom}}$ is the value of the digital phantom in the simulation.

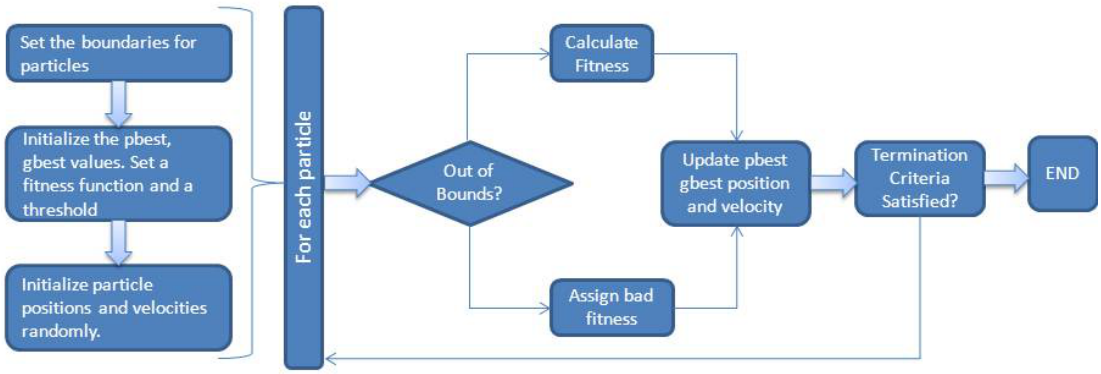

Figure 4.14: Flow chart of the PSO algorithm.

As long as the threshold is satisfied, the optimization technique can result in random values for A and l_{eff} within the given solution space. In order to obtain an increasing set of data, the feasible solution space for l_{eff} is reassigned for each simulation where as the solution space for A remained between 0 to 1. In the PSO algorithm utilized, the invisible boundary condition was used; that is, the particles can fly out of the defined solution space and these values are assigned simply a bad fitness value. By limiting the solution space for l_{eff} for each simulation, we limit the l_{eff} values that the algorithm can come up with and, in this way, an increasing set of data is obtained. Note that there is no single solution of A and l_{eff} to the problem, so we must limit the number of solutions by defining a solution space. The solutions are reached using 50 particles within 10 to 30 iterations. Flow chart of the algorithm is given in Fig. 4.14. The algorithm allowed independent A and l_{eff} values to be found. The point estimations of two unknowns are then used to fit a function to the obtained data set, given in Table 4.6, with the MLR method.

Multiple Linear Regression

Next, the filling factor and effective length are expressed as a function of resonant frequency and the relative permittivity of the phantom material by using an MLR model [23]. Different models of the relationships between frequency, phantom relative permittivity and filling factor or effective lengths were examined. Some were obviously worse than others; here are shown two forms that were qualitatively similar, as examples. Equations for the first model of l_{eff} and A are given in (4.5) and (4.6), respectively. The regression coefficients in (4.5) and (4.6) were calculated with the method of least squares [23].

$$l_{\text{eff}_{(f_n,\varepsilon_{\text{p}})}} = a_1 + a_2\frac{c_0}{f_n} + a_3\frac{1}{\varepsilon_{\text{p}}} \tag{4.5}$$

$$A_{(f_n,\varepsilon_{\text{p}})} = b_1 + b_2\frac{c_0}{f_n} + b_3\frac{1}{\varepsilon_{\text{p}}} \tag{4.6}$$

The regression coefficients a_1, a_2, a_3 are 0.2954 units, -0.0644 units , -0.8083 units for (4.5), and b_1, b_2, b_3 are 1.7446 units, -1.5472 (1/m), -14.1472 units for (4.6), respectively. Note that the coefficients are calculated based on the data from the simulation response.

The second model is given by:

$$l_{\text{eff}_{(f_n,\varepsilon_{\text{p}})}} = a_4 + a_5\frac{c_0}{\sqrt{f_n}} + a_6\frac{1}{\sqrt{\varepsilon_{\text{p}}}} \tag{4.7}$$

$$A_{(f_n,\varepsilon_{\text{p}})} = b_4 + b_5\frac{c_0}{\sqrt{f_n}} + b_6\frac{1}{\sqrt{\varepsilon_{\text{p}}}} \tag{4.8}$$

In 4.7, a_4, a_6 is in units and a_5 is in $\sqrt{s}$. In 4.8, b_4, b_6 is in units and b_5 is in $\sqrt{s}$/m. Fig. 4.16 (a) shows a graphical representation of the l_{eff} output for simulations from the PSO algorithm and the two models fitted by MLR. From Fig 4.16 (a), it can be seen that the two functions are fairly similar; however, the function given in (4.5) has a numerically better fitting to the PSO output than that of (4.7). Similarly, Fig 4.16 (b) shows the functions fitted to the A coefficient PSO output; the function given in (4.6) has a better fitting. Alternative representations of (4.5)–(4.6) obtained for A and l_{eff} are shown in Fig. 4.15 (a) and Fig. 4.15 (b), respectively, where the functions are shown as surface plots. These demonstrate the solution spaces of (4.5) and (4.6) for the stated regression coefficient values, and the need for additional information (in this case, the

simulations and PSO results derived from them) to determine the expected single-valued relationships.

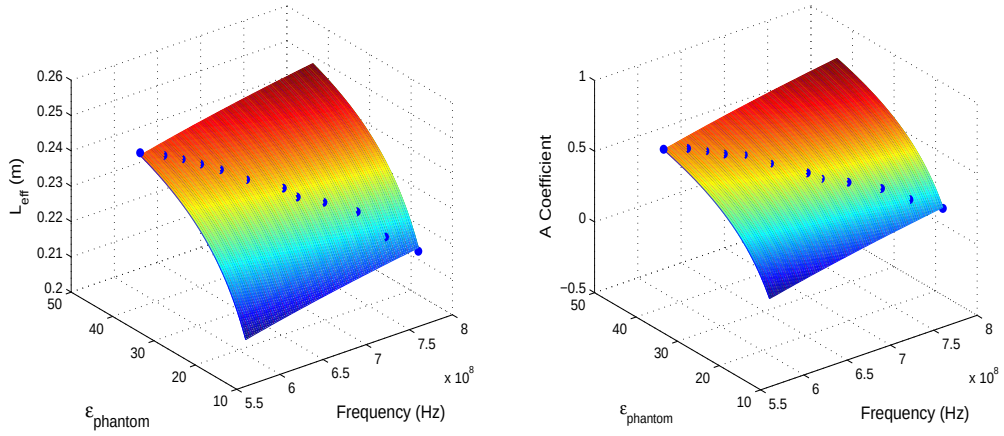

(a) (b)

Figure 4.15: Fitted functions: (a) l_{eff} as a function of f and ε_{p}, (b) A as a function of f and ε_{p}. The blue dots show the data obtained from the PSO algorithm and the surface is the function with the coefficients obtained through the MLR method.

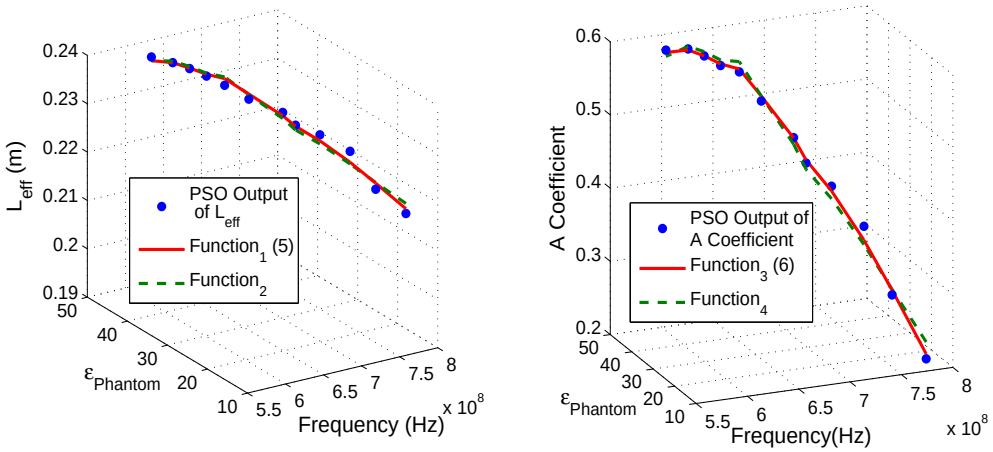

(a) (b)

Figure 4.16: Fitted functions with MLR for l_{eff} and A coefficient: (a) comparison between function$_1$ (4.5) and function$_2$ (4.7); (b) comparison between function$_3$ (4.6) and function$_4$ (4.8). The blue dots show the data obtained from the PSO algorithm.

Statistical analysis of both fitting functions ((4.5) and (4.6)) was performed to determine the reliability of the regression coefficients. Both A and l_{eff} are within the 95% confidence interval and the coefficient of determination is 0.997 and 0.983

for A and l_{eff}, respectively. For both functions, the p value is much smaller than $\alpha = 0.05$. Thus, the outputs of the fitting function for the obtained data sets are deemed statistically significant.

The right side of (4.2) is equated to the right side of (4.3), giving:

$$\left(\frac{nc_0}{l_{\text{eff}_{(f_n,\varepsilon_{\text{p}})}} f_n}\right)^2 = A_{(f_n,\varepsilon_{\text{p}})}\varepsilon_{\text{r}} + \left(1 - A_{(f_n,\varepsilon_{\text{p}})}\right)\varepsilon_{\text{p}} \tag{4.9}$$

Finally, the functions (4.5) and (4.6) for A and l_{eff} are inserted into (4.9), to be solved numerically.

4.3.4 Results and Discussion

Simulated and measured operating frequencies are inserted into (4.9) for each phantom and the equation solved with the Newton-Raphson (NR) method. The initial guess for the NR method was chosen as 20 and the solution space was constrained between 0 and 100, in order to prevent the method from finding negative and very high roots. These values were selected as the dielectric properties of human body tissues are located in this range.

Table 4.6 shows a comparison of the retrieved phantom relative permittivity, the known relative permittivity given to the digital phantom during the simulation, and retrieval error, along with the operation frequencies. The retrieval error for all 12 digital phantoms is less than 2.7%. The sources of retrieval error are, first, the error resulting from the PSO algorithm's threshold and, second, the fitting functions for A and l_{eff}. The final error source is the solution space constraint for the NR model. The NR model suggests the following:

$$x_{\text{n+1}} = x_{\text{n}} - \frac{f_{(x_{\text{n}})}}{f'_{(x_{\text{n}})}} \tag{4.10}$$

Where $\text{x}_{\text{n+1}}$ is the current guess of phantom relative permittivity, x_{n} is the former guess of the phantom relative permittivity, $\text{f}_{(x_{\text{n}})}$ is the function given in 4.9 with the former guess of phantom relative permittivity, and $\text{f}'_{(x_{\text{n}})}$ is the derivative of the function given in 4.9. Since the solution space is restricted in this case study, the left side of (4.10) should be replaced with $x_{\text{n+1}} + \triangle(n)$, with $\triangle(n)$ representing the error due to the feasible solution space constraint. The constraint directly

Table 4.6: Relative Permittivity retrieval from simulation results, with 33 by 95 mm and 30 mm thick phantoms.

Parameter	Value											
Sugar %				30	25	20	15	10	5			
Retrieved $\varepsilon_{\text{digital phantom}}$	14.9	16.8	18.8	21.7	24.4	25.8	29.7	32.1	34.5	36.3	38.0	40.4
Given $\varepsilon_{\text{digital phantom}}$	15	17	19	21.6	23.8	25.37	29.41	32.7	34.47	36.5	38.5	40.5
Error % of Retrieved $\varepsilon_{\text{digital phantom}}$	0.67	1.18	1.05	0.46	2.6	1.69	0.99	1.83	0.09	0.55	1.3	0.25
Simulated f_c (MHz)	784.4	755.0	732.0	706.1	685.8	677.1	653.9	639.4	624.9	613.3	601.7	584.3
Measured f_c (MHz)				672.99	662.37	653.17	647.91	634.46	628.58			
A	0.203	0.291	0.385	0.438	0.469	0.502	0.547	0.582	0.589	0.600	0.607	0.604
L_{eff} mm	0.215	0.221	0.228	0.231	0.233	0.235	0.237	0.239	0.240	0.241	0.242	0.243

affects the retrieved relative permittivity; however, without the restriction of the solution space, the NR method might give very high or low roots, meaning such a restriction is necessary.

Finally, the error in extracted phantom relative permittivity (ε_{p_s}), compared with the given or measured relative permittivity (ε_{p_c}), is determined from equation (4.4).

Table 4.7: Retrieved and Measured Relative Permittivity Comparison of the Solid Phantoms With the Modified Analytic Formulation

Parameter	Value					
Sugar %	30	25	20	15	10	5
Retrieved $\varepsilon_{\text{phantom}}$	26.5	28.3	29.8	30.7	33.0	34.0
Measured $\varepsilon_{\text{phantom}}$	21.6	23.8	27.6	29.3	33.0	34.38
Error %	22.2	18.85	7.85	4.67	0	0.87
f_c (MHz)	672.99	662.37	653.17	647.91	634.46	628.58

Table 4.7 shows the comparison between the retrieved and measured dielectric properties. The error sources are explained in the remainder of the chapter and an error comparison with the previous method is given. The resonant frequencies are obtained by averaging all ten measurements taken with the spiral resonator. The measured $\varepsilon_{\text{phantom}}$ values are the electrical property measurements performed by using Agilent's open ended high temperature dielectric probe at the corresponding frequencies. Note that, as the measurements are taken between 300 MHz to 3 GHz with sixteen hundred points, the resonant frequencies may not correspond to the measurement frequencies. In such cases, the closest frequency of the dielectric probe measurement is chosen as the reference dielectric property measurement. The dielectric properties are a smooth function of the frequency; thus, such an approximation is valid.

The error percentage is calculated using (4.4), which gives less than 23% for all measurements. As can be seen from Table 4.7, the error is increasing as the phantom relative permittivity decreases. In Table 4.6, the retrieval results for 30 and 25 % sugar phantoms are higher than those given in Table 4.5. This is due to the frequency difference between the two tables: note that in Table 4.5, four successive measurements have been chosen and averaged. The dielectric

properties are also calculated for successful measurement frequencies previously shown in Table 4.5, by using the modified analytical formulation, giving values for ε_p of 25.3, 27.1, 28.6, and 30.2, for frequencies of 680.273, 669.148, 660.046, and 650.943 MHz, respectively. The retrieval error in this case for 30% and 25% sugar phantoms are 16.8% and 13.8%, respectively. In addition to the error sources given for the simulation results in Table 4.6, the discrepancy between the retrieved and measured phantom dielectric properties can also be partially attributed to measurement errors. Two different measurement errors may have occurred: 1) measurement error due to the spiral resonator; and 2) measurement error due to the coaxial probe.

Measurement Error due to the Spiral Resonator

During the simulations, the size and shape of the phantoms are considered ideal and homogeneous. However, the shape and condition (i.e., the surface hydration) of the phantom may not be ideal for the measurements. Thus, such imperfections can introduce measurement errors.

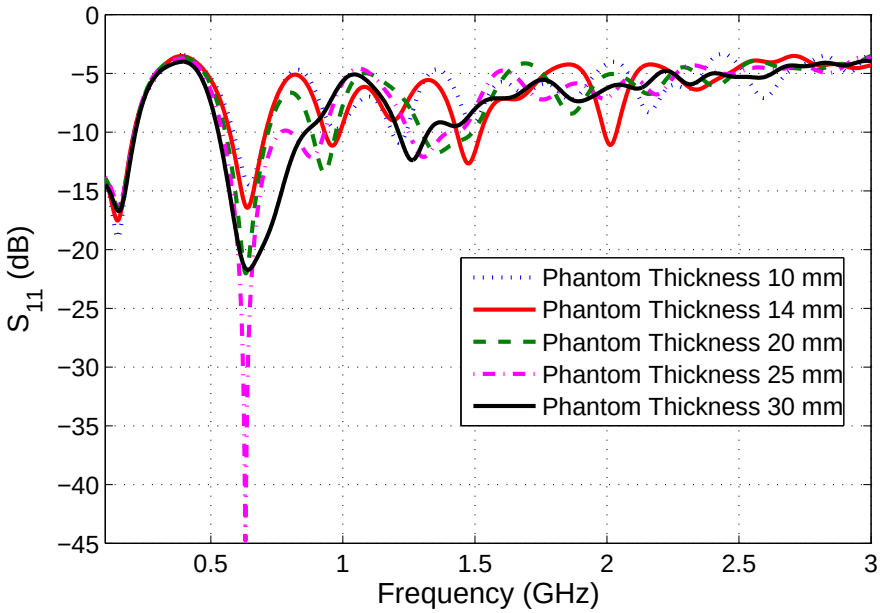

Figure 4.17: S_{11} response of the resonator to the changes in the thickness of the phantoms.

From the simulations, we know that the thickness of the sample phantom affects the resonance of the spiral sensor. As the sample thickness increases, the

effective permittivity increases; thus, the resonator starts to operate at lower frequencies. Which means that around 0.6 GHz there is a need to use a thicker phantom for the wave to attenuate before the boundary of the phantom with the air. As the wave is not attenuating within the phantom the effective permittivity is including the air as well. However, when the phantom thickness is increased the percentage of phantom relative permittivity contribution to effective permittivity increases while the contribution from air is decreasing making the permittivity higher. Thus, the sensor starts to resonate at lower frequencies.

The effect of thickness is investigated by simulating the spiral structure with five phantom samples having a thickness of 10 mm to 30 mm. The dielectric properties of the phantoms are kept constant ($\varepsilon_r = 32.7$ and $\sigma = 0.284$ S/m) and the size of the phantoms are 95 by 33 mm. The change in the S_{11} response is given in Fig. 4.17. From the simulation response, we can conclude that the response of the resonator is affected by the phantom thickness, increasing the resonance response by around 17 MHz for the samples studied; however, the linearity changes with the 30 mm phantom.

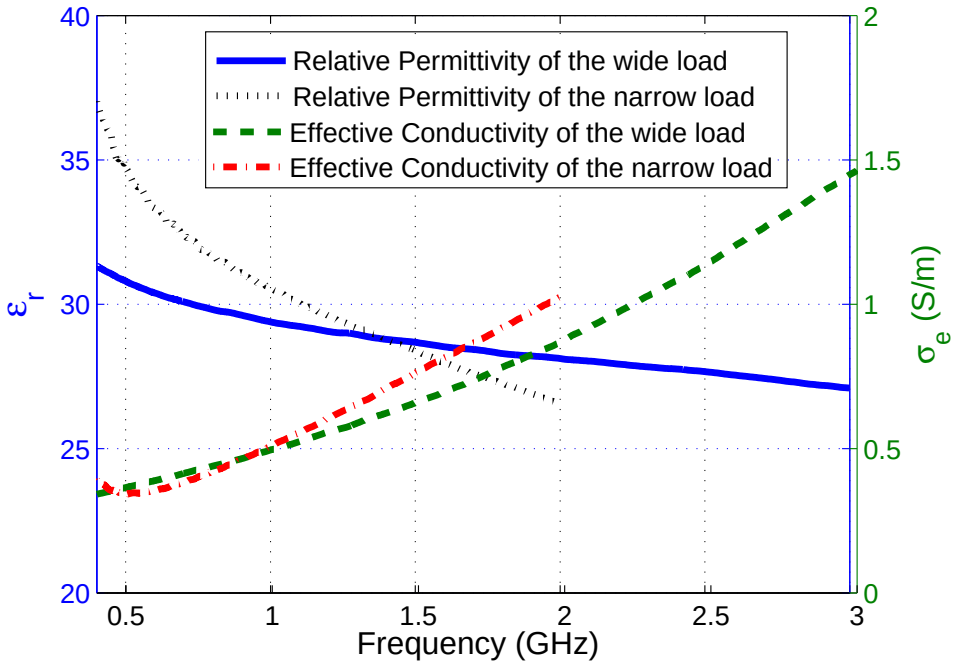

Figure 4.18: Effective conductivity and relative permittivity measurements of the wide-load and narrow-load with (10% sugar) phantom.

To examine the real effect of the load size on the response of the spiral resonator, it was simulated with two phantoms of different sizes. The phantoms are named wide and narrow load phantoms and both had the same dielectric properties: $\varepsilon_r = 32.7$ and $\sigma = 0.284$ S/m. Note that the dielectric properties correspond to the 10% sugar concentration phantom. The surface dimensions of the wide load phantom are 125 mm by 125 mm, and the dimensions of the narrow load phantom are 95 mm by 33 mm; both phantoms have the same thickness of 30 mm. The structure is modelled by placing a box above the spiral resonator and assigning the dielectric properties and sizes of the wide and narrow load phantoms.

(a) (b)

Figure 4.19: Measurement setup: (a) S_{11} measurement with wide load phantom; and (b) resonator mounted in a container with the wide load phantom above.

The resonator response was also measured with an equivalent wide load physical phantom. The wide load phantom was composed by following the recipe of oil-in-gelatine phantoms, that has been used to mimic the dielectric properties of biological tissues [24]. The wide load phantom was a liquid phantom when first composed; it solidified over night at room temperature. To perform the measurement, the resonator was mounted at the bottom of a plastic container, facing upwards, with the container dimensions of 125 mm by 125 mm. The liquid wide load phantom was poured into the container to a thickness of 30 mm and left overnight to solidify. The S-parameter response of the resonator was then collected.

After the measurements of spiral resonator response were complete, the dielectric properties of the phantom were measured with Agilent's high temperature dielectric probe. Dielectric property measurements were collected at 10 points, twice from each point (including above and below surfaces of the phantom, a total of 20 measurements) and averaged to obtain the properties given in Fig. 4.18. The measured dielectric properties at 600 MHz are $\varepsilon_r = 30.53$ and $\sigma = 0.5043$ S/m. The measurement set-up with the spiral structure is shown in Fig. 4.19. Note that all measurements were collected within 24 hours of the phantom composition.

The comparison of the S_{11} is given in Fig. 4.20. Although there is a dielectric property discrepancy between the physical and digital phantoms, simulated and the measured S_{11} for the wide load phantom agrees well with 19.5 MHz discrepancy in resonant frequency. The narrow load phantom measurement and simulation are given in Fig. 4.20, where a relatively small 13.7 MHz discrepancy is observed between measured and simulated S_{11} responses. However, when the simulations for narrow and wide load phantoms are compared, we observed a 95.7 MHz discrepancy between the resonance frequencies.

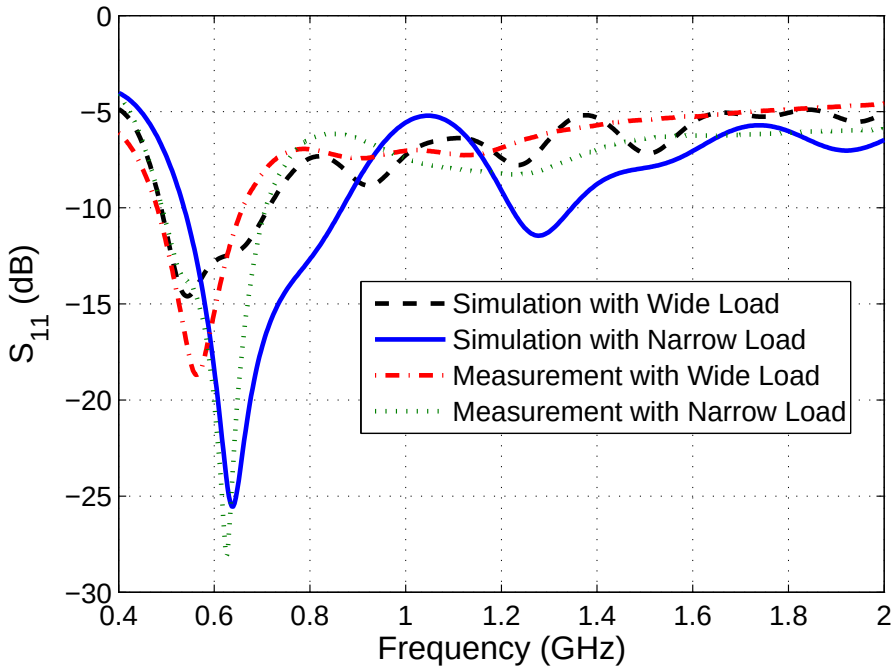

Figure 4.20: S_{11} response of the resonator with wide and narrow load phantoms.

From the presented analysis, we can state that the thickness and other dimensions of the phantoms have a significant effect on the S_{11} response of the resonator. Thus, the phantom shape and size results in retrieval errors. We can conclude that for the intended application of non-invasive blood glucose monitoring, the sensor is subject-specific and would require some form of calibration as a result, particularly if absolute BGL measurements are desired.

The spiral resonator is also sensitive to the surface condition of the phantom; in addition, the applied force/pressure also contributes to the measurements taken with the spiral resonator. From Table 4.7, it can be seen that the error has increased for 25% and 30% sugar measurements. In the simulation results, the resonator operates at 706.1 MHz and 685.8 MHz when phantoms with 30% and 25% dielectric properties are placed above, respectively. Due to the discrepancy between measured and simulated resonant frequencies with similar dielectric phantom properties, the error is attributed the measurement errors. However, it is very unlikely in the application of non-invasive sensing of diabetes patients, that blood glucose level can reach up to 25% sugar level. The glucose levels of a healthy person is ranging from 72 mg/dl to 216 mg/dl. The upper limit namely 216 mg/dl corresponds to 0.22%. Thus the derived formulas are valid for such application can be derived using the proposed technique for other resonator designs.

Measurement Error due to the Coax Probe

The second error source is the dielectric property measurements performed with the Agilent's open ended coaxial probe. The repeatability of coaxial probe measurements was not confirmed during the measurement routine of the semi-solid phantoms. The dielectric probe can pick up faulty measurements if the probe is not in good contact with the sample; the flange at the tip of the high temperature probe obstruct eye inspection to ensure the proper contact with the sample, especially when an opaque sample has been used. Apart from the physical limitations, the probe itself may introduce measurement errors. The accuracy of the high temperature dielectric probe is given as follows [25]:

$$\varepsilon_{\mathrm{r}}' = \varepsilon_{\mathrm{r}}' \mp \ 0.05 \ |\varepsilon_{\mathrm{r}}^*| \tag{4.11}$$

$\varepsilon_{\mathrm{r}}'$ is the relative permittivity and $\varepsilon_{\mathrm{r}}^*$ complex dielectric property of the sample. In this study, the measured relative permittivity of the phantoms varies between 21 and 34 and the measured conductivity varies between 0.19 S/m and 0.4 S/m at the frequency of interest. Therefore, it is expected that the error in the phantom relative permittivity measurement is in the range of 1 to 1.7.

To examine the measurement errors that can be introduced by the coax probe, the dielectric property measurements given in Fig. 4.18 was analyzed. Considering the frequency of interest, the mean and standard deviation for 20 measurements taken from the same sample were calculated. The mean relative permittivity at 600 MHz is 30.5 and the standard deviation is 3.04. This implies a potential error of more than 10% for measured values outside one standard deviation, which could be a significant source of error when using the coax probe measurements as the reference for evaluating the performance of the spiral resonator.

4.4 Conclusions

In this Chapter, two prototypes of a microstrip resonator were designed and fabricated for dielectric property retrieval of biological tissues. The first prototype was tested with solutions containing different amounts of sugar and by placing the solutions stored in plastic bags above the transmission line. Significant shifts in S_{11} nulls were observed when the solutions with different sugar content were placed on the sensor. The relative permittivity were retrieved from the S_{11} response of the planar transmission line by tracking the resonance frequency. The equations used for relative permittivity retrieval have been given. The electrical properties of the phantoms were measured with the MCL coaxial probe for verification purposes. Reconstructed relative permittivities are compared with the previously collected MCL slim probe measurements.

The second prototype was tested with six physical phantoms, composed of flour, distilled water, and sugar. The amount of sugar in the physical phantoms

was altered from 5 % to 30 % in 5% increments. The S_{11} response of the transmission line was measured and, at the resonance frequency, the relative permittivity of the phantoms with 15, 20, 25, and 30 percent sugar were calculated using analytical formulations. Retrieved relative permittivities are compared with the reference data collected with the Agilents high temperature open ended coaxial probe. An error analysis was carried out and it has been observed that the retrieval error is less than 12.1 % for all measurements. The measurements are performed with gel-like phantoms, since using liquid phantoms required an additional material, such as a plastic layer or a superstrate, between the phantom and the resonator. The repeatability of the measurements was also examined by performing the measurements ten times within 24 hours of the characterisation of the phantoms. The proposed approach was a promising application for monitoring dielectric property change in biological tissues; however, better calibration is needed to increase the accuracy.

In order to modify the analytical formulation, the resonator was simulated with twelve digital cuboid phantoms, with different relative permittivities, placed above the resonator and the S_{11} response of the resonator was recorded. The analytical formulation was adjusted, termed as the *modified analytical formulation*, by using the simulated S_{11} response of the transmission line. This was done by finding an optimal solution for the analytical formulation with the PSO algorithm for each simulation response. This approach provided an insight on the behavior of the resonator when the physical phantoms were placed above.

The obtained data was utilized to express A and l_{eff} as a function of frequency and the relative permittivity of the phantom. The functions for A and l_{eff} were written using an MLR model. The retrieval of the relative permittivities of the phantoms was performed by inserting the operating frequency of the resonator obtained from the measurements. The retrieved dielectric properties were compared with the dielectric property measurements taken with Agilent's open-ended high temperature dielectric probe. The retrieval error was found to be less than 23 % for all phantoms. Dielectric property retrieval algorithm was also applied to the obtained simulation results and the retrieval error was found to be less than 2.7 % for all twelve digital phantoms.

It has been demonstrated that the dielectric properties of high water content tissues can be retrieved for narrow bands by employing an analytical equation. However, it is apparent that various error sources must be better understood and compensated for in a practical system. Moreover, the effect of the tissue thickness, shape, and reference dielectric property measurement techniques have a significant effect on dielectric property reconstruction. Thus, the performance of a potential on-body resonator for blood glucose monitoring will be dependent on the tissue composition, age, gender, and body mass index of the patient. These issues may imply the need for periodic calibration using conventional bio-sensor monitoring techniques in a practical system; however, it may still be possible to significantly reduce the frequency of blood sampling required compared to existing solutions. These findings may therefore form the basis for the development of an on-body resonator for dielectric property change monitoring that could have applications in non-invasive blood glucose monitoring or stroke detection.

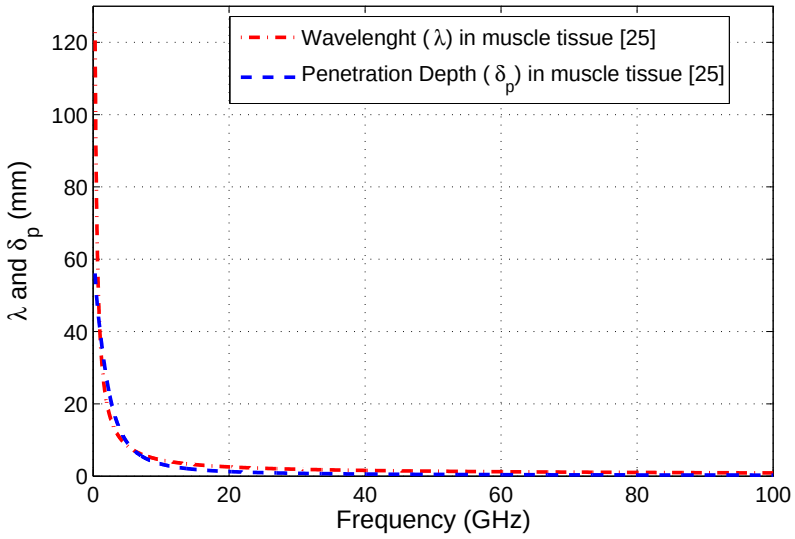

Figure 4.21: Wavelength and penetration depth change in the muscle tissue with respect to frequency [26].

Further analysis of the error sources may help refine the analytical model and improve performance when applied to measured results. Application to other types of resonator is another avenue for exploration. Note that, the concentrations of sugar used in this study are far from normal blood sugar levels; refinement of the model and resonator for a more restricted range are discussed in Chapter

5, with evaluations of the sensitivity and repeatability of the measurements of particular interest. One issue needing careful consideration and further work is how to separate the effect of the change in BGL from the effect from other physiological processes on the relative permittivity of the human body tissue. Similar studies will also be performed, therefore, examining the other factors that affect effective permittivity.

Finally, the non-invasive blood glucose monitoring resonator is intended to operate at relatively low frequencies due to the high loss of the body tissues at higher end of the microwave spectrum. Although 600 MHz frecuency band is mainly allocated for TV broadcasting, both current operation frequency of the resonator and the phantoms does not represent the final design. Note that the semi-solid phantom relative permittivities are ranging between 20 to 35; thus, it is not representing the real tissue environment.

Table 4.8: Penetration depth and wavelength at different frequencies in muscle tissue

$Frequency$ MHz	$Permittivity$ ε_r	$Conductivity$ σ (S/m)	$Wavelength$ mm	$Penetration$ $Depth\ mm$
403.5	57.1	0.797	94.2	52.5
600	55.9	0.849	65.2	47.8
2450	52.7	1.73	16.7	22.3
5800	48.4	4.9	7.3	7.5
24125	27.2	29.5	2.2	1.0
61250	12.6	53.2	1.2	0.4

Fig 4.21 shows the change of penetration depth and wavelength change in the muscle tissue with respect to frequency. To roughly determine the best frequency of operation the muscle tissue is chosen due to the wide usage in the literature to represent the whole body permittivity [27, 28]. Table 4.8 shows the exact wavelength and penetration depths at different frequencies. Recently expanded Med-radio band (401 - 406 MHz) [29] is a good candidate for frequency of operation. Also $2.40 - 2.48$ GHz and $5.725 - 5.875$ GHz ISM bands are well suited for the intended diagnostic applications.

References

[1] E. Topsakal, E. C. Moreland, T. Karacolak, and M. Acar, "The impact of glucose concentration in blood plasma on relative dielectric constant and conductivity," in *National Science Meeting URSI*, 2008.

[2] B. Freer and J. Venkataraman, "Feasibility study for non-invasive blood glucose monitoring," in *Antennas and Propagation Society International Symposium (APSURSI), 2010 IEEE*, july 2010, pp. 1 –4.

[3] C. Hancock and S. Chaudhry, "A non-invasive monitoring system," in *Microwave Conference, 2007. European*, oct. 2007, pp. 313 –316.

[4] B. R. Jean, E. C. Green, and M. J. McClung, "A microwave frequency sensor for non-invasive blood-glucose measurement," in *Sensors Applications Symposium, 2008. SAS 2008. IEEE*, Feb. 2008, pp. 4–7.

[5] C. Gabriel, S. Gabriel, and E. Corthout, "The dielectric properties of biological tissues: I. literature survey," *Physics in Medicine and Biology*, vol. 41, no. 11, p. 2231, 1996. [Online]. Available: http://stacks.iop.org/0031-9155/41/i=11/a=001

[6] M. Lazebnik, E. L. Madsen, G. R. Frank, and S. C. Hagness, "Tissue-mimicking phantom materials for narrowband and ultrawideband microwave applications," *Physics in Medicine and Biology*, vol. 50, no. 18, p. 4245, 2005. [Online]. Available: http://stacks.iop.org/0031-9155/50/i=18/a=001

[7] Y. Hayashi, L. Livshits, A. Caduff, and Y. Feldman, "Dielectric spectroscopy study of specific glucose influence on human erythrocyte membranes," *Journal of Physics D: Applied Physics*, vol. 36, no. 4, pp. 369–374, 2003. [Online]. Available: http://stacks.iop.org/0022-3727/36/i=4/a=307

[8] D. Hagl, D. Popovic, S. Hagness, J. Booske, and M. Okoniewski, "Sensing volume of open-ended coaxial probes for dielectric characterization of breast tissue at microwave frequencies," *Microwave Theory and Techniques, IEEE Transactions on*, vol. 51, no. 4, pp. 1194–1206, 2003.

[9] M. Lazebnik, D. Popovic, L. McCartney, C. B. Watkins, M. J. Lindstrom, J. Harter, S. Sewall, T. Ogilvie, A. Magliocco, T. M. Breslin, W. Temple, D. Mew, J. H. Booske, M. Okoniewski, and S. C. Hagness, "A large-scale study of the ultrawideband microwave dielectric properties of normal, benign and malignant breast tissues obtained from cancer surgeries," *Physics in Medicine and Biology*, vol. 52, no. 20, p. 6093, 2007. [Online]. Available: http://stacks.iop.org/0031-9155/52/i=20/a=002

[10] M. Lazebnik, M. C. Converse, J. H. Booske, and S. C. Hagness, "Ultrawideband temperature-dependent dielectric properties of animal liver tissue in the microwave frequency range," *Physics in Medicine and Biology*, vol. 51, no. 7, p. 1941, 2006. [Online]. Available: http://stacks.iop.org/0031-9155/51/i=7/a=022

[11] T. S. Bird, "Definition and misuse of return loss [report of the transactions editor-in-chief]," *Antennas and Propagation Magazine, IEEE*, vol. 51, no. 2, pp. 166–167, 2009.

[12] S. Seewattanapon, T. Wattakeekamthorn, T. Somwong, and P. Akkaraekthalin, "A microstrip folded resonator sensor for measurement of dielectric constant," in *Electrical Engineering/Electronics, Computer, Telecommunications and Information Technology, 2008. ECTI-CON 2008. 5th International Conference on*, vol. 1, may 2008, pp. 245 –248.

[13] A. Petosa and A. Ittipiboon, "Design and performance of a perforated dielectric fresnel lens," *Microwaves, Antennas and Propagation, IEE Proceedings* -, vol. 150, no. 5, pp. 309 – 314, Oct. 2003.

[14] B. Jean, E. Green, and M. McClung, "A microwave frequency sensor for non-invasive blood-glucose measurement," in *Sensors Applications Symposium, 2008. SAS 2008. IEEE*, Feb. 2008, pp. 4–7.

[15] T. Karacolak, R. Cooper, J. Butler, S. Fisher, and E. Topsakal, "In vivo verification of implantable antennas using rats as model animals," *Antennas and Wireless Propagation Letters, IEEE*, vol. 9, pp. 334 –337, 2010.

[16] P. Soontornpipit, C. Furse, and Y. C. Chung, "Miniaturized biocompatible microstrip antenna using genetic algorithm," *Antennas and Propagation, IEEE Transactions on*, vol. 53, no. 6, pp. 1939 – 1945, june 2005.

[17] T. Yilmaz and Y. Hao, "Electrical property characterization of blood glucose for on-body sensors," in *Antennas and Propagation (EUCAP), Proceedings of the 5th European Conference on*, april 2011, pp. 3659 –3662.

[18] E. Topsakal, T. Karacolak, and E. Moreland, "Glucose-dependent dielectric properties of blood plasma," in *The XXX General Assembly of the International Union of Radio Science*, August 2011.

[19] T. Yilmaz and Y. Hao, "Sensing of dielectric property alterations in biological tissues at microwave frequencies," in *Antennas and Propagation Conference (LAPC), 2011 Loughborough*, nov. 2011, pp. 1 –4.

[20] J. Kennedy and R. Eberhart, "Particle swarm optimization," in *Neural Networks, 1995. Proceedings., IEEE International Conference on*, vol. 4, nov/dec 1995, pp. 1942 –1948 vol.4.

[21] T. Karacolak, A. Hood, and E. Topsakal, "Design of a dual-band implantable antenna and development of skin mimicking gels for continuous glucose monitoring," *Microwave Theory and Techniques, IEEE Transactions on*, vol. 56, no. 4, pp. 1001 –1008, april 2008.

[22] N. Jin and Y. Rahmat-Samii, "Parallel particle swarm optimization and finite- difference time-domain (pso/fdtd) algorithm for multiband and wide-band patch antenna designs," *Antennas and Propagation, IEEE Transactions on*, vol. 53, no. 11, pp. 3459 – 3468, nov. 2005.

[23] D. C. Montgomery and G. C. Runger, *Applied Statistics and Probability for Engineers*, 3rd ed. John Wiley and Sons, Inc., 2003.

[24] T. Yilmaz, R. Foster, and Y. Hao, "Patch resonator for non-invasive detection of dielectric property changes in biological tissues," in *Antennas and Propagation Society International Symposium (APSURSI), 2012 IEEE*, July 2012.

[25] "Agilent 85070e dielectric probe kit 200 mhz to 50 ghz technical overview." [Online]. Available: http://cp.literature.agilent.com/litweb/pdf/5989-0222EN.pdf

[26] Itallian National Research Council, URL: http://niremf.ifac.cnr.it/tissprop/.

[27] S. Jacobsen, H. Olav Rolfsnes, and P. Stauffer, "Characteristics of microstrip muscle-loaded single-arm archimedean spiral antennas as investigated by fdtd numerical computations," *Biomedical Engineering, IEEE Transactions on*, vol. 52, no. 2, pp. 321–330, 2005.

[28] W. Xia, K. Saito, M. Takahashi, and K. Ito, "Performances of an implanted cavity slot antenna embedded in the human arm," *Antennas and Propagation, IEEE Transactions on*, vol. 57, no. 4, pp. 894–899, 2009.

[29] "Federal communications commission," 2012. [Online]. Available: http://www.fcc.gov

Chapter 5

Glucose Dependence of Cole-Cole Parameters of Blood and Testing of a Patch Resonator

Radio frequency (RF) techniques in the literature are mostly focused on telemetry and BGL sensing is usually performed with a chemical sensor [1, 2, 3]. A limited number of studies have been published employing RF techniques for sensing changes in BGL. One of the studies published in this area is given in [4] and [5]; in this work, a two-port spiral resonator is presented. The S_{21} response of the resonator is tracked by placing the resonator radiating towards the tissue while the BGL is fluctuated with a procedure named the *Soda Test*. The experiments are performed with healthy volunteers without *a priori* knowledge of the dielectric properties of the blood. The study is aimed to relate the glucose levels with the output of the spiral resonator. However, from reported studies, it is known that the pressure can have an effect on the performance of the spiral resonator.

An ultra-wide band (UWB) antenna is presented in [6] and the return loss

response of the antenna is tracked while changing the dielectric properties of the blood layer. The study reports significant changes in the simulated return loss response of the UWB antenna. The dielectric property data given to the simulation software, namely hyperglycaemic and hypoglycaemic, was derived from the previously reported study which is analysing the effect of glucose to the dielectric properties of erythrocyte membranes [7]. However, traditionally glucose level measurements performed through the analysis of blood plasma [8]. It suggests that whole blood glucose levels can be measured and it is usually 1.1 times higher than plasma glucose levels; thus, whole blood levels can be converted into plasma glucose levels. However the erythrocyte membranes are not representative of either whole blood or plasma glucose levels.

In order to fully understand the potential of an RF application, the relationship between glucose level change of blood and the change of dielectric properties as a consequence should be established. Previously reported studies suggest that the dielectric properties of blood are glucose-dependent; thus, the dielectric properties of the blood can be changed with the alterations in blood glucose levels [9, 10].

In [9], dielectric property dependence of the human erythrocyte membranes to the D-glucose and L-glucose is examined to determined the mechanism of cell reactions to glucose. Human erythrocyte is the red blood cells which functions mainly as an oxygen carrier. D-glucose is the naturally occurring form of glucose, so-called dextrose, and L-glucose is a synthetic form of glucose produced in the laboratories. The study reports that the dielectric properties of the erythrocyte membranes are independent of L-glucose change; however, dependent to the D-glucose change. However, this article reports the membrane dielectric property change up to 100 MHz and the plasma glucose is not included in the results. Note that, for the sake of convenience, it is recommended to report the plasma glucose levels during both home and clinical testing of blood glucose [8]. Also, [8] reports that whole blood glucose levels (combination of erythrocyte and plasma glucose) is 11% lower than plasma glucose levels. Therefore, [9] is hypothesizing the glucose reaction mechanism on the erythrocyte membranes rather than the glucose dependance of whole blood dielectric properties.

A recently reported study suggests that the dielectric properties of blood decrease as the blood glucose levels are increased [10]. The normal range for BGL is 72 mg/dl to 216 mg/dl (given in Table 5.1); however, previously reported studies carried out measurements with a very large amount of glucose. In [10], the dielectric properties of blood plasma were measured with varying glucose levels from 0 mg/dl to 16000 mg/dl, starting with an increment of 250 mg/dl, which is much higher than the normal blood glucose range.

In [11], a study was performed with real blood samples collected from 10 patients, with BGL ranging from 87 mg/dl to 330 mg/dl in the 1 GHz to 10 GHz frequency band. The study reports the dielectric property measurements of whole blood samples. However, there is a need to analyze the plasma glucose levels and also the paper does not provide detailed information about the measurement steps. In [12], dielectric properties of the blood mimicking phantom materials were reported between 0.5 GHz to 3 GHz. However, both of these studies do not provide detailed information and conclusions regarding the change of permittivity within the range of realistic BGL change.

The concept in using RF techniques for blood sugar level monitoring has, to the authors' knowledge, not yet examined with the sensitivity issues related to normal BGL values and the associated dielectric properties. In addition, there are trade-offs regarding the RF resonator (e.g., size, sensitivity, and operating frequency) that remain poorly understood. This study addresses two vital issues that have not been reported in detail in the previous studies, that are necessary to understand the viability of RF methods for BGL monitoring: (1) establishing a clear relation between the dielectric properties and the realistic glucose levels of the blood, in an extremely wide frequency range; and (2) performing controlled experiments with a minimum effect from the measurement conditions, to allow some assesment of the sensitivity requirements under realistic conditions. To do so, a patch resonator was designed to operate in the $2.4-2.48$ GHz ISM band when placed radiating against a four-layered tissue phantom; then, by decreasing the relative permittivity of the blood layer, the simulated response of the resonator was analyzed. The ISM band is chosen because of the reasonable penetration depth comparing to other ISM and MICS bands (7.5 mm in muscle tissue) and

ISM band is also licensed for medical use [13]. The proposed spiral resonators were bulky; thus, there was a need to miniaturize the design and increase the Q factor. Therefore, a new and much smaller patch design is proposed.

In order to study the effect of blood glucose on the dielectric properties of the blood through experiments, tissue mimicking materials were fabricated and characterized (see Chapter 3 for details). Powdered dextrose (glucose) was added to the blood mimicking material and dielectric property measurements were performed. A Cole-Cole analysis was performed to quantify the dielectric property change in the blood mimicking material. The resonator was tested with the four-layered tissue mimicking material and simulations are replicated by changing the blood layer with blood mimicking materials with differing amount of glucose content.

Section 5.1 provides the design of the patch resonator and the experimental methodology for testing. The dielectric property measurement for blood mimicking material having different dextrose levels is also explained in Section 5.1. Analysis methods are presented in Section 5.2; the results are presented in Section 5.3. Finally, conclusions are drawn in Section 5.5.

5.1 Design and Experimental Methodology

5.1.1 Dielectric Property Measurements of Blood Mimicking Material with Varying Realistic Blood Glucose Levels

This section describes the experimental method used to quantify the dependence of the dielectric properties of blood to the blood glucose levels. To this end, an oil-in-gelatin dispersion blood mimicking material was made, using the recipes given in Chapter 3. The blood mimicking material was divided into five 200 ml beakers, each beaker containing around 200 grams of blood mimicking phantom. Next, 0 g, 0.14 g, 0.24 g, 0.34 g, and 0.44 g of powdered dextrose (glucose) was added to the beakers, respectively, at 28 °C. Corresponding mmol/l and mg/dl values for glucose are given in Table 5.1. The phantoms were poured into 78 mm by

111 mm containers with the thickness of 24 mm. The samples were left overnight to solidify. Five samples in total were prepared. Dielectric property measurements were taken within 18 to 30 hours of phantom characterization with the Agilent's open ended high temperature dielectric probe, following the dielectric property measurement routine described in Chapter 3.

Table 5.1: Blood Mimicking Material with Corresponding Glucose Index

Dextrose (g)	Glucose (mmol/l)	*Glucose* (mg/dl)
0.14	4	72
0.24	7	126
0.34	9	162
0.44	12	216

Dielectric property measurements were collected from the top and bottom sides of the phantoms, from at least 5 points on each side and two measurements collected from each point. The total number of measurements collected from all the phantom samples was 107, with 2500 data points across the frequency range for each measurement.

5.1.2 Design of Patch Resonator

In order to obtain some initial insights into the use of resonators for BGL monitoring, an on-body patch resonator is designed to operate in the $2.40 - 2.48$ GHz ISM band when radiating towards the tissue. The resonator was designed using CST Microwave Studio software when a four-layered (skin, fat, blood, and muscle) digital phantom was placed above the resonator as a superstrate, to represent the lossy biological tissue.

Table 5.2: Dielectric properties and Thicknesses of the Digital Phantoms at 2.45 GHz

Tissue Type	ε_r	σ_e(S/m)	Thickness (mm)
Wet Skin	42.923	1.562	1.0
Fat	5.283	0.103	1.0
Blood	58.347	2.502	2.5
Muscle	52.791	1.705	15.1

All tissues had planar dimensions of 127 mm by 127 mm and the thicknesses of the phantoms are given in Table 5.2. The phantoms were given non-dispersive dielectric properties of the biological tissues at the designed operation frequency (2.45 GHz), also given in Table 5.2 [14, 15].

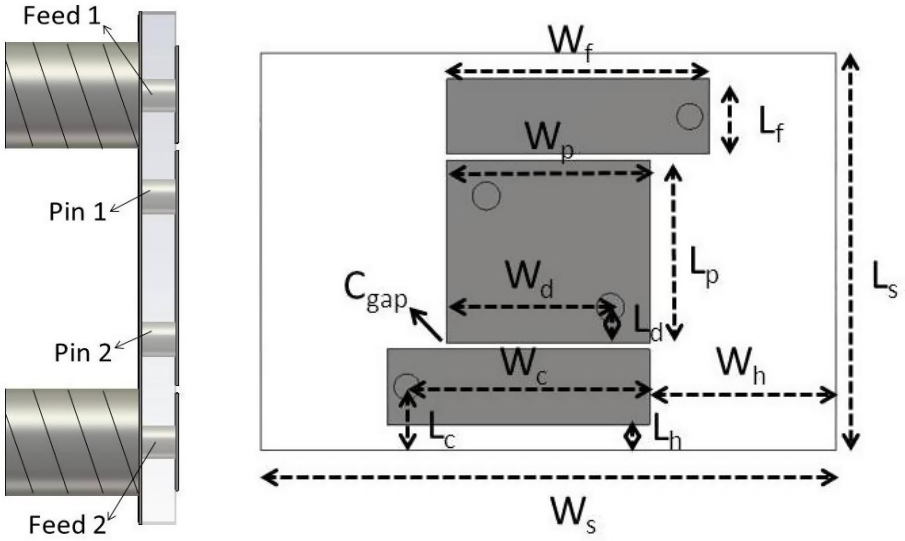

(a) (b)

(c)

Figure 5.1: Patch Resonator: (a) side view; (b) top view; (c) printed resonantor.

Table 5.3: Dimensions of the Patch Resonator

Parameter	*Value (mm)*	*Parameter*	*Value (mm)*	*Parameter*	*Value (mm)*
W_s	29.00	W_h	9.365	L_d	1.8
W_f	13.27	L_p	9.2	L_p	9.2
W_p	10.27	L_s	20.0	L_h	1.3
W_c	12.27	L_c	3.2	L_c	3.2
W_d	8.27				

The configuration of the resonator is given in Fig. 5.1 and the dimensions are given in Table 5.7. The resonator was printed on Rogers 3210 substrate with $\varepsilon_r = 10.2$ and a dissipation factor of 0.0027 at 10 GHz. Note that the Rogers substrate is not frequency dispersive over the frequency of interest. The high relative permittivity of the substrate enables the miniaturization of the resonator. The size of the substrate is 29 mm by 20 mm, which is comparable to a conventional implantable antenna. Two shorting via pins were used to connect the patch to the ground plane symmetrically. The shorting vias enabled further miniaturization of the resonator. The patch resonator is a two-port structure and the energy is capacitively coupled to the patch with two feeding lines. The feeding lines are fed with SMA connectors. The return loss measurement and simulations results for both air and tissue medium are given in Section 5.3.

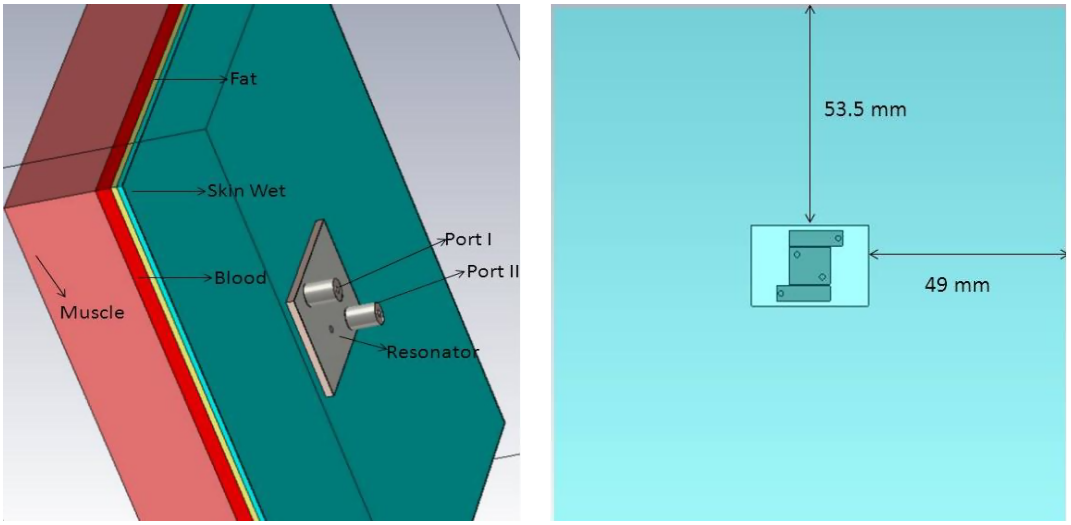

(a) (b)

Figure 5.2: Patch Resonator: (a) simulation with four-layered tissue; (b) patch distance from the digital phantom edges.

5.1.3 Testing of the Resonator with Tissue Mimicking Materials

In this section, the resonator is tested with tissue mimicking materials. Dextrose was added to the blood mimicking material (BMM) in different indices which corresponds to the real values of the glucose in the human blood. The response of the resonator was recorded while the BMM layer was replaced with another

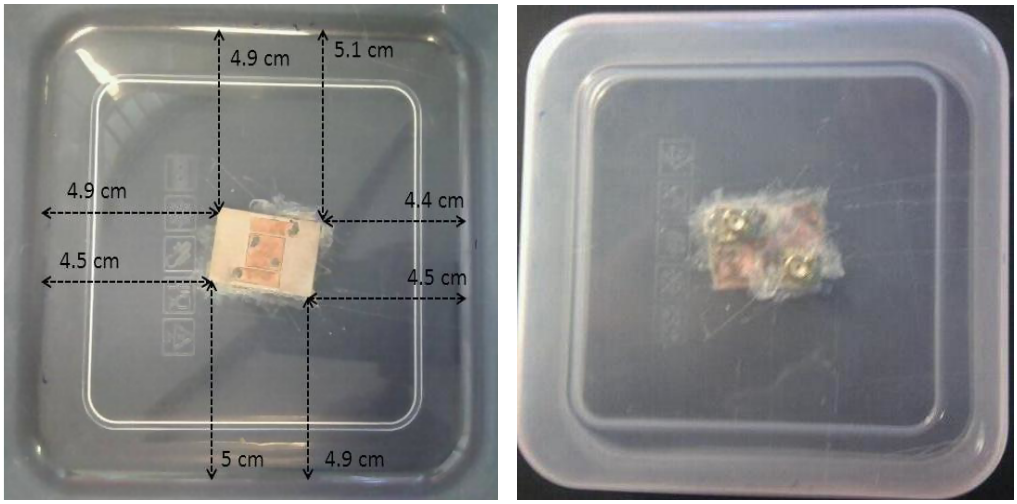

(a) (b)

Figure 5.3: Resonator mounted at the bottom of the container: (a) top view; (b) bottom view.

BMM layer containing a different amount of dextrose. The aim of this experiment was to examine the effect of dextrose change on the response of the resonator.

The fabricated patch resonator was mounted at the bottom of a container. The container had dimensions of 127 mm by 127 mm. During the fabrication of the resonator, SMA coaxial feeds were soldered with a slight angle (i.e., the resonator was tilted 1.98° upwards on the longer side of the substrate); thus, the resonator was tilted up when mounted to the container. Note that SMA connectors was mounted with a slight angle due to the fabrication limitations. The distances from the edges of the container were measured and are given in Fig. 5.3.

Wet skin, fat, blood, and muscle mimicking materials were made using the recipes and characterization process given in Chapter 3. Four samples of BMM were characterized and 0.24 g, 0.34 g, and 0.44 g of dextrose were added to three of the BMM samples. The wet skin mimicking material was poured in to the container with the resonator mounted at the bottom with 1 mm thickness from the top of the resonator. The other phantoms were poured into identical containers with thicknesses of 1 mm, 2.5 mm, and 15 mm for fat, blood, and muscle mimicking materials, respectively. BMM phantoms with different dextrose index values were also poured in identical containers with a 2.5 mm thickness.

(a) (b)

Figure 5.4: Patch resonator: (a) four-layered tissue placed on top of the resonator; (b) measurement set-up.

The fat, blood, and muscle layers were placed on top of the wet skin layer and the S-parameter response of the resonator collected, with the blood layer using one from the set of blood mimicking materials. The measurement set-up is shown in Fig. 5.4.

5.2 Analysis of the Collected Data

5.2.1 Dielectric Property Analysis of Blood Mimicking Phantoms

The collected data from blood mimicking materials with different dextrose indices were analyzed in two steps. The first step was the elimination of poor data. To do so, measured dielectric properties, for one phantom at a time, were plotted

Table 5.4: Feasible solution space given to the Cole-Cole parameters in the PSO algorithm

Parameter	ε_∞	$\Delta\varepsilon_n$	τ_n	α_n	σ_i
Minimum	2	2	7	0	0.01
Maximum	6	70	14	1	3

in MATLAB and plots deviating vastly from the majority of measurements were eliminated. By doing so, 12 out of 107 measurements was eliminated.

The second step was to minimize the parameters of the remaining data (95 measurements) for comparison with respect to glucose indices, because the collected data contains over a million data points. To this end, a single-pole Cole-Cole model was used to express the measured dispersive dielectric properties as a function of frequency. Cole-Cole fitting has often been used to compare the dielectric properties of the biological tissues in the literature: to express the measured data with a compact equation and to compare the variations of dielectric properties in biological tissue due to the changes in water content, heat, and glucose level [10, 16, 17, 18]. It has been also shown [18] that the single-pole Cole-Cole fitting is more efficient than two-pole Cole-Cole fitting, because the number of parameters is smaller and the single-pole fitting represents the measured data just as well as two-pole fitting. The single-pole Cole-Cole equation is shown in (5.1):

$$\varepsilon_\omega = \varepsilon_\infty - \sum_n \frac{\Delta\varepsilon_n}{1 + (j\omega\tau_n)^{(1-\alpha_n)}} + \frac{\sigma_i}{j\omega\varepsilon_0} \tag{5.1}$$

where $\Delta\varepsilon_n$ is the difference between static permittivity and permittivity at higher frequencies $\varepsilon_s - \varepsilon_\infty$, ω is the angular frequency and ε_∞, τ_n, α_n, σ_i are the Cole-Cole parameters. The Cole-Cole parameters were found with particle swarm optimization (PSO) [10, 19]. PSO returns all Cole-Cole variables by minimizing the fitness function. The fitness function of the PSO was chosen as the Euclidean distance [20] between the raw data input and the Cole-Cole equation output. The equation for Euclidean distance is given in (5.2):

$$e = \frac{1}{N}\sum_{i=1}^{N}\left[\left(\frac{\varepsilon'_{\omega_i} - \hat{\varepsilon}'_{\omega_i}}{median\left[\varepsilon'_{\bar{\omega}_i}\right]}\right)^2 + \left(\frac{\varepsilon''_{\omega_i} - \hat{\varepsilon}''_{\omega_i}}{median\left[\varepsilon''_{\bar{\omega}_i}\right]}\right)^2\right] \tag{5.2}$$

where ε'_{ω_i} and ε''_{ω_i} are the real and imaginary part of measured dielectric properties. $\hat{\varepsilon}'_{\omega_i}$ and $\hat{\varepsilon}''_{\omega_i}$ represent the output of the Cole-Cole equation for real and imaginary part of the dielectric properties, respectively, and N is the number of points picked across the frequency range of 0.3 GHz to 20 GHz (2500 for this

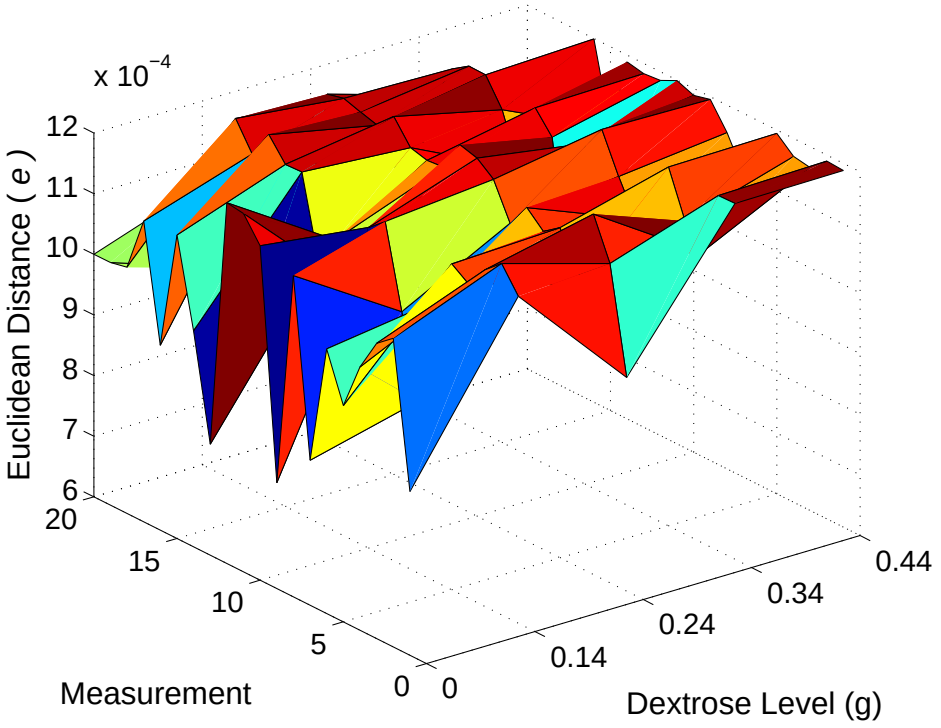

Figure 5.5: Euclidean distance 5.2, also referred as Euclidean space is the distance between two points, from the PSO algorithm's output.

study). The PSO algorithm stops and returns values for the five set of parameters if the Euclidean distance is smaller than the threshold of 0.00012. The pre-determined feasible solution space given to the parameters in the algorithm is shown in Table 5.4. To verify the validity of Cole-Cole fitting, the Euclidean distance for each fitting was computed, shown in Fig. 5.5. The number of particles chosen in the PSO algorithm was 30. The algorithm would end after 500 iterations if the threshold were not reached before this point. Note that an additional measurement was excluded, since the Cole-Cole equation could not be fitted to the measurement; thus, 13 measurements in total were excluded. The solutions were reached within 10 to 150 iterations.

5.2.2 Input Impedance Analysis of the Resonator

From the literature, it is known that an increase in BGL decreases the relative permittivity of blood. To study this effect in terms of the response of the patch resonator, simulations were performed where the relative permittivity of the blood

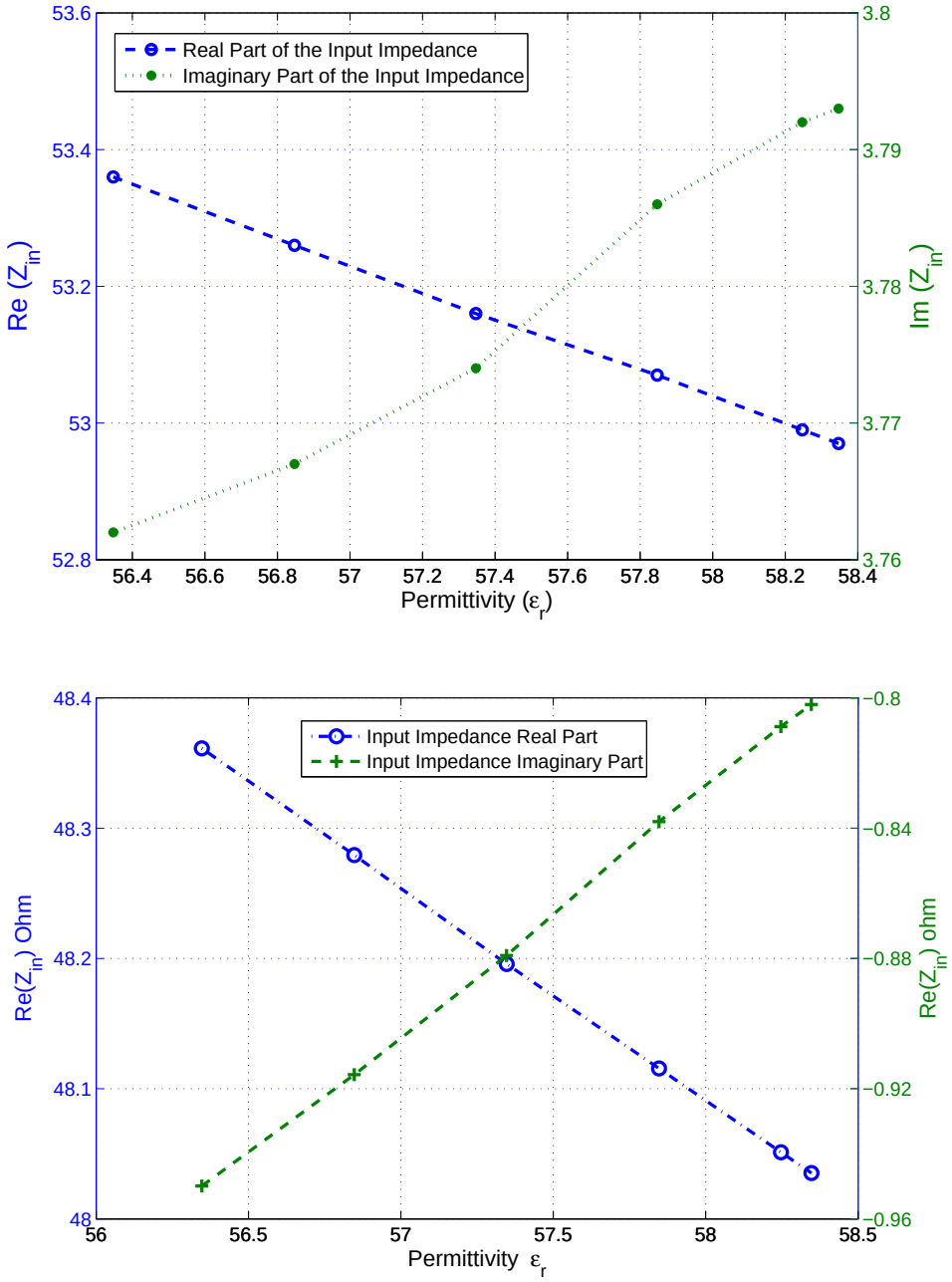

Figure 5.6: Simulated change of input impedance with respect to change in blood layer relative permittivity: a) at 2.4 GHz, b) at 2.4512 GHz.

layer in a four-layered digital phantom was decreased and the response of the resonator was observed. Firstly, the return loss response was observed, with the resonator was operating at 2.4512 GHz; when the relative permittivity was decreased by 2, the operation frequency remained unchanged. From reported studies, we can conclude that the relative permittivity alterations at 2.45 GHz is lower than 2 within the range of $4 - 12$ mmol/dl change in blood. Thus,

the relative permittivity change can not be sensed with the current structure at 2.45 GHz when only tracking the resonance frequency.

However, we observed a mismatch in the return loss response when the relative permittivity of blood layer was changed. To investigate this, the input impedance of the resonator was calculated from the Z parameter response of the resonator:

$$Z_{in} = Z_{11} - \frac{Z_{12}Z_{21}}{Z_{22} + Z_L} \tag{5.3}$$

Z-parameters were calculated with CST Microwave Studio, and the load impedance Z_L was considered matched (50 Ω). The change of input impedance of the resonator with the decrease in relative permittivity of the blood layer is given in Fig. 5.6 a and Fig. 5.6 b. The real part of the input impedance is increasing as the relative permittivity is decreasing. On the other hand, the imaginary part of the input impedance is decreasing as the relative permittivity is decreasing.

For the experiment proposed in Section 5.1.1, the input impedance was calculated from the recorded S-parameter response. First, the S-parameters were converted to Z-parameters; next, the input impedance was calculated using (5.3). The results are given in Section 5.3.2.

5.3 Results and Discussion

5.3.1 Cole-Cole Analysis of the Blood Mimicking Materials with Different Glucose Indices

The median values of the measured dielectric properties were calculated at each frequency for the five samples of blood mimicking material, categorized as 0 g, 0.14 g, 0.24 g, 0.34 g, and 0.44 g of dextrose index. Measured dielectric properties of the blood mimicking phantom with varying dextrose levels are given in Fig 5.7 and Fig 5.8 for relative permittivity and effective conductivity, respectively. No0te that the measurements are performed 20 times for each sample and the median of 20 measurements is taken.

Table 5.5: Cole-Cole parameters of Median Curves for Realistic Dextrose Levels

Parameter	0 g	0.14 g	0.24 g	0.34 g	0.44 g
ε_∞	3.41	2.24	2.67	3.62	3.26
$\Delta\varepsilon_n$	57.13	59.31	56.6	57.56	56.79
τ_n	11.29	11	11.12	10.85	10.71
α_n	0.09	0.07	0.04	0.05	0.04
σ_i	1.05	1.08	1.03	1.05	1.07

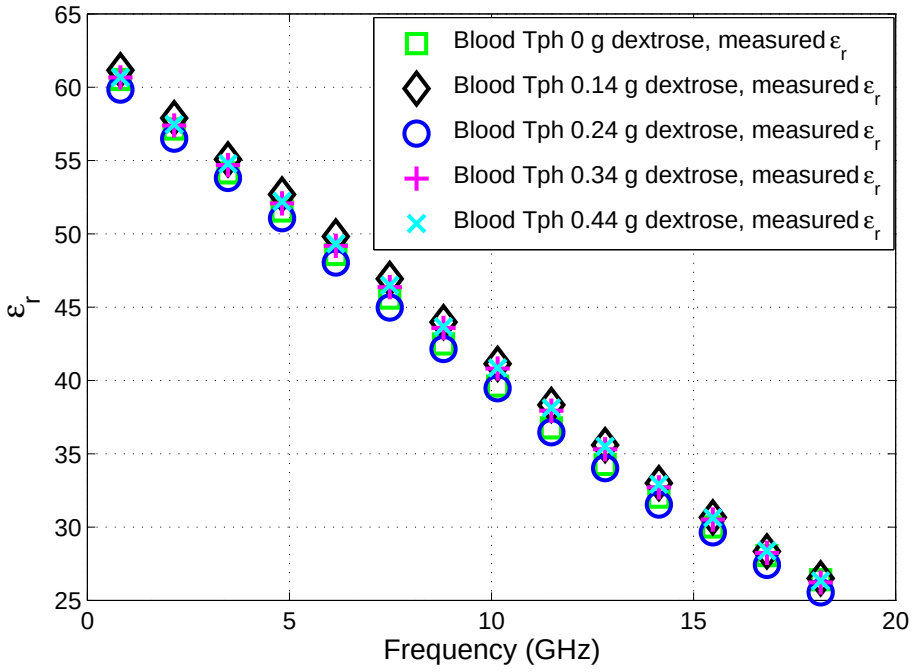

Figure 5.7: Relative permittivity measurements of blood mimicking material with 0, 0.14, 0.24, 0.34, and 0.44 g dextrose.

In order to show the validity of the Cole-Cole fitting, the median of the 0 g dextrose blood mimicking material and fitted Cole-Cole models are shown in Fig. 5.9 as an example. Calculated Cole-Cole parameters for each phantom sample are shown in Table 5.5. Next, the Cole-Cole parameters were expressed as a linear function of the amount of glucose in the sample. The coefficients for each phantom are shown in Table 5.6. An example of the linear fitting for the $\Delta\varepsilon_n$ parameter is plotted in Fig 5.10.

After the linear fitting, the trends of the Cole-Cole parameters were observed; apart from ε_∞ and σ_i, all the parameters demonstrate a decreasing trend with the increase in the dextrose levels. The ε_∞ trend is slightly increasing, whereas

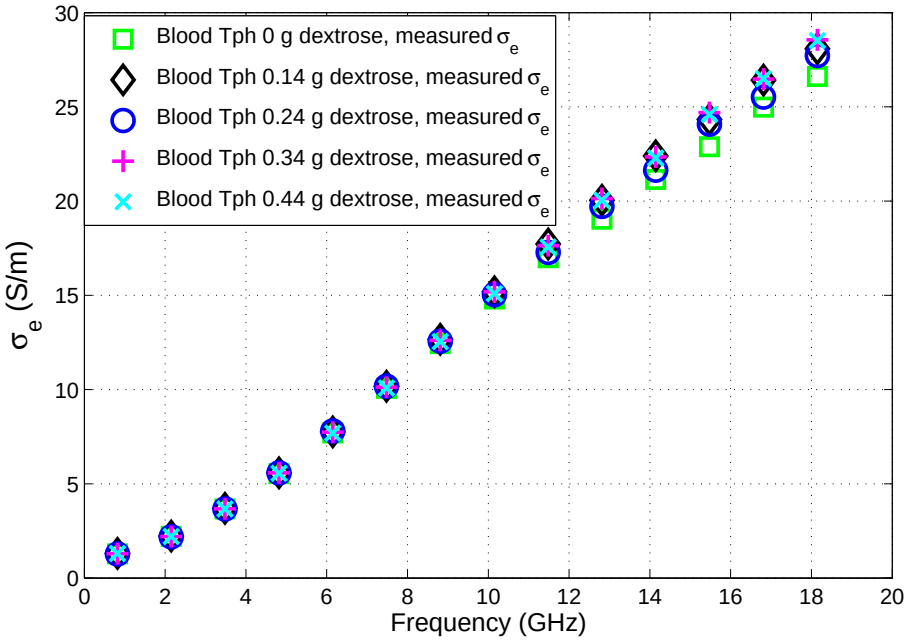

Figure 5.8: Effective conductivity measurements measurements of blood mimicking material with 0, 0.14, 0.24, 0.34, and 0.44 g dextrose.

Table 5.6: Coefficients of the Linear Function $y = ax + b$ Fitted to Cole-Cole Parameters with respect to Glucose Concentration

Coefficient	ε_∞	$\Delta\varepsilon_n$	τ_n	α_n	σ_i
a	0.795	-1.953	-1.218	-0.113	0.011
b	2.86	57.93	11.28	0.084	1.05

σ_i remains almost constant while the dextrose levels are increasing. The trend observed for ε_∞ and $\Delta\varepsilon_n$ agrees with previously published results [10]. The increase of ε_∞ with dextrose content implies that an increase in relative permittivity is expected at high frequencies. From Fig. 5.10, the relative permittivity is expected to vary by approximately 1 unit when the minimum and maximum levels of glucose are considered. The τ_n parameter displays only minor variation with differing glucose index. Finally, from the analysis of the σ_i parameter, no significant changes in the effective conductivity of the phantoms are expected for minimum and maximum glucose content.

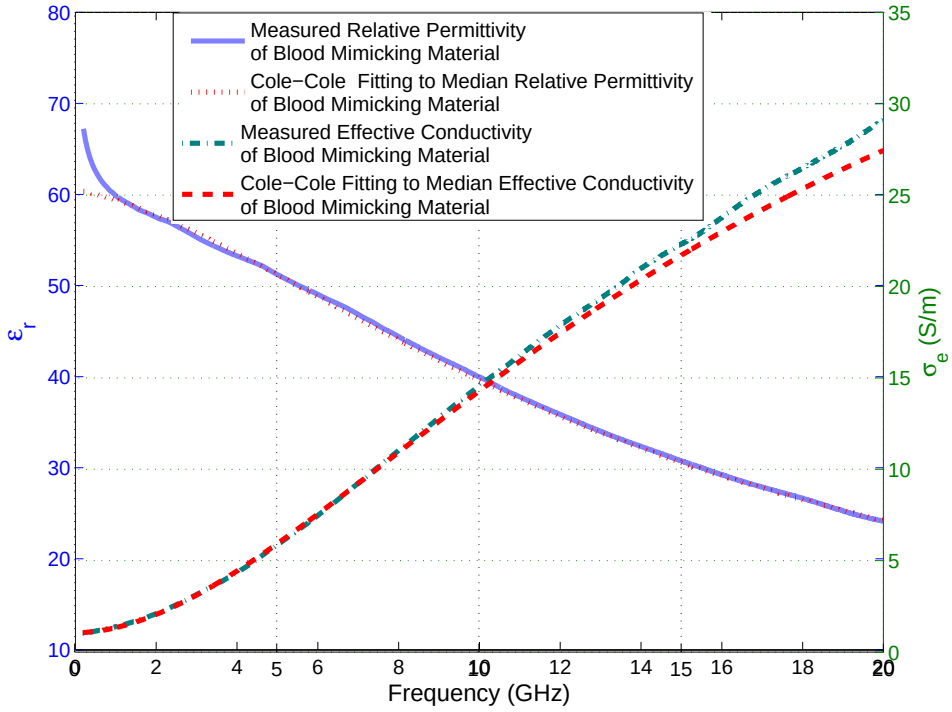

Figure 5.9: Comparison between the median of the dielectric property measurement and Cole-Cole fitting performed for blood mimicking material with 0 g of dextrose.

5.3.2 Patch Resonator Measurement Results with Four-Layered Tissue Mimicking Phantom

An S-parameter measurement in air media was performed, to verify the proper functioning of the resonator. Results from simulation in air media, measurement in air media, and measurement in air media with the resonator mounted at the bottom of the container, are shown in Fig. 5.11. The difference between measured and simulated air media results shows that resonance shifts occurred due to the fabrication process. Namely, the first notch is shifted 216 MHz to left and the second notch 218 MHz to right. Additionally, due to the plastic box, the first notch shifts 17 MHz to left and the second notch shifts 70 MHz to right. The overall difference between simulation and mounted resonator performance is 233 MHz to left and 148 MHz to right, for first and second notches, respectively.

The simulated and measured return loss of the resonator with the four-layered tissue mimicking phantom are shown in Fig. 5.12. Note that the blood

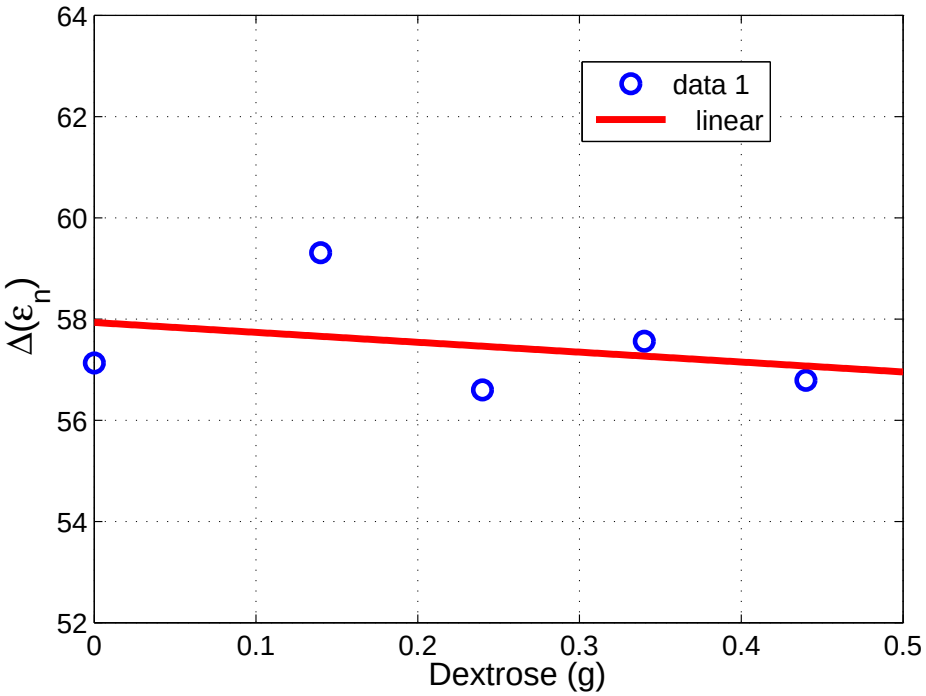

Figure 5.10: Linear fitting to the $\Delta\varepsilon_n = \varepsilon_s - \varepsilon_\infty$ Cole-Cole variable with respect to dextrose levels.

layer has no dextrose. The simulated resonance frequency is 2.451 GHz, whilst the measured resonance frequency is 2.143 GHz. The measured resonance frequency is shifted to the left by 308 MHz, when compared with the simulation. From Fig. 5.11, the first notch is shifted to the left by 233 MHz due to fabrication and plastic (polypropylene) container, since the plastic container was not included in the simulations. The relative permittivity of polypropylene is 2.2 and the dissipation factor is 0.0003 at 1 GHz. The other factors that can affect the resonance frequency could be the mismatch in relative permittivity and effective conductivity of the physical phantoms with respect to human tissues. Note that non-dispersive, in terms of frequency, dielectric properties at 2.45 GHz were considered during the simulation, shown in Table 5.2, whereas the physical phantoms used in the experiments were frequency dispersive.

Next, the blood layer without dextrose was exchanged with the blood layers with higher dextrose content and the S-parameter response of the resonator collected. From the Cole-Cole parameter results, a maximum change in the relative permittivity of the blood layer of 1 unit is expected.In Fig. 5.6, a 1 unit change in

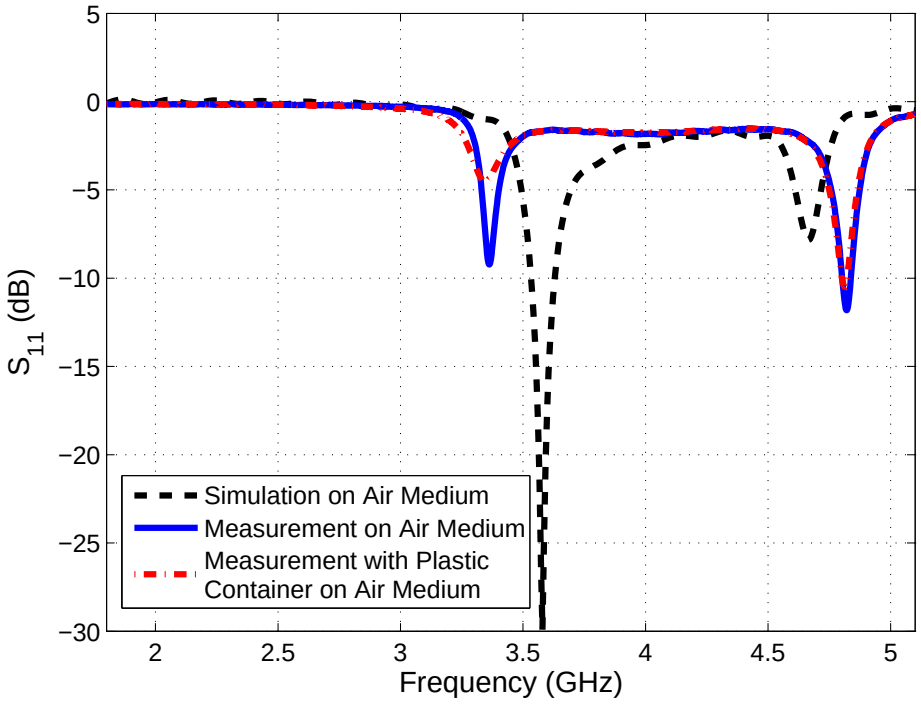

Figure 5.11: Measured and simulated return loss of the resonator in air media.

the relative permittivity of the blood layer corresponds to a $+0.2\ \Omega$ and $-0.02\ \Omega$ change in the real and imaginary parts of the input impedance, respectively. Fig. 5.13 shows the calculated input impedance from the measured S-parameter results at the resonance frequency. The change in the real and imaginary part of the input impedance is $-0.08\ \Omega$ and $+0.05\ \Omega$, respectively. The discrepancy between the measurement and simulations could be due to the resonance frequency shift in the measurement, when compared to the simulation.

The experiment was then repeated with the other BMM layers of different glucose indexes, starting from 7 mmol/dl. The results are also shown in Fig. 5.13. As this work represents an initial study, there is still a need to perform additional measurements within the realistic BGL range, to provide a baseline for further studies. In particular, the experiment will be repeated with smaller glucose index values, to identify the minimum detectable glucose index with the patch resonator; this is important for hypoglycemia, for example. In addition, the step size in glucose index values should be increased and more data points should be collected, to further verify the initial results shown above. The maximum glucose level can also be increased, to allow for the response to extreme values (e.g., in

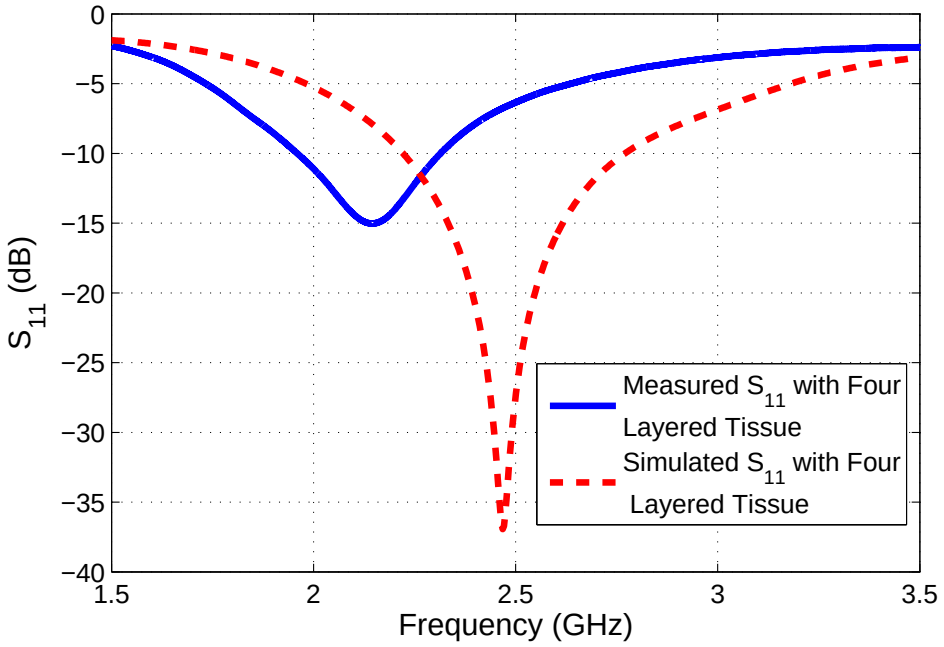

Figure 5.12: Measured and simulated return loss of the resonator with four-layered tissue mimicking material.

hyperglycemia) to be determined. These experiments must also be performed with more sensitive resonators.

It is apparent that the realistic changes in BGL (i.e., restricted to a narrow range) result in restrictions in the degree of change in the measurable dielectric properties. Whilst this study has demonstrated laboratory-level measurements can still detect the observable changes, this is a long way from practical applications, especially when considering that other physiological processes can potentially produce similar, or even larger, changes in the dielectric properties. However, the results above are useful to set the boundaries of what must be detected, allowing the resonator performance to be specified. Typically, resonators are specified in terms of their operating frequency and bandwidth; an alternative figure-of-merit to bandwidth is the quality factor (Q-factor, or Q). One method for estimating the total Q is using

$$\frac{\Delta f}{f_r} = \frac{\mathrm{VSWR} - 1}{Q_t \sqrt{\mathrm{VSWR}}} \tag{5.4}$$

where f_r is the resonant frequency, Δf is the operating bandwidth for the resonator and VSWR is the voltage standing wave ratio level used to determine the

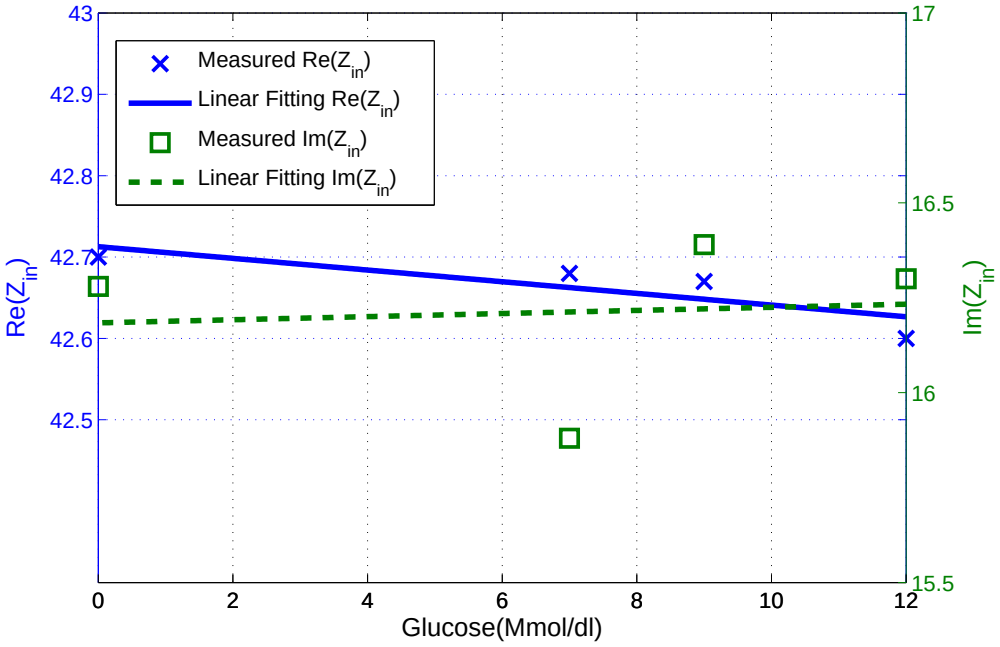

Figure 5.13: Measured input impedance with four-layered tissue mimicking material by alternating the blood layer with four different glucose index.

relevant bandwidth. Low-Q resonators thus have wide bandwidths and correspondingly low frequency selectivity; high-Q resonators have narrow bandwidths and high selectivity. The total Q is affected by various losses in the system, some of which are unavoidable in this application (in particular, the losses in the tissues).

It is obvious that a high-Q resonator would be preferred to measure BGL, given the narrow variation of dielectric properties related to normal variations in BGL (and resulting small changes in resonant frequency and input impedance magnitude). The total Q of the patch resonator used in this study is estimated using (5.4) as $Q_t = 4.0653$, for a VSWR of 1.92 (this is equivalent to $S_{11} = -10$ dB) and $f_r = 2.143$ GHz. The lower and upper limits of the resonant band are 1.962 GHz and 2.312 GHz, respectively. Hence, this resonator is low-Q and not optimal for this application. Higher-Q resonators will be investigated to improve performance. It is also worth noting that resonators operating at higher frequencies can provide higher Q-values for the same absolute bandwidth Δf. This provides two avenues for investigation: higher frequency operation, which may have limitations related to penetration of the RF signal into the body

tissue, and resonator designs with inherently higher Q, which are likely to be more complex in geometry, or fabrication, or both.

5.4 ISM Band Spiral Resonator

In this section, we propose a simulation comparison of input impedances between the patch resonator and spiral resonator. To do so, we introduced new version of the spiral resonator, proposed in Chapter 4, tuned to operate in the 2.45 GHz ISM Band (2.4-2.48 GHz) when radiating against the four-layered (skin-wet, fat, blood, and muscle) digital tissue mimicking materials. The digital tissue mimicking materials were given non-dispersive dielectric properties representing the tissues at 2.45 GHz. The thicknesses and the dielectric properties of the tissues used in the simulation are given in Table 5.2. Width and length of the phantoms are 127 mm by 127 mm. The simulation configuration is shown in Fig. 5.14

The spiral resonator was designed by optimising the configuration of the spiral resonator proposed in Chapter 4. First, the length of the spiral was truncated; then, two via pins were placed symmetrically, shorting the arms of the spiral resonator to the ground plane. By changing the location of the via pins, the operation frequency is tuned. For example, as the pins moved towards the ports, the spiral resonator starts to operate at higher frequencies. In Fig. 5.15, the configuration of the resonator is given; the shorting via pins are shown with black dots and ports are shown with red dots.

Two identical coaxial feeds are designed to feed the spiral resonator in the simulation. The dimensions of the coaxial feeds are as follows: diameter of inner conductor is 1.3 mm, diameter of dielectric is 4.1 mm with a 1.3 mm hole inside for the inner conductor; the length of the coax is 5 mm, and finally, thickness of the outer shell is 0.05 mm. The substrate of the spiral resonator is Rogers 3210 substrate with $\varepsilon_r = 10.2$ and a dissipation factor of 0.0027 at 10 GHz. The dimensions of the spiral resonator are shown in Table 5.7. Note that the spiral resonator has a full ground plane. A return loss comparison of the patch and spiral resonators with normal blood glucose ($\varepsilon_r = 58.347$) is given in Fig. 5.16.

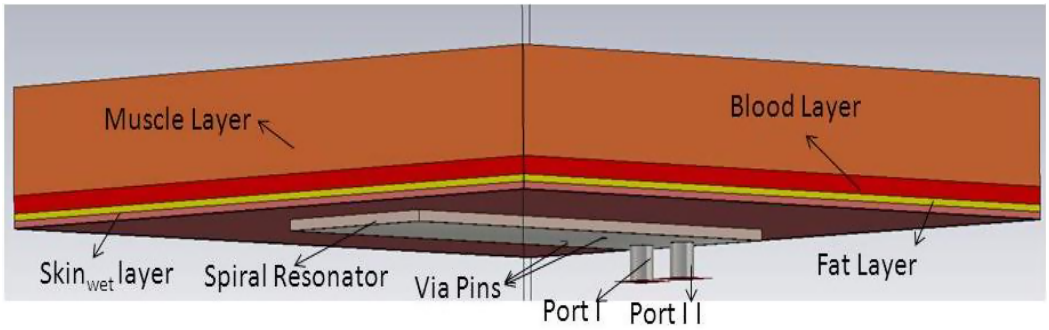

(a)

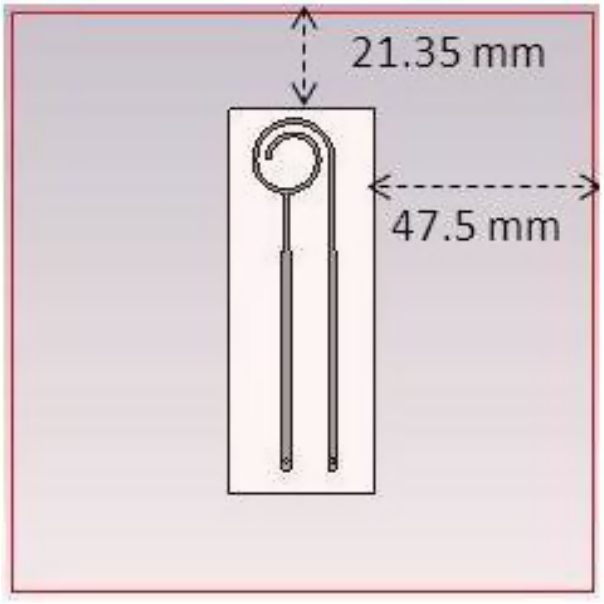

(b)

Figure 5.14: Simulation configuration of the ISM band spiral resonator: (a) digital tissue blocks and resonator; (b) the location of the resonator.

Center frequencies are 2.452 GHz and 2.451 GHz for spiral and patch resonator, respectively. The center frequencies are very close; however, a better matching was obtained for the patch resonator.

To examine the sensitivity of spiral resonator's input impedance to the changes in relative permittivity, digital blood mimicking material block's relative permittivity is decreased. From the simulated S-parameter response, Z-parameters are calculated for each case. There is no shift in the frequency of operation of the both resonators for minimum and maximum values of the blood phantom 56.347 and 58.347, respectively. However, the matching changes for both of the resonators. The change of the input impedance for patch resonator is given for 2.4 GHz in

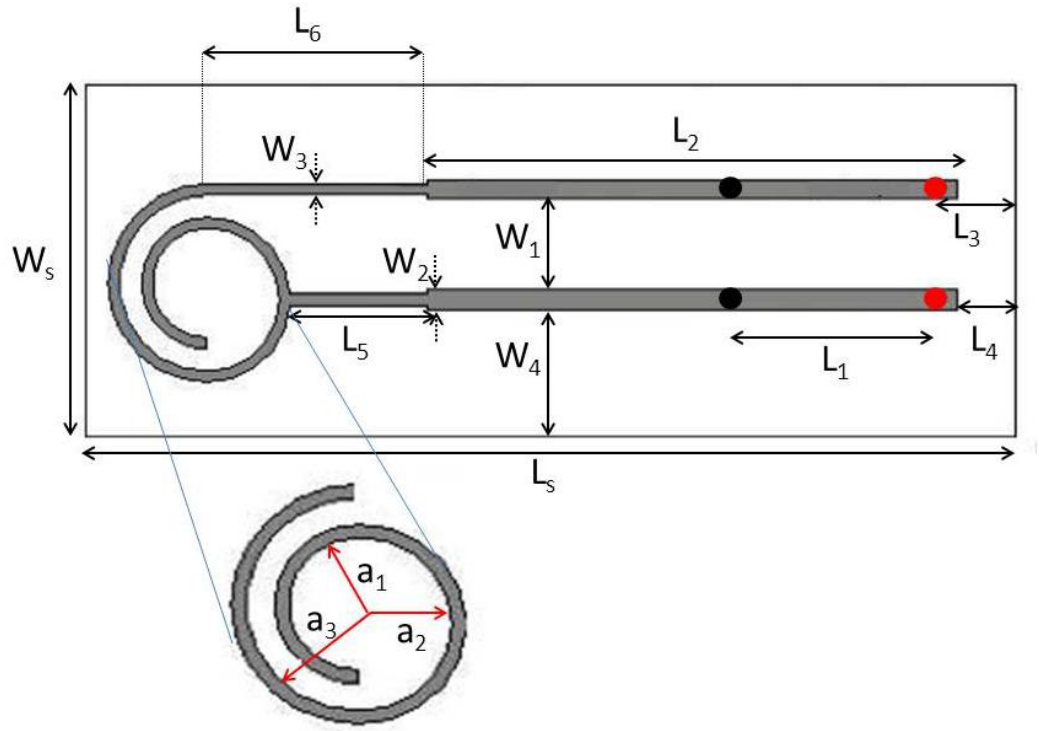

Figure 5.15: Configuration of the ISM band spiral resonator.

Table 5.7: Dimensions of the ISM Band Spiral Resonator

Parameter	*Value (mm)*	*Parameter*	*Value (mm)*	*Parameter*	*Value (mm)*
W_s	32.00	L_s	84.3	L_5	12.51669
W_1	8.193	L_1	19.4	L_6	20
W_2	1.807	L_2	48	a_1	5
W_3	1	L_3	7.3	a_2	6.5
W_4	11.5965	L_4	5.3	a_3	8.5

Fig. 5.6, and the formulation for the input impedance calculation is shown in equation 5.3. The same equation is used to calculate the input impedance of the spiral resonator.

In Table 5.8, a comparison between the input impedance of the spiral resonator and patch resonator at center frequency is shown. From the results, we can state that both of the resonators are somewhat sensitive to the changes in the dielectric properties of the blood layer. However, assuming that the dielectric property change will be 1 unit, the corresponding change for the spiral resonators input impedance will be 0.06 Ω and 0.002 Ω for real and imaginary parts, respectively. Similarly, the corresponding change for the patch resonator will be 0.16 Ω and 0.067 Ω for real and imaginary parts, respectively. From the comparisons, we

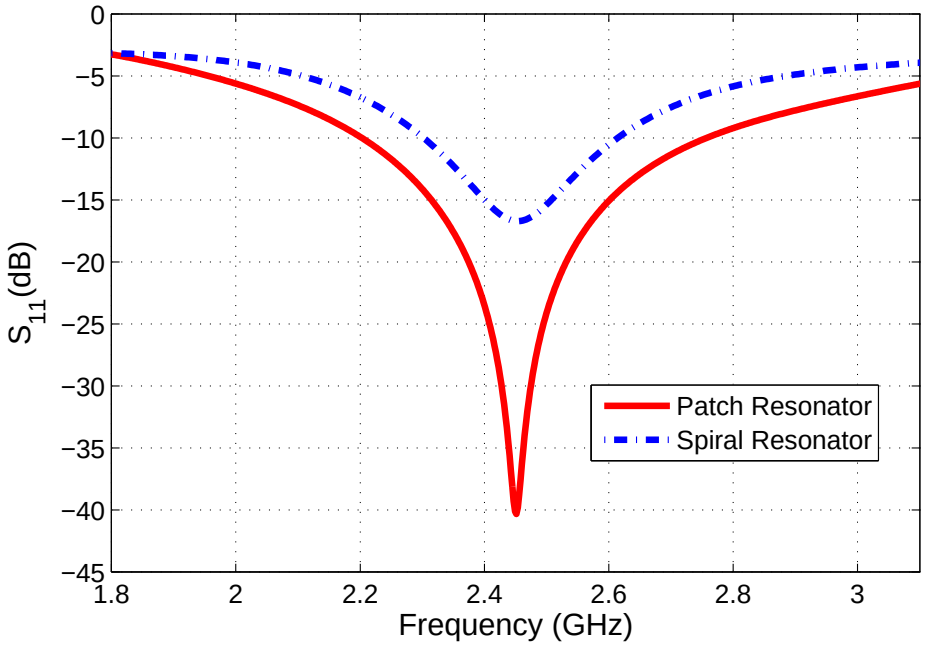

Figure 5.16: Return loss comparison of the spiral and patch resonator.

Table 5.8: Calculated Input Impedance of the Resonators (Spiral: 2.452 GHz; Patch: 2.451 GHz)

Glucose levels(mmol/l)	*Blood* ε_r *Units*	*Patch*		*Spiral*	
		$Re(Z_{in})$ Ω	$Im(Z_{in})$ Ω	$Re(Z_{in})$ Ω	$Im(Z_{in})$ Ω
0	58.347	48.04	−0.802	37.15	6.820
1.2	58.247	48.05	−0.809	37.16	6.820
6	57.847	48.12	−0.804	37.18	6.820
12	57.347	48.20	−0.879	37.21	6.818
18	56.847	48.28	−0.916	37.24	6.817
24	56.347	48.36	−0.950	37.27	6.815

can conclude that the patch resonator is more sensitive to the dielectric property change of the blood layer.

5.5 Conclusions

In this Chapter, experimental validation of simulations and investigations of more realistic levels of blood sugar are presented. Also, some poorly-understood trade-offs regarding the RF resonator (size, sensitivity, operating frequency) are examined.

This chapter also presents dielectric spectroscopy results of the blood mimicking material with realistic blood glucose levels. The results of the dielectric

spectroscopy suggest that there is only a slight change in the relative permittivity of the blood with altering realistic glucose levels and the effective conductivity is expected to remain constant.

In addition, the wide-band TM materials were used in measurements performed with a patch resonator, with varying quantities of dextrose added to the blood layer. This work examines the possibility of measuring the blood glucose levels non-invasively and continuously within the realistic blood glucose level range. It has been shown that the input impedance response of the patch resonator is sensitive to the changes in the relative permittivity of the blood layer. The trend of the measured input impedance has been shown to be consistent with the simulated response. The proposed approach presents a potential for non-invasive continuous monitoring of changes in blood glucose level.

A spiral resonator, operating in the popular 2.45 GHz ISM band, was compared to the patch resonator, with respect to its ability to detect small changes in blood glucose level, via simulations using a four-layered digital phantom. These small changes are detectable in principle, but results suggest the system sensitivity must be optimised.

References

[1] T. Karacolak, A. Hood, and E. Topsakal, "Design of a dual-band implantable antenna and development of skin mimicking gels for continuous glucose monitoring," *Microwave Theory and Techniques, IEEE Transactions on*, vol. 56, no. 4, pp. 1001 –1008, april 2008.

[2] T. Karacolak, R. Cooper, J. Butler, S. Fisher, and E. Topsakal, "In vivo verification of implantable antennas using rats as model animals," *Antennas and Wireless Propagation Letters, IEEE*, vol. 9, pp. 334 –337, 2010.

[3] M. Ahmadi and G. Jullien, "A wireless-implantable microsystem for continuous blood glucose monitoring," *Biomedical Circuits and Systems, IEEE Transactions on*, vol. 3, no. 3, pp. 169 –180, june 2009.

[4] B. Jean, E. Green, and M. McClung, "A microwave frequency sensor for non-invasive blood-glucose measurement," in *Sensors Applications Symposium, 2008. SAS 2008. IEEE*, feb. 2008, pp. 4 –7.

[5] E. C. Green and R. Jean, "Design of a microwave sensor for non-invasive determination of blood-glucose concentration," Master's thesis, Engineering and Computer Science, Baylor University, 2005. [Online]. Available: http://beardocs.baylor.edu/xmlui/handle/2104/3000

[6] B. Freer and J. Venkataraman, "Feasibility study for non-invasive blood glucose monitoring," in *Antennas and Propagation Society International Symposium (APSURSI), 2010 IEEE*, july 2010, pp. 1 –4.

[7] Y. Hayashi, L. Livshits, A. Caduff, and Y. Feldman, "Dielectric spectroscopy study of specific glucose influence on human erythrocyte membranes," *Journal of Physics D: Applied Physics*, vol. 36, no. 4, pp. 369–374, 2003. [Online]. Available: http://stacks.iop.org/0022-3727/36/i=4/a=307

[8] "Recommendation on reporting results for blood glucose," *eJIFCC*, vol. 12, no. 4, 2009, iFCC Scientific Division Working Group on Selective Electrodes. [Online]. Available: http://www.ifcc.org/ifccfiles/docs/vol12no4a4.pdf

[9] Y. Hayashi, L. Livshits, A. Caduff, and Y. Feldman, "Dielectric spectroscopy study of specific glucose influence on human erythrocyte membranes," *Journal of Physics D: Applied Physics*, vol. 36, no. 4, pp. 369–374, 2003. [Online]. Available: http://stacks.iop.org/0022-3727/36/i=4/a=307

[10] E. Topsakal, T. Karacolak, and E. Moreland, "Glucose-dependent dielectric properties of blood plasma," in *The XXX General Assembly of the International Union of Radio Science*, August 2011.

[11] J. Venkataraman and B. Freer, "Feasibility of non-invasive blood glucose monitoring: In-vitro measurements and phantom models," in *Antennas and Propagation (APSURSI), 2011 IEEE International Symposium on*, july 2011, pp. 603 –606.

[12] K. Beam and J. Venkataraman, "Phantom models for in-vitro measurements of blood glucose," in *Antennas and Propagation (APSURSI), 2011 IEEE International Symposium on*, july 2011, pp. 1860 –1862.

[13] "Federal communications commission," 2012. [Online]. Available: http://www.fcc.gov

[14] C. Gabriel, S. Gabriel, and E. Corthout, "The dielectric properties of biological tissues: I. literature survey," *Physics in Medicine and Biology*, vol. 41, no. 11, p. 2231, 1996. [Online]. Available: http://stacks.iop.org/0031-9155/41/i=11/a=001

[15] S. Gabriel, R. W. Lau, and C. Gabriel, "The dielectric properties of biological tissues: Ii. measurements in the frequency range 10 hz to 20 ghz," *Physics in Medicine and Biology*, vol. 41, no. 11, p. 2251, 1996. [Online]. Available: http://stacks.iop.org/0031-9155/41/i=11/a=002

[16] A. Peyman and C. Gabriel, "Colecole parameters for the dielectric properties of porcine tissues as a function of age at microwave frequencies," *Physics in Medicine and Biology*, vol. 55, no. 15, p. N413, 2010. [Online]. Available: http://stacks.iop.org/0031-9155/55/i=15/a=N02

[17] C. Gabriel, R. W. Lau, and S. Gabriel, "The dielectric properties of biological tissues: Iii. parametric models for the dielectric spectrum of tissues," *Physics in Medicine and Biology*, vol. 41, no. 11, p. 2271, 1996. [Online]. Available: http://stacks.iop.org/0031-9155/41/i=11/a=003

[18] M. Lazebnik, M. C. Converse, J. H. Booske, and S. C. Hagness, "Ultrawideband temperature-dependent dielectric properties of animal liver tissue in the microwave frequency range," *Physics in Medicine and Biology*, vol. 51, no. 7, p. 1941, 2006. [Online]. Available: http://stacks.iop.org/0031-9155/51/i=7/a=022

[19] A. Hood and E. Topsakal, "Particle swarm optimization for dual-band implantable antennas," in *Antennas and Propagation Society International Symposium, 2007 IEEE*, june 2007, pp. 3209 –3212.

[20] M. Lazebnik, D. Popovic, L. McCartney, C. B. Watkins, M. J. Lindstrom, J. Harter, S. Sewall, T. Ogilvie, A. Magliocco, T. M. Breslin, W. Temple, D. Mew, J. H. Booske, M. Okoniewski, and S. C. Hagness, "A large-scale study of the ultrawideband microwave dielectric properties of normal, benign and malignant breast tissues obtained from cancer surgeries," *Physics in Medicine and Biology*, vol. 52, no. 20, p. 6093, 2007. [Online]. Available: http://stacks.iop.org/0031-9155/52/i=20/a=002

Chapter 6

Observational Study with Patch and Spiral Resonators

The ultimate testing domain for devices intended to be used in the vicinity or on the human body is using the human subjects. Testing of a blood glucose monitoring system ultimately requires human subjects and blood samples from those subjects. The study can be elaborated by using diabetic human subjects. However, such experiments are subject to tight regulations [1, 2]. In particular, usage and collection of human blood and it's components is highly regulated [3, 4]. Major reasons for such tight regulations on blood usage is experiments requiring blood collection posses high risk of infection to the subject and experimenter. Thus, the laboratory should be organized and equipped according to the requirements, that includes a medical waste, disposable personal lancets and blood collection items, and hygiene standards should be met. Also, unsuitable subjects, namely donors with serious medical condition including carriers of transmissible blood diseases, should be identified before the experiments to prevent experimental misconduct. Although clinical tests are vital to asses the efficiency and the safety of such devices, there is a need to perform preliminary

human tests to assess the feasibility of the proposed technique. Non-ionizing radio wave emitting devices that is designed to operate in the vicinity or on the body have been tested with humans in the literature without obtaining rigorous ethical approvals [5, 6, 7, 8]. Such tests are not subject to tight regulations. Thus, under certain constraints and assumptions, for example in this study by eliminating the blood sample collection, human tests can be carried out with the previously proposed patch and spiral resonators. Through the proposed experimental study, this chapter lays out the foundations for the requirements and necessary improvement in the proposed system to carry out a successful clinical tests.

In this chapter, the patch resonator proposed in Chapter 5 and the first prototype of the microstrip spiral transmission line proposed in Chapter 4, Section 4.2 are used. Although the proposed resonators were previously tested with tissue mimicking phantoms and with liquid phantoms to verify the proper functioning of the resonators, the ultimate test domain, to understand the true performance of the structure, is using human subjects. However, human tests requires carefully designed experiments to minimize the effects of other changes in the body to the resonator response. One factor that is known to effect the resonator response from earlier observations is the applied force. This effect is due to the change in superstrate geometry and in return effective permittivity changes when the tissue is pressed, squeezed or stretched. Thus, there is a need to calibrate the response of the resonator in order to gather the data relating to the permittivity change due to the glucose levels. However, this approach not only requires a multiple sensor system but also a smart algorithm to detect the relevant data. As a necessary preliminary step towards this objective, in this chapter we are proposing initial human experiments performed under controlled conditions. Note that the QMUL Antenna laboratory is authorized by the QMUL research ethics committee to investigate the interaction between RF/microwaves and biological tissues.

One of the constraints for both patch and spiral resonator tests is the subjects are required to go through the procedure named *soda test*. The soda test is similar to the *oral glucose tolerance* (OGT) test, a conventional test performed in hospitals to diagnose the diabetes disease. To perform the OGT, the patient is

required to fast for at least 6 hours, and when the patient arrives to the hospital their fasting state glucose levels are measured. For a non-diabetic the fasting state glucose level is around 3.5 to 5 mmol/l [9, 10, 11]. After this measurement, the subject is given a glucose-rich drink, then the glucose levels are tracked over time. For a non-diabetic, two hours after the glucose-rich drink intake, the levels should be less than 7.8 mmol/l [9]. The soda test, described in more detail in Section 6.1.2, is a very similar procedure; essentially, in the soda test the glucose-rich drink is substituted with soda containing 36 grams sugar. The OGT is an effective way to alternate the blood glucose levels very rapidly. In Fig. 6.1 [12, 13, 14], the graphs for the glucose levels of the healthy subject and diabetes patient during OGT test is shown.

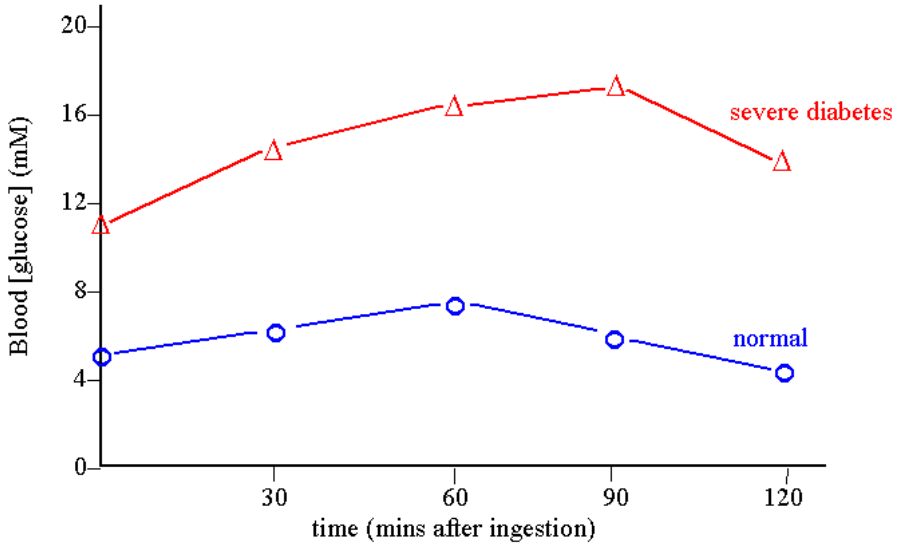

Figure 6.1: Change of blood glucose levels during an oral glucose tolerance test for diabetic patient and non-diabetic subjects [12] .

The other constraint considered during the patch resonator measurements is keeping the applied force constant. To do so, dual sensor system is designed by combining commercial force sensors with the patch resonator. The experimental set-up and the force measurements are explained in Section 6.1.1.

In this work, due to the health and safety regulations only healthy subjects are considered. The remainder of the chapter is organised as follows. The experimental methodology for both of the resonators is presented in Section 6.1.

Calibration procedure the force sensors is described in section 6.1.1. The experimental methodology used for patch resonator elaborated in section 6.1.2. Experimental procedure for spiral resonator is defined in 6.1.3. Calibration results are given in section 6.2.1. Soda test results for patch resonator and spiral resonator are given in section 6.2.3 and 6.2.3, respectively.

6.1 Experimental Methodology

6.1.1 Force Tests for Patch Resonator

Patch resonator presented in Chapter 5 was mounted on a wooden test bench with the dimensions of 140.5x360x18 mm^3. Dielectric properties of the wooden bench is ε_r=1.8, tan(δ)=0.15 at 2.45 GHz. Two flexible commercial thin-film force sensors were taped at both end of the resonator leaving 2 mm space between the resonator and the force sensors. The force sensors are identical and the length, width, and thicknesses of the sensors are 100 mm, 14 mm, and 0.203 mm, respectively. Both of the force sensors used in this study are A201 type *flexiforce* commercial thin-film type sensors [15]. Transparent cover of the commercial sensors is polyester (Mylar) with the dielectric properties of ε_r=3.2, tan(δ)=0.005. Experimental configuration of the test bench is shown in Fig. 6.2. Simulation configuration is identical to experimental set-up. Note that the force sensors are considered as homogeneous Mylar during the simulations.

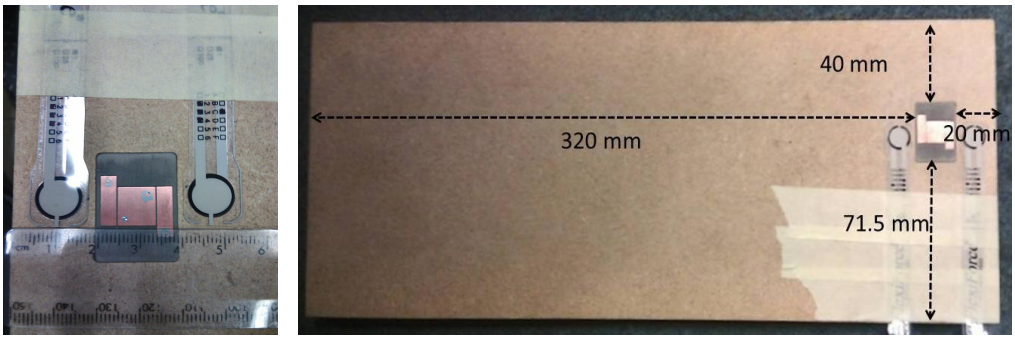

(a) (b)

Figure 6.2: Configuration of the test bench: (a) the resonator and force sensors; (b) wooden test bench.

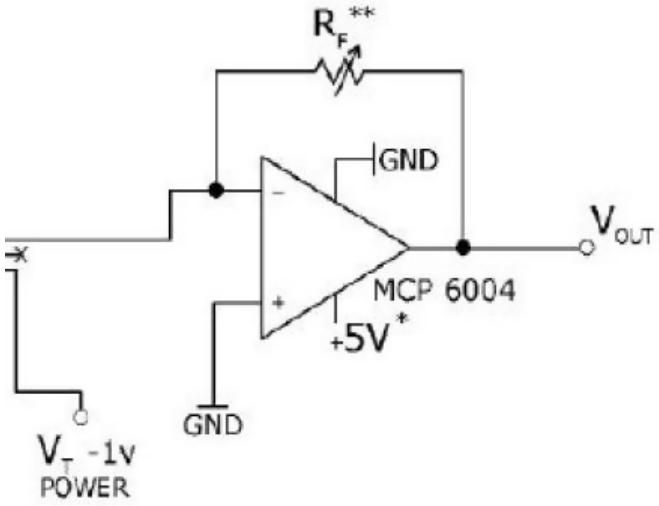

Figure 6.3: Feeding circuit for thin-film force sensors.

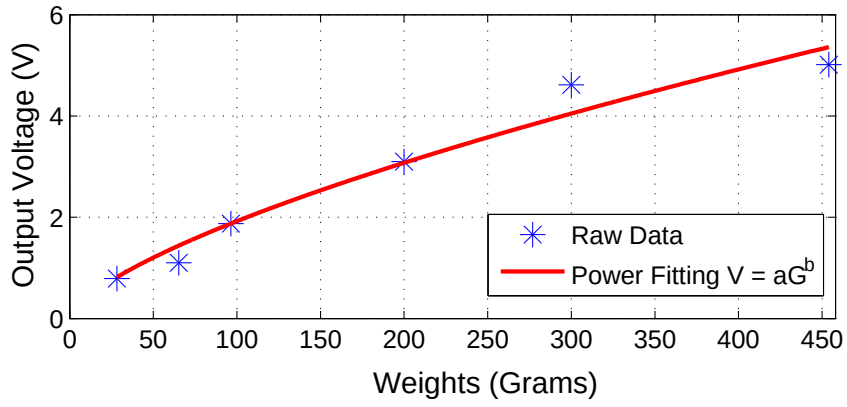

(a)

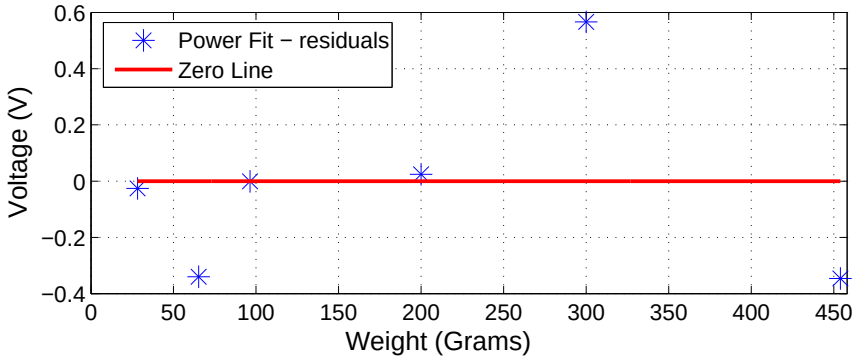

(b)

Figure 6.4: Calibration measurements: (a) the power fitting to the calibration values; (b) residual plots of the power fitting.

The commercial force sensors can measure the applied force up to 400 grams.

Feeding circuit for force sensors is shown in Fig. 6.3. Feeding circuits were built on a breadboard and output voltage of the force sensors were measured with multimeters. The variable resistances were fixed to 203 kΩ.

To express the applied force in terms of weight the sensors are calibrated. Calibration is performed by placing a disk to the sensing area of the force sensors to concentrate the weight only on the sensing area of the sensors. Then the previously known precise weights are placed on top of the disk and the output voltage of the sensors are measured with multimeters. The calibration graph for the sensor are shown in Fig. 6.4 (a). Two sets of data are taken from the first and second sensors and the median of those data is plotted in the Fig. 6.4 (a). The coefficients for the power fitting function is a= 0.085 and b= 0.678. The R square is 0.965 defines the goodness of the fitting. Residual plots are given in Fig. 6.4 (b).

Force measurements are performed with four female and one male healthy subjects. The Body Mass Index (BMI) of the each subject is given in Table 6.1. The age of the subjects are ranging from 25 to 40. The blood glucose levels of the subjects were constant and were expected to be low (4 to 5 mmol/dl) as the subjects were fasting more than 6 hours before the experiment. The subjects were asked to press the inner part of their right arms to the bench where the resonator and the sensors are mounted on top. The subject's arms were also marked with an arm band, 45 mm distance from the wrist was placed on the edge of the test bench, to measure the same tissue block on each subject. Also the location of the arm is marked with bands and on each measurement experimenter checked the placement of the arm to ensure that the sample placement was matching with the previous measurements for each subject. Note that such restriction maximises the repeatability.

Table 6.1: Body mass index (BMI) of the subjects

Subject	*BMI*	*Subject*	*BMI*
$Female_1$	22.1	$Female_4$	21.9
$Female_2$	25.0	$Male_1$	22.1
$Female_3$	22.5		

During the force experiments the subjects were asked to apply the same

amount of force to both force sensors located next to the resonator. When the same level of force was reached on both sensors the experimenter recorded the resonator response. For each force level 5 resonator response was recorded. The subjects applied four different levels of force, from 0.5 V to 2 V with 0.5 V increments.

6.1.2 Soda Test for Patch Resonator

In this test, the objective is to increase the blood sugar levels of a healthy human subject rapidly. The subject is required to fast at least six hours before starting the experiment. While the subject is still fasting the force measurements are performed and the subjects asked which force level was more comfortable. Each subject indicated 1 V output force level as the most comfortable force level. Then the subject is asked to give another set of measurement while still fasting by applying 1 V force. The subject is then asked to consume the soda drink. After the ingestion of the 330 ml sugar-rich soda drink response of the resonator is recorded for two hours with approximately 8 minute intervals. The work flow during the patch resonator experiments is shown in Fig. 6.5.

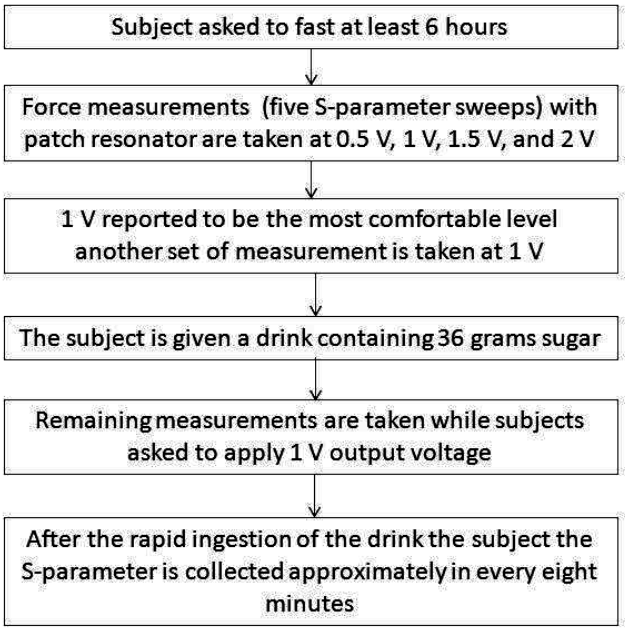

Figure 6.5: Work flow during force and soda test experiments with patch resonator.

During the data analysis the median of the five measurements are taken and each considered as a single data point at the time of the measurement. The purpose of taking the median is to minimize the faulty readings.

6.1.3 Soda Test for Spiral Resonator

The first prototype (presented in Chapter 4, Section 4.2) is strapped to the subject's arm, radiating towards the tissue. One female and one male subject aged between 23 to 25 are tested. The subject is asked to place the arm to a desk and asked to not to remove or move the arm during the experiment. The subjects remained in the same position during the experiment especially the arm where the spiral resonator is strapped is kept in the same position. Thus, the applied pressure kept constant. The sensor is then connected to a HP 8720ESVNA vector network analyzer; the measurement set up is shown in Fig 6.6. The S_{21} response of the sensor is recorded continuously, every six seconds, for 10 minutes for each subject. The data is saved with LabView program by recording the transmission S_{21} response. As the program was able to record one parameter at a time (e.g. the Labview program can not record both S_{11} and S_{21}), only transmission response S_{21} is recorded. Additionally, the sensor is given 0 dBm input power.

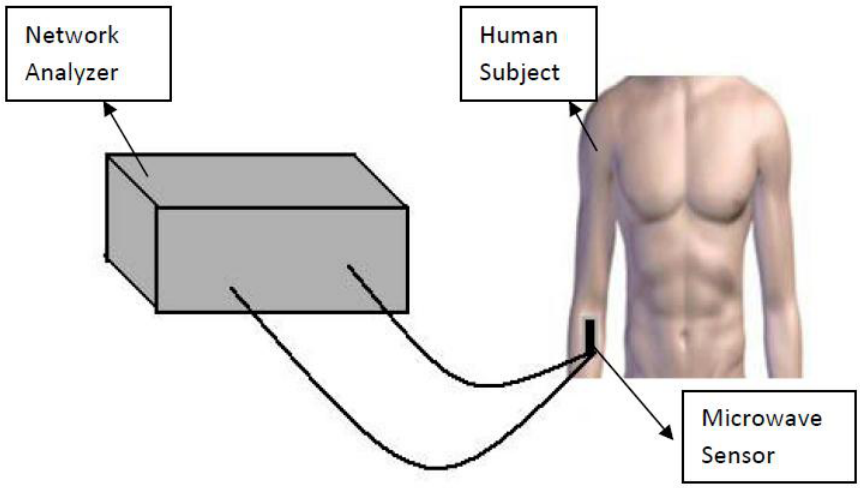

Figure 6.6: Measurement set-up of soda test resonator attached to the arm of the human subject and connected to the network analyzer .

After 10 minutes of continuous monitoring of the sensor response, the subject is given a soda drink. The volume of the soda drink is 330 ml, with a sugar

content of 36 grams. During and after the consumption of soda drink, the sensor response is tracked continuously. Measurements were performed first on a female subject with a BMI of 22, with no serious health condition. Next on a healthy male subject with a BMI of 21.8.

6.2 Results

6.2.1 Force Measurements with Patch Resonator

For each force level five resonator response was recorded during the experiments. The median of the collected response is taken for each force level for each subject, shown in Fig. 6.7. In Fig. 6.7, the red curve, expressed by $y = ax^b + c$ where $a = 0.12$, $b = -1.13$, $c = 2.49$, shows the median of all measurements.

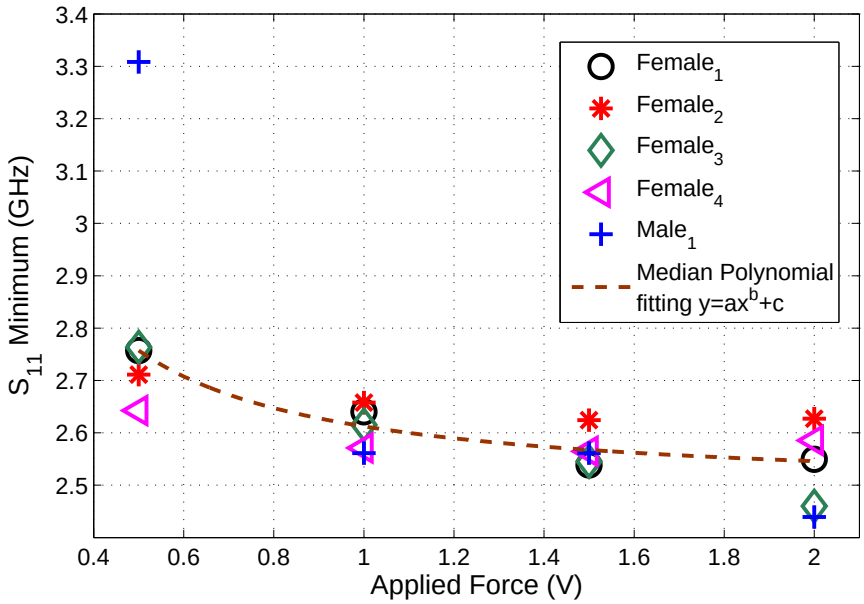

Figure 6.7: Change in sensor S_{11} response with the applied force voltage output.

The median fitting indicates that the with the increase in applied force the superstrate permittivity increases. While the applied force is very low, for example at 0.5 V output, an air gap might be introduced between the tissue and the resonator. Note that the resonance shift is sharp between 0.5 V and 1 V output, 5.3% decrease. As the applied force increased, the resonance shift becomes more smooth. The decrease in resonance is 1.7% and 0.8% for increase in applied force

from 1 V to 1.5 V and 1.5 V to 2 V, respectively. This is due to the tissue displacement, in this case it is hypothesized that the fat tissue is displaced with the increase in applied force. This experiment is important to assess the effect of the force. From the change observed in Fig. 6.7, we can state that the applied force has a significant effect on the resonator response; thus, it should be kept constant to differentiate the effect of the glucose change to the resonator response. Note that during the experiments subjects could not be able to apply more force. The sensor output can reach up to 5 V.

After the measurements the subjects are asked which force level was more comfortable. The subjects reported that the 1 V output was the most suitable force level. After the experiments the standard deviation from the mean (σ) on each applied force level among 5 measurement is also calculated. Table 6.2 shows the calculated standard deviations. From Table 6.2 1 V applied force level shows less deviation. Thus, 1 V force level is considered to be the standard force level during the soda test with patch resonator.

Table 6.2: Standard deviation from the mean (σ) on each applied force level

$Force$ (V)	$Female_1$ $\sigma\ (MHz)$	$Female_2$ $\sigma\ (MHz)$	$Female_3$ $\sigma\ (MHz)$	$Female_4$ $\sigma\ (MHz)$	$Male_1$ $\sigma\ (MHz)$
0.5	25.954	9.5513	24.954	13.257	29.681
1	4.2943	4.6416	8.5015	1.1808	12.343
1.5	17.162	4.7459	25.373	12.159	10.428
2	6.7883	2.4348	2.7803	0.88977	19.459

6.2.2 Patch Resonator Observational Study

For each subject 120 measurements in total were taken. The resonance frequency is derived by taking the median frequency of the S_{11} minimum. S-parameters are then converted to Z-parameters and the input impedance is calculated with equation 6.1. Median of the input impedance real part is taken for five measurements. With the median representation the collected data are then reduced to 24 points from 120 measurements.

$$Z_{in} = Z_{11} - \frac{Z_{12}Z_{21}}{Z_{22} + Z_L} \tag{6.1}$$

Real part of input impedance at the median frequency are plotted against the time for each subject. Then the values are normalised and a second degree gaussian function is fitted to each measurement set. The function is given in equation 6.2.

$$f(t) = a_1 * e^{(-\frac{t-b_1}{c_1})^2} + a_2 * e^{(-\frac{t-b_2}{c_2})^2} \tag{6.2}$$

where t is the time in minutes and f(t) is the fitting function to normalized values and OGT test in Fig. 6.8, Fig. 6.9, and Fig. 6.10. Note that the function gives normalized values for the real part of the input impedance. The normalized fitting to the collected data from female$_1$ is shown in Fig. 6.8 (a). The residuals are also shown in Fig. 6.8 (b). Fig. 6.8 (a) also shown the fitting while the data outliers are excluded from the data set.

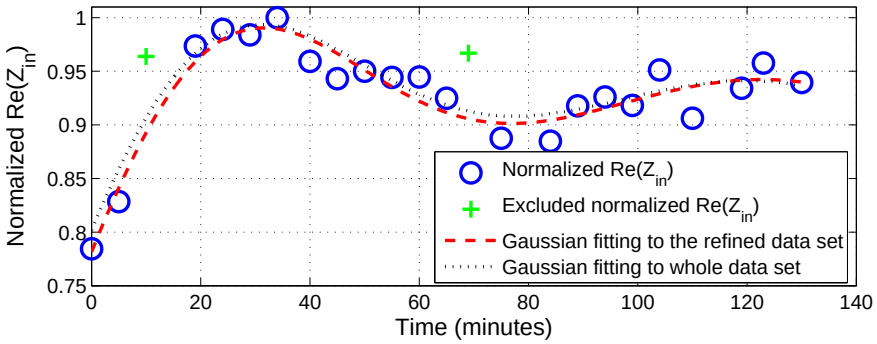

(a)

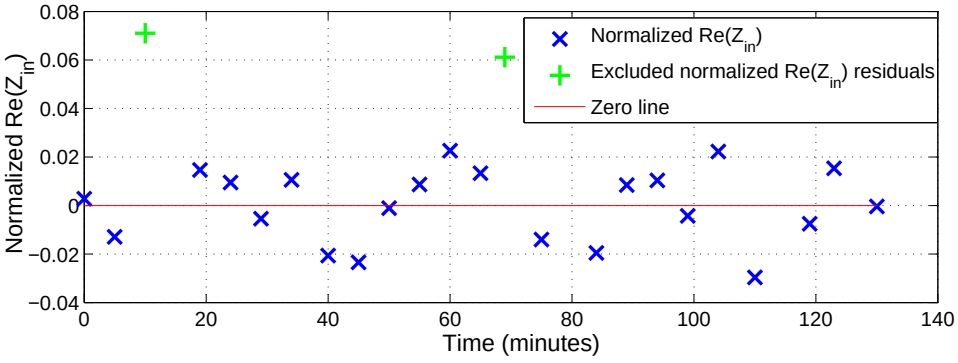

(b)

Figure 6.8: Normalized Re(Z_{in})data for female$_1$:(a) Gaussian fitting to the normalized 24 data points and for the 22 points excluding the data points resulting high residuals; (b) Residual plots including excluded data points .

The outliers are identified through the residual plots. If the data is showing a

residual that is more than 0.06, it is identified as a residual. For female$_1$ 3^{rd} and 14^{th} data set is excluded and the fitting is done according to remaining 22 data points. The R-square value, indicating the goodness the fitting, for female$_1$ is 0.78 while the outliers are included. The R-square value is 0.91 when the outliers are excluded from the data set. The outliers could be due to the misplacement of the arm and failing to apply the aimed pressure to the structure. The gaussian fitting coefficients for each subject is given in Table 6.3. The given values are representing data without the outliers. The omitted outliers are 1, 3, 4, and 6 of the measurements for female$_2$, female$_3$, female$_4$, and male$_1$, respectively. The residual based exclusion criteria is considered for all subjects. Also OGT test results performed on healthy subjects are taken from the literature and a 2^{nd} degree polynomial fitting is performed on the results given in Table 6.3. Due to the ethical restrictions during the experiments the glucose levels of the subjects were not collected. Thus a comparison with the literature data [16] is given.

Table 6.3: Coefficients for gaussian fitting functions for each experiment subject and R^2 values

$Variables$	$Female_1$	$Female_2$	$Female_3$	$Female_4$	$Male_1$	$OGT\ Fitting$
a_1	0.44	0.93	0.97	0.93	0.27	153.4
b_1	17.77	135.5	78.28	111	39.67	43.42
c_1	42.93	172.7	233	104.4	33.96	50.89
a_2	0.94	0.37	123.5	0.60	0.81	88.56
b_2	124	2.96	−62.54	−1.78	125.9	121
c_2	136.4	75.24	23.17	53.88	178.6	38.2
R^2	0.91	0.55	0.36	0.36	0.79	0.99

Fig. 6.9 shows the comparison between the gaussian fittings for three subjects and the literature data. The best correlation with the literature data [16] is obtained for male$_1$. Female$_1$ and female$_2$ shows correlation with the literature data [16] with a tolerable time lag. Comparisons for female$_3$ and female$_4$ shown in Fig. 6.9 (a) and (b), respectively, does not show a significant correlation with the literature data [16].

The time lag could be due to the different amount of glucose injection. In the experiment the subjects are asked to ingest 36 grams of sugar. However, in [16], the subjects are given a drink containing 75 grams of sugar. Thus the glucose

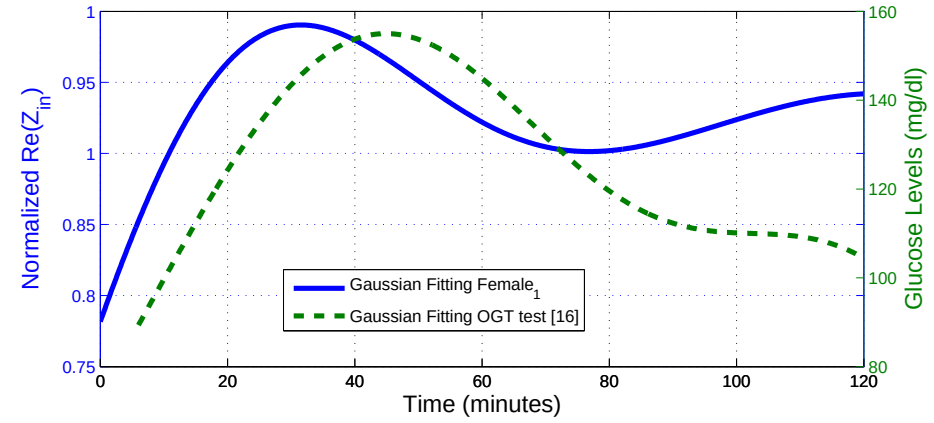

(a)

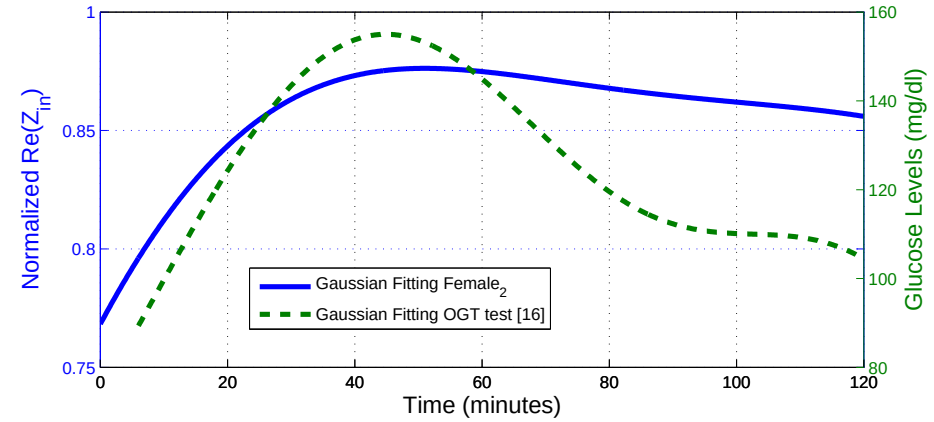

(b)

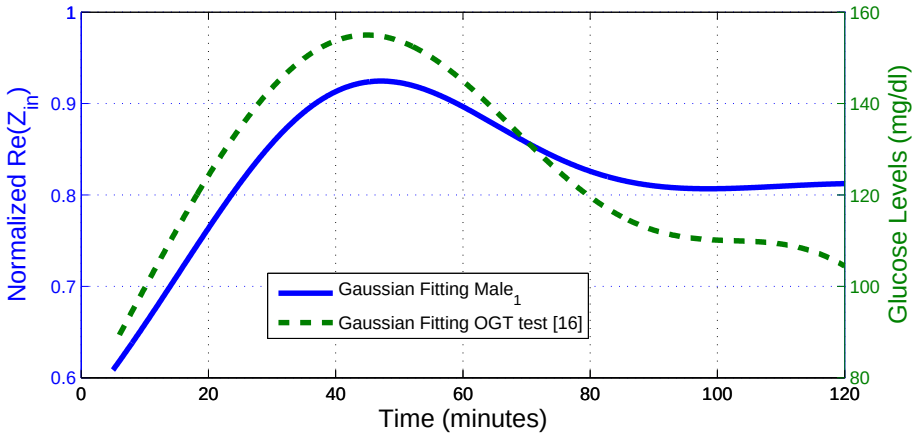

(c)

Figure 6.9: Comparison of the normalized input impedance $\mathrm{Re}(Z_{in})$ measurements and oral glucose tolerance test results from the literature [16]: (a)Female_1; (b) Female_2; (c)Male_1.

levels of female_1 and female_2 might not be able to reach an upper limit. Also the gender and age difference effects the metabolism of the subjects, suggesting the

reaction to the glucose intake is highly likely to differ. Nevertheless, the results shown in Fig. 6.9 and Fig. 6.9 gives promising results with 60% success rate. The preliminary results suggests that the patch resonator is sensitive to the blood glucose change. However, there is still a need to investigate further the potential contributing factors to dielectric property change in the tissue such as insulin and temperature change.

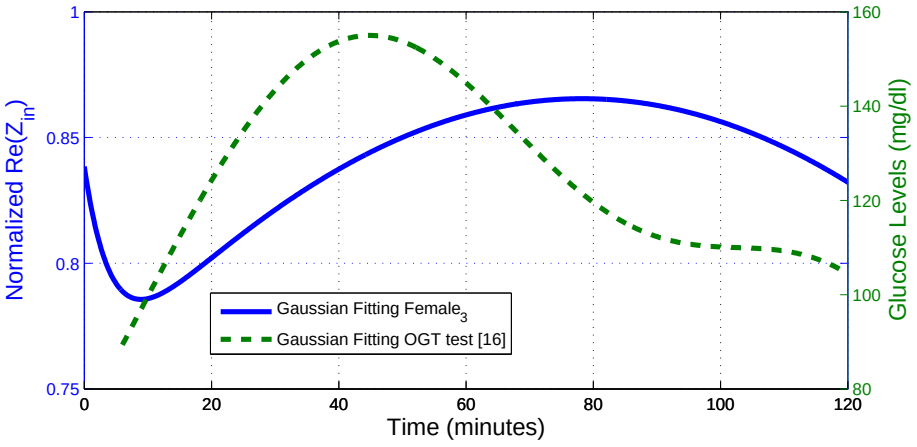

(a)

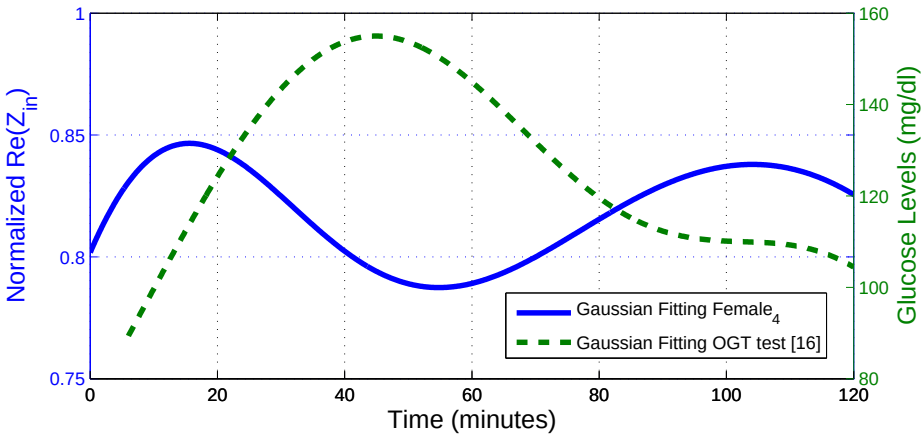

(b)

Figure 6.10: Comparison of the normalized input impedance Re(Z_{in}) measurements and oral glucose tolerance test results from the literature [16]: (a)Female$_3$; (b) Female$_4$.

6.2.3 Spiral Resonator Observational Study

For each subject a total of 1000 measurements are taken. The subjects were observed for 90 minutes after the ingestion of the soda drink with 36 grams of sugar. Note that the same soda drink is used for both patch and spiral resonator

human tests. The S_{21} response for female and male subject is shown in Fig. 6.11 (a) and (b), respectively. The difference between the S_21 measurements is due to the difference in subjects. The measurement for male subject shows a clear peak around 500 MHz; however, transmission is better for female subject at the first peak around 600 MHz.

The frequency of first maximum for both of the measurements is tracked. The results are shown in Fig. 6.12 (a) and (b) for female and male subjects, respectively. The frequency of the first maximum is now changing. This is expected as the relative small change in the permittivity is expected to change the resonance for a very high Q resonator. However, the planar spiral resonator does not possess such property.

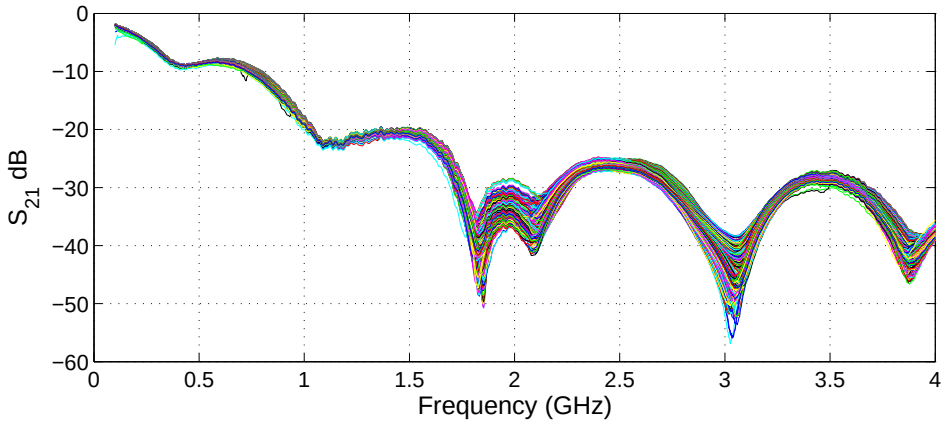

(a)

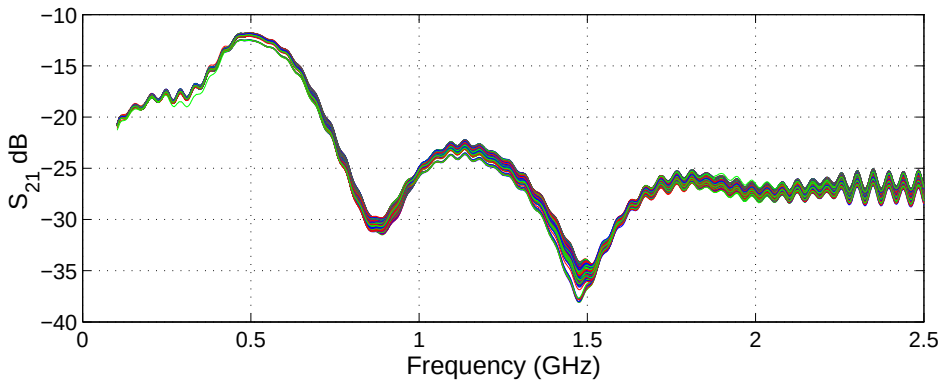

(b)

Figure 6.11: Continuous measurement of the magnitude of the transmission S_{21} response:(a) S_21 response for female subject; (b) S_{21} response for the male subject.
.

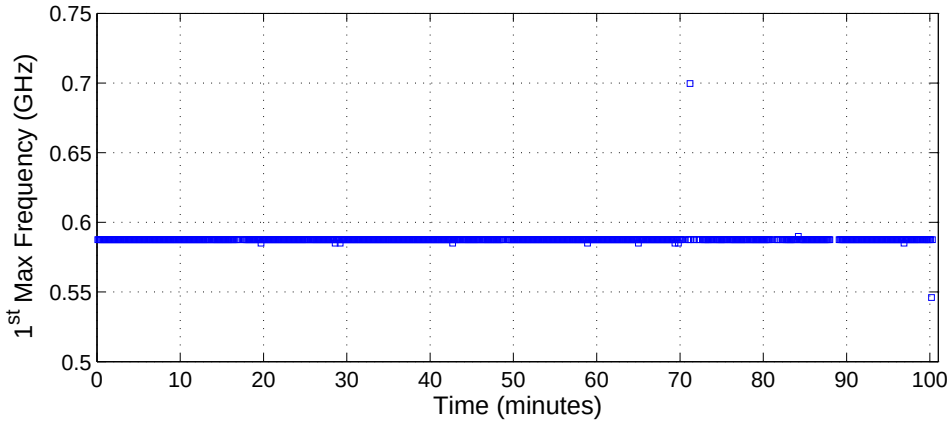

(a)

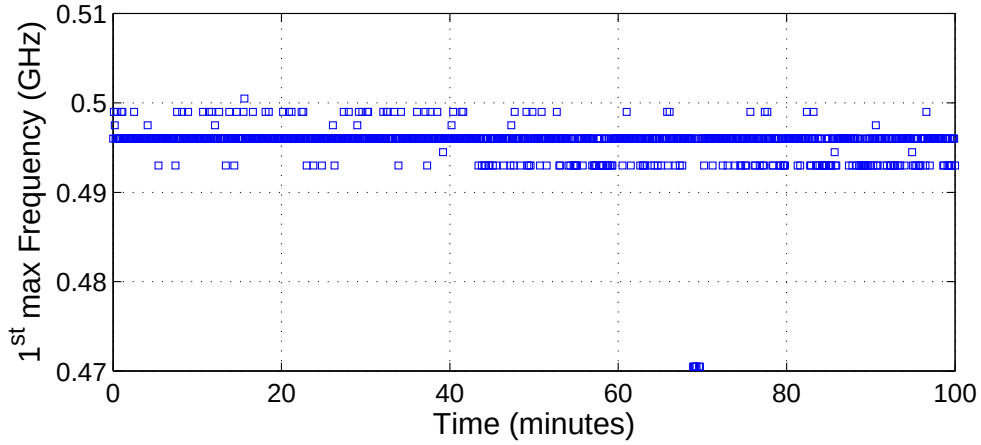

(b)

Figure 6.12: Tracking the frequency of the first maximum namely the frequency of the peak transmission :(a) first maximum of the S_21 response for female subject; (b) first maximum of the S_{21} response for the male subject. .

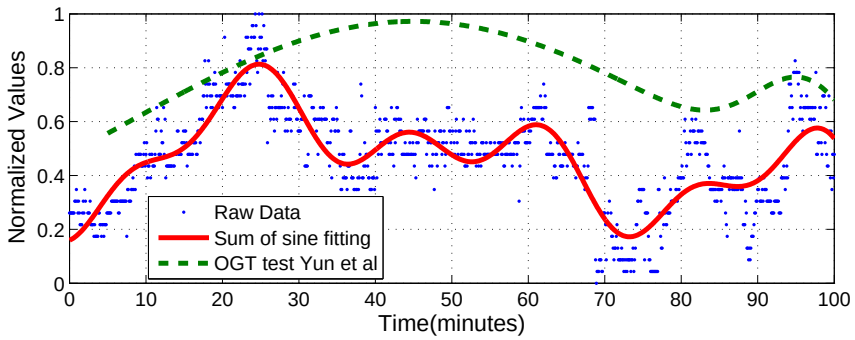

Figure 6.13: Comparison of the normalized frequency at the −29 dB of the male S_21 measurement and the oral glucose tolerance test results from the literature [16].

The frequency of occurrence of −29 dB is tracked. The frequency are normalized a 4^{th} degree sum of sine function is fitted to the normalized data. Then the

data is compared with the normalized OGT test results from the literature [16].

The comparison is shown in Fig. 6.13. The trend of the frequency change agree with the OGT results. However, the rise between 40^{th} and 70^{th} minutes are expected to be higher. This could be due to the lower sugar intake during the experiments. Also note that the reference glucose tests might not match exactly with the subject's glucose levels.

6.3 Conclusions

The patch resonator is fabricated and embedded into a wooden bench. Two commercial force sensors are taped to the two sides of the resonator and the effect applied force to the resonator response is quantified with five subjects. Applied force is effecting the resonator response significantly thus there is a need to minimize such effect.

A soda test is performed with five subjects and the patch resonator under constant applied force. The S-parameter response of the resonator is recorded during the soda test. Input impedance at the resonance frequency is calculated from the measured S-parameter results. The normalized input impedance is than compared with the literature data. Comparisons showed correlation with the literature data with 60% success rate.

The Soda test was also performed with two healthy individuals and the measured frequency shift for male subject showed correlation with the expected rise in blood glucose levels. The transmission response of the spiral resonator was recorded and compared with the reference data. The planar resonator approach shows promising results for non-invasive continuous assessment of the blood glucose levels. However, there is a need to improve the sensors and implement and multi parameter monitoring system to measure the blood glucose levels in a casual environment.

References

[1] "Fda clinical trial regulations." [Online]. Available: http://www.fda.gov/ScienceResearch/SpecialTopics/RunningClinicalTrials/ucm155713.htm

[2] "Medical device regulations." [Online]. Available: http://www.legislation.gov.uk/uksi/2002/618/contents/made

[3] "Mhra blood regulations." [Online]. Available: http://www.mhra.gov.uk/Howweregulate/Blood/#l1

[4] "Fda blood regulations." [Online]. Available: http://www.fda.gov/BiologicsBloodVaccines/BloodBloodProducts/default.htm

[5] A. Alomainy, Y. Hao, C. Parini, and P. Hall, "Comparison between two different antennas for uwb on-body propagation measurements," *Antennas and Wireless Propagation Letters, IEEE*, vol. 4, pp. 31–34, 2005.

[6] Y. Yao, J. Zheng, and Z. Feng, "Diversity measurements for on-body channels using a tri-polarization antenna at 2.45 ghz," *Antennas and Wireless Propagation Letters, IEEE*, vol. 11, pp. 1285–1288, 2012.

[7] T. S. P. See and Z. Chen, "Experimental characterization of uwb antennas for on-body communications," *Antennas and Propagation, IEEE Transactions on*, vol. 57, no. 4, pp. 866–874, 2009.

[8] M. Munoz, R. Foster, and Y. Hao, "On-body channel measurement using wireless sensors," *Antennas and Propagation, IEEE Transactions on*, vol. 60, no. 7, pp. 3397–3406, 2012.

[9] [Online]. Available: http://www.diabetes.co.uk/

[10] A. Tirosh, I. Shai, D. Tekes-Manova, E. Israeli, D. Pereg, T. Shochat, I. Kochba, and A. Rudich, "Normal fasting plasma glucose levels and type 2 diabetes in young men," *New England Journal of Medicine*, vol. 353, no. 14, pp. 1454–1462, 2005, pMID: 16207847. [Online]. Available: http://www.nejm.org/doi/full/10.1056/NEJMoa050080

[11] D. M. Nathan, M. B. Davidson, R. A. DeFronzo, R. J. Heine, R. R. Henry, R. Pratley, and B. Zinman, "Impaired fasting glucose and impaired glucose tolerance: Implications for care," *Diabetes Care*, vol. 30, no. 3, pp. 753–759, 2007. [Online]. Available: http://care.diabetesjournals.org/content/30/3/753.short

[12] [Online]. Available: http://www2.gvsu.edu/chm463/diabetes/diabetes-mellitus-good.htm

[13] M. Stumvoll, A. Mitrakou, W. Pimenta, T. Jenssen, H. Yki-Jrvinen, T. Van Haeften, W. Renn, and J. Gerich, "Use of the oral glucose tolerance test to assess insulin release and insulin sensitivity." *Diabetes Care*, vol. 23, no. 3, pp. 295–301, 2000. [Online]. Available: http://care.diabetesjournals.org/content/23/3/295.abstract

[14] K. V. Larin, M. S. Eledrisi, M. Motamedi, and R. O. Esenaliev, "Noninvasive blood glucose monitoring with optical coherence tomography: a pilot study in human subjects," *Diabetes Care*, no. 12, pp. 2263–2267, 2002.

[15] "Thin-film force sensors." [Online]. Available: http://www.tekscan.com/flexiforce.html?gclid=CKWnrq-3rrQCFaTKtAodDWAAgQ

[16] J. W. Yun, Y. K. Cho, J. H. Park, H. J. Kim, D. I. Park, C. I. Sohn, W. K. Jeon, and B. I. Kim, "Abnormal glucose tolerance in young male patients with nonalcoholic fatty liver disease," *Liver International*, vol. 29, no. 4, p. 525529, 2009.

Chapter 7

Conclusion and Future Work

In this thesis, the possibility of monitoring the realistic blood glucose levels by means of RF devices is explored. In order to relate the blood glucose level with the response of an RF device, it is vital to explore the relationship between glucose levels and dielectric properties of the blood and the subcutaneous tissue. Thus, there is a significant need to quantify two important issues: 1) establishing glucose dependent dielectric properties of the blood and subcutaneous liquid; and 2) relating the dielectric properties with the resonator response. To this end, two activities were carried out: 1) a dielectric property retrieval study; and 2) establishing a relation between glucose and dielectric properties of blood.

This thesis has presented a spiral resonator that was designed and tested with phantoms. The dielectric properties of the phantoms were retrieved with an improved analytical formulation. Also, a blood mimicking material was proposed and the realistic glucose dependance of dielectric properties of the blood mimicking material investigated though Cole-Cole analysis. Next, a patch resonator was designed and simulated with a four-layered digital tissue block and the sensitivity response of the resonator to the relative dielectric constant change in blood layer investigated. Finally, the resonator was fabricated and tested with tissue

mimicking materials. A detailed description of the chapters is given below.

In Chapter 2, off-the-shelf devices and scholarly articles for monitoring of chronic diseases, including diabetes, are described. The current state of the art for monitoring chronic diseases using different technologies and methods are summarised. This chapter presents an extensive overview of chronic diseases, as well as the advantages and disadvantages of the current monitoring systems and techniques.

Chapter 3 presents novel, extremely wide band, high and low-water content tissue mimicking material recipes and dielectric property measurements. The materials are composed with off-the-shelf, low-cost ingredients that are widely available. The dielectric property measurements of the tissue mimicking materials are also compared to the dielectric properties of the biological tissues reported in the literature. The TM phantoms reflect the dielectric properties with maximum deviations of 7.7 units and 3.9 S/m for relative dielectric constant and conductivity, respectively, for the whole frequency range. In addition, previously reported dielectric properties of tissue mimicking phantoms are also compared to those presented in this thesis, which demonstrated similar performance.

A spiral resonator was presented in Chapter 4 to establish a relation between the sensor response and dielectric property change in the biological tissue. The spiral resonator is tested with liquid and semi-solid phantoms. In order to retrieve the relative dielectric constant of the phantoms from the resonator response, an empirical analytical method is used. To improve the empirical method, the analytical formulation is modified by utilising Particle Swarm optimisation and Multiple Linear Regression methods. This is done by utilizing the simulated S-parameter response of the resonator. The new non-linear analytical equation is then solved with the Newton-Raphson iterative method for measurements and simulations. The dielectric properties of the phantoms are measured with the open-ended dielectric probe to verify the retrieved dielectric properties. Measured and retrieved relative dielectric constants are compared and a good agrement is obtained. The analysis of the possible error sources are also described in this chapter.

In Chapter 5, in order to quantify the glucose-dependent dielectric properties of blood, a blood mimicking material is characterized. By adding realistic glucose amounts to the blood mimicking phantoms, the glucose change in blood is mimicked. The dielectric properties of the blood mimicking materials with different glucose concentrations are measured for an extremely wide frequency range (0.3 GHz to 20 GHz). Next, a single-pole Cole-Cole model is fitted to the median of the dielectric property measurements. The Cole-Cole parameters are expressed as a function of blood glucose levels and it has been concluded that the relative dielectric constant variation between the minimum and maximum glucose levels in the blood mimicking phantoms will be 1 unit and the conductivity will remain constant. In addition, a patch resonator operating in the 2.4 - 2.48 GHz ISM band, when placed radiating against human tissue, was studied for non-invasive monitoring of blood glucose levels. The resonator was simulated with a four-layered non-dispersive digital phantom. The fabricated resonator is tested with the four-layered physical frequency-dispersive phantom. Four samples of the blood mimicking phantom were characterized, where the glucose concentration was changed for each sample. While alternating the blood layer with different concentrations of glucose, the S-parameter response of the patch resonator was measured. From the resonator experiments, it has been observed that the input impedance of the resonator is sensitive to the realistic glucose level changes in the blood layer.

Chapter 6 presented human tests. The first set of human tests were conducted with the patch resonator. First the patch resonator is combined with the commercial force sensors and the effect of the applied force is identified. Then under constant applied force five subjects went through a soda test. The S-parameter response of the patch resonator is recorded. During the post processing the input impedance at the resonance is calculated. The results are compared with the literature glucose data, 60% correlation is obtained between the resonator response and literature data. Next, two subjects went though soda test with the first prototype of spiral resonator. Transmission response of the spiral resonator is recorded. After the analysis the data is compared with the literature data.

7.1 Key Contributions

Major contributions proposed in this study are:

- New recipes for wide-band tissue mimicking phantoms based on oil-in-gelatine dispersion materials, including wet skin, blood, muscle, and fat mimicking materials, are proposed. Two recipes for narrow-band tissue mimicking materials are also proposed. These materials can be characterized easily by using off-the-self ingredients and the shelf-life of the tissue mimicking phantoms are at least two weeks when kept in air tight containers at low temperatures. The proposed wide-band phantoms can mimic the dielectric properties of the given biological tissues for an extremely wide frequency range.

- Realistic glucose-dependent dielectric properties of blood mimicking material are characterized by fitting Cole-Cole parameters to measured dielectric properties. It has been found that the relative dielectric constant change for maximum and minimum glucose range (where these values are the expected extremes for a normal, healthy subject from the literature) is 1 unit and the conductivity will remain constant. To the best of the author's knowledge, the realistic glucose changes, in terms of dielectric property values, have not previously been reported in the literature.

- Spiral resonators are designed and tested with phantoms. An analytical formulation is used to retrieve the dielectric properties of the liquid and semi-solid phantoms. Reference dielectric properties are collected with an open-ended coaxial probe. Collected reference dielectric properties and retrieved dielectric properties are compared. A good agreement obtained, which indicates that a real-time narrow band relative dielectric constant measurement fixture for high-loss biological tissues can be developed.

- A patch resonator operating at the ISM band when placed towards to skin is presented. The resonator is tested with four-layered tissue mimicking materials, by changing the glucose content of the blood layer. The input impedance of the resonator at the resonance frequency is calculated from the

S-parameter response, and it has been found to be sensitive to the dielectric property changes within the minimum and maximum glucose change.

- The effect of applied force to the patch resonator response is quantified and it was concluded that the applied force has a significant effect on the response of the resonator. It should be noted that there is a need to control the applied force during the measurements with such resonators.

7.2 Suggestions for Future Research

This thesis presents the methodologies and results that lays the foundations for non-invasive monitoring of the blood glucose levels by means of electromagnetics. Presented work have the potential that can be exploited both experimentally and numerically. Future experimental research suggestions are given in section 7.2.1, suggestions on numerical future investigation is given in 7.2.2.

7.2.1 Experimental Aspects

Dielectric Spectroscopy

Dielectric properties of the biological tissues is the vital parameter for designing resonators and antennas that is aimed to operate inside or in the vicinity of the human tissue. This study investigates the realistic glucose dependance of the blood mimicking material's dielectric properties. Logical expansion of this line of research, is the investigation of the glucose dependance of the blood and other tissue dielectric properties. One important parameter that can be exploited quickly is the effect of the temperature on the glucose-dependent dielectric properties of blood.It is also well known that dielectric properties of water is highly dependent on the temperature [1]. Temperature dependant static permittivity of water is given in Fig. 7.1. Thus, dielectric properties of the biological tissues, which most of the tissues are high water content, are dependant on the temperature [2, 3, 4]. Note that this thesis reports the measurements taken at room temperature (25°); however, the body's temperature is much higher (37°). Therefore, it is vital to

perform measurements at the body's temperature; one important research contribution could be the potential discrepancy of dielectric properties occurring due to the variation of glucose levels at (37°). That at (37°) is the discrepancy between two glucose levels could be different from the (25°).

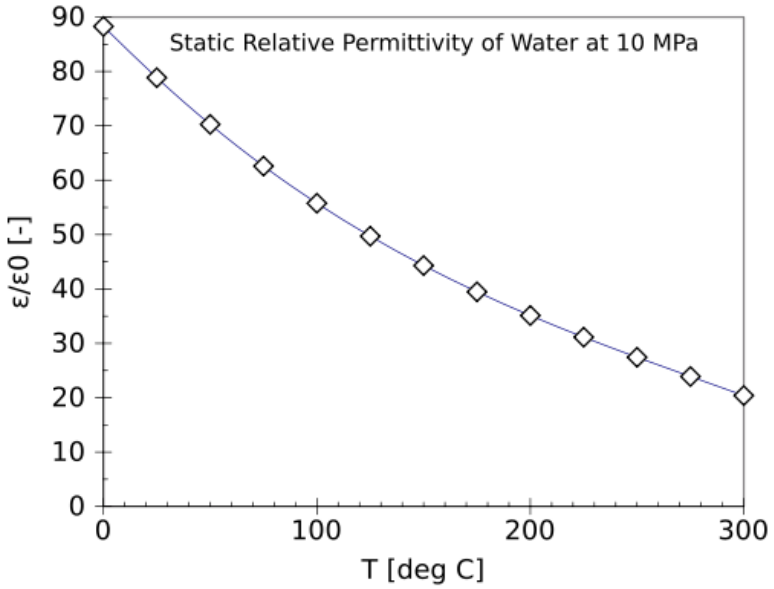

Figure 7.1: Temperature dependance of water static permittivity [5].

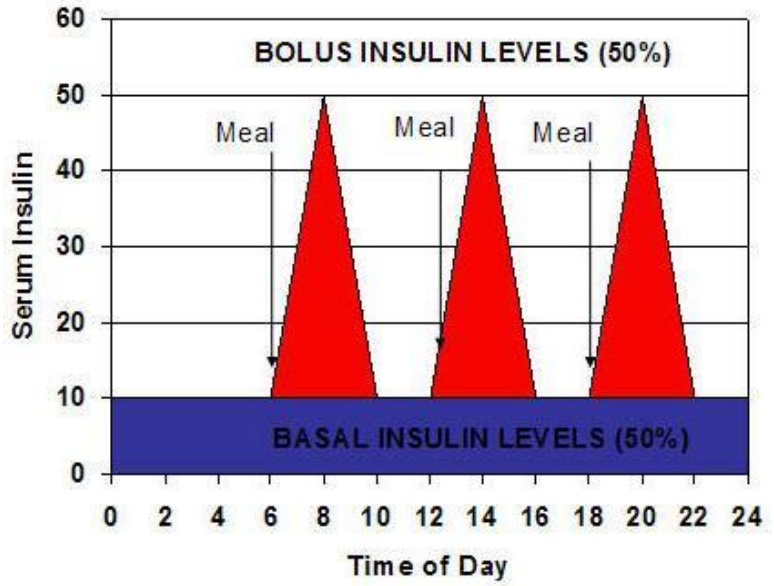

Figure 7.2: Insulin, blood glucose regulating hormone, secretion after meals for a healthy subject [6].

The amount of other hormones, specifically insulin levels [7], should be determined and the dielectric property dependance of such hormones should be

investigated. The investigation of insulin dependance is important as insulin level elevates with the increase in glucose levels in blood 7.2. Such study can be carried out in vitro with blood plasma, body temperature also needs to be considered during such experimental work.

Further investigation of glucose-dependent dielectric property changes of biological tissues, including skin, fat, and muscle tissues is needed, since the resonator is sensing the effective change in the dielectric properties for blood layer. Thus, it is important to quantify the changes occurring in the other tissues. Then, by applying a correction technique (which will require further work in itself), the information regarding the blood glucose levels can be withdrawn from the collected sensor response. Investigating the effect of other parameters, such as sweat levels, blood pressure, daily activity, and the psychological condition of the subject to the sensor response. A multi-sensor system is needed to perform such experiments.

Human Tests

Performing the soda test with more subjects under controlled and uncontrolled environments is important. There is a need for more data in human experiments and the tests should be performed with the other resonators proposed in this thesis. Also, the tests should be performed with diabetes patients as well, since the ultimate testing domain is the diabetes patients. Such experiments provides advanced data; thus, it is vital to verify the proper functioning of the end product with diabetes patients.

7.2.2 Numerical Aspects

Due to the relatively small glucose-dependent change in the dielectric properties of blood, the sensitivity of the resonators should be increased. To do so, one vital parameter to consider is the Q factor of the resonator. Designing a high Q structure is challenging, one example of a high Q resonator is the cavity resonators. However, due to the application specific physical constrains the resonator should be a planar structure that can be evolved into a flexible sensor in the future.

Finally, improvement of the numerical model is needed. In this thesis numerical simulations are limited with layered phantoms. However, the human body is more complicated and it can be now represented in the computer domain. Within the last decade, the human body have been constructed in computer domain and represented during the solution of numerical electromagnetic problems [8, 9, 10, 11].

References

[1] "Dielectric properties of materials." [Online]. Available: http://www.clippercontrols.com/pages/Dielectric-Constant-Values.html#W

[2] F. Jaspard and M. Nadi, "Dielectric properties of blood: an investigation of temperature dependence," *Physiological Measurement*, vol. 23, no. 3, p. 547, 2002. [Online]. Available: http://stacks.iop.org/0967-3334/23/i=3/a=306

[3] M. Lazebnik, M. C. Converse, J. H. Booske, and S. C. Hagness, "Ultrawideband temperature-dependent dielectric properties of animal liver tissue in the microwave frequency range," *Physics in Medicine and Biology*, vol. 51, no. 7, p. 1941, 2006. [Online]. Available: http://stacks.iop.org/0031-9155/51/i=7/a=022

[4] L. Chin and M. Sherar, "Changes in dielectric properties of ex vivo bovine liver at 915 mhz during heating," *Physics in Medicine and Biology*, vol. 46, no. 1, p. 197, 2001. [Online]. Available: http://stacks.iop.org/0031-9155/46/i=1/a=314

[5] "Temperature dependent static dielectric contant of water." [Online]. Available: http://en.wikipedia.org/wiki/File:Water_relative_static_permittivity.svg#filehistory

[6] "Insulin levels." [Online]. Available: http://www.columbia.edu/itc/hs/medical/clerkships/primcare/case/diabetes/diabetes01_07.html

[7] A. A. Laogun, R. J. Sheppard, and E. H. Grant, "Dielectric properties of insulin in solution," *Physics in Medicine and Biology*, vol. 29, no. 5, p. 519, 1984. [Online]. Available: http://stacks.iop.org/0031-9155/29/i=5/a=004

[8] "Numerical human models." [Online]. Available: http://www.itis.ethz.ch/itis-for-health/virtual-population/human-models/

[9] D. L. Collins, A. P. Zijdenbos, V. Kollokian, J. G. Sled, N. J. Kabani, C. J. Holmes, and A. C. Evans, "Design and construction of a realistic digital brain phantom," *Medical Imaging, IEEE Transactions on*, vol. 17, no. 3, pp. 463–468, 1998.

[10] I. G. Zubal, C. R. Harrell, E. O. Smith, Z. Rattner, G. Gindi, and P. B. Hoffer, "Computerized three-dimensional segmented human anatomy," *Medical Physics-New York-Institute of Physics*, vol. 21, no. 2, pp. 299–302, 1994.

[11] M. Caon, "Voxel-based computational models of real human anatomy: a review," *Radiation and environmental biophysics*, vol. 42, no. 4, pp. 229–235, 2004.

Appendix A

Particle Swarm Optimization

PSO is a novel population based meta-heuristic technique developed by Eberhart and Kennedy in 1995. It is inspired by the behavior of bird flocking or fish schooling and utilizes the swarm intelligence generated by the cooperation and competition between the particles in a swarm. Compared with evolutionary algorithms (genetic algorithm (GA), evolutionary programming, evolutionary strategy, and genetic programming), PSO still maintains the population based global search strategy but adopts the velocity-displacement model with more efficient information flow and easier implementing procedures.

The swarm intelligence suggests that when the swarm is in search for the best place for food gathering in an unfamiliar field the swarm moves to reach it's goal with a collective search technique. Each member remembers the visited individual best position with the most food (personal best) and each member also stores the best position found by the swarm (global best). When the member is moving another position it changes it's directory based ont he personal best and global best. Through this search the animals eventually swarm around the position in the field with the most food. The PSO terminology is given in Table A.1.

Table A.1: Particle Swarm Optimization Terminology

Term	Explanation
Partical/Agent	Single individual in the swarm
Location/Position	An Agent's N dimensional coordinates which represents a solution to the problem
Swarm	The entire collection of particles
Fitness	A single number representing the goodness of a given solution
Pbest	The location in parameter space of the best fitness returned for a specific particle (personal best)
Gbest	The location in parameter space of the best fitness returned for the entire swarm (global best)
Velocity	The velocity of the particle that is decided according to pbest and gbest

The swarm is composed of members so called particles. Each particles position is a set of coordinates in the preassigned n-dimensional solution space and position of each particle represents one solution. A fitness function determines the closeness of each solution relative to other solutions to the desired result. Each particle stores the personal and global best. According to the stored best values the particle flies in the pre-determined solution space with the velocity and position equations. The velocity and position update expressions are given in equations (A.1) and (A.2), respectively.

$$\upsilon_n(t + \Delta(t)) = \omega \cdot \upsilon_n(t) + c_1 \cdot \mathrm{r}()(pb_n - x_n(t)) + c_2 \cdot \mathrm{r}()(gb_n - x_n(t)) \quad \text{(A.1)}$$

$$x_n(t + \Delta(t)) = x_n(t) + \Delta(t) \cdot \upsilon_n(t) \quad \text{(A.2)}$$

In the equations above, n is the number of particles, $\Delta(t)$ is the time step,c_1 and c_2 are constants typically assigned the scalar value of 2, pb and gb are personal and global best, and r calls for a random number on each iteration. ω is the inertial weight which decreases linearly with the iteration.Such implementation encourages the trajectory influenced by the personal best rather than the global best initially; thus, the solution space is searched thoroughly.

Although being relatively new optimization method, PSO is simple to implement to optimization of both for binary and real variables. Another desirable property of the PSO is the flexibility of assigning multiple design and optimisation

goals. For example, in an antenna problem both bandwidth and center frequency can be chosen as design goals namely the fitness function can be defined as a weighted function of each goal. This properties makes PSO a great algorithm to be implemented to solve electromagnetics optimisation problems effectively.